

# CANADIAN THESES ON MICROFICHE

I.S.B.N.

# THESES CANADIENNES SUR MICROFICHE



National Library of Canada  
Collections Development Branch

Canadian Theses on  
Microfiche Service

Ottawa, Canada  
K1A 0N4

Bibliothèque nationale du Canada  
Direction du développement des collections

Service des thèses canadiennes  
sur microfiche

## NOTICE

The quality of this microfiche is heavily dependent upon the quality of the original thesis submitted for microfilming. Every effort has been made to ensure the highest quality of reproduction possible.

If pages are missing, contact the university which granted the degree.

Some pages may have indistinct print especially if the original pages were typed with a poor typewriter ribbon or if the university sent us a poor photocopy.

Previously copyrighted materials (journal articles, published tests, etc.) are not filmed.

Reproduction in full or in part of this film is governed by the Canadian Copyright Act, R.S.C. 1970, c. C-30. Please read the authorization forms which accompany this thesis.

THIS DISSERTATION  
HAS BEEN MICROFILMED  
EXACTLY AS RECEIVED

## AVIS

La qualité de cette microfiche dépend grandement de la qualité de la thèse soumise au microfilmage. Nous avons tout fait pour assurer une qualité supérieure de reproduction.

S'il manque des pages, veuillez communiquer avec l'université qui a conféré le grade.

La qualité d'impression de certaines pages peut laisser à désirer, surtout si les pages originales ont été dactylographiées à l'aide d'un ruban usé ou si l'université nous a fait parvenir une photocopie de mauvaise qualité.

Les documents qui font déjà l'objet d'un droit d'auteur (articles de revue, examens publiés, etc.) ne sont pas microfilmés.

La reproduction, même partielle, de ce microfilm est soumise à la Loi canadienne sur le droit d'auteur, SRC 1970, c. C-30. Veuillez prendre connaissance des formules d'autorisation qui accompagnent cette thèse.

LA THÈSE A ÉTÉ  
MICROFILMÉE TELLE QUE  
NOUS L'AVONS REÇUE



National Library  
of Canada

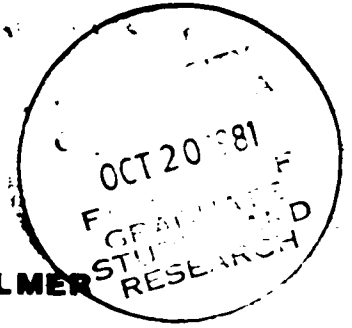
Bibliothèque nationale  
du Canada

Canadian Theses Division / Division des thèses canadiennes

Ottawa, Canada  
K1A 0N4

54072

6-315-06152-7



**PERMISSION TO MICROFILM — AUTORISATION DE MICROFILMER**

• Please print or type — Écrire en lettres moulées ou dactylographier

Full Name of Author — Nom complet de l'auteur

BRYAN DAVID WATTS

Date of Birth — Date de naissance

MARCH 1, 1951

Country of Birth — Lieu de naissance

CANADA

Permanent Address — Residence fixe

13479 Waterford Place  
V3W 6V2

Title of Thesis — Titre de la thèse

Lateral Creep Deformations in the Foundation of a High Dam

University — Université

UNIVERSITY OF ALBERTA

Degree for which thesis was presented — Grade pour lequel cette thèse fut présentée

MASTER OF SCIENCE

Year this degree conferred — Année d'obtention de ce grade

1981

Name of Supervisor — Nom du directeur de thèse

N.R. MORGENSTERN

Permission is hereby granted to the NATIONAL LIBRARY OF CANADA to microfilm this thesis and to lend or sell copies of the film

L'autorisation est, par la présente, accordée à la BIBLIOTHÈQUE NATIONALE DU CANADA de microfilmer cette thèse et de prêter ou de vendre des exemplaires du film.

The author reserves other publication rights, and neither the thesis nor extensive extracts from it may be printed or otherwise reproduced without the author's written permission

L'auteur se réserve les autres droits de publication; ni la thèse ni de longs extraits de celle-ci ne doivent être imprimés ou autrement reproduits sans l'autorisation écrite de l'auteur.

Date

October 12, 1981

Signature

Bryan D. Watts

THE UNIVERSITY OF ALBERTA

LATERAL CREEP DEFORMATIONS IN THE FOUNDATION OF A HIGH DAM

by



BRYAN DAVID WATTS

A THESIS

SUBMITTED TO THE FACULTY OF GRADUATE STUDIES AND RESEARCH  
IN PARTIAL FULFILMENT OF THE REQUIREMENTS FOR THE DEGREE

OF MASTER OF SCIENCE

IN

CIVIL ENGINEERING

EDMONTON, ALBERTA

Fall 1981

THE UNIVERSITY OF ALBERTA

RELEASE FORM

NAME OF AUTHOR BRYAN DAVID WATTS  
TITLE OF THESIS LATERAL CREEP DEFORMATIONS IN THE FOUNDATION OF A HIGH DAM

DEGREE FOR WHICH THESIS WAS PRESENTED MASTER OF SCIENCE

YEAR THIS DEGREE GRANTED Fall 1981

Permission is hereby granted to THE UNIVERSITY OF ALBERTA LIBRARY to reproduce single copies of this thesis and to lend or sell such copies for private, scholarly or scientific research purposes only.

The author reserves other publication rights, and neither the thesis nor extensive extracts from it may be printed or otherwise reproduced without the author's written permission.

(SIGNED) *Bryan D. Watts*

PERMANENT ADDRESS:

*13419 Waterford Place  
Surrey, British Columbia*

DATED ..... *September 16 1981*

THE UNIVERSITY OF ALBERTA  
FACULTY OF GRADUATE STUDIES AND RESEARCH

The undersigned certify that they have read, and recommend to the Faculty of Graduate Studies and Research, for acceptance, a thesis entitled Lateral Creep Deformations in the Foundation of a High Dam submitted by Bryan David Watts in partial fulfilment of the requirements for the degree of Master of Science in Civil Engineering.

*B. Hyatt*  
.....  
Supervisor  
*B. Simpson*  
.....  
*Edw. Roberts*  
.....  
*W. S. ...*  
.....

Date... *September 16, 1981* .....

To my mother

## ABSTRACT

The time dependent lateral deformations of the clay foundation of an oilsands mine tailings dyke are analysed in this thesis. The lateral deformations analysed were recorded by several inclinometers over a period of approximately four years. Based on the nature of the lateral deformations and piezometer readings in the clay foundation it is postulated that the movements are a result of a drained creep mechanism.

On the basis of laboratory tests the foundation clay is normally consolidated, stiff, medium plastic and contains approximately two percent organic matter and four percent calcium carbonate. A series of oedometer tests demonstrate that the clay has a 'low' secondary compressibility according to Mesri's (1973) classification.

Incremental drained creep triaxial tests were performed on samples with the bedding plane horizontal and at an angle of  $45^\circ$ . It is shown that the creep behaviour of the clay is isotropic and insensitive to normal stress. Furthermore, it is demonstrated that the axial creep strain rate, after all excess pore pressures have dissipated, follows a relationship of the Singh-Mitchell (1968) type.

An analysis of one set of inclinometer readings is presented which illustrates a method whereby the creep parameters in the Singh-Mitchell (1968) equation can be derived from field shear strain versus time curves. The time from the actual initiation of creep to the time at which the

inclinometer was installed it is identified as a key parameter in the field creep relationship.



## Acknowledgments

This thesis programme was undertaken in the Department of Civil Engineering at the University of Alberta under supervision of Professor N.R.Morgenstern. I wish to thank Dr.Morgenstern for his guidance, support and patience. I also wish to thank Dr.H.K.Mittal for originally suggesting the thesis topic.

Suncor Inc. and Hardy Associates(1978) Ltd. kindly provided the instrumentation data from Tar Island Dyke. I am grateful to the numerous people at Hardy Associates(1978) Ltd. who gave of their time to discuss the performance of the dyke.

The personal financial support provided by the University of Alberta and the National Research Council is gratefully acknowledged.

I am indebted to Mr. A. Muir for fabrication of the laboratory equipment and to Messrs. G. Cyre and O. Wood for their assistance in the design of the laboratory equipment. I am grateful to Mrs. Linda Nielsen for her excellent typing of the thesis into the computer and to Mr. G. Cyre for drafting the figures.

I am especially grateful to my fellow graduate students for the many hours spent discussing this research. Special thanks are extended to Mr. J. Sobkowicz for his critical review of the entire thesis, Mr. J. Simmons for his guidance in the use of his finite element program and Dr. D. Segó for his review of Chapter 3.

Finally, I wish to express my sincere appreciation to my mother and my two sisters, Cathie and Lisa, who always provided support and understanding.

## Table of Contents

Chapter	Page
1. Introduction .....	1
1.1 General .....	1
1.2 Lateral Displacements Beneath Embankments .....	3
1.3 Objective and Scope .....	6
2. Tar Island Dyke - Site Conditions and Instrumentation ..	8
2.1 Introduction .....	8
2.2 Construction History .....	8
2.3 Foundation Characteristics .....	13
2.3.1 Geology .....	13
2.3.2 Geotechnical Properties of Silt and Clay Deposit .....	15
2.4 Field Sampling Program .....	16
2.5 Foundation Instrumentation .....	18
2.5.1 General .....	18
2.5.2 Foundation Piezometers .....	19
2.5.3 Inclinometers .....	23
2.6 Nature of Foundation Movements .....	24
3. A Review of the Creep Behaviour of Soils .....	27
3.1 Introduction .....	27
3.2 The Fundamental Approach .....	29
3.2.1 General .....	30
3.2.2 Considerations Based on Viscosity of Adsorbed Water .....	30
3.2.3 Rate Process Theory .....	33
3.2.4 A Model Based on a Cavity Channel Network ...	35
3.3 The Phenomenological Approach .....	36

3.3.1	Drained Creep .....	40
3.3.1.1	Volumetric Component .....	40
3.3.1.2	Deviatoric Component .....	51
3.3.2	Undrained Creep .....	53
3.4	Creep Rupture .....	58
3.4.1	Undrained Conditions .....	60
3.4.2	Creep Rupture Life .....	62
3.4.3	Drained Conditions .....	66
4.	Laboratory Testing Equipment and Procedures .....	68
4.1	Introduction .....	68
4.2	Oedometer Creep Tests .....	69
4.2.1	Testing Equipment .....	69
4.2.2	Sample Preparation .....	72
4.2.3	Testing Procedure .....	73
4.3	Triaxial Creep Tests .....	75
4.3.1	General .....	75
4.3.2	Triaxial Testing Equipment .....	76
4.3.2.1	General .....	76
4.3.2.2	Triaxial Cells .....	76
4.3.2.3	Pressure Systems .....	81
4.3.2.4	Monitoring of Sample Deformation .....	86
4.3.2.5	Suggested Modifications To Equipment .....	91
4.3.3	Sample Preparation .....	92
4.3.4	Testing Procedure .....	92
4.3.4.1	General .....	92
4.3.4.2	B Tests* .....	95

4.3.4.3	Isotropic Consolidation .....	95
4.3.4.4	Incremental Creep Tests .....	96
5.	Experimental Results .....	100
5.1	Introduction .....	100
5.2	Soil Composition .....	101
5.2.1	Index Tests .....	101
5.2.2	Mineralogy .....	103
5.2.3	Scanning Electron Microscope Analysis .....	104
5.3	Oedometer Test Results .....	107
5.3.1	General .....	107
5.3.2	Coefficient of Secondary Consolidation .....	112
5.3.3	Vertical Strain Rate .....	115
5.4	Triaxial Creep Test Results .....	119
5.4.1	General .....	119
5.4.2	Isotropic Consolidation .....	121
5.4.3	Incremental Creep .....	125
5.4.4	Factors Influencing Creep Parameters .....	135
5.4.4.1	Stress State .....	135
5.4.4.2	Anisotropy .....	136
5.4.4.3	Octahedral Stress .....	136
5.4.4.4	Testing Procedure .....	137
5.5	Shear Strength Results .....	139
5.5.1	General .....	139
5.5.2	Stress-Strain Behaviour .....	141
5.5.3	Strength Envelope .....	143
5.6	Concluding Remarks .....	145
6.	Analysis of Lateral Creep Movements in the Tar Island Dyke Clay Foundation .....	146

6.1	Introduction .....	146
6.2	State of Stress in Foundation Clay .....	149
6.2.1	Introduction .....	149
6.2.2	Total Stress Analysis .....	151
6.2.2.1	General .....	151
6.2.2.2	Boundary Conditions .....	152
6.2.2.3	Parametric Study .....	155
6.2.3	Rationale for Simple Shear .....	159
6.3	Formulation of <i>In Situ</i> Creep Equation .....	161
6.3.1	Introduction .....	161
6.3.2	Multiaxial Form of Singh-Mitchell Equation .....	164
6.3.3	Derivation of Stress Level Term .....	165
6.3.4	Derivation of $t_c$ and $m$ .....	167
6.4	Concluding Remarks .....	172
7.	Conclusions and Recommendations .....	174
7.1	Introduction .....	174
7.2	Conclusions .....	174
7.2.1	General .....	174
7.2.2	Laboratory Creep Tests .....	175
7.2.3	<i>In Situ</i> Lateral Strains .....	176
7.3	Recommendations For Further Study .....	177
7.3.1	Drained Laboratory Creep Experiments .....	178
7.3.2	Lateral Creep Strains Beneath Tar Island Dyke .....	179
References	.....	180
Appendix A	Field Instrumentation Data .....	194
Appendix B		

Grain Size Curves, Scanning Electron Micrographs and Oedometer Test Results .....	203
B.1 Derivation of Equation 4.3 .....	203
Appendix C	
Triaxial Creep Test Results .....	217
Appendix D	
Derivation of Formulas for Analysis .....	245
D.1 Definition of Nonlinear Elastic Material Parameters .....	245
D.2 Transformation of Singh-Mitchell Equation To a Multiaxial State of Stress .....	246
D.3 Definition of Stress Level For Simple Shear Stress Conditions .....	248
D.4 Sample Calculation of $\bar{\sigma}$ .....	250
D.5 Procedure For Determining $t_f$ .....	251

## List of Tables

Table	Page
5.1 Summary of index test results .....	102
5.2 Oedometer test results ,sample C1 .....	108
5.3 Summary of isotropic consolidation results, vertical samples .....	122
5.4 Summary of isotropic consolidation results, inclined samples .....	123
5.5 Summary of incremental creep test results ,sample T4 .....	126
5.6 Summary of incremental creep test results,all samples .....	132
6.1 Summary of material constants used for linear elastic analyses .....	156
6.2 Summary of material constants used for nonlinear elastic analyses .....	156
B.1 Oedometer test results ,sample C2 .....	204
B.2 Oedometer test results ,sample C3 .....	205
C.1 Summary of incremental creep test results ,sample T1 .....	218
C.2 Summary of incremental creep test results ,sample T2 .....	220
C.3 Summary of incremental creep test results ,sample I1 .....	221
C.4 Summary of incremental creep test results ,sample I2 .....	222
C.5 Summary of incremental creep test results ,sample I3 .....	223



## List of Figures

Figure		Page
1.1	Location of major oilsands deposits in Canada .....	2
1.2	Total and effective stress paths under an embankment during construction (after Tavenas <i>et.al</i> , 1979) .....	5
2.1	Tar Island Dyke, section at Station 65+00 .....	10
2.2	Isopach map of silt and clay deposit .....	14
2.3	Atterberg limit test results .....	17
2.4	Tar Island Dyke, location of instrumentation .....	20
2.5	Summary of foundation pore pressures, upper-303 m berm and lower-291 m berm .....	21
2.6	Summary of foundation pore pressures, upper-277 m berm and lower-264 m berm .....	22
2.7	Inclinometer S76-101, calibrated January 26, 1976 .....	25
3.1	Variation in creep behaviour of soils (after Mitchell and Campanella, 1963) .....	28
3.2	Strain rate versus time during undrained creep of alluvial Osaka clay (after Murayama and Shibata, 1958) .....	38
3.3	Variation of strain rate with deviator stress for undrained creep of San Francisco Bay Mud (after Mitchell, 1976) .....	38
3.4	Relation between applied stress and rate of secondary compression in oedometer (after Murayama and Shibata, 1964) .....	46
3.5	Relationship between $C_a$ and $C_c$ and consolidation pressure for (a) Mexico City clay (b) Leda clay (c) Undisturbed New Haven organic silt (after Mesri and Godlewski, 1977) .....	46
3.6	Effect of load increment ratio on secondary compression index (after Bjerrum, 1967) .....	47

Figure	Page
3.7 Effect of stress level on volumetric creep rate, left - triaxial tests, right - simple shear tests (after Walker, 1969a) .....	50
3.8 Lines of equal volumetric strain rate at $t = 100$ min in the stress space for drained tests (after Tavenas <i>et.al</i> , 1978) .....	50
3.9 Lines of equal shear strain rates at $t = 100$ min in the stress space for drained and undrained tests (after Tavenas <i>et.al</i> , 1978) .....	54
3.10 Effect of stress level on shear creep rate, left - triaxial tests, right - simple shear tests (after Walker, 1969a) .....	54
3.11 Creep parameter, $m$ , versus void ratio (after Krizek <i>et.al</i> , 1977) .....	57
3.12 Excess pore pressure development following cessation of drainage after secondary compression for different time periods (after Holzer <i>et.al</i> , 1973) .....	59
3.13 Excess pore pressure development during undrained creep of San Francisco Bay mud after consolidation at $1.0 \text{ kg/cm}^2$ for 10 min (after Holzer <i>et.al</i> , 1973) .....	59
3.14 Determination of upper yield stresses (after Campanella and Vaid, 1974) .....	61
3.15 Creep rate behaviour of $K_0$ -consolidated undisturbed Haney clay under axially symmetric loading (after Campanella and Vaid, 1972) .....	61
3.16 Relationships between rupture life and minimum creep rate--normally consolidated undisturbed Haney clay (after Campanella and Vaid, 1974) .....	65
3.17 Axial strain at minimum strain rate as a function of creep stress for undisturbed Haney clay (after Campanella and Vaid, 1974) .....	65
4.1 Typical oedometer compliance test results .....	70

Figure	Page
4.2 Typical ram friction test results .....	80
4.3 Schematic of cell pressure systems .....	82
4.4 Schematic of back pressure system and volume change indicator .....	83
5.1 Void ratio versus logarithm of time curves ,sample C1 .....	109
5.2 Void ratio versus vertical stress, sample C1 .....	111
5.3 Coefficient of secondary consolidation versus vertical stress .....	113
5.4 Coefficient of secondary compression for natural soil deposits, after Mesri, 1973 .....	114
5.5 Vertical strain rate versus time ,sample C2 .....	116
5.6 Unit strain rate versus vertical stress, oedometer tests .....	118
5.7 Vertical strain and strain rate versus logarithm of time ,sample I2, consolidation pressure=1386 kPa .....	124
5.8 Vertical strain versus time ,sample T4 .....	127
5.9 Vertical strain rate versus time ,sample I3-left, sample t4-right) .....	128
5.10 Strain rate versus time for Pancone clay (after Lovenbury, 1969) .....	130
5.11 Creep parameter, m, versus octahedral stress .....	133
5.12 Unit strain rate versus stress level, triaxial tests .....	134
5.13 Strain versus time relationship for step-creep test (after Mitchell <i>et.al</i> , 1969) .....	140
5.14 Stress-strain curve ,sample I3 .....	142
5.15 P-q plot, from creep tests and previous	

Figure	Page
work .....	144
6.1 Lateral creep movements of the Tar Island Dyke clay foundation, Station 65+00 .....	147
6.2 Dyke crest and pond level rise with time .....	150
6.3 Tar Island Dyke stress analysis, finite element mesh .....	153
6.4 Horizontal shear stress in the upper half of the foundation clay along the downstream slope .....	157
6.5 Total vertical stress with time in the upper half of the foundation clay for the 291 m and 277 m berms .....	157
6.6 Shear stress with time in upper half of clay foundation below 291 m berm .....	160
6.7 Shear stress with time in upper half of clay foundation below 277 m berm .....	160
6.8 Shear strain versus time, inclinometer S76-103, above-upper half of clay, below-lower half of clay .....	162
6.9 Shear strain versus time, inclinometer S76-103, basal sand .....	163
6.10 Actual and predicted field shear strain versus time curves .....	171
6.11 Field shear strain versus time curves and curves predicted from laboratory equation .....	171
A.1 Test hole log S79-109 at which samples for laboratory testing were obtained .....	195
A.2 Inclinometer S78-101S, calibrated November 26, 1978 .....	196
A.3 Inclinometer S75-102, calibrated January 19, 1976, shear strain .....	197
A.4 Inclinometer S75-102, calibrated January 19, 1976, horizontal displacement .....	198
A.5 Inclinometer S76-103, calibrated November 2, 1976, shear strain .....	199

Figure	Page
A.6	Inclinometer S76-103,calibrated November 2,1976,horizontal displacement .....200
A.7	Inclinometer S75-104,calibrated September 16,1976, shear strain .....201
A.8	Inclinometer S75-104,calibrated September 16,1976,horizontal displacement .....202
B.1	Room temperature versus time .....206
B.2	Cell pressure and back pressure versus time,sample I2 .....207
B.3	Grain size analysis,samples C1, C2 and C3 .....208
B.4	Grain size analysis,samples T1, T2 and T4 .....209
B.5	Grain size analysis,samples I1, I2 and I3 .....210
B.6	Void ratio versus time, sample C2 .....211
B.7	Void ratio versus time, sample C3 .....212
B.8	Void ratio versus effective stress,sample C2-left,sample C3-right .....213
B.9	Vertical strain rate versus time,sample C1 .....214
B.10	Vertical strain rate versus time,sample C1 .....215
B.11	Vertical strain rate versus time,sample C3 .....216
C.1	Vertical strain and strain rate versus time, sample I1, consolidation pressure=365 kPa .....224
C.2	Vertical strain and strain rate versus time, sample I1, consolidation pressure=743 kPa .....225
C.3	Vertical strain and strain rate versus time, sample I2, consolidation pressure=334 kPa .....226
C.4	Vertical strain and strain rate versus time, sample I2, consolidation

Figure	Page
pressure=672 kPa .....	227
C.5 Vertical strain and strain rate versus time, sample I3, consolidation pressure=271 kPa .....	228
C.6 Vertical strain and strain rate versus time, sample I3, consolidation pressure=548 kPa .....	229
C.7 Vertical strain and strain rate versus time, sample I3, consolidation pressure=1097 kPa .....	230
C.8 Vertical strain versus time, sample T1 .....	231
C.9 Vertical strain versus time, sample T2 .....	232
C.10 Vertical strain versus time, sample I1 .....	233
C.11 Vertical strain versus time, sample I2 .....	234
C.12 Vertical strain versus time, sample I3 .....	235
C.13 Vertical strain rate versus time, left-sample T1, right-sample T2 .....	236
C.14 Vertical strain rate versus time, left-sample I2, right-sample I1 .....	237
C.15 Stress strain curves, sample T1-upper, sample T2-lower .....	238
C.16 Stress strain curve, sample T4 .....	239
C.17 Stress strain curve, sample I1 .....	240
C.18 Stress strain curve, sample I2 .....	241
D.1 Regression analysis of shear strain versus time at depths 67.06 m (upper) and 62.18 m (lower) for inclinometer S76-103 .....	25

## List of Plates

Plate	Page
2.1 Tar Island Dyke, aerial photographs .....	11
4.1 Triaxial cell .....	77
4.2 Sample with membrane .....	77
4.3 Cell pressure board .....	84
4.4 Volume change indicators and back pressure board .....	84
4.5 Inclined sample before trimming .....	93
4.6 Inclined sample after trimming .....	93
5.1 Scanning electron micrographs .....	106
C.1 Sample T1-upper, sample T2-lower, after failure .....	242
C.2 Sample T4-upper, sample I1-lower, after failure .....	243
C.3 Sample I2-upper, sample I3-lower, after failure .....	244

## 1. Introduction

### 1.1 General

Surface mining of the vast reserves of the Athabasca oilsands deposit began in 1967 on a large scale when the Suncor (then G.C.O.S. - Great Canadian Oil Sands) oilsands plant began production. In 1978 a second plant, Syncrude, began production and others are planned for construction in the 1980's. The location of the Athabasca oilsands deposit and the forementioned plants are shown on Figure 1.1.

Extraction of the bitumen from the sand by the Clark hot water process creates large volumes of tailings consisting of sand, silt, clay, water and small quantities of bitumen. For an oilsands plant producing 100,000 barrels of oil per day approximately 150,000 cubic meters of tailings are produced daily.

The disposal of these tailings creates the need for large capacity tailings ponds. Tailings cannot be disposed of in the open pit mine during the first years of production so a separate tailings structure has traditionally been built close to the plant site. The tailings structures at the Suncor and Syncrude plants have been constructed according to the upstream method (see Mittal and Morgenstern, 1977). Compacted tailings sand comprises the supporting shell and the remainder of the tailings forms the beach and pond of the tailings disposal structure.



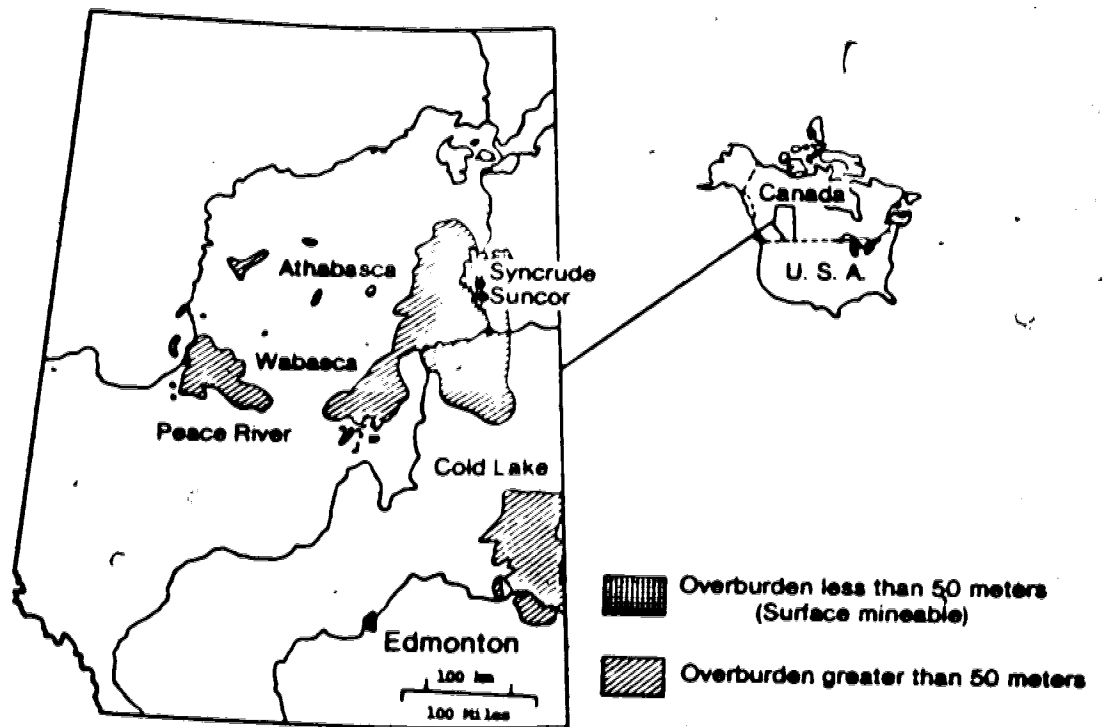


Figure 1.1 Location of major oilsands deposits in Canada

The tailings dykes at the Suncor and Syncrude plants are raised in stages usually with a freeboard of one year in tailings output. The stage construction of these structures allows the performance of the supporting shells to be monitored with instrumentation. Design can be optimized through rational interpretation of the structure's performance. Such a policy of performance monitoring has been pursued at Suncor's Tar Island tailings dyke and provided the impetus for this thesis.

In 1975 at the request of a Design Review Panel, convened by Alberta Environment to review the feasibility of the continued raising of Tar Island Dyke, several inclinometers were installed to monitor the lateral movements of the clay foundation. The time dependent lateral movements displayed by these inclinometers are the focus of this thesis. As the inclinometer readings were accompanied by a plethora of information on foundation geology, geotechnical properties, pore pressures and construction history this case history represented a unique opportunity for the investigation of time-dependent lateral displacements beneath embankments.

### 1.2 Lateral Displacements Beneath Embankments

It is of value to briefly review the possible stress paths in soft clay foundations in order to cast the lateral deformations beneath Tar Island Dyke in a conceptual

4

framework. The prediction and analysis of lateral displacements in soft foundations beneath embankments has been afforded much less attention in the literature than vertical displacements. Perhaps this is because lateral displacements are much harder to predict and recorded less often than vertical displacements. Poulos (1972) suggests a number of reasons for their poor prediction. Recently Tavenas *et.al* (1979) and, earlier, Rutledge and Gould (1973) documented numerous case histories concerning lateral displacements beneath embankments.

Tavenas *et.al* (1979) presented some simple empirical methods for predicting lateral displacements of normally consolidated clay foundations. Figure 1.2 is taken from their paper and shows possible stress paths in clay foundations during construction of embankments. It is of value to follow the stress paths shown on Figure 1.2 with a view to understanding the mechanisms causing lateral deformations.

From O' to P' the clay consolidates and the stresses move towards the limit state or yield surface. Lateral deformations in this region of overconsolidation are usually rapid because of high values of  $C_v$ . When the stress path intercepts the yield surface all deformations become undrained. The stress path will follow the yield surface to failure as shown by Tavenas *et.al* (*op.cit.*) unless construction is halted.

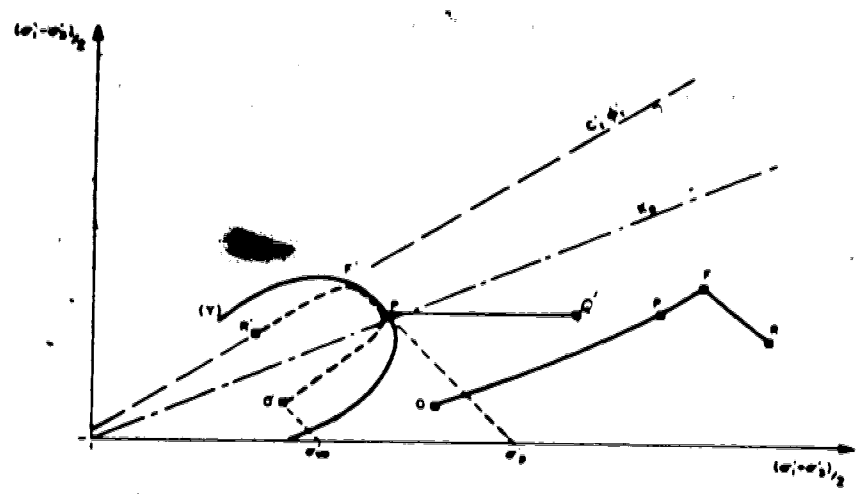


Figure 1.2 Total and effective stress paths under an embankment during construction (after Tavenas *et.al*, 1979)

The writer has added stress path P'-Q' to Figure 1.2. The foundation clay will follow this stress path if it is allowed to consolidate before reaching failure. It should be noted that creep movements can occur along any of the previously mentioned stress paths. The importance of creep to lateral movements depends upon the geometry of the embankment and foundation, the creep susceptibility of the clay and the construction sequence of the embankment.

Piezometers in the foundation clay of Tar Island Dyke are recording either dissipation of excess pore pressures with time or steady state pore pressure conditions. This indicates that the stress path for the foundation clay is on a line similar to P'-Q' in Figure 1.2. It therefore follows that the lateral deformations are a result of consolidation, creep or some combination of both.

### 1.3 Objective and Scope

The objective of this thesis is the understanding of the time dependent lateral displacements beneath Tar Island Dyke.

Chapter 2 presents the construction history, site conditions and selected instrumentation readings for the clay foundation. Chapter 3 is a review of the available literature on the creep behaviour of soils. The laboratory program to investigate the creep behaviour of the foundation clay is detailed in Chapters 4 and 5.

Chapter 6 examines the characteristics of the lateral displacement versus depth and time curves from the inclinometers. Chapter 7 outlines the overall conclusions of the investigation and presents recommendations for future research.

## 2. Tar Island Dyke - Site Conditions and Instrumentation

### 2.1 Introduction

The purpose of this chapter is to present a brief summary of the construction history of Tar Island Dyke and selected data concerning foundation conditions and instrumentation. Most of the material regarding construction history is taken from Mittal and Hardy (1977) and the Design Review Panel (1977). The information regarding foundation conditions and instrumentation has been provided by the designers of Tar Island Dyke, Hardy Associates Ltd (1978). The field program to secure soil samples for laboratory testing is also recounted in this chapter.

### 2.2 Construction History

Tar Island Dyke was originally conceived as a low, 12 m high conventional earthfill dyke of waste overburden with sufficient volume to store tailings until exploited portions of the mine became available for disposal of tailings. Construction began on this low dyke in 1965 and continued intermittently until 1967 when it was apparent that tailings volumes were greater than anticipated and that the continued construction of a conventional earthfill dyke to store the tailings would be prohibitively expensive. It should be stated that during these early pioneering days even essential tailings dam design parameters such as the bulking

factor could, at best, only be estimated.

In November of 1967 application was made to the Energy Resources Conservation Board (ERCB) of Alberta to raise the dyke with hydraulically placed sand tailings instead of continuing with the conventional earthfill dyke. The application was approved and since 1968 the dyke has been built with hydraulically placed sand tailings according to the upstream method of construction. Aerial photographs of Tar Island Dyke at different stages of construction are shown in Plate 2.1. It is of benefit to briefly summarize the construction procedure for the dyke.

The dyke consists of a compacted downstream zone and an uncompacted beach zone which retain a pond as shown in Figure 2.1. The compacted zone is constructed by spigotting from a tailings pipeline into a cell which is enclosed by a peripheral berm, 1.5 m to 2.0 m high. A cell typically has dimensions of 30 m to 90 m by 300 m to 460 m. Attached to the spigot point on the tailings pipeline is a deflector spoon which has the effect of spraying the exiting tailings and thereby inhibits the formation of a stilling basin beneath the spigot point. Consequently, the tailings velocity in the cell is increased which prevents premature sedimentation of fines in the cell. Sand settles from suspension in the tailings stream in the cell and is subsequently distributed within the cell by a caterpillar tractor. The action of the tractor is sufficient to increase the relative density of the sand in the cell to above 75



Legend

Inclinometers Piezometers

- A S76-101\*
  - S76-1018\*
  - B S76-103
  - C S76-102\*
  - D S76-104
  - 1 P79-37
  - 2 Ap79-46
  - 3 AP75-14A,B
  - 4 AP75-19
  - 5 AP79-46
  - 6 AP79-47
  - 7 AP75-18
  - 8 P79-38
  - 9 AP76-20
  - 10 AP76-21
- \* Station 56+00

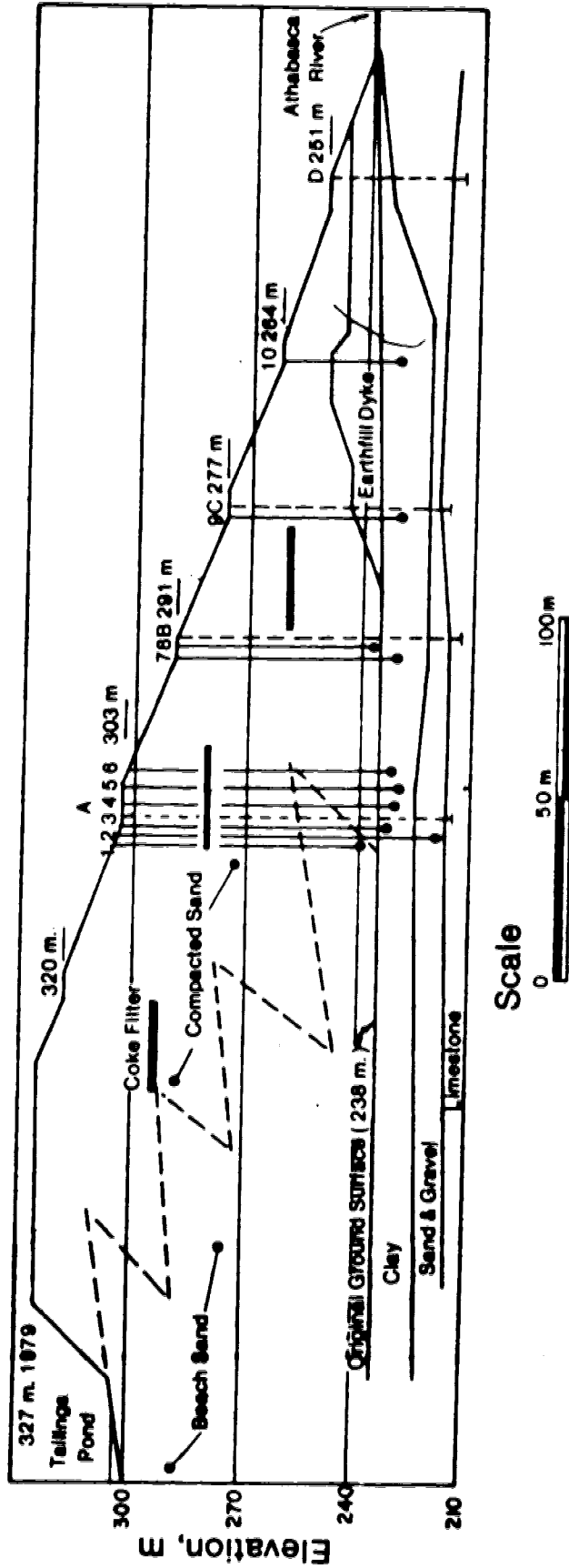


Figure 2.1 Tar Island Dyke, section at Station 65+00



August 31, 1967  
Scale 1:31,680



September 27, 1976  
Scale 1:31,680



September 15, 1950  
Scale 1:40,000

Plate 2.1 Tar Island Dyke,  
aerial photographs

percent. The tailings stream with sand and fines in suspension exits from one corner of the cell through a spillway box. The suspended sand and fines sediment from the tailings stream and form the beach which has an average slope of approximately 8 percent to the center of the pond. A layer of sludge, composed of fines and oily water, overlies the beach sand in the tailings pond. Sufficient storage capacity is created each year by constructing the compacted section of the dyke for only part of the year. During the rest of the year tailings are over-boarded directly into the pond.

The forementioned method of construction has been very successful with the exception of a few minor downstream liquefaction failures of the compacted zone in 1972, 1973 and 1974. These failures have since been avoided with local improvements in construction procedure. The stability of the Tar Island Dyke is discussed in detail in the Design Review Panel (1977) report and will not be discussed in this thesis.

The downstream face of the dyke has an overall slope of three horizontal to one vertical. There are berms for access at approximately 13 m vertical intervals. Seepage through the dyke is controlled by blanket drains composed of plant coke. All seepage collected in the drains is now returned to the pond. In 1979 the dyke had reached a height of 89 m and ultimately it is planned to raise it to 97.5m.

## 2.3 Foundation Characteristics

### 2.3.1 Geology

Tar Island Dyke rests on the active floodplain of the Athabasca River. The abutments of the dyke are the Athabasca River valley walls which are composed of Clearwater Formation shale and McMurray Formation oilsand. The common stratigraphic sequence in the general area consists of Recent deposits overlying Pleistocene glacial deposits which rest unconformably on the Cretaceous Clearwater and McMurray Formations which, in turn, unconformably overlie a Devonian limestone. The meandering incised Athabasca River has completely eroded all Pleistocene and Cretaceous sediments in the site specific area. The foundation stratigraphy consists of muskeg overlying a Recent deposit of silt and clay overlying sand which, in turn, rests on the Devonian limestone. Cobbly gravel is usual just above the sand/limestone contact. The clay deposit, which will occasionally be referred to as Tar Island clay, should not be confused with the basal clay shales of the McMurray Formation (see Dusseault and Scafe, 1979).

The original foundation investigations for the dyke were undertaken in 1964 and 1965. Since then there have been numerous other investigations (see summary in Design Review Panel, 1977). An isopach map of the silt and clay deposit based on the 1964 and 1965 borehole logs is given in Figure 2.2. The thicknesses of silt and clay encountered in

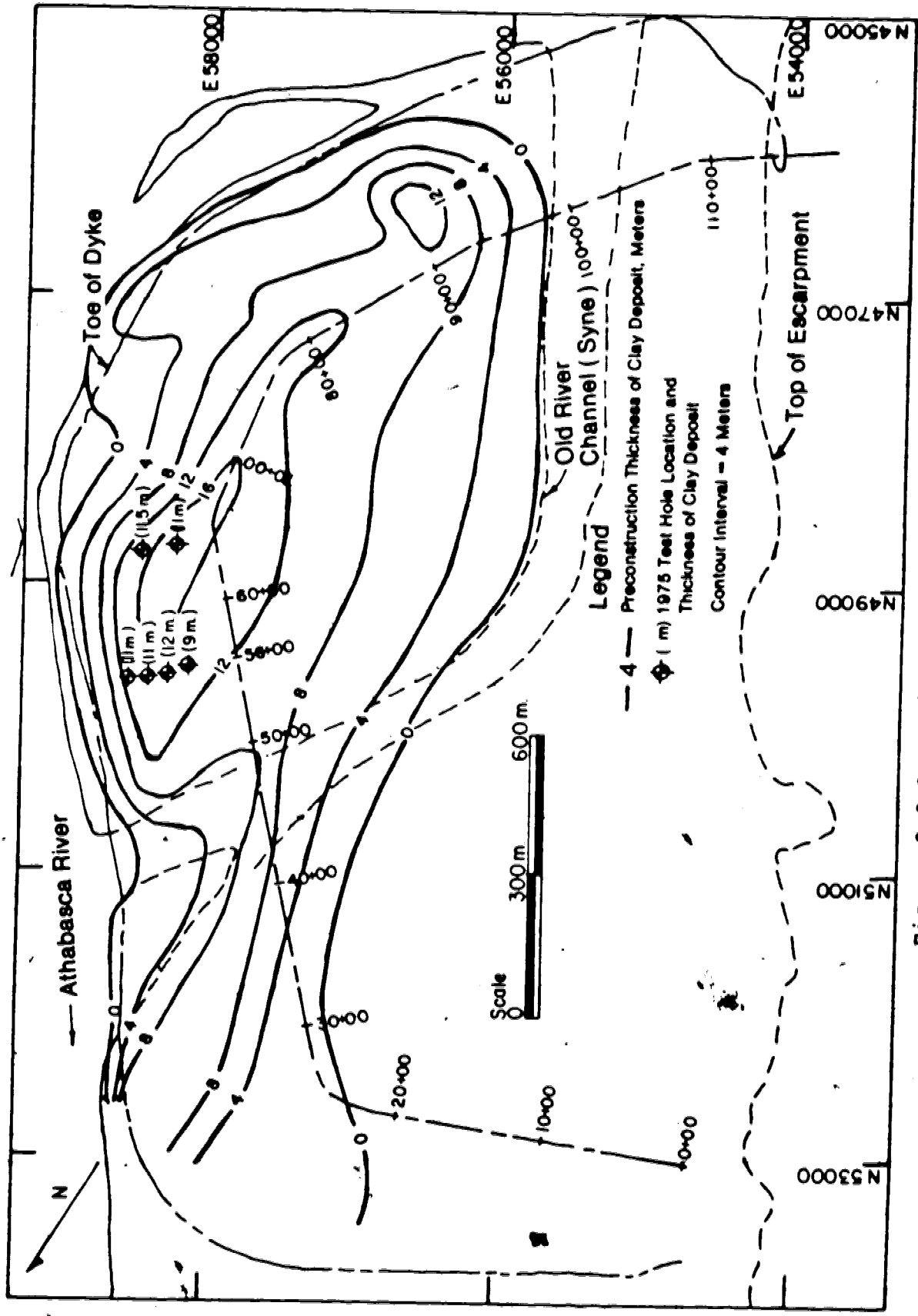


Figure 2.2 Isopach map of silt and clay deposit

selected boreholes drilled in 1975 are also shown on the isopach map.

The silt and clay deposit originated by sedimentation in an abandoned meander of the Athabasca River. The basal sands represent an Athabasca River bed load sediment which was deposited prior to complete cutoff of the meander. The major source of sediment to the meander was undoubtedly suspended silt and clay from overbank flows when the Athabasca was in flood. This genesis implies that the deposit should be coarser at its margins. There is also evidence of essentially still water deposition in the form of numerous calcium carbonate shells throughout the deposit.

### 2.3.2 Geotechnical Properties of Silt and Clay Deposit

The deposit consists of interbedded silt and clay with occasional sand lenses. Silt and sand predominate towards the margins of the deposit: From 34 grain size analyses on 1964 and 1965 samples the deposit averages 20 percent sand, 63 percent silt and 17 percent clay. The deposit also contains varying amounts of coal fragments, calcium carbonate shell material and organic material.

Before imposition of the dyke the deposit was medium stiff with undrained strengths ranging from 45 kPa to 90 kPa. The undrained strength over effective stress ratio ( $C_u/p'$ ) was 0.45. Of course, the undrained strength has increased with time as the deposit has consolidated under the weight of the dyke.

The liquid limit of the deposit varies from 24 percent to 65 percent and the plasticity index varies from 4 percent to 37 percent. The Atterberg limit test results from the early investigations are presented in Figure 2.3. The plasticity is greatest where the clay is thickest. The compression index,  $C_c$ , from the results of 16 oedometer tests averages 0.28. The results of effective shear strength tests performed by Hardy Associates Ltd. (1978) are presented in Chapter 5.

#### 2.4 Field Sampling Program

A sampling program was undertaken in the fall of 1979 to obtain samples of the foundation clay. The program was coordinated with the annual installation of instrumentation by the dyke designers, Hardy Associates (1978) Ltd., in the critical section of the dyke between Stations 56+00 and 65+00. A Mayhew 1000 wet rotary rig mounted on a Nodwell tracked vehicle was used for all sampling.

The main requirements for the samples were that they be representative of the clay in the critical section and, furthermore, that they be as undisturbed as practicable. To this end, it was attempted initially to obtain samples from beneath the 303 m berm using 10.2 cm- $\phi$  Shelby tubes. Unfortunately, continual sloughing of the hole within the tailings sand precluded sampling at the chosen location on the 303 m berm. The instrumentation program dictated that

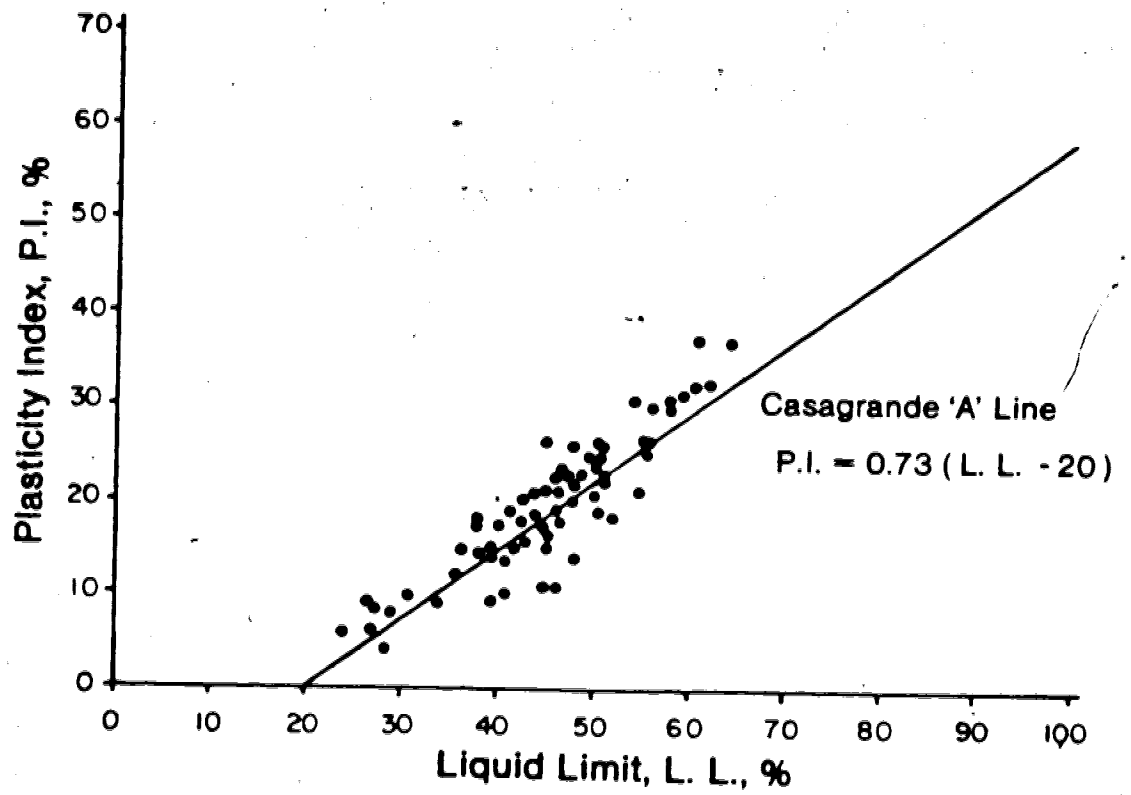


Figure 2.3 Atterberg limit test results



the rig be moved to the 291 m berm so samples were eventually obtained there. The inside diameter of the shelby tube sampler had to be decreased from 10.2 to 7.3 cm as the rig did not have sufficient capacity to pull or drive the larger shelby tubes.

The test hole log, S79-109, at which the samples were obtained is included in Appendix A. The location of the test hole is shown on Figure 2.4. The description of the samples is given in Chapter 5.

## 2.5 Foundation Instrumentation

### 2.5.1 General

Tar Island Dyke is heavily instrumented with piezometers to monitor the seepage regime in the tailings sand and in the foundation. Foundation piezometers are concentrated at Stations 56+00 and 65+00 where the clay deposit is thickest. Numerous inclinometers to monitor lateral deformation of the clay deposit are also located at these two stations. Vertical deformation of the clay deposit is not monitored directly but is routinely estimated from water content change and thickness change as determined by aperiodic drilling programs.

Because of the abundance of instrumentation data, only the readings from selected instruments will be reported here. Figure 2.4 shows the locations of selected

instrumentation in plan while Figure 2.1 presents the same instrumentation in section.

### 2.5.2 Foundation Piezometers

The readings from the foundation piezometers at Station 65+00 from the 303 m and the 291 m berm are illustrated in Figure 2.5. The readings from the 277 m and 264 m berms are shown in Figure 2.6. On every pore pressure plot a 'steady state' line is shown. This line represents the estimated pore pressure regime in the clay layer at the end of consolidation. The pore pressure at the base of the clay layer is equal to that in the basal sand which is in direct communication with the Athabasca River. The pore pressure at the top of the clay is governed by the seepage regime in the tailings sand and has been determined from piezometer readings or estimated.

It can be seen from Figure 2.5 that the clay deposit beneath the 303 m berm has excess pore pressures and is consolidating. Recently piezometers have been installed upstream of the 303 m berm and these instruments indicate that the clay deposit there has excess pore pressures and is consolidating. From Figures 2.6 and 2.7 it can be seen that the clay deposit from the 291 m berm downstream is essentially fully consolidated. It follows that stresses on the foundation caused by recent dyke construction are not significant enough to induce pore pressures in the foundation clay downstream of the 291 m berm.

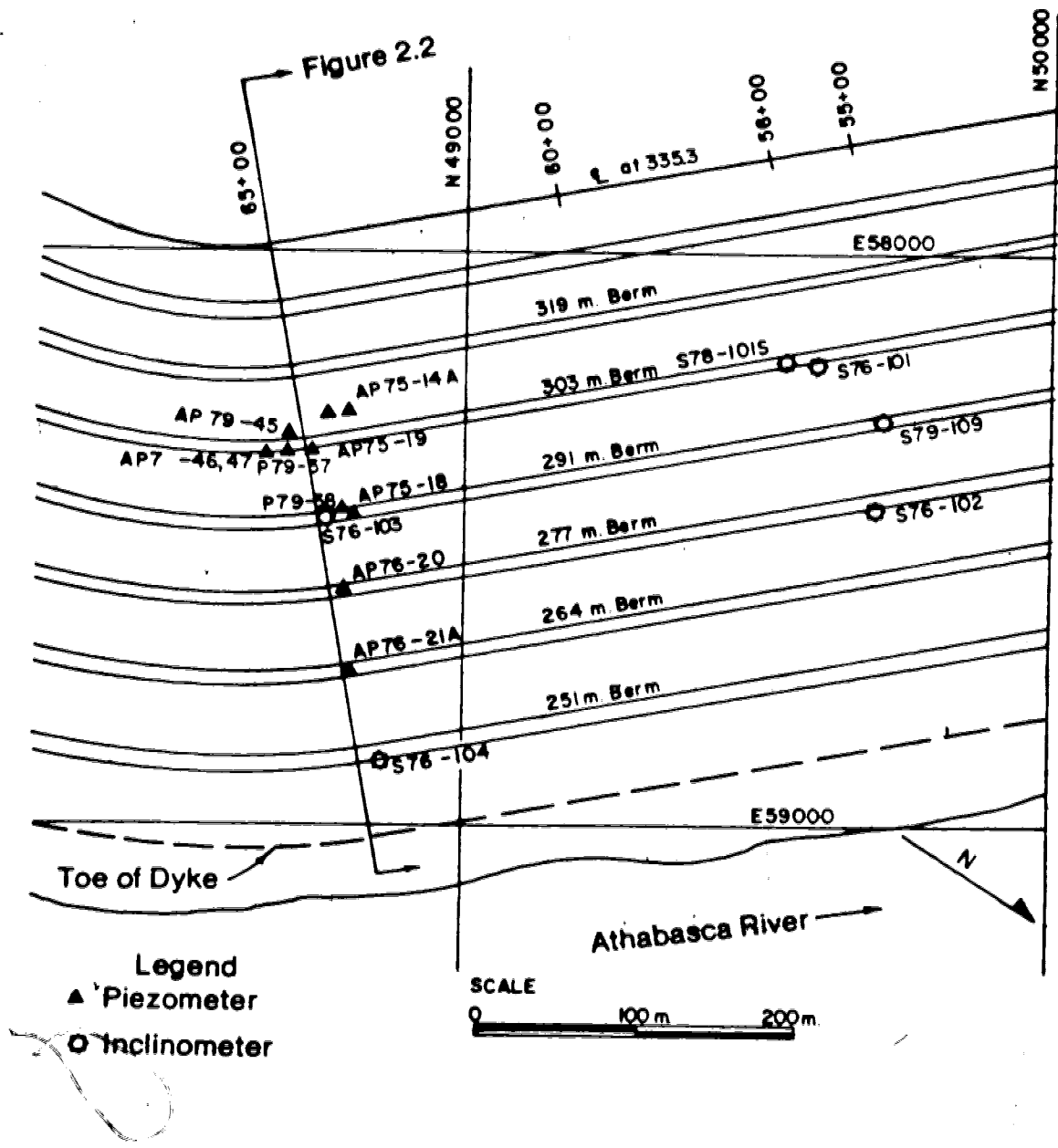
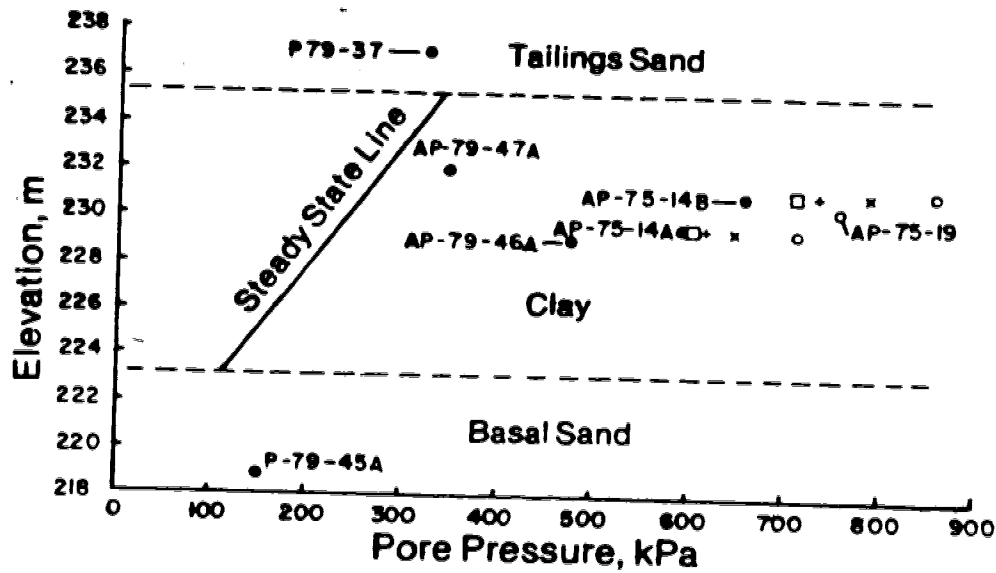


Figure 2.4 Tar Island Dyke, location of instrumentation



**Legend**

- December, 1975
- × December, 1976
- + December, 1977
- December, 1978
- April, 1980
- AP - Pneumatic
- P - Standpipe

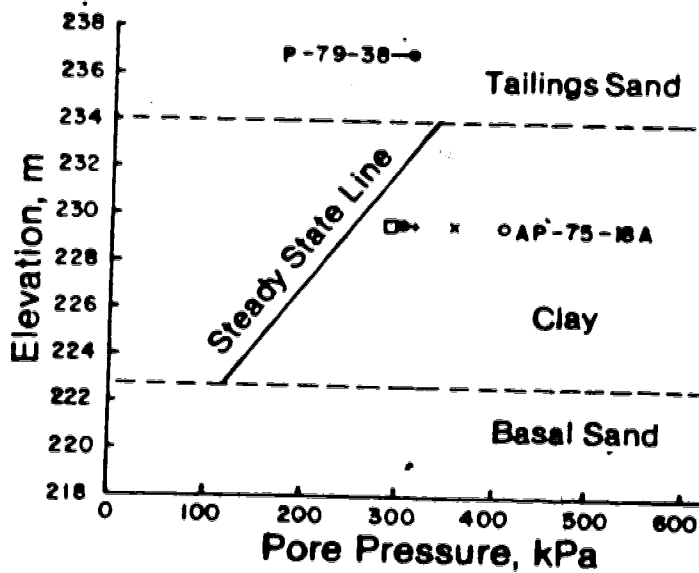
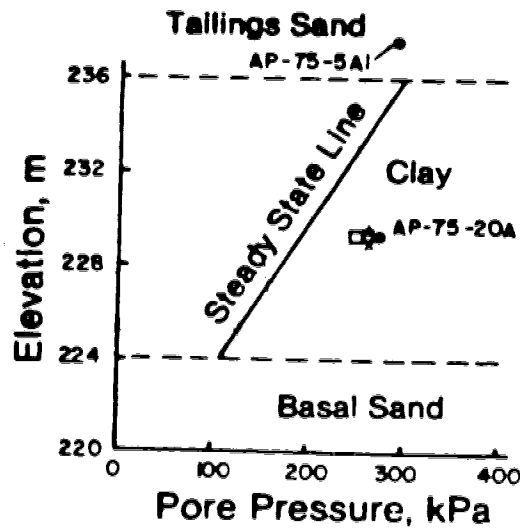


Figure 2.5 Summary of foundation pore pressures, upper-303 m berm and lower-291 m berm



**Legend**

- December, 1975
  - × December, 1976
  - + December, 1977
  - December, 1978
  - April, 1980
- AP - Pneumatic  
P - Standpipe

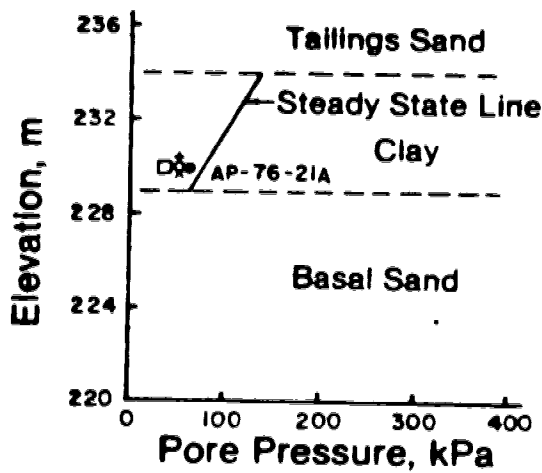


Figure 2.6 Summary of foundation pore pressures, upper-277 m berm and lower-264 m berm

### 2.5.3 Inclinerometers

A number of inclinometers have been installed in the dyke since 1976 to monitor lateral movements of the foundation. The Sinco Digitilt inclinometer has been used for all slope indicator installations at Tar Island Dyke (see Savigny, 1980 for description of inclinometer characteristics). The readings from five inclinometers, numbered S76-101, S78-101s, S76-102, S76-103 and S76-104, have been selected for review. Their plan location is shown on Figure 2.4 while their position in section is shown on Figure 2.1.

The bases of all inclinometers are founded in the limestone to provide a fixed reference point for calculation of lateral movements. Inclinometer readings covering the period September, 1976 to May, 1980 were made available to the writer by Hardy Associates (1978) Ltd. on magnetic tape. Hardy Associates (1978) Ltd. also made their inclinometer data reduction computer program available. Several modifications were made to the program and it is of value to briefly review the important data reduction steps.

As a first step, the average of the A component and the B component readings were multiplied by an instrument constant to give the horizontal displacement in each of the A and B directions. The vector sum of the A and B displacements was then computed to give the maximum horizontal displacement, irrespective of orientation, at each depth. The tacit assumption was made in this

calculation step that the maximum displacement is in the normal section to the longitudinal axis of the dyke. The displacements were then cumulated from the fixed base reference point in the standard manner. The program was modified to incorporate computer graphics and a plot of cumulative horizontal displacement with depth for inclinometer S76-101 is illustrated in Figure 2.7.

The shear strain was calculated in a similar manner and is given by:

$$\delta = \text{Arcsin}(A \cdot C) \cdot 100\% \quad 2.1$$

where  $\delta$  = shear strain  
 A = vector sum of average A and average B component readings  
 C = instrument constant

A plot of shear strain versus depth for inclinometer S76-101 is given in Figure 2.7. Similar plots to those presented for inclinometer S76-101 are included in Appendix A for the other inclinometers enumerated previously.

## 2.6 Nature of Foundation Movements

The inclinometer plots illustrate that the clay deposit is experiencing time dependent shear strain. The basal sand is also exhibiting shear strain with time. However, the tailings sand above the clay deposit does not show any shear

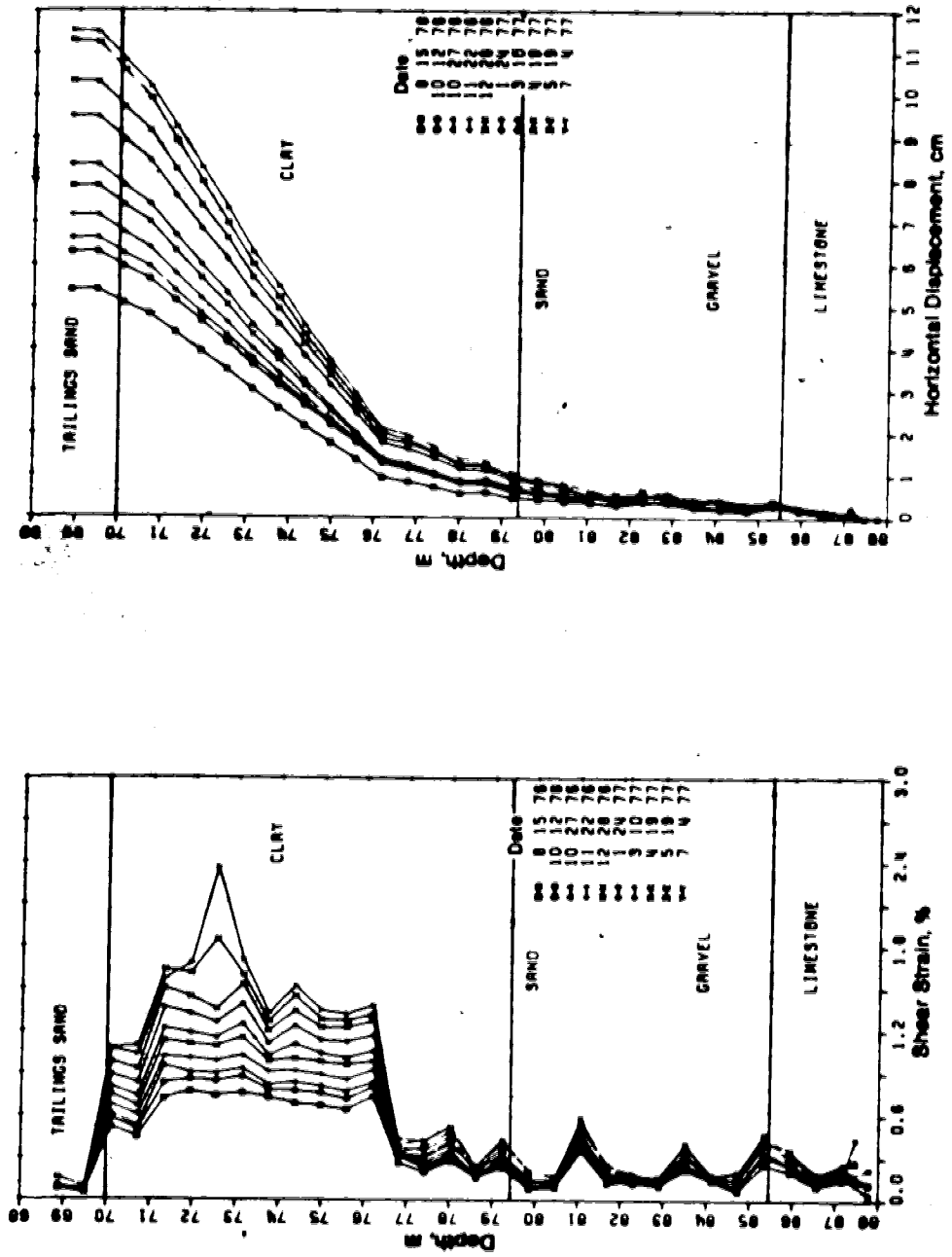


Figure 2.7 Inclinometer S76-101,calibrated January 26, 1976



straining. The dyke appears to be moving essentially as a rigid body on its foundation.

The time dependence of the shear strain in the foundation materials may either be a consequence of creep or of lateral consolidation. It is considered that creep is the dominant mechanism causing the time dependent shear strains since:

1. Shear straining is occurring in portions of the foundation where any excess pore pressures have already dissipated. This is apparent in the top and bottom portions of the clay deposit and in the full thickness of the clay deposit downstream of the 291 m berm.
2. A mechanism of lateral consolidation necessitates compression in the horizontal direction. However lateral strains are in the order of 0.04 percent which is insignificant compared to the shear strains of 1 percent to 3 percent over the same time period.

As a consequence of these observations the remainder of the thesis is directed towards defining the creep behaviour of the clay deposit.

### 3. A Review of the Creep Behaviour of Soils

#### 3.1 Introduction

The creep deformations of soils are an important consideration in a wide variety of geotechnical problems. These problems range from the time dependent settlements of foundations, after all excess pore pressures have dissipated, to the time dependent deformation of soft embankment foundations which may eventually fail in creep rupture before any excess pore pressures have dissipated. The estimation and importance of creep deformation in design has been the subject of considerable research, especially over the last twenty years. Most research has been directed towards understanding the creep behaviour of soils in the laboratory. Regretably, there are few case histories of field behaviour, with the exception of long term settlement of foundations, which link a rational design approach to actual field behaviour. Of necessity then, this review of creep behaviour is restricted to a review of laboratory investigations.

Creep is defined here as time dependent deformation under a sustained change in stresses, exclusive of hydrodynamic effects. Creep in soils depends upon a host of factors which include time, temperature, soil type, soil structure, stress history, stress state and drainage conditions. Figure 3.1 illustrates the wide variation of

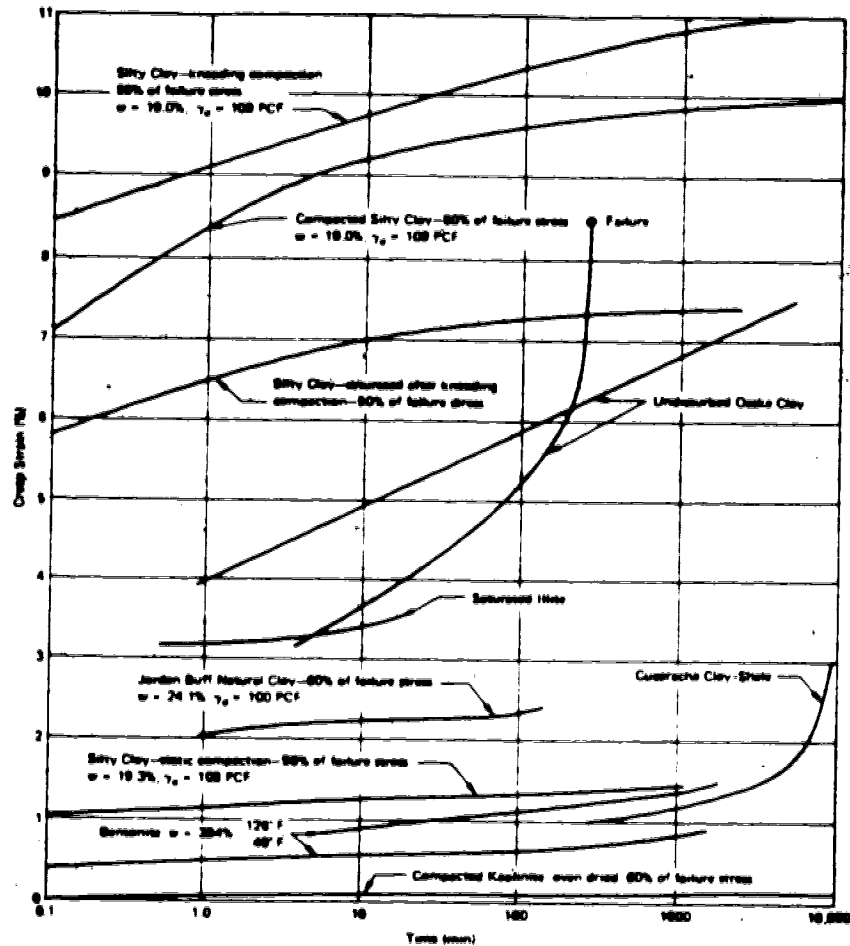


Figure 3.1 Variation in creep behaviour of soils (after Mitchell and Campanella, 1963)

creep response among different soil types.

There are two approaches to the investigation of the creep behaviour of soils according to Ladanyi (1972). The first is a fundamental approach, which he termed the micromechanistic approach, in which creep behaviour is related to events occurring at the particle level. The second is a phenomenological approach, which he termed the microanalytical approach, in which creep behaviour is related to macroscopic experimental findings. A brief outline of the principal work in soil mechanics in relation to the fundamental approach is presented in section 3.2. This outline has been included because it adds to our understanding of soil behaviour, but kept brief because it has not yet been successful in providing constitutive relationships that can be used in practice.

The phenomenological approach is presented in section 3.3 in more detail than the fundamental approach as constitutive relationships, albeit empirical, have evolved from this approach which are used in practice. The creep rupture strength of soils as determined from laboratory creep tests is discussed in Section 3.4.

### **3.2 The Fundamental Approach**

### 3.2.1 General

There have been a number of researchers who have developed theories to explain and predict the creep behaviour of soils on a particle interaction level. Most of these theories can be grouped into three categories. The first category is that based upon the viscosity of the adsorbed water layers around clay particles which was first advocated by Terzaghi (1941) and Taylor (1942). The second is rate process theory which was popularized in soil mechanics in the 1960's by a number of researchers including Christensen and Wu (1964) and Mitchell *et.al* (1968). The third category is that originated by de Jong (1968) which is based upon considerations of a cavity channel network model for the soil pores. A brief review of the main elements of each of these theories will now be given.

### 3.2.2 Considerations Based on Viscosity of Adsorbed Water

Clay particles are surrounded by a layer of adsorbed water that has a bonding and structure which is different than the pore water (see Mitchell, 1976). The presence of these adsorbed water layers was known in the early 1940's and attempts were made to explain secondary consolidation in terms of their viscosity. Taylor (1942) was one of the first researchers in soil mechanics to hypothesize that the viscosity of the adsorbed water layers were of substantially higher magnitude than that of the pore water and, furthermore, that the adsorbed water was responsible for the

viscous component in the effective stress-strain-time behaviour.

Terzaghi (1941) postulated that, after primary consolidation, the load carried by the soil was somehow distributed between grain to grain contacts and adsorbed water bonds. Secondary consolidation was thought to be the time dependent transfer of load from the adsorbed water to the grain to grain contacts. He also held that the viscosity of the adsorbed water bonds increased as the particles moved together and, therefore, the load transfer occurred at an ever decreasing rate.

Walker (1969a) used this hypothesis to explain the independence of volume creep rate on stress level. He contended that the increase in the structural viscosity of the adsorbed water bonds was counteracted exactly by the increased shear stress.

One method of validating the influence of the viscosity of the adsorbed water bonds on secondary consolidation is to replace the adsorbed water and pore water in a soil by an inert liquid such as carbon tetrachloride or benzene. Both Leonards and Girault (1961) and Mesri (1973) have conducted such experiments and have found that the nature of the pore fluid has some influence on the rate of secondary consolidation. However, both authors agree that the presence of adsorbed water is not necessary in order for secondary consolidation to occur.

Barden (1965) summarized the work of Terzaghi and Taylor and contended that they are in agreement on the following points:

1. Primary and secondary consolidation are part of a single continuous process.
2. The seat of secondary or creep effects is gradual readjustment or remoulding of the soil structure initiated during primary consolidation.
3. The rate at which the secondary compression proceeds is strongly influenced by the viscous effects of the adsorbed water layer.

The hypothesized influence of the viscosity of the adsorbed water bonds lends some fundamental basis to the development of rheological models to predict secondary consolidation. A rheological model is some combination of springs, dashpots and sliders that has a mathematical analogy that fits observed soil behaviour. The dashpots represent the adsorbed water bonds. Because the viscosity hypothesis is tenuous rheological models must remain primarily phenomenological.

Numerous rheological models have been proposed for the stress-strain-time behaviour of soils. Barden (1965), de Jong (1968) and Mitchell (1976) summarize the majority of these models. The more important rheological models are those by Gibson and Lo (1961), Christensen and Wu (1964) and Komamura and Huang (1974). Gibson and Lo (*op.cit.*) developed a rheological model that accounts for both primary and

secondary consolidation. Taylor and Merchant (1940) were the first to include secondary compression in a consolidation theory but did not relate their theory to a rheological model. Christie (1964) demonstrated that the rheological model developed by Gibson and Lo (1961) is equivalent to the Taylor and Merchant (1940) theory.

Mitchell (1976) notes that most mathematical expressions from rheological models are complicated and none has yet been proposed which is as simple as the three parameter relationship presented later as Equation 3.2. Simple rheological models which would have potential use are not used because they incorrectly predict infinite settlement. Due to their complexity rheological models are not used extensively in creep modelling of soils and will not be discussed further.

### 3.2.3 Rate Process Theory

Rate process theory is based upon the proposition that atoms, molecules or particles (termed flow units) participating in a time dependent deformation process are constrained from movement relative to each other by virtue of energy barriers which separate adjacent energy positions. In order for a flow unit, a soil particle in this case, to move to a new equilibrium position it must acquire sufficient energy to surmount the imposed energy barrier. This energy is called the activation energy and it has some frequency of occurrence. A shear stress distorts the energy



barriers allowing flow units to move preferentially in the direction of distortion.

Rate process theory was first proposed by Eyring (1936) and became popular in the soil mechanics literature in the 1960's. Mitchell (1976) provides a compact overview of its significance to different aspects of soil mechanics. Mitchell *et al* (1968) proposed the following equation derived from rate process theory to determine the creep strain rate:

$$\dot{\epsilon} = (2 X) (kT/h) \exp(-\Delta F/RT) \sinh(f\lambda/2kT) \quad 3.1$$

where  $X$  = a function of the number of flow units in the direction of deformation and the average component of displacement due to a single unit mounting the energy barrier

$k$  = Boltzmann's constant,  $1.38 \times 10^{-16}$  erg/ $^{\circ}$  K

$h$  = Planck's constant,  $6.624 \times 10^{-27}$  erg/sec

$T$  =  $^{\circ}$  K

$\Delta F$  = free energy of activation calories/mole

$R$  = universal gas constant, 1.98 cal/ $^{\circ}$ K-mole

$f$  = average shear force on each flow unit, dynes

$\lambda$  = separation distance between successive equilibrium positions

Several authors, including Murayama and Shibata (1964), Mitchell (1964), Christensen and Wu (1964), Wu *et. al* (1966) and Krizek *et. al* (1977), have shown how shear strength, consolidation and creep of soils can be related to rate process theory. Due to its complexity rate process theory has not been widely used in practice and remains primarily a research tool.

#### 3.2.4 A Model Based on a Cavity Channel Network

De Jong (1968) introduced a concept of primary and secondary consolidation that models the soil pores as cavities of differing compressibilities linked together by channels with differing permeabilities. During primary consolidation pore water drains from the accessible cavities and the ambient excess pore water pressure eventually goes to zero. However, in a certain number of cavities linked to the network by channels of low permeability, the excess pore pressure remains greater than zero. The slow drainage of water from these cavities gives rise to secondary consolidation.

De Jong (*op.cit.*) develops a constitutive relationship from this model in a rigorous stochastic manner and proves that the cavity channel model yields the same equations as a rheological model also developed in the same paper. Due to its complexity the model has only been employed by a few other researchers (see Holzer *et. al*, 1973).

### 3.3 The Phenomenological Approach

The phenomenological approach is the endeavor to produce empirical relationships that predict creep behaviour based solely on observed creep behaviour in the laboratory. Singh and Mitchell (1968) contend that an empirical creep relationship must satisfy the following general requirements:

1. It must be applicable to a reasonable range of creep stresses.
2. It must describe the behaviour of a range of soil types.
3. It must account for both linear and curved relationships between strain and the logarithm of time.
4. It must contain parameters that are easily determined.

The most widely accepted empirical relationship for soil is that by Singh and Mitchell (1968) which has the following form:

$$\dot{\epsilon} = Ae^{\alpha D} (1/t)^m \quad 3.2$$

- where  $\dot{\epsilon}$  = strain rate  
 $A$  = a constant, the strain rate at unit time and zero deviator stress  
 $\alpha$  = slope of the natural logarithm of strain rate versus deviator stress curves  
 $D$  = deviator stress  
 $t$  = time  
 $1$  = unit time  
 $m$  = slope of the natural logarithm of the

strain rate versus natural logarithm of  
time curves

The stress level term in Equation 3.2 can be replaced by:

$$\bar{\sigma} \bar{D} = \alpha D \quad 3.3$$

where  $\bar{\sigma} = \alpha D_{max}$

$\bar{D} = D/D_{max} = \text{stress level}$

$D_{max} = \text{deviator stress at failure}$

In order to determine the constants in Equation 3.2 it is necessary to perform at least two creep tests at the same consolidation stress but at different stress levels. The data is then plotted as the natural logarithm of strain rate versus the natural logarithm of time for each stress level to determine  $m$  as shown in Figure 3.2. The same data is then plotted in a natural logarithm of strain rate versus arithmetic deviator stress plot to determine  $\alpha$  and  $A$  as shown in Figure 3.3.

Mitchell (1976) presented a detailed derivation of Equation 3.2. Numerous investigations of the creep behaviour of natural materials since 1968 have demonstrated that Equation 3.2 applies to a wide range of soils both in undrained and drained conditions and, also, to some types of rock (see da Fontoura, 1979). Singh and Mitchell (1968) have shown that Equation 3.2 can be derived, in part, from rate process theory. A most important feature of Equation 3.2 is

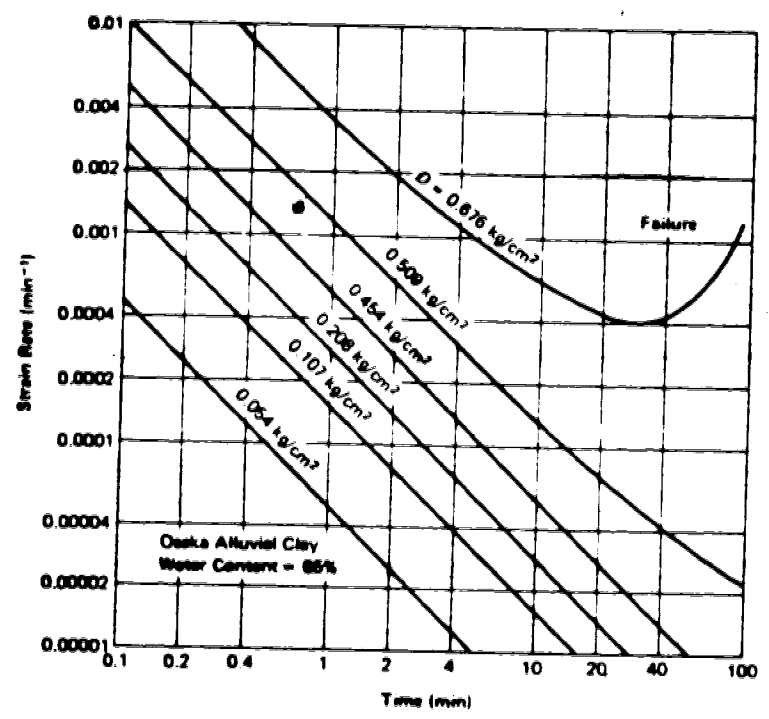


Figure 3.2 Strain rate versus time during undrained creep of alluvial Osaka clay (after Murayama and Shibata, 1958)

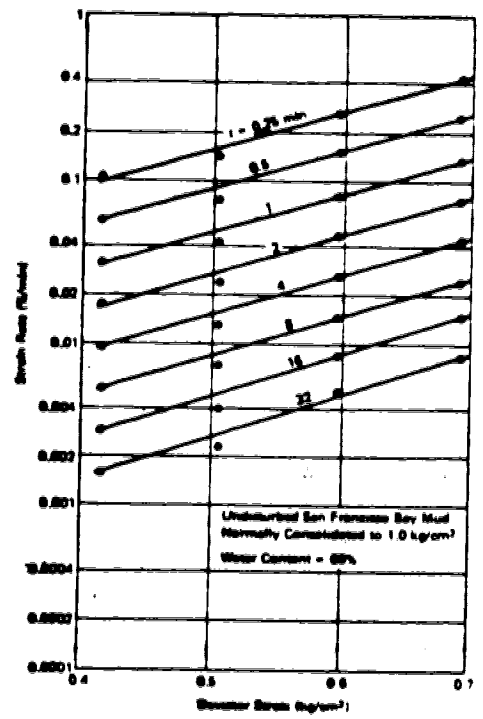


Figure 3.3 Variation of strain rate with deviator stress for undrained creep of San Francisco Bay Mud (after Mitchell, 1976)

that it predicts a continual decrease of strain rate with time. In other words, steady state creep does not exist for the materials described by this equation. Equation 3.2 only applies for stresses below the long term strength.

Equation 3.2 was derived on the basis of laboratory data taken primarily from the triaxial test. In an attempt to develop creep relationships that adequately describe soil in a general state of stress, Kavazanjian and Mitchell (1977) found it convenient to decompose the general creep strain and stress tensor into its volumetric and deviatoric components as follows:

$$\sigma = \sigma_v + \sigma_D \quad 3.4$$

$$\epsilon = \epsilon_v + \epsilon_D \quad 3.5$$

where  $\sigma$  = general stress tensor  
 $\sigma_v$  = volumetric stress tensor  
 $\sigma_D$  = deviatoric stress tensor

and  $\epsilon$  = general strain tensor  
 $\epsilon_v$  = volumetric strain tensor  
 $\epsilon_D$  = deviatoric strain tensor

The definition of the stress and strain tensors are as given in Fung (1965). They state that each strain tensor component is related to each stress tensor component by a pseudo

elastic formulation of the type:

$$\epsilon = 1/R \Delta \sigma_v + 1/G \Delta \sigma_d \quad 3.6$$

where  $R$  = volumetric tensor operator

$G$  = deviatoric tensor operator

The characteristics of the tensor operators have been discussed in detail by Kavazanjian and Mitchell (*op.cit.*)

It is convenient to review the creep deformation of soils in terms of the Kavazanjian and Mitchell (*op.cit.*) formulation and in terms of the drainage conditions. The volumetric and deviatoric components of the strain tensor for drained creep will be discussed first. This is followed by a discussion of undrained creep.

### 3.3.1 Drained Creep

Drained creep is time dependent deformation under sustained constant effective stress where the boundary conditions during testing allow volume change. Drained creep deformation has a volumetric and deviatoric component in all stress states in the laboratory with the exception of isotropic consolidation in a triaxial test where the deviatoric component is zero.

#### 3.3.1.1 Volumetric Component

The volumetric component of drained creep is traditionally referred to in the literature as secondary

compression or secondary consolidation. It is referred to as 'secondary' because it has been considered as deformation occurring after primary consolidation. This notion is, of course, incorrect (see Gibson and Lo, 1961) as creep deformations must also occur during the dissipation of excess pore pressures. Both terms will be used interchangeably in this thesis. The writer prefers the term drained creep.

A substantial amount of research has been conducted in the laboratory on the factors influencing secondary compression. Most researchers have chosen to use the oedometer for the investigation of secondary compression because of its simplicity and because the measurement of volume change in other testing devices over long periods of time presents difficulties. Since oedometer testing is so common it is of value to review briefly the boundary conditions of this testing device.

$$\epsilon_2 = \epsilon_3 = 0$$

3.7

It follows that:

$$\epsilon = \epsilon_1 = \gamma_{max}$$

3.

where  $\epsilon_{1,2,3}$  = principal strains

$\epsilon$  = volumetric strain

$\gamma_{max}$  = maximum engineering shear strain

The effective stresses are related by:



$$\sigma_1 = \sigma_3 = K. \sigma_2$$

3.9

where  $\sigma_1, \sigma_2, \sigma_3$  = principal stresses

K. = coefficient of earth pressure at rest

Other testing equipment such as the triaxial test, the plane strain test and the simple shear plane strain test have also been used to investigate the volumetric component of the drained creep tensor. It is customary in all tests to determine the amount of secondary compression by plotting the void ratio,  $e$ , against the logarithm of time. The slope of the curve, shown in Figure 5.1, after the dissipation of excess pore pressures is referred to as the secondary compression index (after Mesri and Godlewski, 1977) and is defined by:

$$a = e / \log t \quad 3.10$$

where  $a$  = secondary compression index

$e$  = void ratio

$t$  = time

The coefficient of secondary consolidation,  $C_{\alpha}$  is given by:

$$C_{\alpha} = a / (1+e) \quad 3.11$$

The secondary compression index may be a function of time, stress history, consolidation stress, load increment ratio, shear stress level, stress state, stress path, duration of previous stress and temperature. The influence

of all these factors will now be discussed. Except where noted, the researchers mentioned in the following discussion have used the oedometer.

### Time

It is widely assumed, as first proposed by Buisman (1936), that  $\alpha$  is independent of time. That is, the slope of the void ratio versus logarithm of time curve is constant. Bjerrum (1967), in his Rankine lecture, assumed that  $C_\alpha$  was independent of time, as did Walker (1969a) and Kavazanjian and Mitchell (1980). However, Lo (1961) examined the behaviour of both remoulded and undisturbed clays and found that  $C_\alpha$  decreased, remained constant or increased with time depending on the soil type.

Lo (*op.cit.*) also found that secondary compression went to zero with time, usually within three weeks. Conversely other researchers, notably Bishop and Lovenbury (1969), found that secondary compression from triaxial and oedometer tests on undisturbed clay continued for over three years.

It is of value to further elaborate on the dependence of  $C_\alpha$  on time. Equation 3.11 can also be written as:

$$\dot{\epsilon} = (C_\alpha)(1/t) \quad 3.12$$

where  $\dot{\epsilon}$  = volumetric strain rate

If the natural logarithm of volumetric strain rate is plotted versus the natural logarithm of time, as shown in

Figure 5.5 the curve can be expressed by a relationship of the type:

$$\dot{\epsilon} = A(1/t)^m \quad 3.13$$

The effect of consolidation shown in Figure 5.5 is neglected in the derivation of Equation 3.13. If Equations 3.12 and 3.13 are equated it is apparent that  $C_a$  is a constant, i.e. independent of time, only if the parameter,  $m$ , is equal to one. This has been previously recognized by Singh and Mitchell (1969), Barden and Poskitt (1969) and Walker (1969c) among others.

Although  $C_a$  may not be independent of time most researchers have found the parameter,  $m$ , in Equation 3.2 to be independent of time. As an example, Tavenas *et al* (1978) have plotted their volumetric creep data from triaxial tests on undisturbed St. Alban clay in the same form as Equation 3.2 and have found the parameter,  $m$ , to be independent of time. This suggests that  $m$  is a more fundamental parameter than  $C_a$ .

#### Consolidation Stress

There is some controversy in the literature concerning the dependence of  $C_a$  on consolidation stress. However, most researchers, including Mesri and Godlewski (1977) and Murayama and Shibata (1964), agree that  $C_a$  increases with increasing stress below the preconsolidation pressure,  $p_c$ , and reaches a maximum in the vicinity of  $p_c$ . It is above the

maximum that the controversy appears. Some researchers, including Murayama and Shibata (1964), Schiffman *et.al* (1964) for one of the soils they tested, Ladd and Preston (1965), Walker (1969a), Lo (1961) and Shen *et.al* (1973), contend that  $C_c$  is a constant above  $p_c$ . Others, including Wahls (1962), Schiffman *et.al* (1964) and Mesri and Godlewski (1977) maintain that  $C_c$  decreases with increasing stress above  $p_c$ . Figures 3.4 and 3.5 illustrate examples of the dependence of  $C_c$  on consolidation stress. It is of interest to note the Mesri and Godlewski (1977) only tested soils that displayed dependence of the compression index,  $C_c$ , on consolidation stress above  $p_c$ .

#### Load Increment Ratio

The load increment ratio is defined here as the net added load divided by the total previous load,  $\Delta p/p$ . Several researchers, including Mesri and Godlewski (1977), Leonards and Girault (1961) and Gibson and Lo (1961) have documented that the shape of the consolidation curve is dependent on the load increment ratio. This is illustrated in Figure 3.6, taken from Bjerrum (1967). However most researchers, including Wu *et.al* (1978), Bjerrum (1967), Barden (1969), Wahls (1962) and Mesri and Godlewski (1977), have concluded that  $C_c$  is independent of the load increment ratio.

#### Shear Stress Level

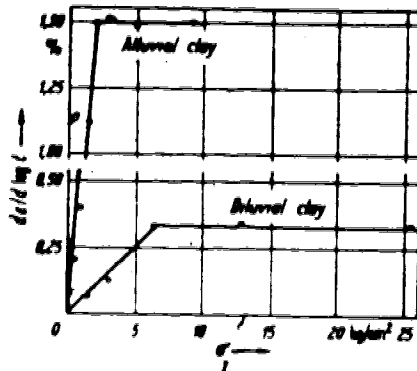


Figure 3.4 Relation between applied stress and rate of secondary compression in oedometer (after Murayama and Shibata, 1964)

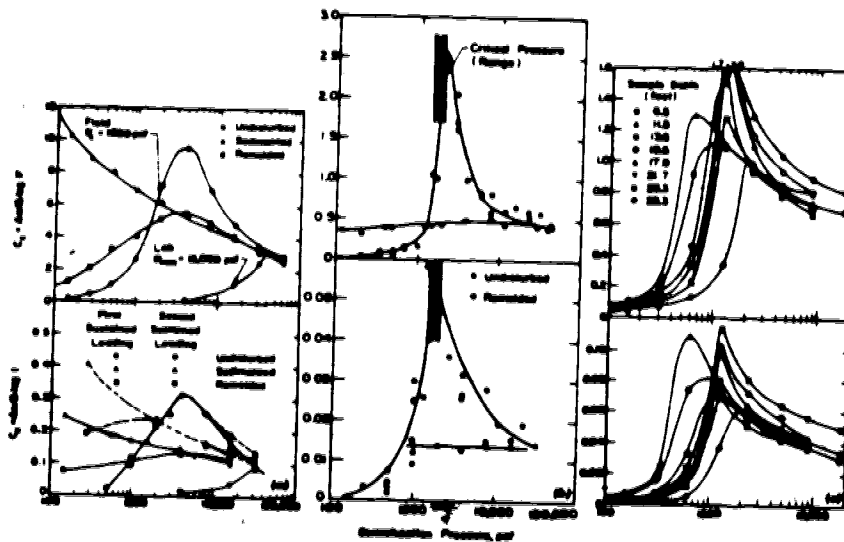


Figure 3.5 Relationship between  $C_a$  and  $C_c$  and consolidation pressure for (a) Mexico City clay (b) Leda clay (c) Undisturbed New Haven organic silt (after Mesri and Godlewski, 1977)

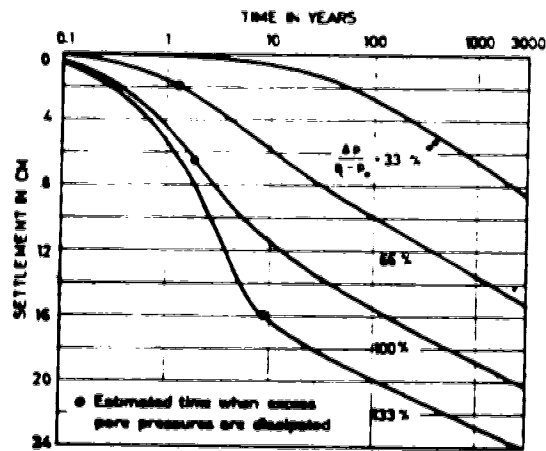


Figure 3.6 Effect of load increment ratio on secondary compression index (after Bjerrum, 1967)

The effect of shear stress level on the magnitude of  $C_\alpha$  has been investigated only sparingly. This is a consequence of most research being undertaken with the oedometer where the shear stress level is a constant. Murayama and Shibata (1961) found a shear stress level dependence of  $C_\alpha$  for undisturbed Osaka clay using the triaxial test. Walker (1969a) using the simple shear plane strain test and the triaxial test found the volumetric creep rate to be independent of shear stress level. His data is illustrated in Figure 3.7. Kavazanjian and Mitchell (1980) cited Walker (1969a) to justify their assumption that  $C_\alpha$  is independent of stress level. Yudhbir and Mathur (1977) found that the volumetric creep rate was independent of shear stress level up to a yield value where it decreased to zero.

Analysing their creep data according to Equation 3.2 Tavenas *et al* (1978) found a dependence of volumetric strain rate in the triaxial test on shear stress level and expressed it in the form:

$$\dot{\epsilon} = Bf(\sigma')(t./t)^m \quad 3.14$$

where B = constant

$f(\sigma')$  = stress function

They found, using different stress paths, that the stress function could be represented by the equations of lines of equal volumetric strain rate in stress space. They did not produce these equations for the stress function but did

suggest they would take the same form as the equation of the limit state surface (yield surface) for the clay. Figure 3.8 illustrates the shape of the stress function.

### Stress State

The effect of stress state on the magnitude of  $C_\alpha$  has been investigated only sparingly. Again, this is a consequence of most research on  $C_\alpha$  being conducted using only the oedometer. Walker (1969a) found a minimal effect of stress state on the value of  $C_\alpha$  between the triaxial and simple shear devices for tests on remoulded kaolinite. Schiffman *et.al* (1964) found little difference between  $C_\alpha$  determined from isotropic triaxial consolidation tests and oedometer tests. Bishop and Lovenbury (1969), from oedometer and triaxial tests, and Wu *et.al* (1978), from triaxial, plane strain and simple shear plane strain tests found little dependence of volumetric creep strain or strain rate on stress state. There appears to be a consensus that stress state has only a minimal effect on volumetric creep. Of course, this conclusion is only valid for soils which have isotropic creep properties.

### Stress Path

Tavenas *et.al* (1978) in a comprehensive series of triaxial tests using different stress paths found the parameter,  $m$ , in Equation 3.2 for the volumetric creep strain rate to be independent of stress path. Conversely,



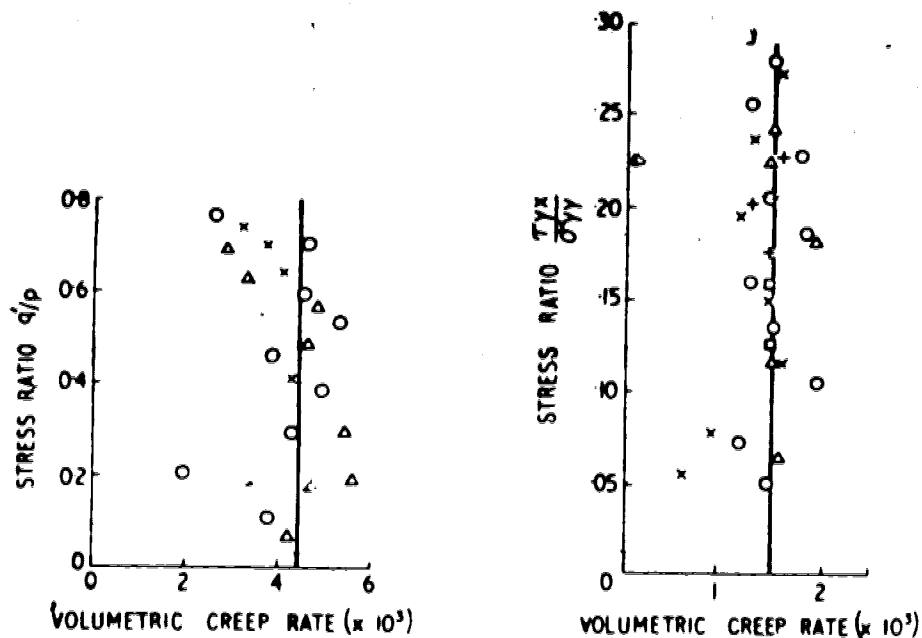


Figure 3.7 Effect of stress level on volumetric creep rate, left - triaxial tests, right - simple shear tests (after Walker, 1969b)

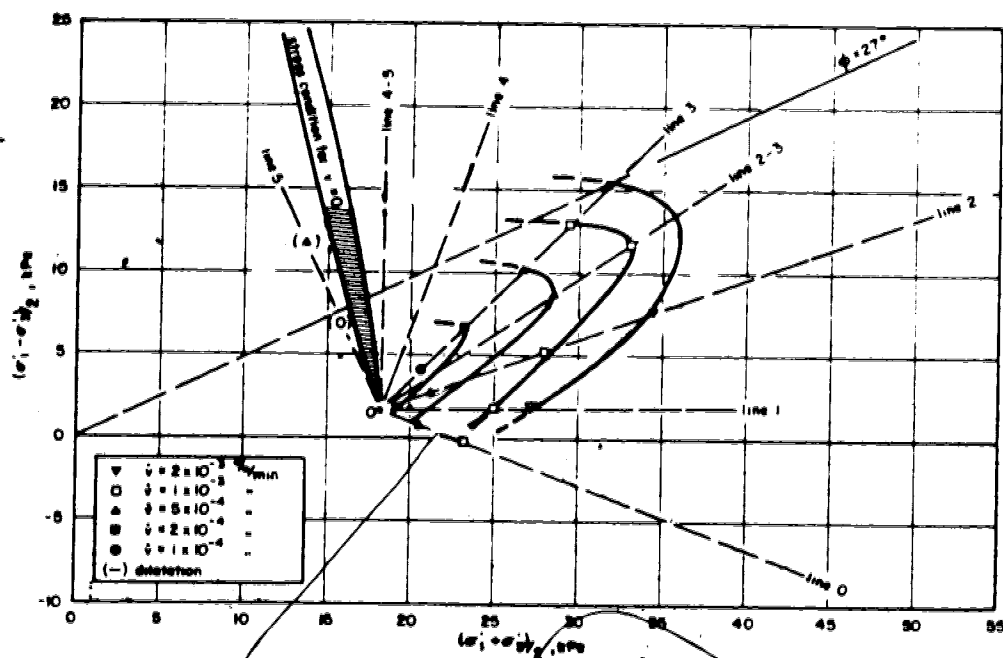


Figure 3.8 Lines of equal volumetric strain rate at  $t = 100$  min in the stress space for drained tests (after Tavenas et.al, 1978)

Yudhbir and Mathur (1977), found that the volumetric creep rate was dependent on stress path.

#### Duration of Previous Stress

The duration of the previous stress may have some effect on the subsequent volumetric creep rate according to Mesri (1973). Bjerrum (1967) demonstrated that delayed compression, i.e. secondary compression, induces a pseudo preconsolidation stress on the sample. It has already been shown in this section that preconsolidation has an effect on the volumetric creep. If, however, the subsequent load is higher than the pseudo preconsolidation stress then the duration of the previous load has a minimal effect. Wu *et.al* (1978) and Barden (1969) found no effect on the subsequent creep of the sample from the duration of the previous consolidation load.

#### Temperature

An increase in temperature will cause an increase in the creep rate for all creep conditions. Rate process theory demonstrates this admirably. However, the temperature must be changed substantially according to Bishop and Lovenbury (1969) and Mesri (1973) before the effect is measurable.

#### 3.3.1.2 Deviatoric Component

The deviatoric component of the drained creep strain tensor has not received much attention in the literature.

Again, this is a consequence of the majority of researchers using the oedometer for the investigation of drained creep behaviour. It is revealing to note that Equation 3.8 demonstrates that the maximum engineering shear strain in the oedometer is equal to the volumetric strain. It then follows that the maximum shear strain rate must be dependent on the same factors as the volumetric strain rate for the oedometer stress state. Furthermore, it should be a function of shear stress level but this cannot be investigated with the oedometer.

Kavazanjian and Mitchell (1980) state that deviatoric component of the drained creep strain tensor can be described by a relationship of the type given by Equation 3.2. The results of Tavenas *et al* (1978) are in agreement with this. Their data fits a relationship of the form:

$$\dot{\gamma} = A[g(\sigma')](\dot{\epsilon}_1/\dot{\epsilon}_v)^m \quad 3.15$$

where  $\dot{\gamma}$  = shear strain rate

A = constant

$g(\sigma')$  stress function

and

$$\dot{\gamma} = \dot{\epsilon}_1 - 1/3\dot{\epsilon}_v \quad 3.16$$

where  $\dot{\epsilon}_1$  = axial strain rate

$\dot{\epsilon}_v$  = volumetric strain rate

Figure 3.9 shows the form of the shear stress function. It is apparent that the shear strain rate is a function of shear stress level but, for their data, not in the simplified form given by Equation 3.2. It is of interest to note that the value of  $m$  in Equation 3.14 is the same as that in Equation 3.15.

Walker (1969a) also investigates the influence of shear stress level on shear creep rate, a parameter which is analogous to  $C_a$ , for triaxial and simple shear tests on remoulded kaolin. His results are illustrated in Figure 3.10. A linear relationship between shear creep rate and shear stress level is indicated in Figure 3.10 which is independent of consolidation stress. Yudhbir and Mathur (1977) also have shown that the shear creep rate is dependent on stress level and also on stress path.

In summary, deviatoric creep strains under drained conditions are a function of stress level, stress path and time. A relationship of the Singh-Mitchell type appears to fit the laboratory data of most researchers reasonably well.

### 3.3.2 Undrained Creep

Undrained creep results from the application of a sustained total stress under conditions of no volume change. It then follows that the creep strain tensor contains a deviatoric component only. During undrained creep the pore pressures change with time and, hence, the effective stress during undrained creep is not constant.

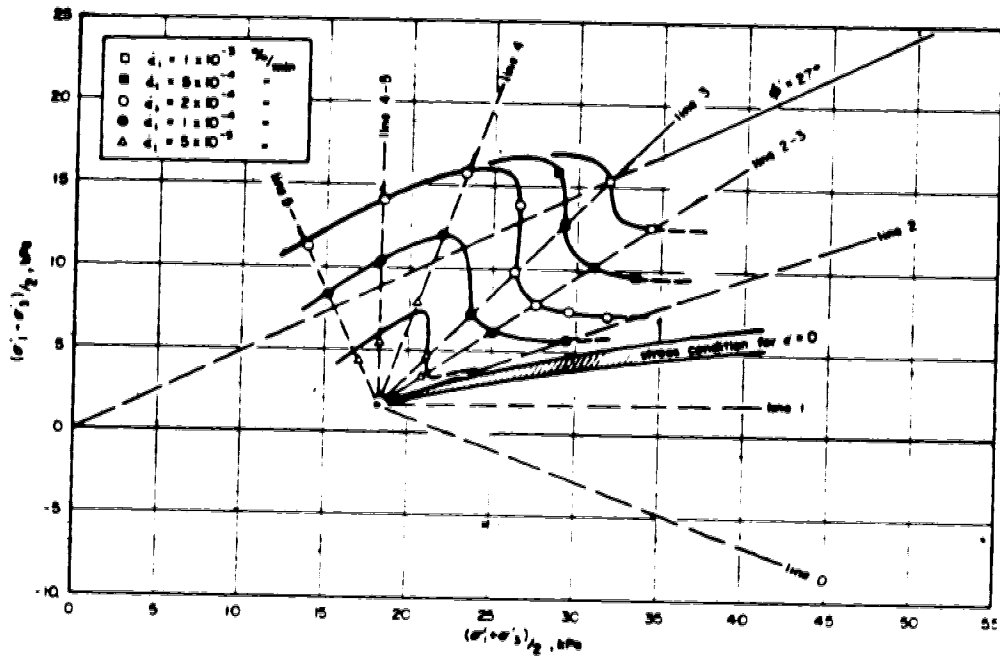


Figure 3.9 Lines of equal shear strain rates at  $t = 100$  min in the stress space for drained and undrained tests (after Tavenas *et al* , 1978)

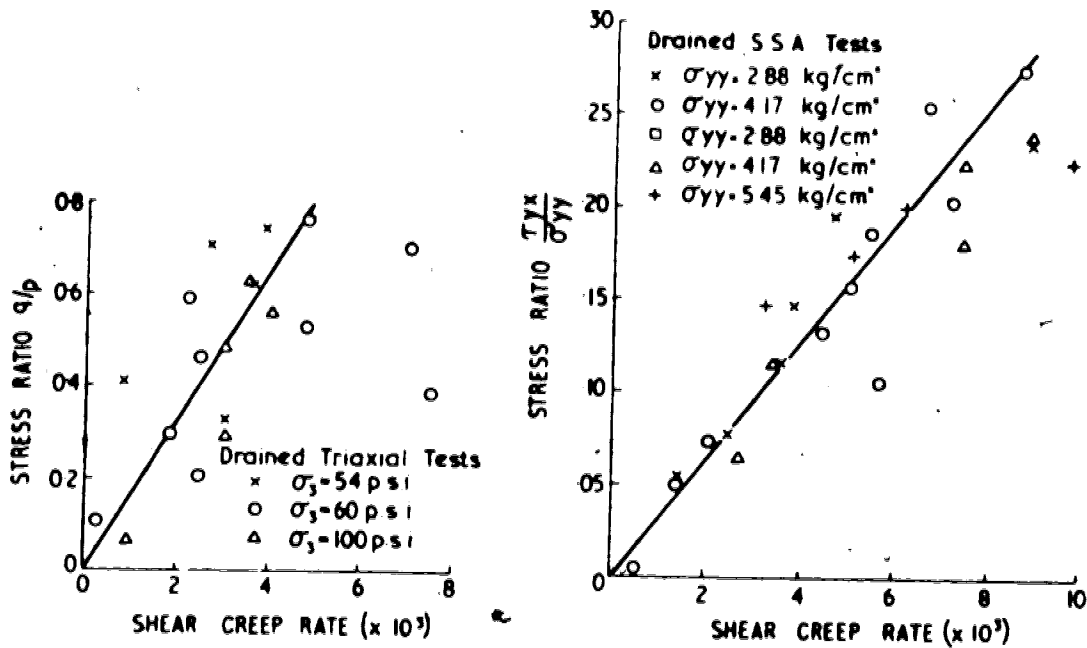


Figure 3.10 Effect of stress level on shear creep rate, left - triaxial tests, right - simple shear tests (after Walker, 1969a)

The most common laboratory apparatus for performing undrained creep experiments is the triaxial test. A few researchers have also used the plane strain device and the simple shear plane strain device. The prevention of leaks during undrained testing in all three devices is difficult. Poulos (1964) presented a comprehensive summary of sources of leaks in the triaxial test which is of great value for designing undrained creep test programs.

For undrained creep testing it is customary to plot the development of axial strain and pore pressure with time for different stress levels. Typical examples of such pore pressure plots are shown in Figures 3.12 and 3.13. Singh and Mitchell (1968), Edgers *et.al* (1973) and Holzer *et.al* (1973) all found the axial strain rate to be adequately represented by Equation 3.2. Tavenas *et.al* (1978) found that axial strain rate can be described by a relationship similar to Equation 3.2 but with a stress function that has a similar form to that shown in Figure 3.9.

It is of interest to note that Tavenas *et.al* (1978) found the parameter,  $m$ , in Equation 3.2 to be independent of drainage conditions and stress path. This is in agreement with Singh and Mitchell's (1968) contention that the parameter,  $m$ , is a material constant. Edgers *et.al* (1973) in an extensive series of simple shear tests with no volume change and undrained triaxial tests on undisturbed, highly plastic, very soft, backswamp clay found that  $m$  was dependent on stress state and, also, a function of whether

the sample was consolidated isotropically or anisotropically. They also found the stress level term,  $\bar{\sigma}$ , in Equation 3.2 to be a function of stress state.

Krizek *et.al* (1977) performed a series of undrained creep tests on remoulded kaolin which was prepared with a number of different microfabrics. The microfabrics varied from highly random to highly oriented and were identified with the scanning electron microscope. They found that  $m$  was a function of void ratio and anisotropy as shown on Figure 3.11. The vertical specimens exhibited larger creep deformations, *i.e.* a lower value of  $m$ , than the samples cut in the horizontal direction. The stress level parameter,  $\alpha$ , was also found to be a function of void ratio and anisotropy.

Walker (1969b) conducted a series of undrained triaxial tests on Leda clay to determine the development of deviatoric strain and pore pressure with time. He chose to plot these two variables against the logarithm of time and found a bilinear relationship for each. The initial linear relationship was attributed to redistribution of pore pressure. He proposed a functional relationship between axial strain and pore pressure which was based on their similar relationship to time. Unfortunately an exact formulation of this function was not given.

Holzer *et.al* (1973) ran a series of undrained triaxial tests on undisturbed San Francisco Bay Mud to investigate the nature of undrained pore pressure response during creep.

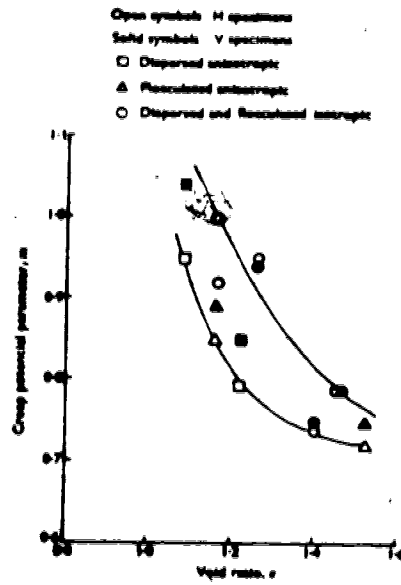


Figure 3.11 Creep parameter,  $m$ , versus void ratio (after Krizek et.al, 1977)



They found that the pore pressure response could be decomposed into two parts. The first was essentially time independent and due to the application of an increased deviator stress. The second was time dependent and due to the arresting of secondary consolidation. They were able to decompose the pore pressure response in this way by determining the pore pressure response of an isotropically consolidated sample at zero deviatoric stress. Their data is presented in Figures 3.12 and 3.13. It can be seen from Figure 3.12 that increased time for secondary consolidation resulted in a lowering of the time dependent pore pressure response during shear.

#### 3.4 Creep Rupture

A soil may fail under the sustained action of a creep stress at undrained strengths substantially lower than the strength measured in 'normal' undrained tests. A failure of this type is referred to as creep rupture. Mitchell (1976) attributes the discrepancy between the normal undrained strength and the creep rupture strength to either deterioration of cemented bonds by creep strains or pore pressure generation under undrained conditions which decrease the effective stresses to failure.

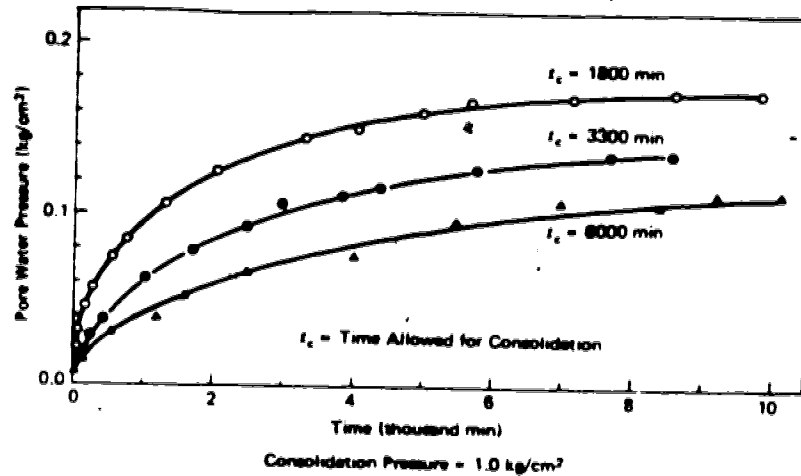


Figure 3.12 Excess pore pressure development following cessation of drainage after secondary compression for different time periods (after Holzer *et al.*, 1973)

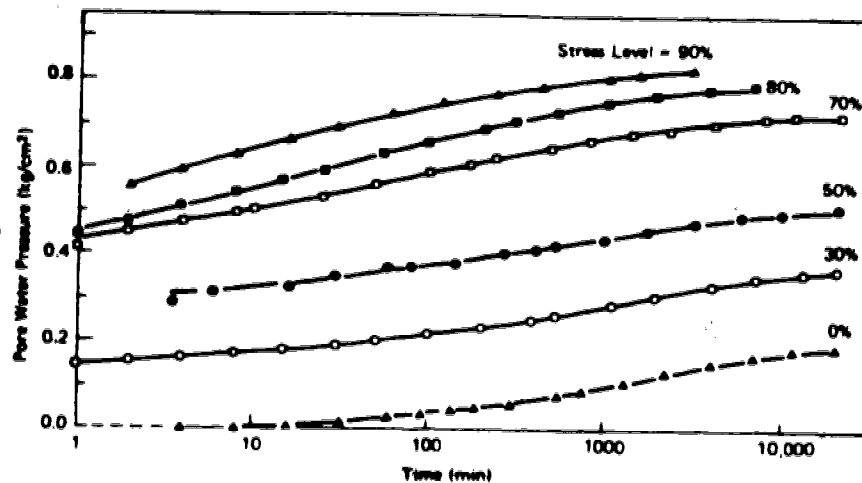


Figure 3.13 Excess pore pressure development during undrained creep of San Francisco Bay mud after consolidation at 1.0 kg/cm<sup>2</sup> for 10 min (after Holzer *et al.*, 1973)

### 3.4.1 Undrained Conditions

It is important to appreciate that, although the undrained creep rupture strength is substantially less than the normal undrained strength, failure is still governed by the effective strength envelope. Campanella and Vaid (1974) demonstrate this fact conclusively using a comprehensive series of undrained creep test results on undisturbed Haney clay.

Finn and Snead (1973) conducted a series of undrained creep rupture tests on undisturbed Haney Clay to determine the cause of the discrepancy between creep rupture strength and the 'normal' undrained strength. They found that the creep rupture strength could be determined from a relationship of the form:

$$\sigma_c = \sigma_{uy} + K \dot{\epsilon}^n \quad 3.17$$

- where  $\sigma_c$  = creep strength  
 $\sigma_{uy}$  = upper yield strength  
 $K$  = a constant  
 $\dot{\epsilon}$  = minimum axial strain rate  
 $n$  = constant, 3 for Haney Clay

Figure 3.14 presents Equation 3.17 in graphical form. The significance of the minimum axial strain rate is shown in Figure 3.15. The upper yield strength, first proposed by Murayama and Shibata (1958) is the creep stress below which failure will not occur. According to Finn and Snead (1973)

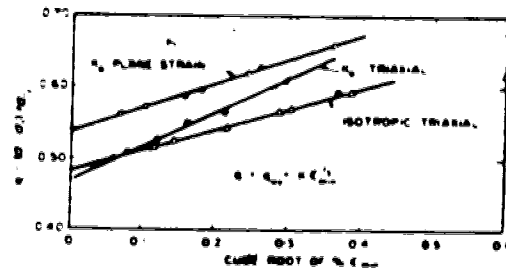


Figure 3.14 Determination of upper yield stresses (after Campanella and Vaid, 1974)

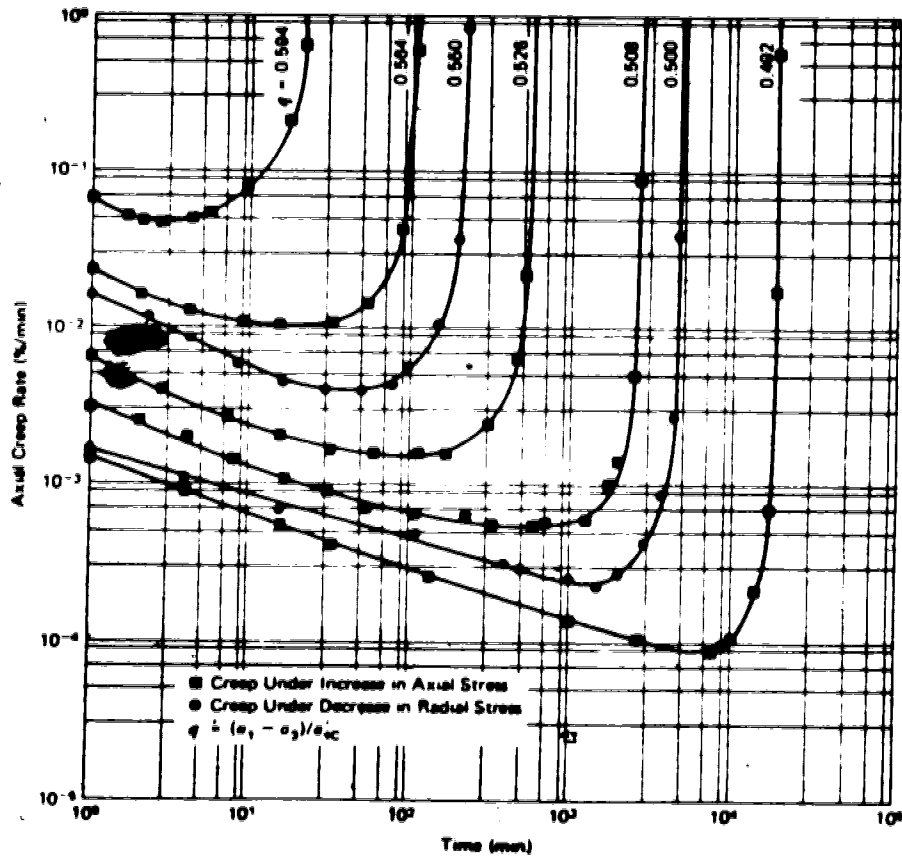


Figure 3.15 Creep rate behaviour of  $K_c$ -consolidated undisturbed Haney clay under axially symmetric loading (after Campanella and Vaid, 1972)

it is equivalent to the undrained strength determined from a constant strain rate test run at a strain rate sufficiently slow to allow complete equilization of pore pressure within the sample. It then follows that the discrepancy between 'normal' undrained strengths and creep rupture strength is a result of the high strain rates, 1 %/min to 2 %/min, usually employed for 'normal' undrained strength tests.

### 3.4.2 Creep Rupture Life

It is of interest to be able to predict the time to rupture in a creep test when the creep stress is greater than the upper yield strength. The time period from the initiation of creep to creep rupture is termed the creep rupture life. Saito (1965) presents a relationship between creep rupture life and any transient strain in the 'tertiary' range as:

$$\dot{\epsilon} = a/(t_r - t) \quad 3.18$$

where  $\dot{\epsilon}$  = transient strain rate in the 'tertiary' range at optional time

$t_r$  = creep rupture life

$t$  = optional time

$a$  = constant

Saito (*op.cit.*) demonstrates by graphical means how Equation 3.18 can be used to correctly predict creep rupture life.

Singh and Mitchell (1969) have also presented an empirical method for predicting the time remaining to failure for creep rupture tests. They plot  $\dot{\epsilon}t$ , which they called the creep coefficient, versus the logarithm of time. This method applies only to soils with the parameter,  $m$ , less than one. They found, for a given soil, that the value of the creep coefficient reached a unique value just preceding the onset of failure. They calculated the time to failure from:

$$(\dot{\epsilon}_f / t_f)^a = \dot{\epsilon}t / \dot{\epsilon}t_r \quad 3.19$$

- where  $t_f$  = time to failure  
 $t_r$  = reference time  
 $a$  = slope of  $\dot{\epsilon}t$  versus  $\log$  of  $t$   
 $\dot{\epsilon}t_f$  = creep coefficient at failure, unique and known  
 $\dot{\epsilon}t_r$  = creep coefficient at reference time

Extending the work of Saito (1965), Finn and Shead (1973) found that creep rupture life was related to minimum strain rate during a creep rupture test by a relationship of the form:

$$\log_{10} t = 0.751 - 0.92 \log_{10} \dot{\epsilon}_{min} \quad 3.20$$

- where  $t$  = creep rupture life  
 $\dot{\epsilon}_{min}$  = minimum creep strain rate

Equation 3.20 is similar to that proposed by Saito and Uezawa, (1961). Finn and Shead (*op.cit.*)state that Equation 3.20 is valid for a variety of soils.

A disadvantage of Equation 3.20 is that the time since initiation of creep must be known in order to calculate the remaining creep rupture life. Finn and Shead (1973) overcame this disadvantage by developing a relationship of the form:

$$t_{tr} = C/\dot{\epsilon} \quad 3.21$$

where  $t_{tr}$  = time remaining to creep rupture

C = constant

$\dot{\epsilon}$  = current accelerating creep rate

Campanella and Vaid (1974) have furthered this approach to include the effect of stress state. They performed a series of creep tests on undisturbed Haney clay with the triaxial device using both anisotropic and isotropic consolidation and with the plane strain device. They found that the total rupture life determined from the isotropic triaxial tests was four times longer than that determined from K. triaxial and plane strain tests. This is illustrated in Figure 3.16 which also shows the relationship given by Equation 3.20. Campanella and Vaid (*op.cit.*) also demonstrated that the axial strain at the minimum strain rate is independent of the creep stress. This is shown in Figure 3.17 which also illustrates the much higher creep strains from the isotropic triaxial tests.

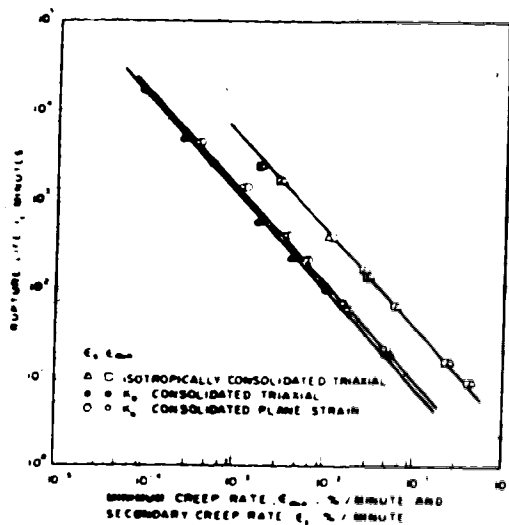


Figure 3.16 Relationships between rupture life and minimum creep rate--normally consolidated undisturbed Haney clay (after Campanella and Vaid, 1974)

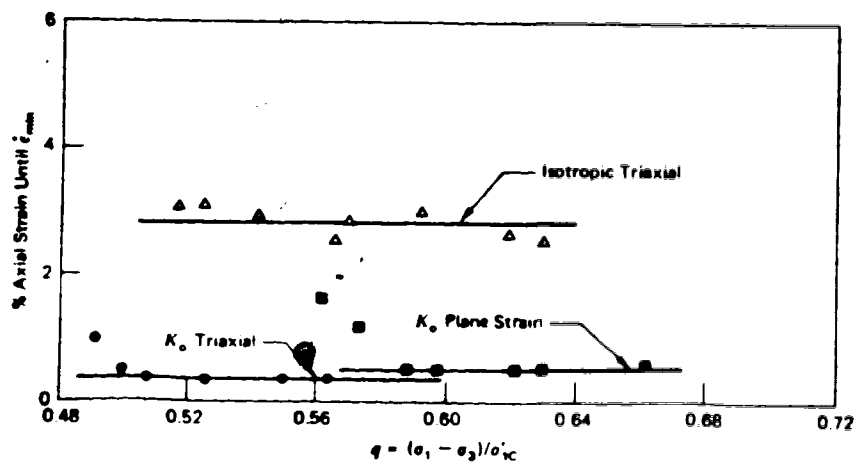


Figure 3.17 Axial strain at minimum strain rate as a function of creep stress for undisturbed Haney clay (after Campanella and Vaid, 1974)



Mitchell (1976) provided a simple method to obtain the constant,  $C$ , in Equation 3.20 using the parameters from Equation 3.2. He demonstrated that  $C$  is equal to:

$$C = (1-m)\epsilon_f \quad 3.22$$

where  $\epsilon_f$  = strain at failure, a constant

The constant,  $C$ , can then be used in the following relationship to find the remaining time to failure:

$$\ln t_f = 1/(1-m) |\ln(C/A) - \alpha D| \quad 3.23$$

Equations 3.20 and 3.23 can be used to predict the remaining time to failure using only the parameters in Equation 3.2.

It must be emphasized that the preceding only applies to stresses above the upper yield strength. Creep rupture will not occur below the upper yield strength given any amount of time.

#### 3.4.3 Drained Conditions

Strength loss during creep under drained conditions has received much less attention in the literature than under undrained conditions. Campanella and Vaid (1974) explained this by suggesting that if creep rupture is a possibility then it is more likely to happen before drainage can strengthen the soil.

Bishop and Lovenbury (1969) performed long term drained creep tests, exceeding three years, at stress levels near peak strength and found no reduction in the effective stress parameters as a result of creep strains. This was demonstrated for both London clay, a strain softening soil, and Pancone clay, a normally consolidated soil. Shibata and Karube (1969) and Tavenas *et al* (1978) also found no strength reduction as a result of creep strains in drained tests. These laboratory results cast doubt on Nelson and Thompson's (1977) hypothesis that the application of creep stresses to strain softening soils at stress levels between residual and peak strength eventually cause a strength reduction of the soil to residual as a result of deterioration of soil bonds.

The laboratory results from the literature demonstrate that strengths derived from long term stress controlled drained creep tests are identical to those obtained from drained strain controlled tests on the same material. Thus, it appears that the concept of creep rupture does not apply to drained creep conditions for soils.

## 4. Laboratory Testing Equipment and Procedures

### 4.1 Introduction

In order to assess the creep behaviour of Tar Island clay a series of drained creep tests were undertaken using the oedometer and the triaxial test. This chapter is devoted to the description and design of the test equipment and to an outline of the test procedures used for creep testing. Recommendations are made for improvements in testing equipment.

Available equipment was used for the oedometer testing. The triaxial systems were designed and fabricated especially for this testing program. The oedometer testing program was undertaken first so that preconsolidation stresses could be calculated and used as a guide in the design of the minimum pressure requirements for the triaxial cells. All triaxial creep tests were performed at consolidation stresses above the apparent preconsolidation stress for the clay. The creep strains determined from the oedometer testing were also used as a guide to the required resolution of the monitoring systems for the triaxial tests.

The results of the testing program described in this chapter are presented in Chapter 5.

## 4.2 Oedometer Creep Tests

### 4.2.1 Testing Equipment

The oedometer tests were performed in a temperature and humidity controlled room which was remote from any source of vibration. Room temperature was maintained within a range of  $20.5^{\circ}\text{C} \pm 1^{\circ}\text{C}$ .

Three samples were tested simultaneously using three floating ring Clockhouse Engineering Ltd. (Model J42) oedometers. Stress was applied to the top of the samples by placing dead weights on a self compensating lever arm system which had an 11 to 1 load enhancement factor. A reduction to the vertical stress was not made for oedometer ring friction because it is generally considered to be negligible. Before testing, the compliance of each oedometer was investigated to ascertain if there were any system time effects.

For the compliance testing an aluminum disc equal in diameter to the inside of the oedometer ring was used in place of the soil sample. The disc was enclosed with a similar filter paper and porous plate arrangement to that used during actual testing. Weights were added in the same increments as for soil testing. Displacement versus time readings were recorded for each load increment until the difference between successive one minute readings was zero. The results from a typical compliance test are shown in Figure 4.1. The top diagram in Figure 4.1 reveals that most of the compliance occurs within 30 seconds of adding the

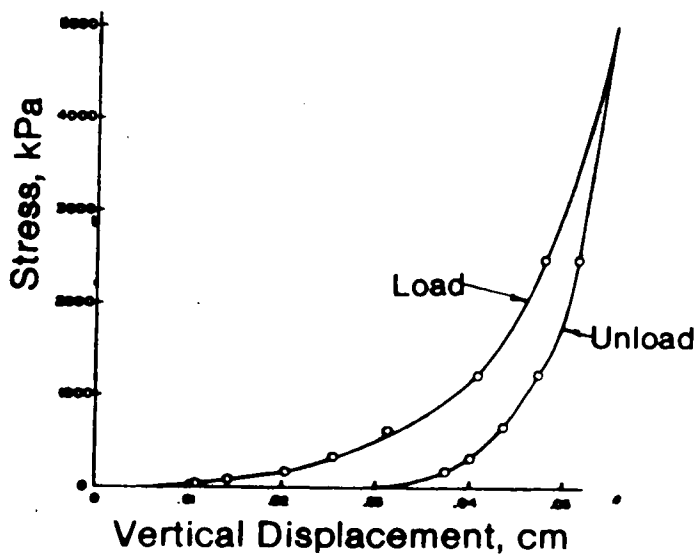
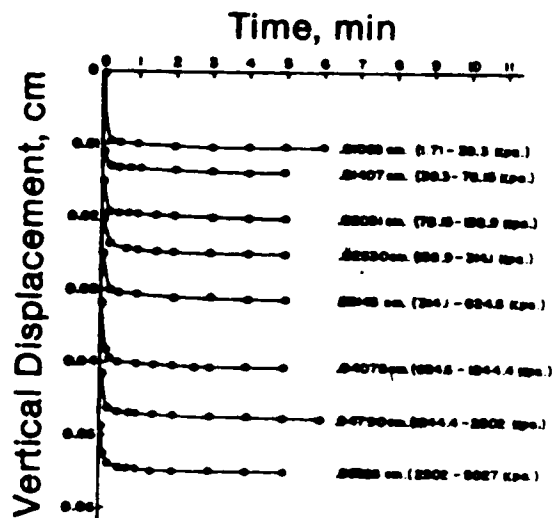


Figure 4.1 Typical oedometer compliance test results

load. The bottom diagram indicates some hysteresis in the loading-unloading compliance curves.

The cause of the hysteresis may be irrecoverable deformation of the porous plates. However, it was observed that a slight change in the alignment of the lever arm system induced a change in the linear variable displacement transducer (LVDT) output. It is considered that most of the hysteresis is caused by this phenomenon which occurs only upon removal of the weights. The immediate compliance displacement from the loading curve was subtracted from the apparent immediate deformation of the soil for each loading increment as part of the data reduction. It was found that the compliance accounted for most of the apparent immediate deformation of soil which is in agreement with the theoretical postulate that immediate deformation of a saturated soil under an oedometer stress state is zero.

Hewlett Packard Model No. 7DCT-1000 LVDT's were used to record displacement. The LVDT's were attached to the oedometers with a bracket. The threaded bottom portion of the LVDT extension rod was screwed into the top of the lever arm immediately above the sample. This mounting configuration reduced the disturbance from accidental knocking or vibration on the displacement readings.

The transducers were calibrated with a micrometer before and after testing. The transducers had a linear travel of 2.54 cm with a concomitant output of 7.500 volts. This corresponds to a theoretical sensitivity for the LVDT

of  $\pm 0.0003$ cm. However, the observed sensitivity was in the order of  $\pm 0.001$ cm. The excitation voltage for each transducer was continually monitored for the duration of each test. This was necessary since a change, for any reason, in the excitation voltage alters the calibration factor for the transducer.

The output voltages of the transducers were monitored with time on a Fluke 33003 2200A data acquisition system which produced a permanent record on paper tape and/or on a magnetic tape cassette which was housed in a Techtrah 8410.

#### 4.2.2 Sample Preparation

Samples for oedometer testing were obtained from the shelby tube samples which were acquired during the drilling program described in Chapter 2. The shelby tube samples, wrapped in cheese cloth and waxed, were stored in a 100 percent humidity room to prevent moisture loss before testing.

Three samples which represented the range in soil properties available from the shelby tube samples were selected for oedometer testing. The description of the samples is given in Chapter 5. The samples were cut to the inner dimensions of the oedometer ring in the conventional way of carefully pushing the cutting edge of the oedometer ring into the sample and simultaneously trimming the excess soil. The top and bottom surfaces of the soil in the ring were trimmed to produce uniform horizontal planes. Gaps were

left between the soil and the top and bottom edges of the ring to allow for proper seating of the porous plates.

The oedometer ring was weighed before and after emplacement of the soil sample. The dimensions of the soil sample were measured and, together with the weight of soil, used to calculate the initial total density. The trimmings were collected for index testing and approximate water content determinations. The entire trimming operation took approximately one hour. Undoubtedly, some drying of the sample occurred during preparation.

#### 4.2.3 Testing Procedure

The oedometer ring containing the sample was taken immediately to the testing laboratory after preparation. Saturated filter papers were placed in contact with the top and bottom soil surfaces. Porous plates which had been saturated in distilled boiling water were then placed adjacent to the filter papers. This assemblage was placed in the oedometer apparatus.

The enclosure around the oedometer ring was filled with distilled water and the lever arm was positioned on the sample. The LVDT was threaded into the lever arm and a small load was applied to the sample to obtain the initial LVDT reading. The first stress increment was applied and the output LVDT voltage was recorded with time. In the first five minutes the readings were recorded manually because the minimum time interval between readings for the data



acquisition system was one minute. Thereafter, the data acquisition system was set to record the LVDT output voltage at predetermined time intervals.

Loads were added to the samples in all three tests in increment ratios,  $\Delta\sigma/\sigma$ , equal to one. The only exceptions were the last two increments for sample C1 where the increment ratio was 0.5. An increment ratio of one ensured that a classical Terzaghi consolidation curve was obtained which allowed an unambiguous determination of the end of primary consolidation. Mesri and Godlewski (1977) have discussed the influence of increment ratio on the shape of the compression-logarithm of time curve as have Leonards and Girault (1961).

The stress at each increment was left for a minimum of one day and, generally, not longer than one week before the next stress increment was applied. All stress increments were maintained for a sufficient time period so that the secondary compression index could be adequately defined. Increment durations were generally longer for stresses above the preconsolidation stress where the creep characteristics were of primary interest.

A computer program was written to reduce the data and present the void ratio versus logarithm of time results on a computer graphics facility. This permitted daily visual monitoring of the test progress and enabled a quick response to any malfunctions.

At the end of testing, the loads were removed in one step without monitoring the swelling of the sample. The sample was immediately taken from the oedometer and weighed for a water content determination.

### 4.3 Triaxial Creep Tests

#### 4.3.1 General

A total of six incremental drained creep triaxial tests were undertaken on Tar Island clay. Three separate triaxial systems were used which allowed creep tests to be performed simultaneously at three different consolidation pressures. The first suite of three tests used vertical samples with horizontal bedding planes. The second suite used inclined samples which had the bedding plane at  $45^\circ$ . In all cases the isotropic consolidation pressure during shear was in excess of the apparent preconsolidation stress determined from the oedometer testing.

The triaxial testing equipment and procedures were designed to determine the influence of anisotropy and consolidation pressure or water content on the creep behaviour of the clay.

### 4.3.2 Triaxial Testing Equipment

#### 4.3.2.1 General

Three identical separate triaxial systems were fabricated. Each system consisted of a triaxial cell, a hanging yoke with no mechanical advantage for adding weights, a system for applying cell pressure, a system for applying back pressure, an LVDT to monitor vertical displacement and a burette to provide volume change measurements. All triaxial tests were performed in the same laboratory as the oedometer tests. The room temperature was monitored daily and the results are given in Appendix B.

The design of the triaxial systems followed conventional standards and only the general aspects of design and operation, as these affect tests results, will be discussed in the following sections.

#### 4.3.2.2 Triaxial Cells

The cells were made of aluminum and were designed for a maximum pressure of 3500 kPa. The inside diameter of the cells was approximately 13 cm and the inside height was approximately 23 cm. The pedestal on the cell base was designed for a sample diameter of 3 cm but, with a change of pedestals, the cells are capable of housing 7.5 cm- $\phi$  x 15 cm samples or 3.8 cm- $\phi$  x 7.6 cm samples with lateral strain gauges. The cell is shown in Plate 4.1

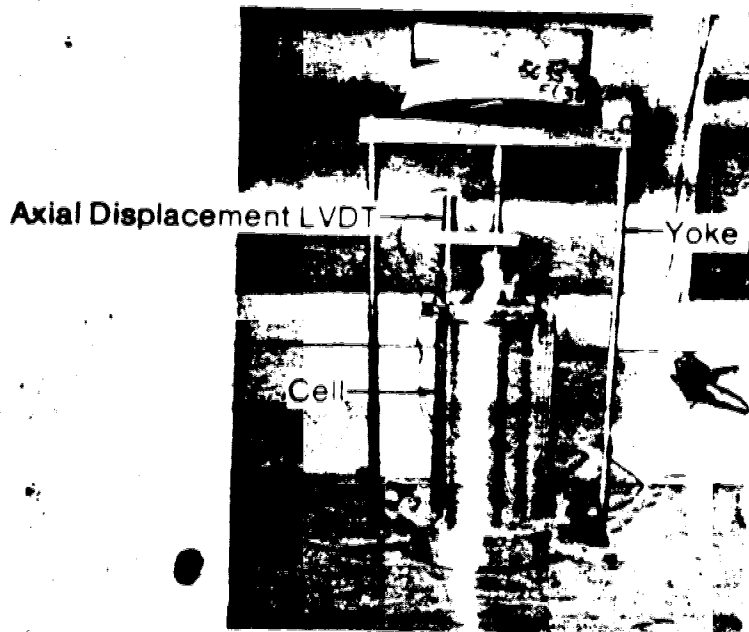


Plate 4.1 Triaxial cell

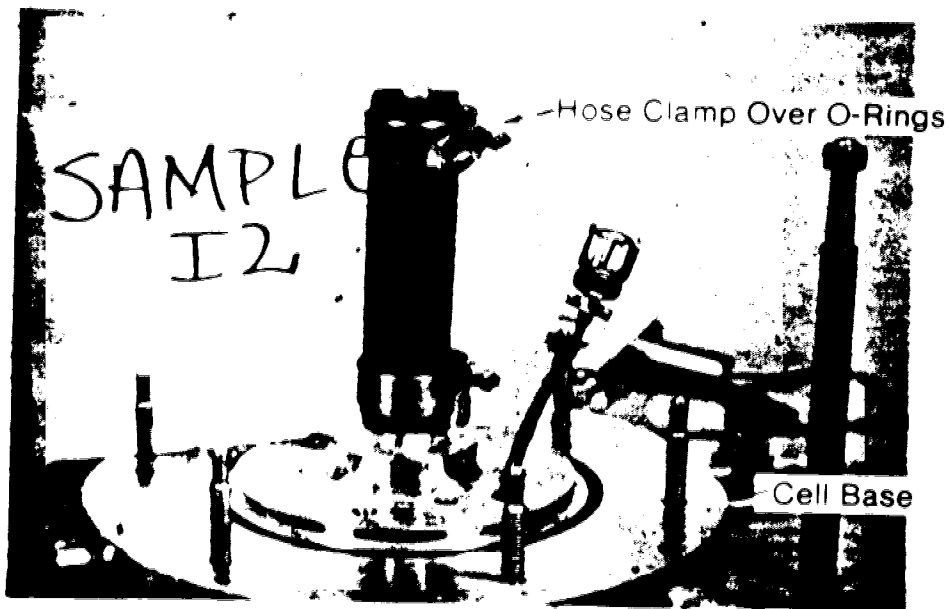


Plate 4.2 Sample with membrane

The top plate of the cell was connected to the cylinder and the cylinder base plate by six steel rods. The pressure seal at the cylinder/top plate contact was provided by an O-ring. The cylinder arrangement was connected to the base plate by six steel threaded studs with wing nuts for easy removal. The pressure seal at the cylinder/base plate contact was again provided by an O-ring.

The base plate had ports which allowed access to the cell interior for sample drainage, measurement of sample pore pressure, cell pressure and electronics. The electronics port can be used for a lateral strain gauge or an interior load cell. The top plate had a port which was used for filling and emptying the cell. The cell fluid was emptied through the cell pressure port by applying air pressure.

The sample arrangement in the cell interior is shown in Plate 4.2. The sample sat on filter paper and a porous plate. The top cap rested directly on the sample. Drainage was permitted from the sample base only but top drainage can be added with only minor modifications to the cell. The sample size of 3 cm- $\phi$  x 6 cm used for testing was not standard so custom membranes were manufactured at the University of Alberta according to Madeiros (1979). The membrane was seated to the top cap and bottom pedestal by two O-rings at each position. The O-rings fitted into grooves and were tightened against the membrane with hose clamps. A correction to the vertical stress on the sample

due to membrane strength was not made because it is generally considered to be small (see Bishop and Henkel, 1962). Membrane leakage was never observed. This is due, in part, to the use of silicone as a cell fluid as recommended by Poulos (1964) and Lovenbury (1969).

Load was applied to the sample by a ram through the cell top. The base of the ram was machined to fit a ball bearing which fitted into the sample top cap. This arrangement ensured that the ram applies load without eccentricity. An O-ring and an oil seal provided the pressure seal for the ram/cell top interface. This seal arrangement resulted in a reduction of external load due to ram friction. The magnitude of the ram friction was determined for each cell before testing.

The magnitude of the ram friction was calculated by comparing the internal load measured with a load cell and the external load applied by the dead weights on the yoke. A typical set of results for a variety of external loads and cell pressures is presented in Figure 4.2. All curves are parallel to the curve passing through the origin which indicates that ram friction is independent of the magnitude of the external load. The intercept of the curves with the ordinate is equal to the load on the ram end from cell pressure plus ram friction. By subtracting the former it was found that ram friction varied from 9 nt to 18 nt and was independent of cell pressure. A common value of 18 nt for ram friction was adopted for all three cells. It should be

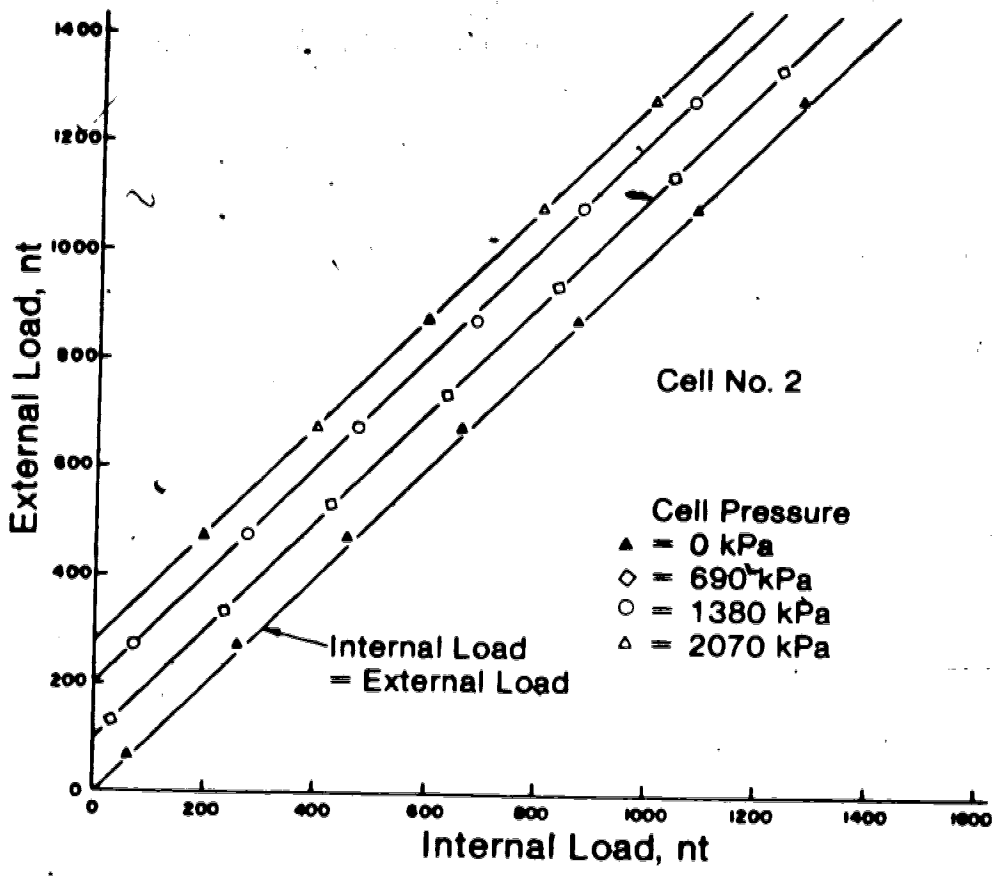


Figure 4.2 Typical ram friction test results

mentioned that this value of ram friction is for static conditions while the magnitude of the kinematic friction is probably more applicable to the testing conditions.

#### 4.3.2.3 Pressure Systems

A schematic of the cell fluid pressure system for each cell is shown in Figure 4.3. The cell pressure was applied by means of two separate systems. One was a low pressure system, 0 to 1380 kPa, that originated from a compressed air supply. A Moore continuous bleed regulator was used to set the desired pressure and an aluminum closed end cylinder served as the compressed air/cell fluid interface. This system was capable of maintaining pressure within  $\pm 3$  kPa over sustained periods of time. A backup generator was available for the compressed air pump in the event of a power outage. Plate 4.3 shows the aluminum plate which supports the regulator and interface. The back pressure system for the sample pore pressure was identical to this system and is shown in Figure 4.4.

For cell pressures above 1380 kPa a high pressure system was fabricated which was similar in detail to other high pressure systems used in the geotechnical laboratories at the University of Alberta. It is illustrated schematically in Figure 4.3 and a portion is shown in Plate 4.2. The pressure source was a 17,200 kPa nitrogen bottle. A simple step regulator attached to the nipple of the bottle was used to decrease the bottle pressure to a lower, safer



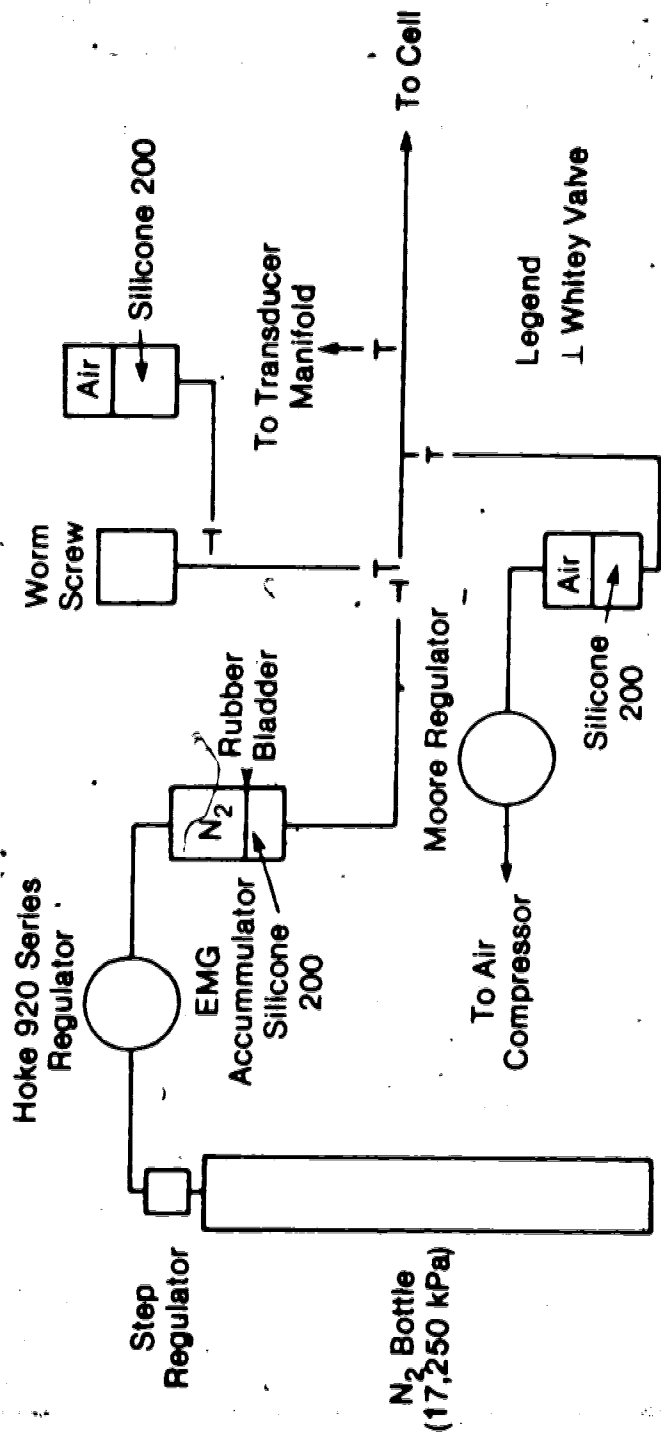


Figure 4.3 Schematic of cell pressure systems

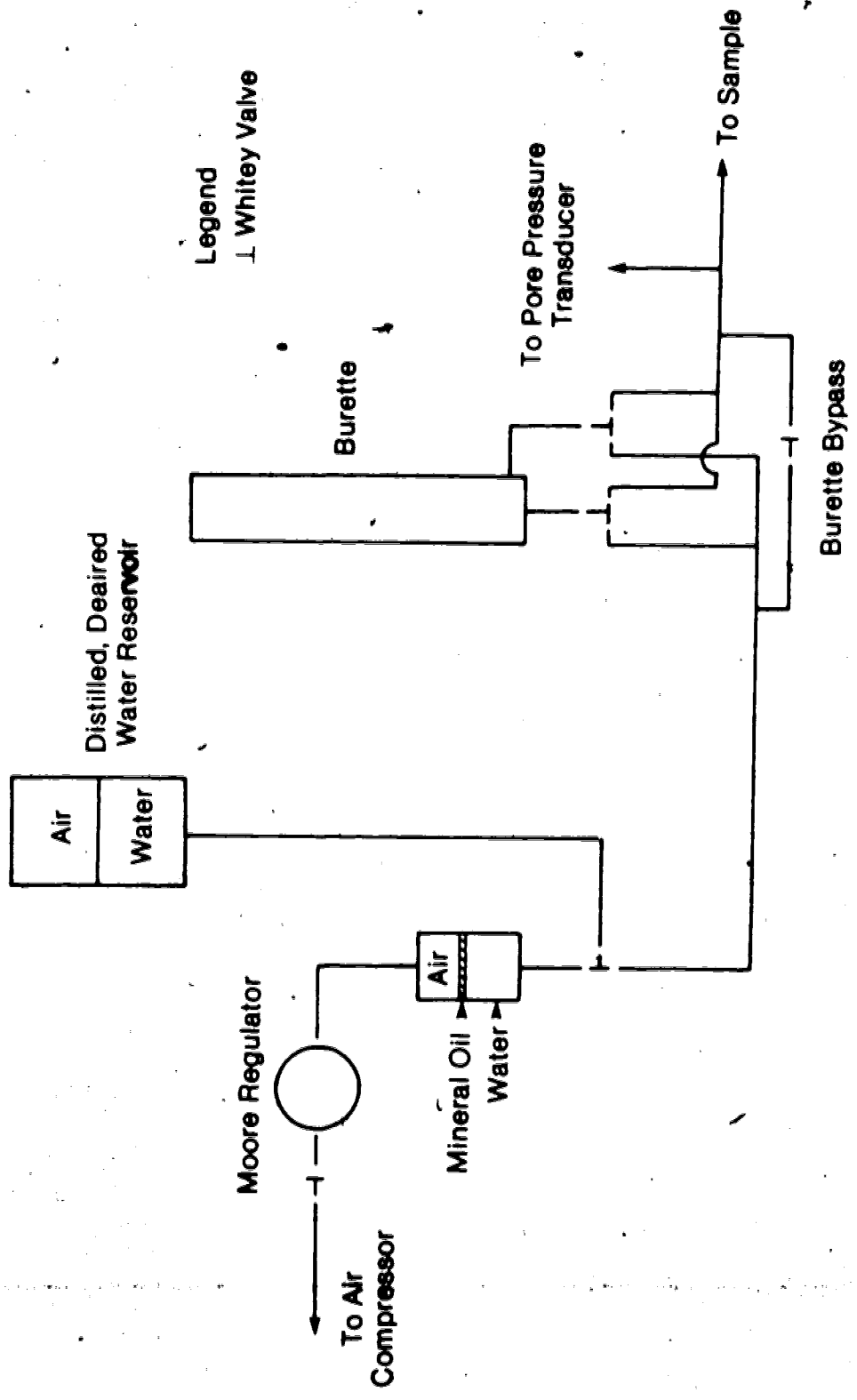


Figure 4.4 Schematic of back pressure system and volume change indicator

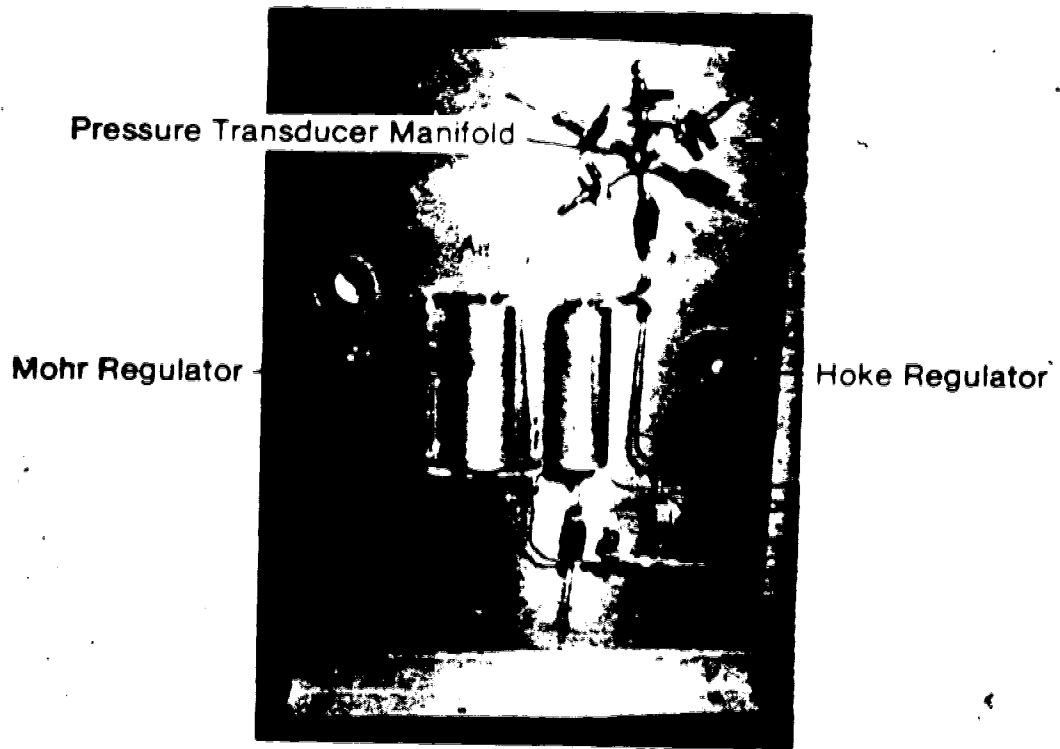


Plate 4.3 Cell pressure board

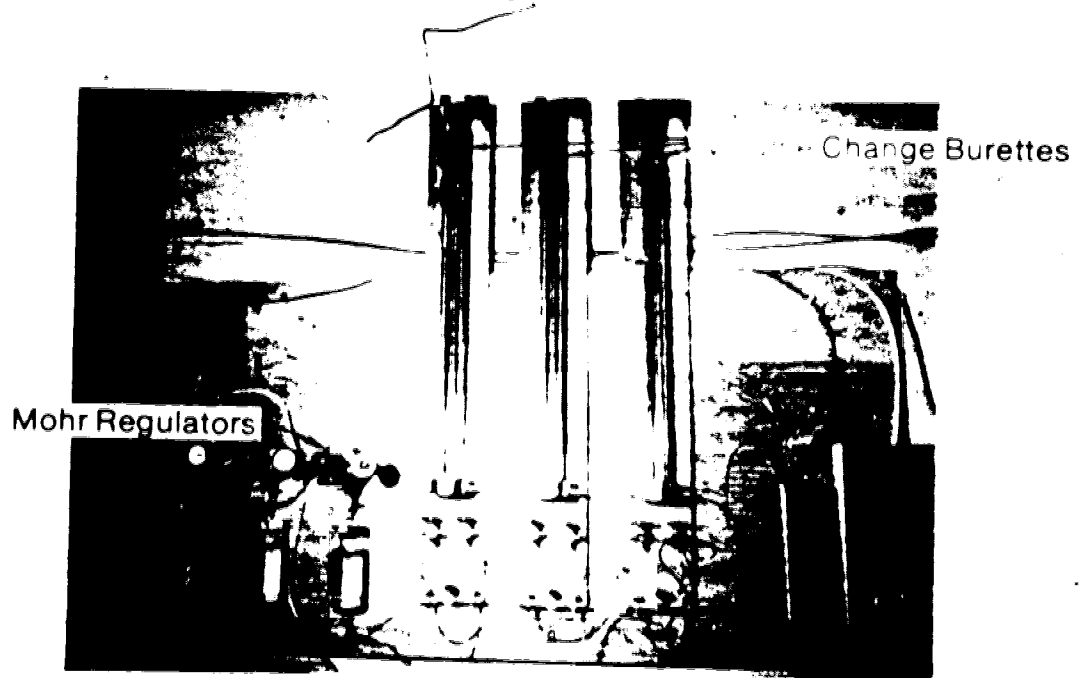


Plate 4.4 Volume change indicators and back pressure board

level of 3500 kPa for this testing program. Downstream of the step regulator was a Hoke 920 regulator which was used to set the desired cell pressure. An EMG Hydraulics Inc., hydropneumatic accumulator with a sliding rubber bladder served as the nitrogen/cell fluid interface. The purpose of the rubber bladder was to isolate the explosive gas pressure from any system leaks. The interior of the accumulator will corrode if in contact with water so another fluid interface is required downstream of the accumulator if, in the future, water is chosen as the cell fluid.

There are some drawbacks to the high pressure system just described. It was difficult to set the Hoke regulator at the desired pressure. The chosen pressure inevitably fell by about 10% (in approximately 12 hours) before it stabilized. It is considered that this was a result of air going into solution. Furthermore, the nitrogen bottles lost pressure due to inevitable leaks in the system. The cell pressure dropped by approximately 7 kPa per week. The bottles had to be changed every few weeks, taking care not to disturb an ongoing creep test. An example plot of pressure versus time for the backpressure system and the high pressure system is included in Appendix B.

Sweglok brass fittings were used for the entire system. These fittings have a maximum capacity of 3500 kPa. If pressures above 3500 kPa are required for future testing all brass fittings must be replaced with stainless steel fittings. Whitey ball valves were used to direct flow for

the entire system. An advantage of ball valves over stem valves is that there is no volume change associated with their operation.

Copper tubing with a diameter of 0.32 cm was used for the cell pressure system and a combination of copper tubing and polyethylene tubing was used for the back pressure system.

A 7000 kPa transducer was used to monitor cell pressure and a 2100 kPa transducer was used to monitor back pressure.

#### 4.3.2.4 Monitoring of Sample Deformation

The axial deformation of the sample was measured with a Hewlett-Packard 24DCT-250 LVDT attached to the ram as shown in Plate 4.1. The LVDT's were calibrated before and after testing. No significant change in the calibration factors were observed. The LVDT's had a linear travel of  $\pm 0.16$  cm with a concomitant voltage output of  $\pm 3.7500$  volts. This corresponds to a theoretical sensitivity of  $\pm 0.000004$  cm. The actual sensitivity observed was closer to  $\pm 0.00004$  cm.

The same Fluke data acquisition which was used for the oedometer testing was also used for this testing. The data acquisition unit was used to monitor the LVDT voltage excitation and output as well as the output voltage of the two pressure transducers.

The volume change of the sample was measured with a burette which had an apparent sensitivity of  $\pm 0.005$  cc. Figure 4.4 presents a schematic of the back pressure/volume

system and Plate 4.4 shows the volume change indicators. Each volume change indicator consisted of an outer perspex cylinder with aluminum end caps which housed a 10 cc glass burette. The pressure seal at the aluminum/perspex contact was provided by an O-ring. A dyed kerosene/water interface recorded the fluid movement in the burette. The inside of the burette had to be kerosene wet before assembly or the meniscus would stick to the glass.

Tests were performed to determine the leakage from the back pressure/volume change system. An aluminum cylinder encased in a membrane in place of the sample was used for these tests. Back pressure and cell pressure were applied and it was found that the system leakage varied between 0.05 and 0.1 cc/day. The possible sources of leakage are considered to be :

1. Leakage through valves and Sweglok fittings
2. Diffusion through and creep of the polyethylene .32 cm  $\phi$  tubing (see Poulos, 1964)
3. Incomplete saturation of the system

Each component of the system was checked and replaced if faulty. For the second suite of creep tests most of the polyethylene tubing was replaced by copper tubing which decreased the leakage rate by 50%. The leakage rate was found to be a direct function of the magnitude of the back pressure. However, cell pressure had no effect on the leakage rate which indicated the sample membranes did not leak. Slight changes in room temperature caused substantial

changes in the burette readings.

It is considered that the leakage rate was reduced to the minimum possible for a system of this design. Further minor reductions could be possible if the number of valves and fittings and the length of tubing were reduced. Tavenas *et al* (1978) did this by incorporating a burette in the cell base. Lovenbury (1969) undertook a series of long term drained creep tests and found leakage rates of between 0.005 and 0.015 cc/day for similar paraffin burettes. He also measured volume change with a mercury jacket around the sample. These measurements were more accurate but reliability problems hampered their long term efficacy.

The problem with measuring volume change with burettes was recognized at the beginning of the testing program. It was considered that a leakage rate correction could be applied to the volume change readings. This view proved to be optimistic as the correction was usually greater than the actual volume change of the sample within one day after beginning a creep increment. Consequently, volumetric strain with time cannot be reported in this thesis. For the sample size used in this testing program a leakage rate of less than 0.001 cc/day was required before volumetric strain with time could be determined reliably for any reasonable period of time. However, it was possible to estimate the total volumetric strain during a creep increment which was used in the calculation of applied stress.

It is of benefit for future long term drained creep research to review the volume change devices for triaxial testing described in the literature and to assess their applicability to creep testing. The devices are in two categories; those that directly measure pore fluid exchange with the sample and those that measure the change in diameter of the sample, usually referred to as lateral strain gauges.

The first category consists mainly of burettes with various adaptations for continuous automatic data logging. A few systems are described in the literature where fluid exchange with the sample caused a shift in a mercury system which was automatically recorded. For descriptions of various types of volume change devices see Lewin (1971), Mitchell and Burn (1971), Rowlands (1972), Klementev (1974), Menzies (1975), Sharpe (1978) and Watts (1980). The sensitivity of the instruments described by these authors ranged from  $\pm 0.002$  cc to  $\pm 0.5$  cc. None of these authors mentioned leakage rates, presumably because the instruments were designed for short term testing. With only a minimum leakage rate superposed on the maximum sensitivity of the instruments it is apparent that none would be suitable for long term drained creep tests of the type undertaken in this testing program.

The alternative to volume change indicators are lateral strain gauges. The most common are adaptations of that described by Bishop and Henkel (1962). Modern versions - such



as those commonly used at the University of Alberta employ a vertically mounted LVDT to measure displacement. Menzies (1976) describes an adaptation which employs a horizontally mounted LVDT. An attempt was made to design a gauge for this testing program for use with 3 cm- $\phi$  samples but problems with mounting the LVDT on a small gauge and bedding errors caused the attempt to be abandoned. In general, lateral strain gauges have sufficient accuracy to be used for long term drained creep tests.

El-Ruwayih (1976) described a lateral strain gauge developed at Imperial College which is superior to the conventional design. It consisted of a spring stainless steel strip which can be shaped to fit any sample size. Lateral displacement was measured with four strain gauges mounted on the strip. One advantage over the conventional design is that several gauges can be mounted on one sample. The device has high sensitivity and is very linear but it appears difficult to calibrate.

In recent years a lateral strain gauge which does not contact the sample has been described in the literature (see Cole, 1978 and Kahn and Hoag, 1979). The device consists of a source transducer and an aluminum target on the sample. It operates on the eddy current loss principle. The device has a sensitivity of  $\pm 2.54 \times 10^{-4}$  mm, is simple to calibrate, insensitive to immersion in most liquids and is operable over a temperature range of at least  $10^{\circ}\text{C}$  to  $-6.7^{\circ}\text{C}$ . It is recommended that the utility of this device be investigated

for long term drained creep tests.

#### 4.3.2.5 Suggested Modifications To Equipment

With the exception of the volume change indicators the testing equipment performed as anticipated. However, several modifications are suggested here which would improve the test results:

1. A noncontacting lateral strain gauge should be adapted for use with this triaxial cell design.
2. The data acquisition system should be upgraded to a unit which allows the time interval between readings to be set for each channel individually. This would preclude having to filter small time interval readings necessary for one creep test from another creep test which has been running for an extended period.
3. Thermistors should be added to each cell so that the temperature of the cell fluid can be continually monitored with a data acquisition unit.
4. A more reliable high pressure system must be developed for long term testing.
5. The dead weight loading system should be replaced by a bellofram so that axial loads can be added more precisely.
6. The transducer manifold system should be replaced by individual transducers for each cell so pressure can be continuously monitored.

### 4.3.3 Sample Preparation

Test specimens for triaxial testing were prepared in a device which allowed rotation of the sample and is shown in Plates 4.5 and 4.6. Both vertical and inclined samples were prepared. The samples were prepared by rotating and trimming away excess material with a sharp knife. Three vertical samples could be trimmed from one 7 cm long section of the shelby tube samples. The diameter of the shelby tube samples was 7.3 cm. However it required 23 cm of shelby tube sample to prepare one sample inclined at 45° to the axis of the shelby tube.

A section of a shelby tube sample cut at 45° before final preparation of an inclined sample is shown in Plate 4.5. The maximum diameter of an inclined sample which could be prepared from a shelby tube sample of the forementioned diameter is This constraint determined the maximum sample size of 3 cm-ø x 6 cm for all triaxial testing.

After trimming the samples were carefully measured and weighed. Trimmings were used for index tests and water content determinations.

### 4.3.4 Testing Procedure

#### 4.3.4.1 General

Each drained triaxial creep test involved three distinct stages. A B test was performed as the first stage to select the back pressure necessary to saturate the

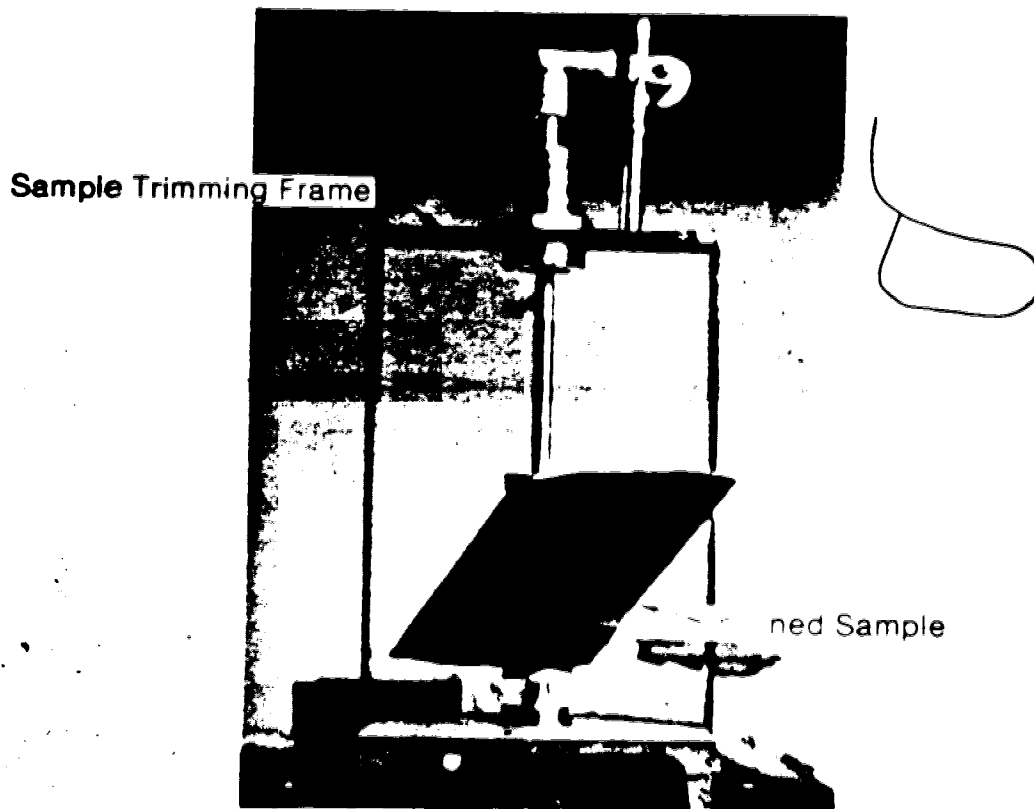


Plate 4.5 Inclined sample before trimming

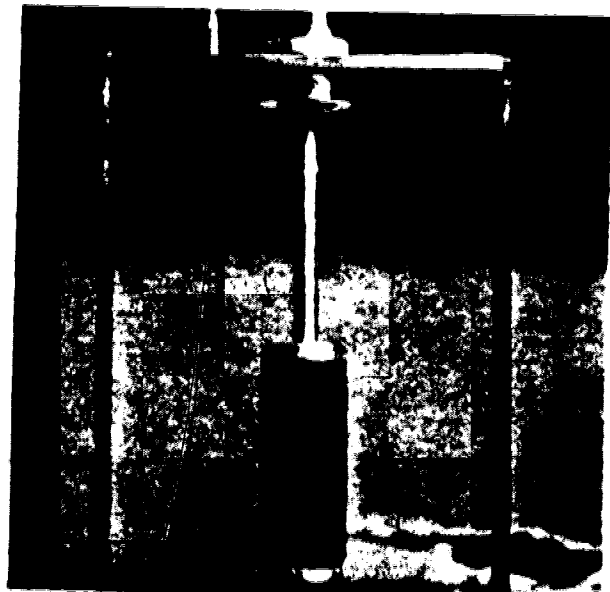


Plate 4.6 Inclined sample after trimming

sample. In the second stage the sample was subjected to isotropic consolidation in steps to the desired consolidation pressure. Finally the sample was sheared at constant cell pressure by incrementally applying axial loads which were maintained for various lengths of time. This latter step constitutes an incremental creep test. The axial deformation and volume change were measured versus time at each creep increment. At the conclusion of the last creep increment the sample was sheared to failure by adding loads slowly enough to ensure drained failure. The stress path just described,  $\sigma$ , constant- $\sigma$ , increasing, was the only stress path studied during the laboratory investigation.

With the available equipment three samples could be tested concurrently. A suite of three vertical samples was tested first. The second and final suite of tests used inclined samples. The vertical samples were tested first because they could be replaced if the test malfunctioned for any reason. Due to the shortage of shelby tube samples the inclined samples could not be replaced if the test malfunctioned. Modifications to the testing technique as a result of experience gained from the first suite of tests led to improved test procedures for the second suite of tests.

A package of computer programs, developed especially for this testing program, were used to monitor the progress of each test daily.

#### 4.3.4.2 B Tests

The samples were saturated with back pressure at the start of each test. The back pressure was applied under a slightly higher cell pressure for 24 hours to allow the sample to saturate before performing a B test. The B tests were performed according to conventional standards. The cell pressure was increased by 70 kPa and the pore pressure was recorded with time until it stabilized. This usually took about five minutes. The calculated value of B was usually in the range of 0.92 to 0.98. It is considered that all the samples were saturated and the B parameter was marginally less than one because of sample stiffness.

#### 4.3.4.3 Isotropic Consolidation

Each sample was consolidated in steps to the desired cell pressure with cell pressure increments,  $\Delta\sigma_c/\sigma_c$ , equal to one. In the first suite of samples the volume change with time was monitored using the burettes only. This proved to be unsatisfactory for volumetric strain rate calculations because of burette leakage, although reliable estimates of the total volume change could be made.

For the second suite of samples, both volume change and axial displacement with time were measured. The axial displacement was monitored with an LVDT connected to the ram. The ram was seated to the sample by an axial load which was just in excess the ram friction and the load on the ram end due to cell pressure. The ram had to be reset with the

sample drainage line closed each time the consolidation pressure was increased.

#### 4.3.4.4 Incremental Creep Tests

Axial loads were added to the sample in steps. At each step or increment vertical displacement and volume change were measured with time. Three increments, referred to here as extended increments, were chosen for each test where the stress was maintained constant for periods in excess of 10,000 mins. Since the cross sectional area of the sample continuously increased during shear loading small loads were added to the sample to maintain constant stress for the extended increments only. The changing area was calculated according to:

$$A = A_0 (1 - \epsilon_s)^2 \quad 4.1$$

where A = area

A<sub>0</sub> = sample cross sectional area at the beginning of present increment

$\epsilon_s$  = lateral strain (always negative for this stress path)

The lateral strain is given by:

$$\epsilon_s = \epsilon_v - \epsilon_v / 2 \quad 4.2$$

where  $\epsilon_v$  = volumetric strain (estimated from volume change readings, based on sample volume at the beginning of the increment)

$\epsilon_a$  = axial strain (based on sample height at the beginning of the increment)

Equation 4.1 is valid only if it is assumed that the soil is cross-anisotropic. Equation 4.1 can be used directly with a lateral strain gauge. Despite the approximations used to estimate  $\epsilon_v$ , the test results indicate that the stress was maintained constant during the extended increments.

Axial loads were added to the sample in small enough increments to preclude undrained failure. The increase in axial stress at any stress level just necessary to cause undrained failure is given by:

$$\Delta\sigma_a = \sigma'_a(1 - \sin\phi') - \sigma'_r(1 + \sin\phi') / (1 - 2A)\sin\phi' - 1 \quad 4.3$$

where  $\Delta$  = change in axial stress necessary to cause undrained failure

$\sigma'_a$  = effective axial stress at the beginning of the increment

$\sigma'_r$  = effective radial stress at the beginning of the increment

$\phi'$  = effective angle of shearing resistance

A = pore pressure parameter

The derivation of Equation 4.3 is given in Appendix B.



Equation 4.3 can be extended to include cohesion. In order to use Equation 4.3 it is necessary to know  $\phi'$  and the variation of  $A$  with stress level. The value of  $\phi'$  for this testing program was estimated initially from strain controlled shear tests by Hardy Associates (1978) Ltd (see Design Review Panel, 1977). The value of  $A$  was estimated for each stress level. Equation 4.3 was used as a check at the beginning of each stress increment to ensure that the applied load would not cause undrained failure. It can easily be shown from Equation 4.3 and a simple consideration of the stress path that  $\Delta\sigma$ , the change in axial load necessary to cause undrained failure, decreases with increasing axial load.

Loads were maintained for periods of 1500 to 5000 mins at the intervening increments between the extended increments. The stress was not maintained constant at the intervening increments. At the conclusion of the third extended increment loads were added until the sample failed. These loads were added slowly enough so that the failure was completely drained.

The creep test just described is referred to as an incremental creep test. A possible alternative to this procedure is the single increment creep test where the desired load is added in one step. This type of test is commonly employed in undrained creep testing of soils and creep testing of rock. A single increment creep test cannot be used in a drained creep examination of normally

consolidated soils at higher stress levels because the sample would fail in undrained shear due to the generation of pore pressures before exhibiting drained creep. The influence of the incremental testing procedure on the test results will be discussed in Chapter 5.

## 5. Experimental Results

### 5.1 Introduction

The results from the oedometer test program, the triaxial test program and an investigation of the soil composition are presented in this chapter. The testing program was conducted primarily to investigate the creep behaviour of the clay. Other information regarding shear strength and compressibility was also acquired during the course of the laboratory program and is detailed herein. It will be shown in Chapter 6 that the relevant state of stress in the portion of the clay deposit to be analysed is one of simple shear. Simple shear laboratory tests were not conducted because Wu *et.al* and Edgers *et.al* have that there are only minor differences between the creep parameters from triaxial and simple shear tests.

It is demonstrated that the creep test results from the triaxial program fit a Singh-Mitchell relationship. The influence of stress state, octahedral stress, test procedure and anisotropy on the creep parameters in the Singh-Mitchell equation are discussed. The applicability of the laboratory results to the field problem under consideration is reviewed in Chapter 6.

## 5.2 Soil Composition

### 5.2.1 Index Tests

The specimens of Tar Island clay were very stiff, medium to highly plastic and contained varying amounts of silt, sand, organic material, coal fragments and calcium carbonate shell material. A series of standard index tests were performed on each sample and the results are presented in Table 5.1. A grain size analysis for each sample is included in Appendix B.

Horizontal bedding was evident throughout the entire soil horizon sampled. Bedding planes were marked by organic material concentrated in thin dark seams, less than .10 cm thick at irregular intervals, and by variations in material properties. The organic material also occurred disseminated throughout the soil. The bedding planes are evident in Plate C.3 in Appendix C.

The plasticity index ranged from 20 to 30 percent and the liquid limit varied from 44 to 54 percent. The average natural water content of the soil tested was approximately 27 percent which is significantly less than the natural water content of approximately 45 percent before dyke construction. The difference in water content, of course, reflects consolidation of the clay due to the imposed dyke load.

Table 5.1 Summary of index test results

Sample No.	Depth (m)	w-%	$\rho$ (1)	Density (mg/m <sup>3</sup> )	%-Silt	%-Clay	PL-% (2)	LL-% (3)
C1	61.3	28.2	2.68	2.00	62	34	-	-
C2	60.0	30.3	2.71	1.98	60	38	-	-
C3	60.5	32.8	2.66	1.89	63	32	-	-
T1	61.5	26.0	2.74	2.02	60	28	23.1	44.6
T2	61.5	26.4	2.74	1.96	60	28	23.1	44.6
T4	59.6	25.9	2.64	1.99	62	34	23.5	50.0
I1	59.1	24.2	2.70	1.98	66	28	23.9	49.8
I2	59.0	26.7	2.69	1.94	58	36	24.3	53.7
I3	60.1	25.0	2.71	1.99	58	34	23.4	51.0

C-oedometer test samples  
T,I-triaxial test samples

- (1)-specific gravity  
(2)-plastic limit  
(3)-liquid limit

The average specific gravity of the soil tested was 2.70 and the average density was 1.97 Mg/m<sup>3</sup>. Approximately 30% of the clay was clay size material with the majority of the remainder in the silt size range.

Although sampling was undertaken only in one location over a limited depth, a comparison with the index tests in Chapter 2 indicate that the samples tested adequately represent the average properties of the entire clay deposit.

### 5.2.2 Mineralogy

An X-ray diffraction analysis was performed by the Alberta Research Council to determine the mineralogy of the clay size fraction. The majority of the clay size fraction is quartz and the remainder is composed of clay minerals. The clay mineral assemblage consists of 40 percent illite, 35 percent montmorillonite, 20 percent kaolinite and 5 percent chlorite. The relative percentage of the clay minerals is based on the 'peak height method'. From the scanning electron microscope analysis described in the next section the particles larger than 2 microns are predominantly quartz.

Two bulk samples were also examined for organic content, pH and CaCO<sub>3</sub>. The laboratory procedures used to determine these quantities are described by McKeague (1978). The organic content is approximately 1.9% by weight, from one test only, although it can be locally much higher because of concentration in thin seams. The pH of the soil

is 7.9, an average of two tests.

The total percentage of  $\text{CaCO}_3$  by weight in the soil is 4 percent, an average of two tests. The quantitative gravimetric method which consists of measuring the amount of  $\text{CO}_2$  liberated after pouring  $\text{HCl}$  on the soil was used to determine the  $\text{CaCO}_3$  content. It is not possible to distinguish among  $\text{CaCO}_3$  in solution in the pore water,  $\text{CaCO}_3$  precipitated on soil particles, perhaps contributing to cementation of the soil, and  $\text{CaCO}_3$  in the form of fossil shells by this method. Because of the consequences of soil cementation on the creep and shear strength behaviour, a scanning electron microscope study was undertaken in an attempt to distinguish the form  $\text{CaCO}_3$  takes in the soil.

### 5.2.3 Scanning Electron Microscope Analysis

A Cambridge Stereoscan 150 scanning electron microscope (SEM) operated by the Department of Entomology at the University of Alberta was used to examine the microfabric of the soil. A Kevex elemental analytical mass spectrometer was used in conjunction with the SEM to determine the predominate elements in the soil. The spectrometer has the capability of analysing the entire screen of the SEM or any selected spot on the screen.

The samples for the SEM were obtained by cutting approximately 1 cm cubes from a fresh fracture surface that was produced by manually breaking a shelly tube sample. Samples were obtained from both horizontal and vertical

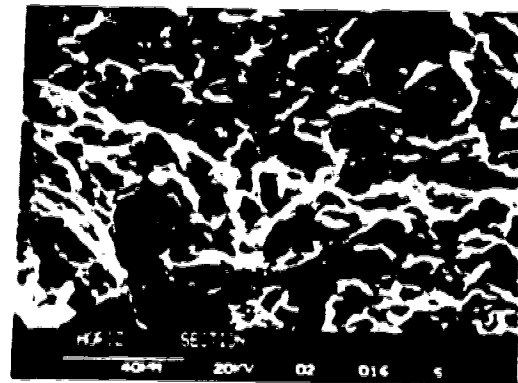
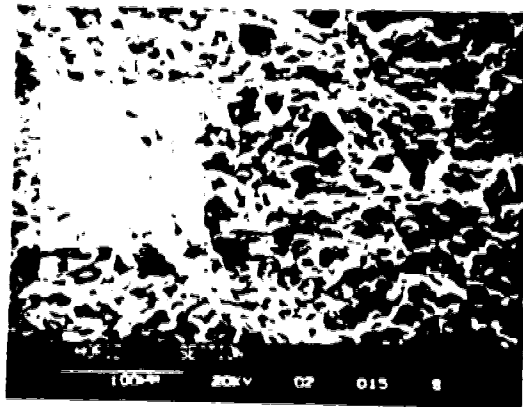
fracture surfaces. Sample moisture was removed by immersing the samples in liquid nitrogen at  $195.8^{\circ}\text{C}$ , then liquid freon and finally sublimating the sample in a dessicator.

The samples were examined at magnifications ranging from 25X to 10,000X. Plate 5.1 illustrates the fabric of the soil at different magnifications. The elemental analysis shown on the spectrometer charts are for the SEM micrographs which show the 4 micron scale designation.

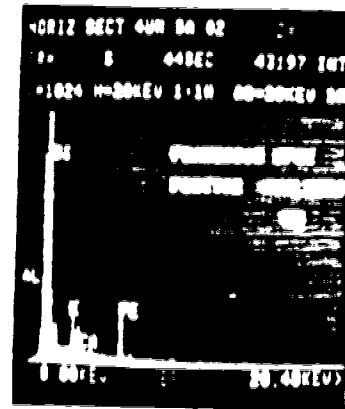
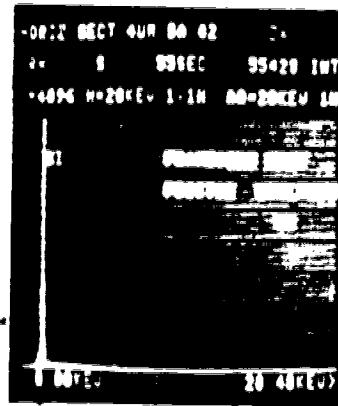
The low magnification micrographs reveal that the soil is dense with little pore space. At higher magnifications it is evident that silica grains predominate. Clay platelets occur in groups or masses surrounding the silica grains. In a number of micrographs silica grains are joined by connectors which may be bonds (see Collins and McGown, 1974).

The mass spectrometer results reveal that the predominate element in the soil is silica with lesser amounts of aluminum, iron, calcium and potassium. The primary sources of the silica are the particle grains as confirmed by several spot analysis. The mineralogy of the clay mineral assemblage accounts for most of the elements present. Aluminum and silica are present in all the clay minerals. Iron and potassium are constituents of illite and chlorite. Calcium may occur in the montmorillonite. Spot analyses with the mass spectrometer revealed that iron and calcium are constituents of most of the connectors between soil grains. These connectors may provide some cohesion but





### Mass Spectrometer Results



Clay Particle

Bridge

Silica Grain

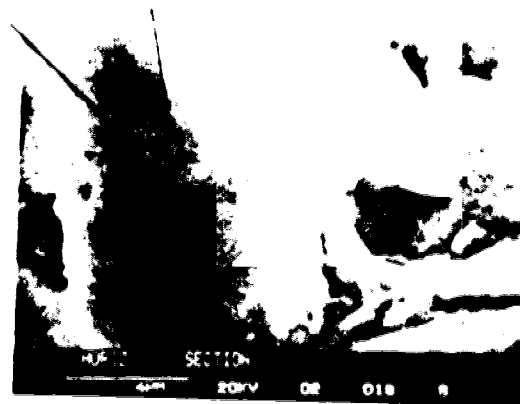
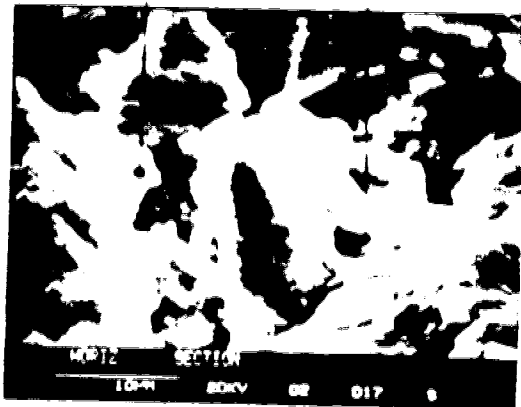


Plate 5.1 Scanning electron micrographs

this can only be confirmed with strength tests.

### 5.3 Oedometer Test Results

#### 5.3.1 General

Oedometer tests were undertaken as a first step in the laboratory creep study to investigate the creep behaviour of the soil in a simple way and, secondly, to ascertain some conventional engineering parameters of the soil such as the coefficient of consolidation and the preconsolidation stress. The conventional analysis of the oedometer test data is given in this section and the creep behaviour of the soil is discussed in the subsequent two sections.

Table 5.2 summarizes the oedometer test results for sample C1. Figure 5.1 presents the void ratio versus logarithm of time curves for each stress increment of sample C1. The test results for samples C2 and C3 are presented in similar fashion in Appendix B.

In order to compile the void ratio versus time curves as shown in Figure 5.1, the initial void ratio was calculated from the initial water content and the specific gravity. The initial water content and the specific gravity was determined on the basis of the entire sample, not on the preparation trimmings. The void ratio curves were then calculated from the displacement readings, allowing for the compliance of the equipment.

Table 5.2 Oedometer test results, sample C1

Incr. No.	Stress (kPa)	Elapsed Time (min)	Void Ratio Change $\Delta e$	$C_v^{(1)}$ (cm <sup>2</sup> /sec)	$C_\alpha$	$m^{(2)}$	Unit Strain Rate <sup>(3)</sup> (%/min)
1	47.9	3093	.0113	-	.0004	1.14	.049
2	98.2	2230	.0096	-	.0009	1.08	.064
3	194.0	2763	.0144	-	.0010	1.04	.065
4	386.4	2890	.0240	-	.0015	1.03	.095
5	770.6	2563	.0382	.0024	.0027	1.05	.171
6	1512	9018	.0628	.0022	.0038	1.08	.307
7	2997	5387	.0754	.0013	.0047	1.06	.333
8	4482	4301	.0472	-	.0051	1.08	.322
9	6000	6707	.0316	-	.0054	1.01	.273

(<sup>1</sup>) Calculated only at stresses above the preconsolidation stress where possible

(<sup>2</sup>) Slope of logarithm of volumetric strain versus logarithm of time curves

(<sup>3</sup>) Intercept of logarithm of volumetric strain versus logarithm of time at  $t=1$  min, ignoring consolidation effects

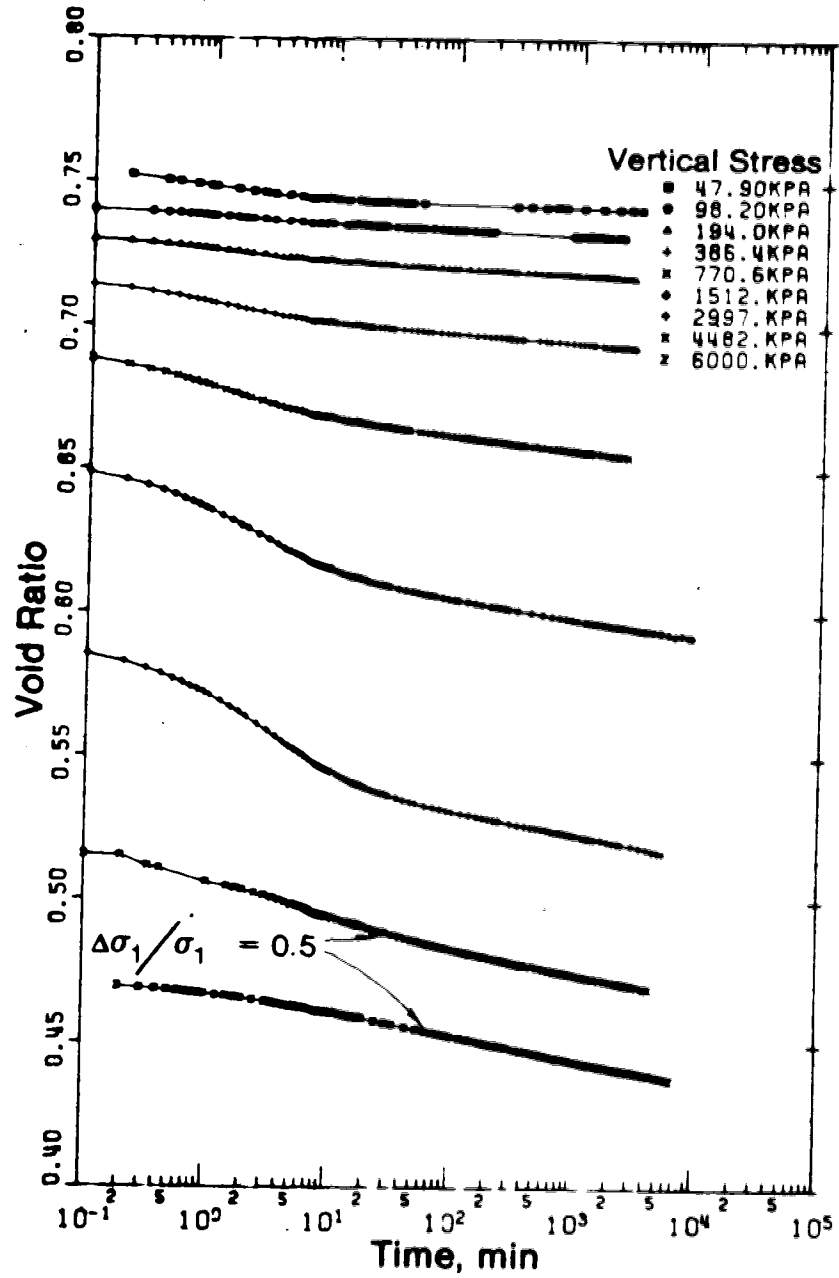


Figure 5.1 Void ratio versus logarithm of time curves, sample C1

Void ratio versus logarithm of vertical effective stress curves,  $e$ -log  $p$  curves, have been compiled for all three samples in order to determine the compression index,  $C_c$ , and the preconsolidation stress,  $p_c$ . The results for sample C1 are given in Figure 5.2 and the results for samples C2 and C3 are included in Appendix B.

Out of interest the  $e$ -log  $p$  curves are plotted for three different time intervals; that corresponding to the end of primary consolidation, the actual duration of the test which is a variable and, finally, an extrapolated time of 10,000 minutes. The value of  $C_c$  is shown on the plots and for the longer time curves ranges from 0.25 to 0.31 with an average of 0.28. The value of  $p_c$  is quite sensitive to the time interval and ranges from 480 kPa to 900 kPa with a mean of 650 kPa. Since the clay is normally consolidated the mean value should be close to the effective stress imposed on the soil by the dyke load at the time and depth of sampling.

The coefficient of consolidation,  $C_v$ , is tabulated for stresses above the preconsolidation stress of 650 kPa on Table 5.2 for sample C1 and on similar tables for samples C2 and C3 in Appendix B. The magnitude of  $C_v$  ranges from 0.0024  $\text{cm}^2/\text{sec}$  to 0.0001  $\text{cm}^2/\text{sec}$  and generally decreases with increasing stress above the preconsolidation stress.

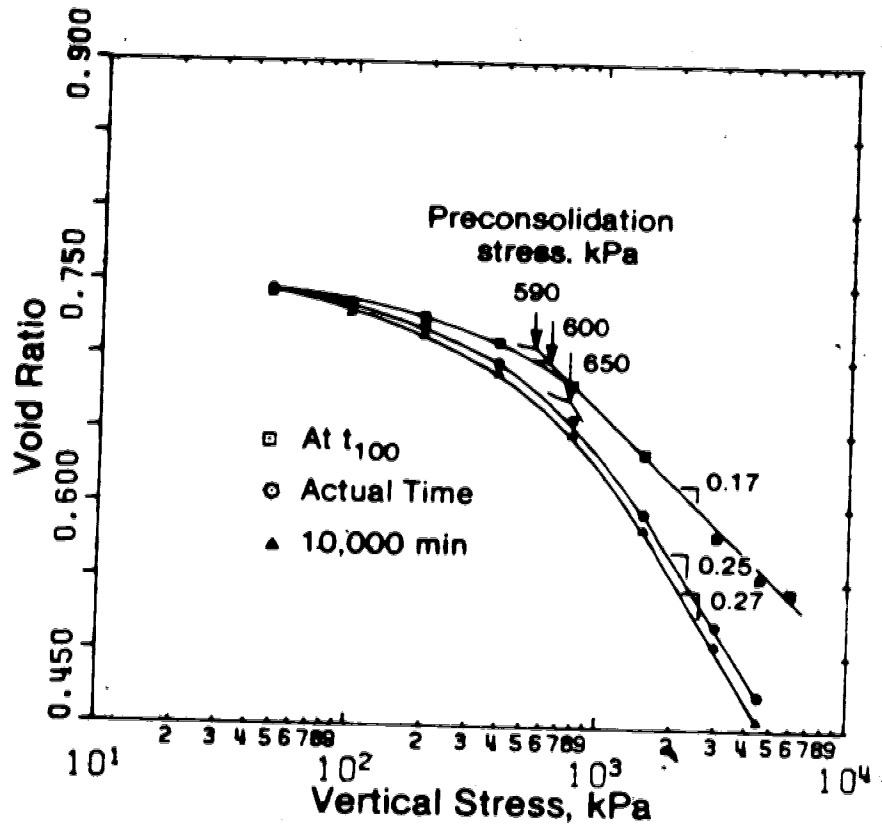


Figure 5.2 Void ratio versus vertical stress, sample C1

### 5.3.2 Coefficient of Secondary Consolidation

It is possible to analyse the creep behaviour of a soil from laboratory test results in a number of ways. The most common for oedometer test results is to determine the coefficient of secondary consolidation,  $C_{\alpha}$ , according to Equation 3.11 and plot it against the vertical stress. This section is devoted to an analysis of this type. Another possible analytical route is to plot the logarithm of vertical strain rate versus the logarithm of time and proceed with an analysis according to Singh and Mitchell (1968). The next section is devoted to this alternate approach.

For each void ratio versus logarithm of time curve  $C_{\alpha}$  was determined graphically assuming that the slope of the curve is independent of time in the secondary range. Figure 5.3 shows the variation of  $C_{\alpha}$  with vertical stress for all three samples. There is some tendency for  $C_{\alpha}$  to level off with increasing stress, especially where the load increment ratio drops below one. This is consistent with other work, such as that by Mesri and Godlewski (1977) and Muryama and Shibata (1964) who found that  $C_{\alpha}$  was a constant at stresses above one to two times the preconsolidation stress.

Mesri (1973) presented a global correlation between water content and the coefficient of secondary compression, an analogous form of  $C_{\alpha}$ , which is given here as Figure 5.4. The oedometer test results are plotted on Figure 5.4 and fit his correlation quite well. According to Mesri's (*op.cit.*)

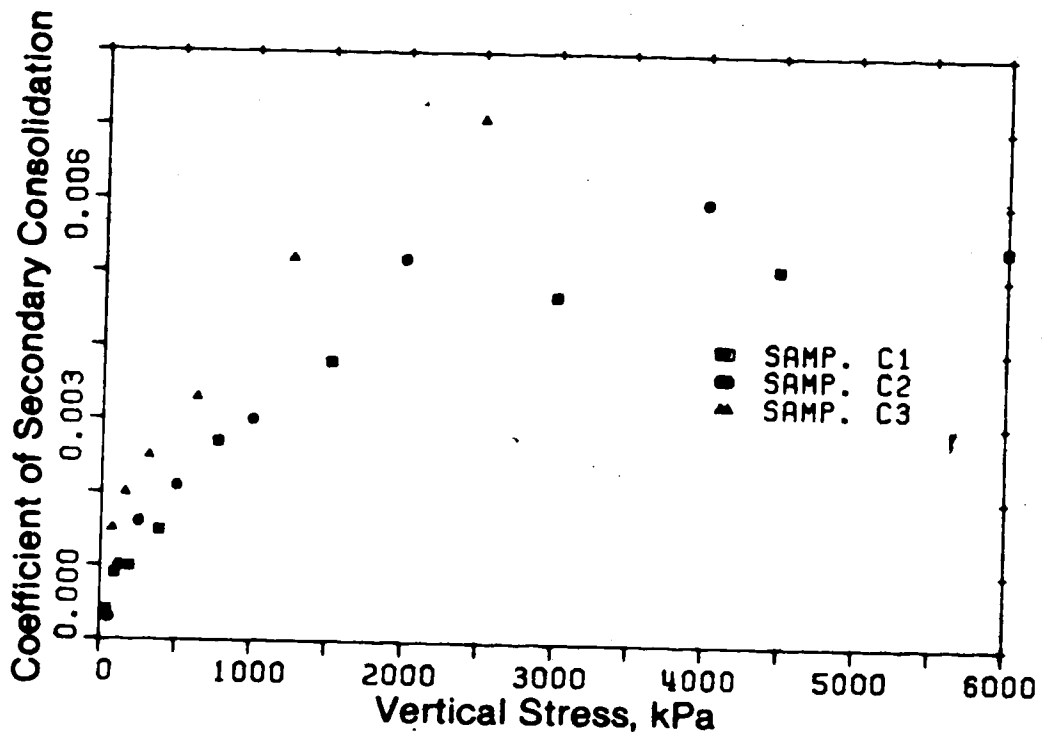


Figure 5.3 Coefficient of secondary consolidation versus vertical stress



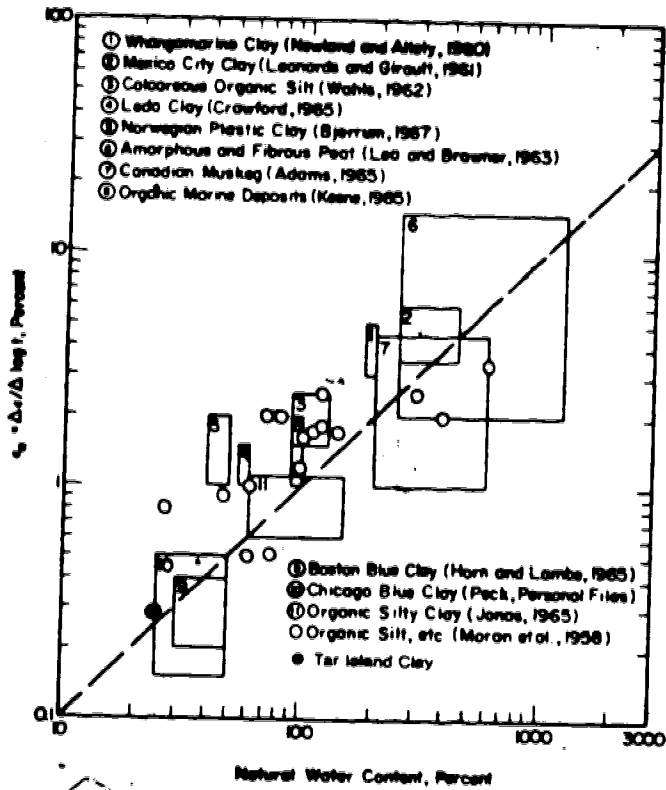


Figure 5.4 Coefficient of secondary compression for natural soil deposits, after Mesri, 1973

creep classification system for the oedometer stress state, the clay test here has a 'low' secondary compressibility.

### 5.3.3 Vertical Strain Rate

As mentioned previously the oedometer data can also be analysed in terms of the logarithm of vertical strain rate versus the logarithm of time. The results from the test on sample C2 are plotted in this manner in Figure 5.5. Similar plots are included in Appendix B for samples C1 and C3. The vertical strain rate was calculated, after da Fontoura (1980), using a moving five point linear regression analysis on the strain versus time data. The vertical strain was calculated on the basis of the sample height at the beginning of each increment. Analysing the data in this fashion is not new. It was first done by Wilson and Lo (1965) and, later, by Lovenbury (1969) and Tavenas *et.al* (1978).

Each strain rate versus time curve in Figure 5.5 can be broken into two sections based on the shape of the curve and time. In the first section which is at times less than  $t_{...}$ , as determined from the void ratio versus time curves, the strain rate continually decreases with time in a nonlinear manner. The time dependent deformation is a result of both transient consolidation and creep effects.

In the second section of the curve at times greater than  $t_{...}$  the strain rate decreases continually with time but in a linear fashion. The deformation is considered to be

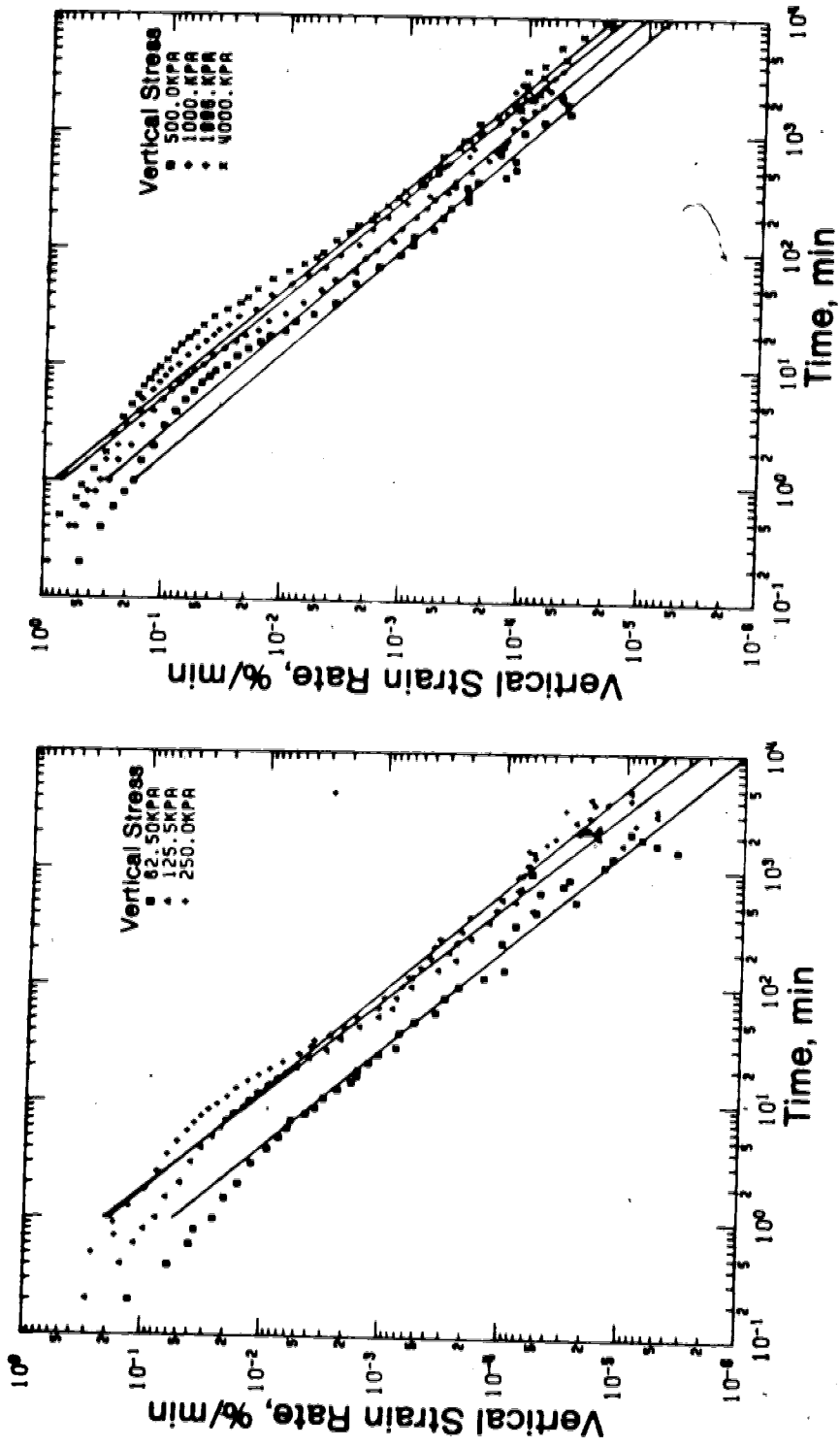


Figure 5.5 Vertical strain rate versus time , sample C2

entirely a result of creep effects. A linear regression analysis was used to best fit a line through the data points of this part of the curve.

The slope of these best fit lines is equivalent to the creep parameter,  $m$ , in Equation 3.2. The value of  $m$  for all three samples ranges from 1.01 to 1.29 with a mean of 1.12 (standard deviation=0.07). The values of  $m$  for each test for each sample are included in the summary tables for the oedometer tests and are plotted in Figure 5.11. The variation in  $m$  is small and is attributable to sample variations. From this data it is apparent that  $m$  is independent of vertical stress and load increment ratio. It is assumed that  $m$  is independent of the duration of the transient consolidation effects.

It is obvious from Figure 5.5 that an increase in the vertical stress causes an increase in the strain rate. To investigate the influence of vertical stress, the strain rate at time equals one minute (unit strain rate) for the best fit lines has been plotted against vertical stress in Figure 5.6. This figure shows that the unit strain rate increases with stress at lower stresses and then appears to level off at higher stresses especially when the load increment ratio drops below one. It is assumed that transient consolidation does not effect the position of the strain rate curves, that is, the magnitude of the unit strain rate. The best fit lines in Figure 5.6 can be described by a relationship of the Singh-Mitchell type as

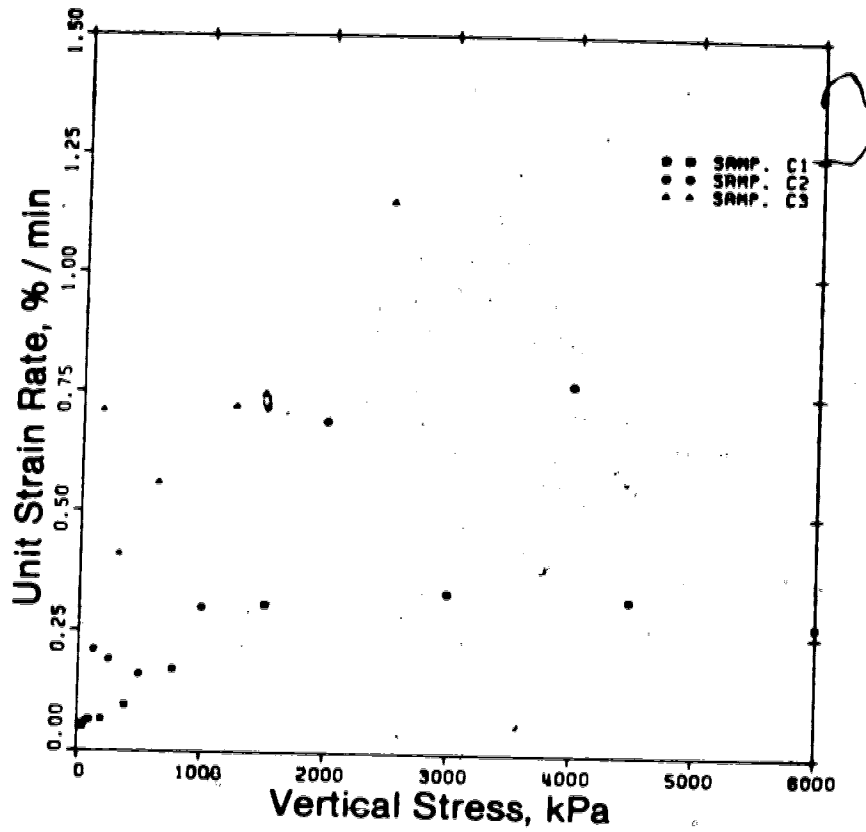


Figure 5.6 Unit strain rate versus vertical stress, oedometer tests

follows:

$$\dot{\epsilon}_v = A(1/t)^m \quad 5.1$$

- where  $\dot{\epsilon}_v$  = vertical or volumetric strain rate  
 $A$  = unit strain rate, a function of vertical stress and load increment ratio  
 $t$  = time  
 $m$  = 1.12, a constant

The difference between Equations 3.2 and 5.1 is the lack of a shear stress level term in Equation 5.1. This is a result of the stress state in the oedometer test. Regardless of the vertical stress the shear stress level is a constant in the oedometer and its effect is therefore included in  $A$ . It follows from this that the dependence of  $m$ , if any, on shear stress level cannot be evaluated with oedometer tests.

It must also be added that since  $m$  is not precisely equal to one then the assumption of  $C_\alpha$  being independent of time in Section 5.3.2 is incorrect.  $C_\alpha$  decreases with time.

#### 5.4 Triaxial Creep Test Results

##### 5.4.1 General

The results of two suites of drained triaxial creep tests are presented in this section. Both suites consist of three samples, each consolidated under different isotropic

consolidation pressures. The samples in one suite were prepared with the bedding plane horizontal and are numbered T1, T2 and T4. The samples in the other suite were prepared with the bedding plane inclined at an angle of  $45^\circ$  and are numbered I1, I2 and I3. The suite of inclined samples was tested at  $45^\circ$  to investigate the anisotropy of the creep behaviour but also to have the maximum shearing stress along the bedding plane. The relevance of this stress orientation to the field problem is discussed in Chapter 6.

All samples were consolidated isotropically to pressures above the average preconsolidation stress determined from the oedometer testing program. The stress range below the preconsolidation stress was not investigated in shear since only the normally consolidated creep behaviour of clays is of interest here and differs from the overconsolidated behaviour. The final isotropic consolidation pressures during shear were varied from 740 kPa to 1500 kPa between samples which allowed an investigation of the influence of normal effective stress or water content on the creep behaviour. This is of importance in a field problem of this type where the effective stresses vary substantially in the lateral and vertical directions.

The test results from the isotropic consolidation stage are presented in the next section. The results from the incremental creep tests are then presented. Following is a discussion of the various factors which influence the creep parameters in the Singh-Mitchell equation derived from this

testing program.

#### 5.4.2 Isotropic Consolidation

All samples were consolidated isotropically in pressure increments,  $\Delta\sigma/\sigma$ , of one to the selected pressure for testing. It is generally considered that a sample consolidated anisotropically along the same stress path it has experienced in the field will yield results that are more indicative of the field behavior than an isotropically consolidated sample. For this field situation consolidating anisotropically would have brought the sample to the 60 % stress level at the beginning of the incremental creep test which would have precluded the study of the creep behaviour below this stress level. Since the proper definition of the stress level term in the Singh-Mitchell equation requires testing at stress levels below 60 %, the samples were consolidated isotropically. )

The isotropic consolidation results for the vertical and inclined samples are presented in Tables 5.3 and 5.4 respectively. The vertical strain and vertical strain rate versus time curves are presented in Figure 5.7 for the last consolidation step of sample I2. Similar plots are contained in Appendix C for the remainder of the consolidation steps for sample I2 and the corresponding curves for samples I1 and I3. The volume changes for the inclined samples given in Table 5.4 are calculated from the axial strain readings assuming that the sample is isotropic. Axial displacement



Table 5.3 Summary of isotropic consolidation results, vertical samples

Sample No.	$\sigma'_v$ (kPa)	Volume Change (cm <sup>3</sup> ) <sup>(1)</sup>	Height (cm)	Volume (cm <sup>3</sup> )	Time (min)	B Test Result <sup>(4)</sup>
T1	0	0	6.39	45.17	-	0.97
	165	-0.9	6.35	44.27	1176	
	559	-1.29	6.29	42.97	5592	
	1103	-1.09	6.24	41.88	4328	
T2	0	0	5.83	40.93	-	0.98
	(*)	+5.07 <sup>(2)</sup>	6.07	46.00	1116	
	190	-3.25	5.93	42.75	5523	
	380	-0.54	5.91	42.21	4433	
	758	-0.79	5.87	41.42	4450	
T4	0	0	6.15	44.34	-	0.97
	187	+0.27	6.16	44.61	4312	
	377	-0.60	6.13	44.01	2740	
	722	-0.74	6.10	43.28	1441	
	1500	-1.38	6.04	41.89	4074	
	0 <sup>(3)</sup>	+1.15	6.09	43.04	613	
	827	-1.51	6.02	41.53	1485	
1507	-0.85	5.98	40.70	5734		

(1) volume change readings are calculated including a leakage correction

(2) burette seriously malfunctioned, replaced, reading only approximate

(3) cell pressure reduced to zero due to leakage of cell fluid through a crack in cell top, replaced, sample reconsolidated

(4) backpressure is 207 kPa for all samples

(\*) sample swelled at 0 kPa

Table 5.4 Summary of isotropic consolidation results, inclined samples

Sample No.	$\sigma_i$ (kPa)	Volume Change (cm <sup>3</sup> ) <sup>(1)</sup>	Height (cm)	Volume (cm <sup>3</sup> )	Time (min)	B Test Result
I1	0	0	6.70	48.63	-	0.92
	365	1.14	6.65	47.49	5790	
	743	0.85	6.61	46.64	4017	
I2	0	0	6.81	49.86	-	0.98
	334	1.05	6.76	48.81	2600	
	672	0.77	6.72	48.04	4145	
	1386	1.80	6.64	46.24	4549	
I3	0	0	6.39	47.35	-	0.96
	271	2.28	6.29	45.08	1405	
	548	0.85	6.25	44.23	1370	
	1090	1.25	6.19	42.98	4539	

(1) calculated from axial strain assuming deformation is isotropic

(2) absolute value of slope of logarithm of axial strain rate versus logarithm of time

(3) backpressure is 310.3 kPa for I3 and 413.7 kPa for I1 and I2

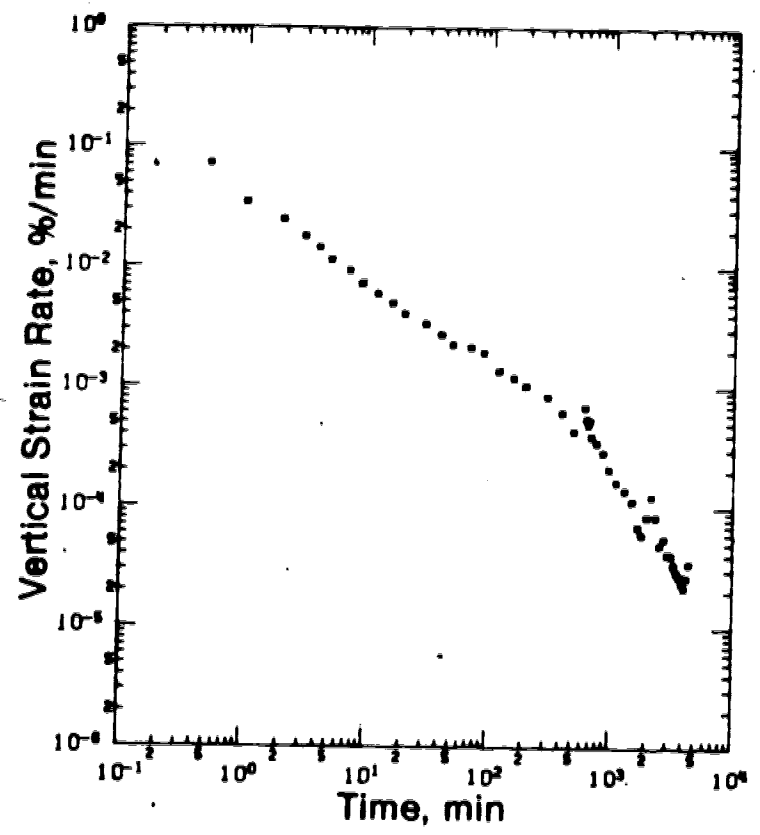
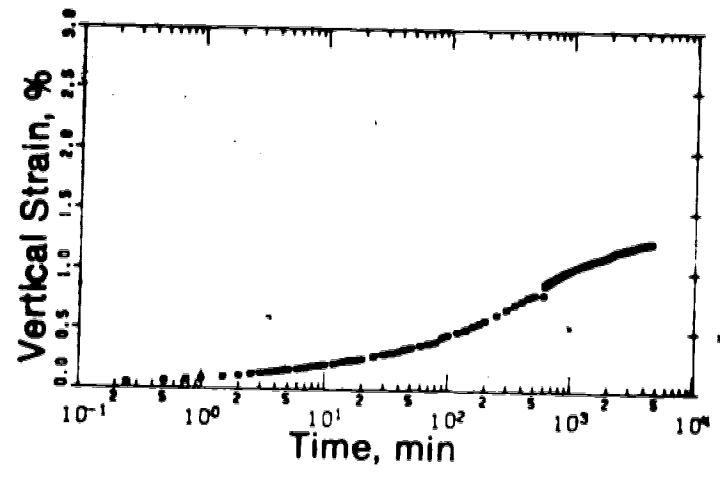


Figure 5.7 Vertical strain and strain rate versus logarithm of time ,sample I2, consolidation pressure=1386 kPa

readings were not taken with time for the vertical samples. The volume changes given in Table 5.3 for the vertical samples are from the burette readings and have been corrected for leakage.

The axial strain in Figure 5.7 is calculated on the basis of the sample height at the beginning of the consolidation increment. The strain rate curve in Figure 5.7 shows the same characteristic shape as the oedometer strain rate curves. The creep portion of the strain rate curves for all the inclined samples have much steeper slope than the oedometer samples. Deformation due to creep under isotropic stresses appears to cease with time especially at the lower consolidation pressures.

#### 5.4.3 Incremental Creep

The results of the incremental creep tests are presented in this section. A summary of the test results for sample T4 is given in Table 5.5. Vertical strain versus time for each creep increment of sample T4 is given in Figure 5.8. The axial strain is calculated on the basis of the sample height at the end of isotropic consolidation. The stress levels included in Table 5.5 and on Figure 5.8 are the ratio of the shear stress during the increment divided by the shear stress at failure. Similar summary plots and tables to those presented for sample T4 are contained in Appendix C for all the other samples.

Table 5.5 Summary of incremental creep test results, sample T4

Incr. No.	Deviator Initial (kPa)	Stress Final (kPa)	Stress Level (%)	Time (min)	Axial Strain (%)	Cumulative Axial Strain (%) <sup>(2)</sup>
1	350	350	13.2	1303	0.34	0.34
2	781	777	29.4	14541	1.32	1.66
3	1070	1068	40.3	1331	0.43	2.09
4	1365	1358	51.4	12747	1.82	3.91
5	1727	1717	65.1	1200	1.14	5.05
6	1982	1947	74.7	2821	2.94	7.99
7	2147	2143	80.9	14538	2.23	10.22
8	2328	2312	87.7	4194	1.02	11.24
9	2434	2395	91.7	7340	2.26	13.50
10	2550	2485	96.1	3317	3.48	16.98
11	2582	2539	97.3	1121	2.24	19.22
12 <sup>(1)</sup>	2654	2619	100.0	130	1.73	20.95

Total duration of test=64583 min,  $\sigma_1=1507$  kPa

<sup>(1)</sup> Failure

<sup>(2)</sup> Strain at the end of the increment

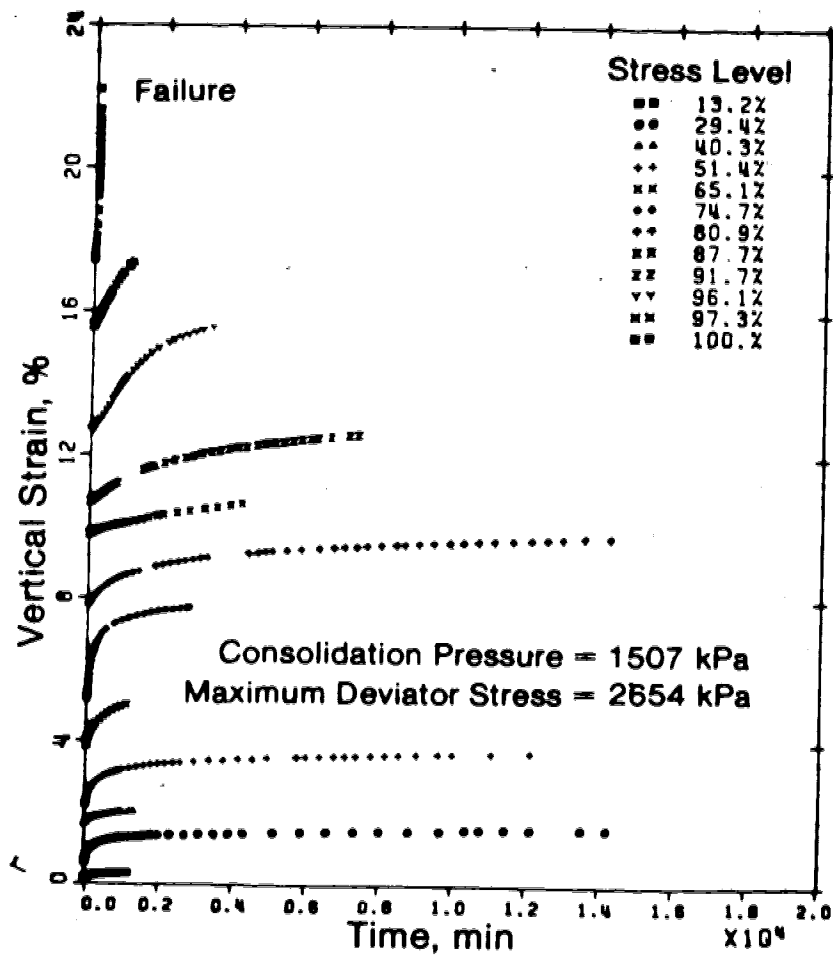


Figure 5.8 Vertical strain versus time ,sample T4

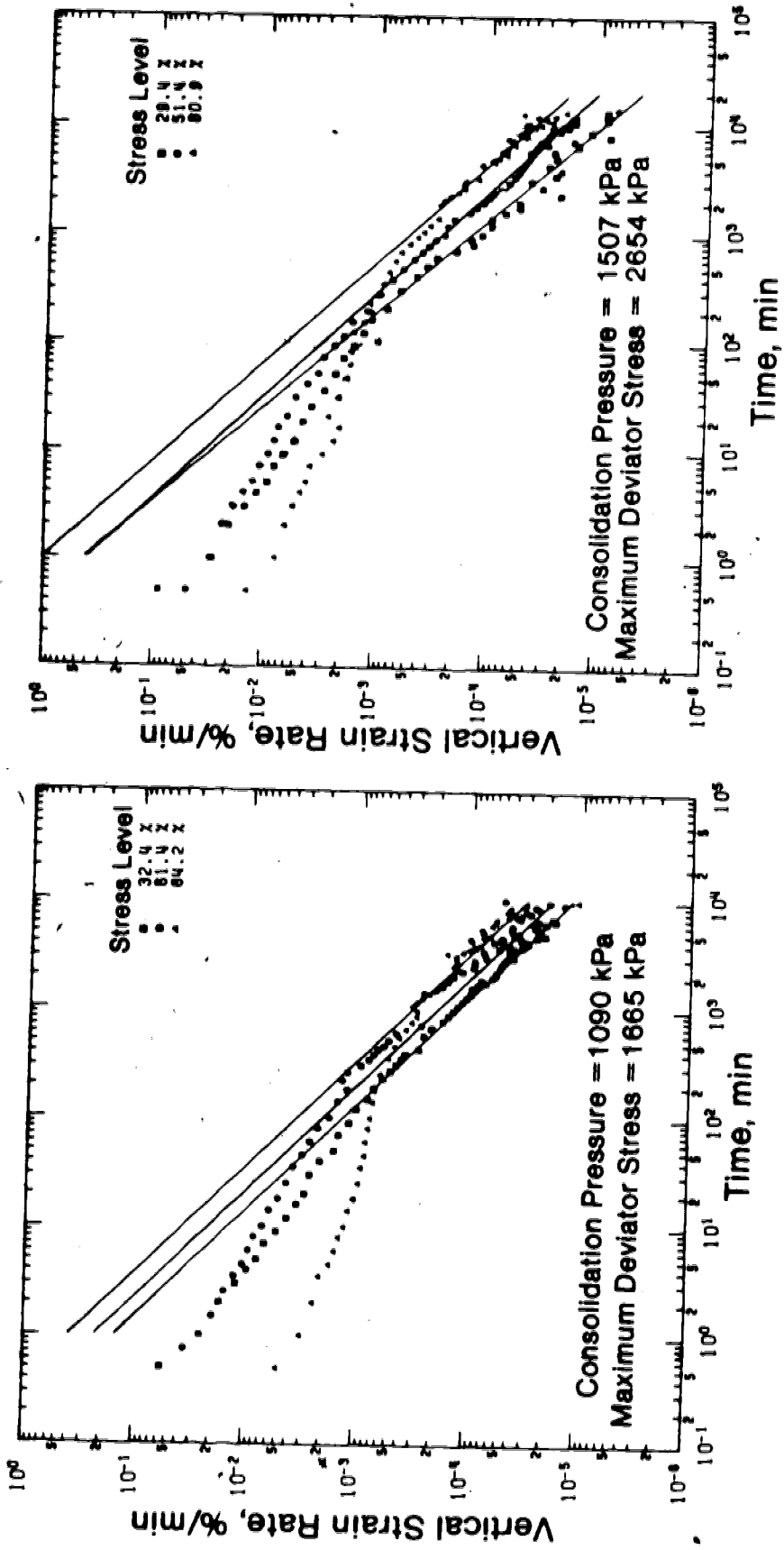


Figure 5.9 Vertical strain rate versus time , sample I3-left, sample t4-right)

The strain rate has been calculated for the incremental creep results in the same manner as for the oedometer test results. A plot of the logarithm of strain rate versus the logarithm of time is shown in Figure 5.9 for samples T4 and I3. The strain rate results for the extended increments only are shown on Figure 5.9. Stress levels for the extended increments are also indicated on Figure 5.9. The strain rate plots for the other samples are included in Appendix C.

The strain rate plot in Figure 5.9 has the same characteristics as the strain rate plot for the oedometer test shown in Figure 5.5. The strain rate decreases continuously with time for the length of the test. The strain rate for the initial portion of the curves decreases continuously but in a nonlinear fashion. This strain is a result of both consolidation and creep effects. In the latter portion of the curve the strain rate decreases continuously in a linear fashion and is entirely due to drained creep.

Other authors, notably Lovenbury (1969) and Tavenas *et.al* (1978) have also recorded transient consolidation effects on strain rate versus time plots for drained triaxial creep tests. As an example, the strain rate versus time for Pancone Clay from Lovenbury (*op.cit.*) is illustrated in Figure 5.10. A strain instability at approximately 40 to 100 days is clearly evident on Figure 5.10. It is considered that the duration of the transient consolidation effect depends upon the coefficient on



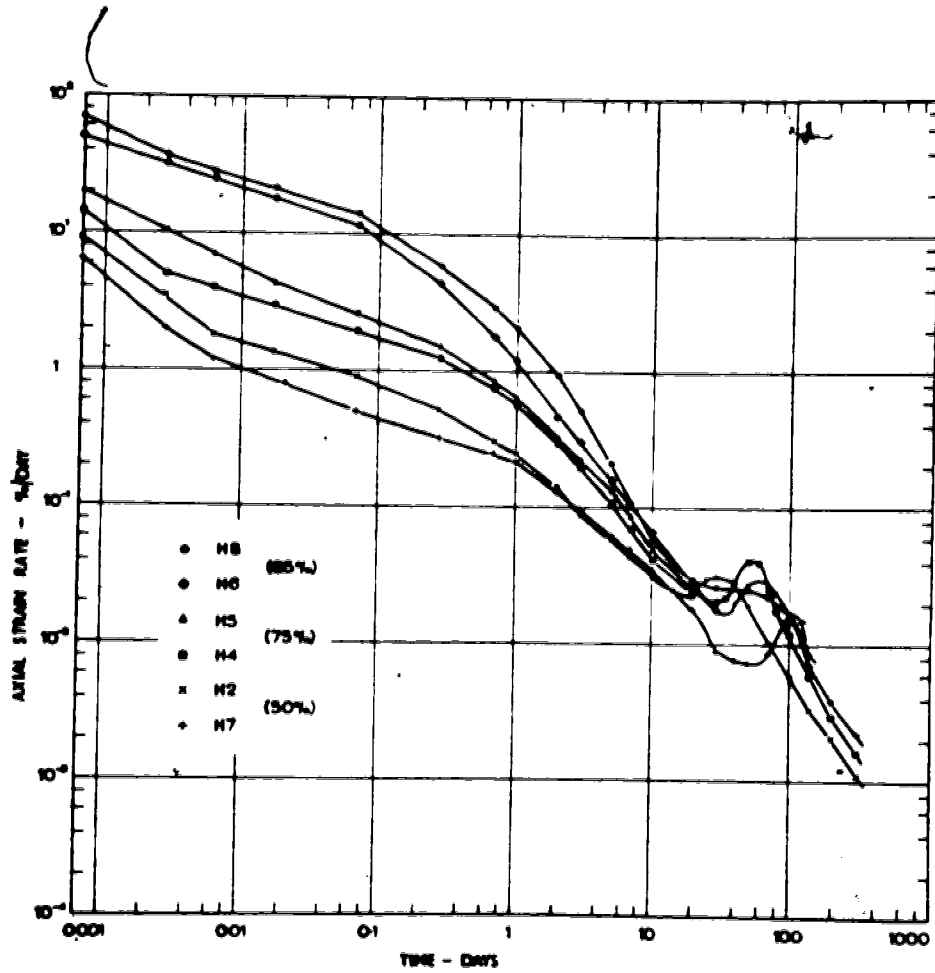


Figure 5.10 Strain rate versus time for Pancone clay (after Lovenbury, 1969)

consolidation,  $C_v$ , the sample drainage conditions, the sample size and the load increment ratio,  $\Delta\sigma/\sigma$ . A drained creep incremental test should be designed so that each of these factors is manipulated to minimize the duration of the transient effect.

For the purposes of the interpretation of the test results reported herein it is assumed that the duration of the transient effect does not influence the slope of the linear portion of the strain rate versus time curves or the position of the curves, that is, the magnitude of the strain rate for any given time after the transient effect. To this end a best fit straight line based on a linear regression analysis has been drawn through the linear portion of the strain rate curves and extrapolated to lesser times ignoring the transient effect.

A summary of the creep parameters for the strain rate plots for all samples is given on Table 5.6. The slope of the lines,  $m$ , is plotted against octahedral stress, the first stress invariant, for all triaxial samples and the oedometer samples in Figure 5.11. The average value of  $m$  for all tests is 1.13. The unit strain rate for all triaxial samples is plotted versus stress level in Figure 5.12. It is observed that the slope of the curves are similar with the exception of sample I2 and average approximately 3.0. The average value of the unit strain rate at zero stress level is approximately 0.18 %/min with a range of 0.54 %/min to 0.04 %/min.

Table 5.6 Summary of incremental creep test results, all samples

Sample No.	Stress Level (%)	σoct (kPa)	n	Unit Strain Rate (%/min)	Duration of Increment (min)
T1	23.6	1446	1.15	0.28	16742
	49.9	1827	1.19	0.84	15754
	67.4	2081	1.19	1.8	27255
T2	26.7	880	1.09	0.11	17171
	53.8	1004	1.10	0.33	17418
	76.9	1110	1.11	0.70	20418
T4	29.4	1767	1.15	0.44	14541
	51.4	1962	1.11	0.59	12747
	80.9	2223	1.10	1.0	14538
I1	36.3	881	1.15	0.25	6800
	68.1	1001	1.21	0.60	1431
	83.4	1059	1.21	0.88	13189
I2	34.2	1618	1.26	1.14	7103
	63.3	1816	1.20	1.80	10180
	88.0	1984	1.20	5.20	8845
I3	32.4	1277	1.00	0.14	7123
	61.4	1438	1.06	0.45	10110
	84.2	1564	1.06	0.70	9915

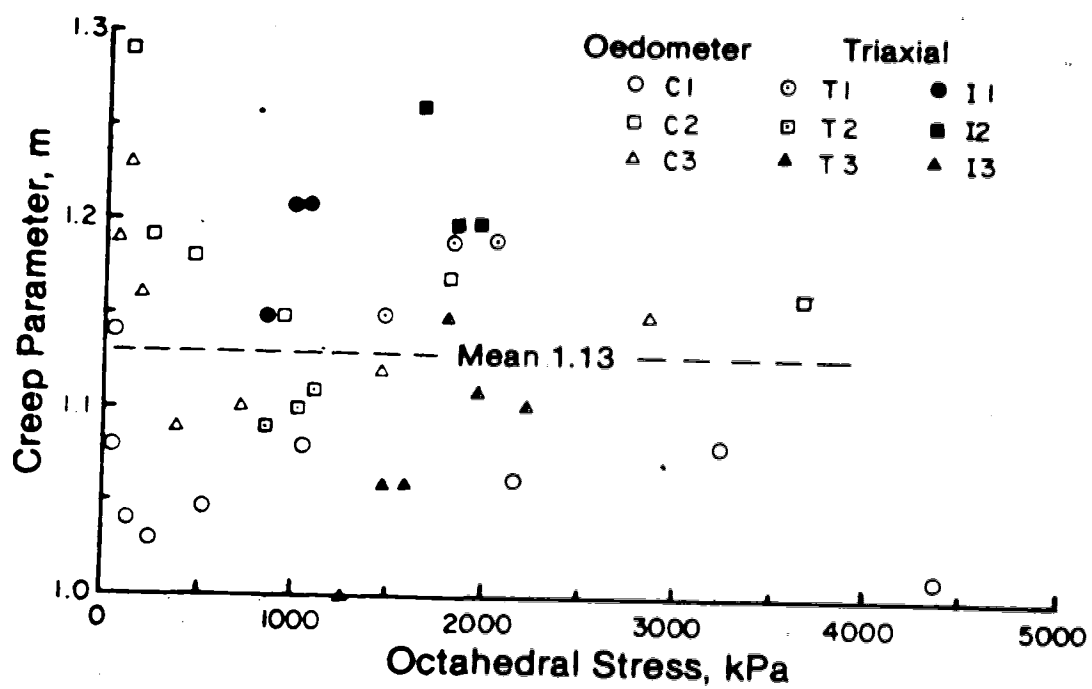


Figure 5.11 Creep parameter,  $m$ , versus octahedral stress

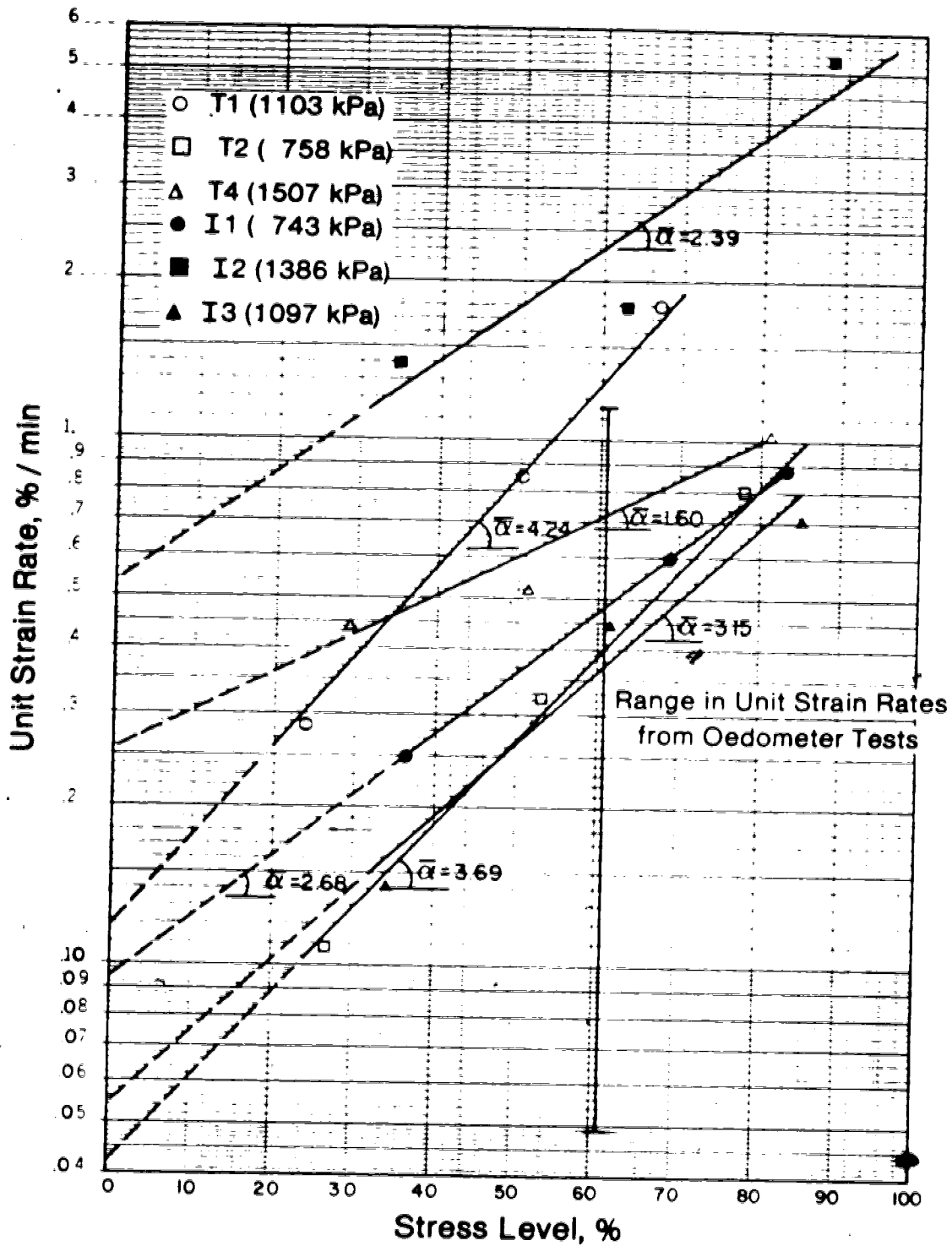


Figure 5.12 Unit strain rate versus stress level, triaxial tests

From Figures 5.11 and 5.12 it is apparent that the creep behaviour of this clay fits a Singh-Mitchell relationship because:

1. The strain rate versus time decreases linearly on a  $\ln-\ln$  plot.
2. The creep parameter,  $m$ , is independent of stress level.
3. The strain rate increases exponentially with stress level for a given time.

If the average parameters from all tests are used the vertical strain rate versus time can be described by a relationship of the form:

$$\dot{\epsilon}_v = .18e^{.35} (1/t)^{.35} \quad 5.2$$

Although Equation 5.2 holds for the average, it is of value to discuss the factors which influence the creep parameters,  $A$ ,  $\bar{\sigma}$  and  $m$  in Equation 5.2 in more detail.

#### 5.4.4 Factors Influencing Creep Parameters

##### 5.4.4.1 Stress State

The influence of stress state on the creep parameters can be evaluated from a comparison of the oedometer and triaxial test results. The value of the creep parameter,  $m$ , as shown on Figure 5.11 is insensitive to stress state. The unit strain rate for the oedometer test results are plotted on Figure 5.12 for an assumed stress level for the oedometer stress state and this soil of 61 percent. Again the

oedometer results are approximately similar to the triaxial test results.

It appears from this limited comparison that the influence of stress state on the creep parameters is small compared to sample variations. This conclusion cannot be extrapolated to other stress states such as plane strain simple shear without additional testing however. The influence of stress state will be discussed further in Chapter 6.

#### 5.4.4.2 Anisotropy

The average values of  $m$  for the vertical and inclined samples are 1.13 and 1.15 respectively. The average values of  $\bar{a}$  for the vertical and inclined samples are 3.18 and 2.74 respectively. It is apparent that any effects due to anisotropy are masked by sample variation. Any effect of the possible cohesion discussed in section 5.2.3 does not manifest itself in the creep behaviour of the clay.

#### 5.4.4.3 Octahedral Stress

The value of the parameter,  $m$ , as shown in Figure 5.11 is insensitive to octahedral stress for both the triaxial and oedometer tests. The value of the stress level term,  $\bar{a}$ , for the triaxial tests does not show a consistent relationship with isotropic consolidation stress for either the inclined or vertical samples. The same is true for the parameter  $A$ . The equivalent parameter  $A$  in the oedometer tests shows some tendency to a constant value above the

preconsolidation stress.

It may therefore be stated that the creep parameters in Equation 5.2 are not influenced by the magnitude of the octahedral stress.

#### 5.4.4.4 Testing Procedure

The effect of the incremental testing procedure on the creep parameters in Equation 5.2 cannot be definitely stated, since it is not possible to compare the results with single increment tests. As discussed in Chapter 4 single increment tests cannot be used to examine drained creep at high stress levels since the soil will fail in undrained shear before drainage occurs. An advantage of an incremental creep test is that the creep behaviour of a single soil sample can be examined at a variety of stress levels. The influence of the variation in properties between soil samples is thus eliminated.

The key variable which can be used to manipulate the results from an incremental creep test is the stress increment ratio,  $\Delta\sigma_1/\sigma_1$ . The magnitude of  $\Delta\sigma_1/\sigma_1$  is governed by Equation 4.3 and must decrease with increasing  $\sigma_1$ . The ratio,  $\Delta\sigma_1/\sigma_1$ , governs the duration of transient consolidation, the relative importance of previous creep strains on the strains during the present increment and the influence of pseudo-preconsolidation on the strains in the succeeding increments.



### Transient Consolidation

Tavenas *et.al* (1978) in a comprehensive series of drained creep tests postulate that the stress increment ratio must be kept less than 0.3 in order to diminish the relative effect of primary consolidation strains to creep strains. The effect of consolidation was probably not pronounced for the results of Tavenas *et.al* (*op.cit.*) because the soil tested, St. Alban clay, is overconsolidated at the low stresses, less than 50 kPa, used during their testing program. It is considered that decreasing the drainage path is more effective than manipulation of stress increment ratio in reducing the effect of consolidation.

### Previous Creep Strains

It is not clear how the previous creep strains affect the creep strains at succeeding increments. Mitchell *et.al* (1969) have examined this problem for undrained creep tests on soil and have related the creep strain rates between increments by a relationship of the form:

$$\xi(D_2, t) / \xi(D_1, t) = (t/t')^m + (t/t' - 1)^m (e^{a(D_2 - D_1)} - 1) \quad 5.3$$

$$a = \ln(Y+1) / (D_2 - D_1) \quad 5.4$$

$$Y = ((t_j - t')/t_i)^m [ \xi(D_2, t_j) / \xi(D_1, t_i - (t_i/t_j)^m ) ]$$

The variables in Equation 5.3 are defined in Figure 5.13. Equation 5.3 was derived from Equation 3.2 with the assumption that the net strain in the second increment is independent of the accumulated strain in the previous increment. Using this equation they find that the creep parameter,  $\bar{a}$ , is the same for multiple increment tests as for single increment tests.

#### Pseudo-Preconsolidation

As a sample experiences drained creep the effective stress state remains constant but the yield surface must move away from the effective stress point of the sample because of the decrease in volume of the sample. The stress increment ratio must be high enough to overcome this pseudo preconsolidation or the soil may behave in an overconsolidated manner. This effect can be reduced by limiting the duration of the intervening stress increments between the extended increments to the minimum necessary to dissipate the pore pressure.

### 5.5 Shear Strength Results

#### 5.5.1 General

Although the primary objective of the incremental tests was to evaluate the creep behaviour of the clay, the results also yield the stress-strain and strength properties of the

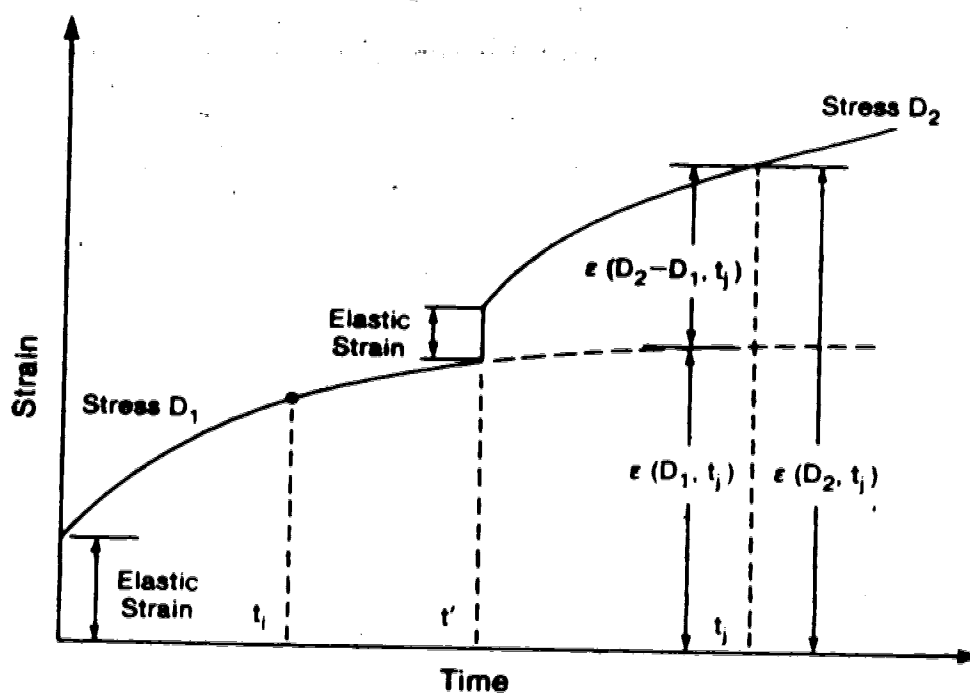


Figure 5.13 Strain versus time relationship for step-creep test (after Mitchell et al., 1969)

141

clay. The stress strain behaviour is discussed in the next section. This is followed by a discussion of the strength properties which includes a comparison with the strain controlled test results from Hardy Associates (1978) Ltd. (see Design Review Panel, 1977).

### 5.5.2 Stress-Strain Behaviour

The results from the incremental tests, as shown in Figure 5.7, can also be plotted in the conventional manner of deviatoric stress versus strain. Such a plot is shown in Figure 5.13 for sample I3. Similar plots for all other tests are included in Appendix C.

The stress and strain at the beginning and the end of each increment on Figure 5.13 are shown and these points are joined by straight lines. This straight line path represents the stress strain path followed by the sample during the test. A smooth line is also drawn through the final stress-strain point of each extended increment. The smooth line represents the long term stress strain behaviour of the clay.

The stress strain curves demonstrate that the material is ductile with strains to failure in excess of 10 percent. The clay continually compresses during shear. The volume change curve levels off at higher stresses.

All samples failed along distinct shear planes and as with all stress controlled tests, failure was catastrophic. It is known that the clay is strain softening (see Design

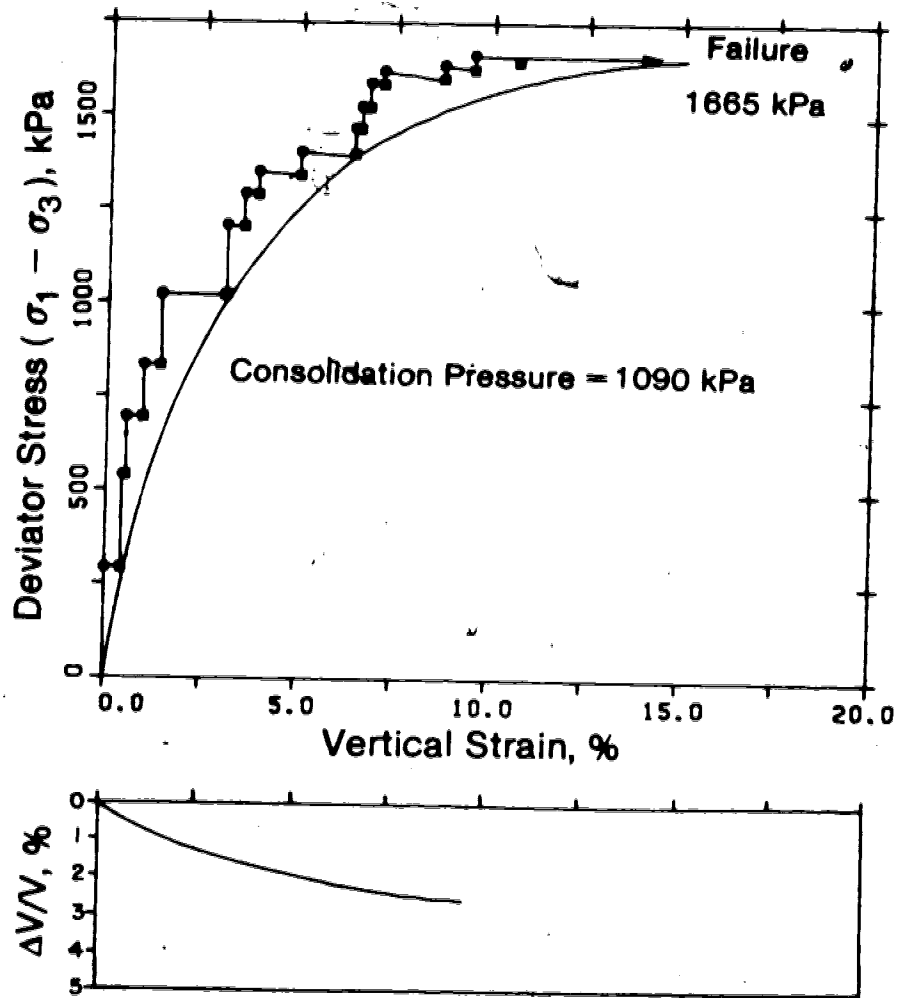


Figure 5.14 Stress-strain curve , sample 13

Review Panel, 1977) but it was not possible to evaluate this characteristic in a stress controlled test. Photographs of all failed specimens are included in Appendix C. The inclined specimens failed along bedding and, usually, along obvious organic layers. The vertical samples failed across bedding.

It must be stated the sample T2 was not taken to failure although the final vertical strain approached 14 %. It is estimated that the final imposed stress is within 5 % of the failure stress.

### 5.5.3 Strength Envelope

A p-q plot of the shear strength results are presented in Figure 5.15 for both the creep tests and the strain controlled tests from Hardy Associate Ltd. The effective angle of shearing resistance,  $\phi'$ , for all tests is  $26.5^\circ$ . The effective cohesion intercept,  $c'$ , is zero. These results are based on a best fit line through all of the data points shown on Figure 5.15. It is apparent that the shear strength results determined from this testing program are consistent with previous work.

An angle of  $24^\circ$  will be used for the computations in Chapter 6 as this value is indicative of the shear strength for the portion of the soil to be analysed.

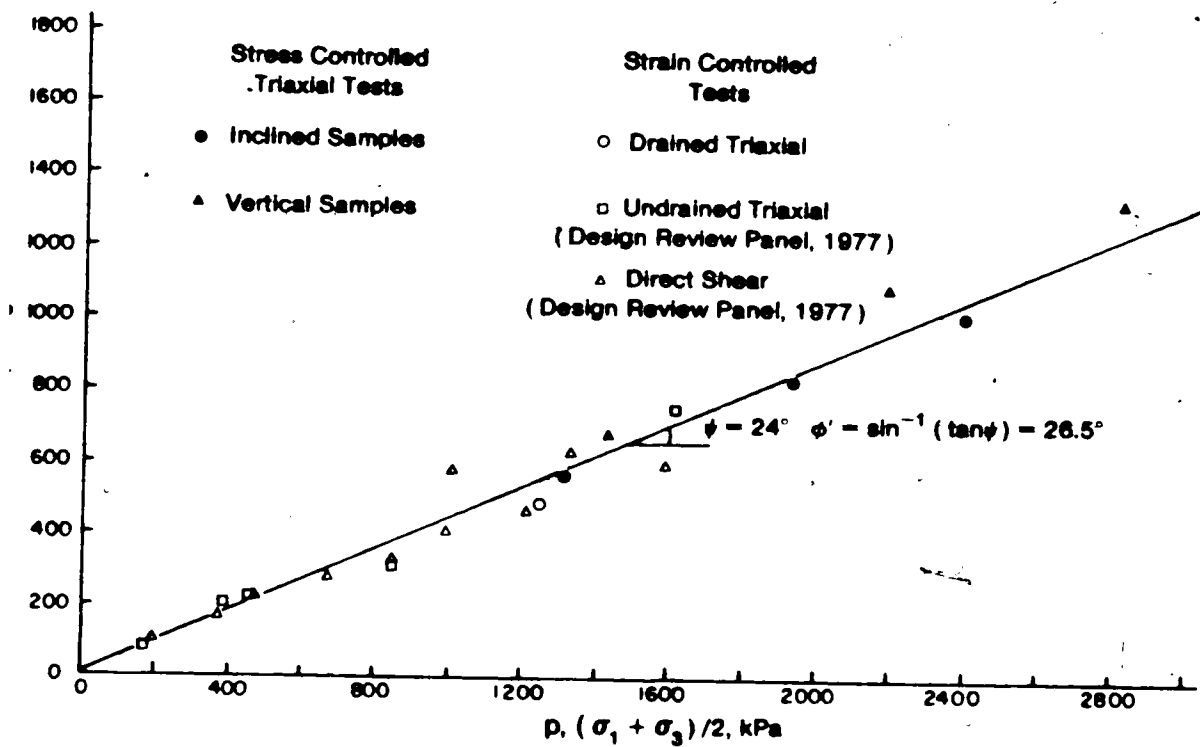


Figure 5.15 P-q plot, from creep tests and previous work

### 5.6 Concluding Remarks

The creep behaviour of Tar Island clay can be described by a Singh-Mitchell relationship. The strain rate continually decreases with time and is proportional to stress level for a given time. The effects of transient consolidation and the incremental test procedure were assumed to be negligible in fitting the creep data to the Singh-Mitchell relationship. The effects of stress state, octahedral stress and anisotropy on the creep parameters are so minor that they cannot be detected due to sample variations. It has also been shown that  $C_\alpha$  is not a constant and decreases with time.

The effective angle of shearing resistance obtained from the stress controlled tests correlates well with the previous strain controlled tests by Hardy Associates. This demonstrates that  $\phi'$  does not decrease due to creep strains over the duration of the stress controlled tests.



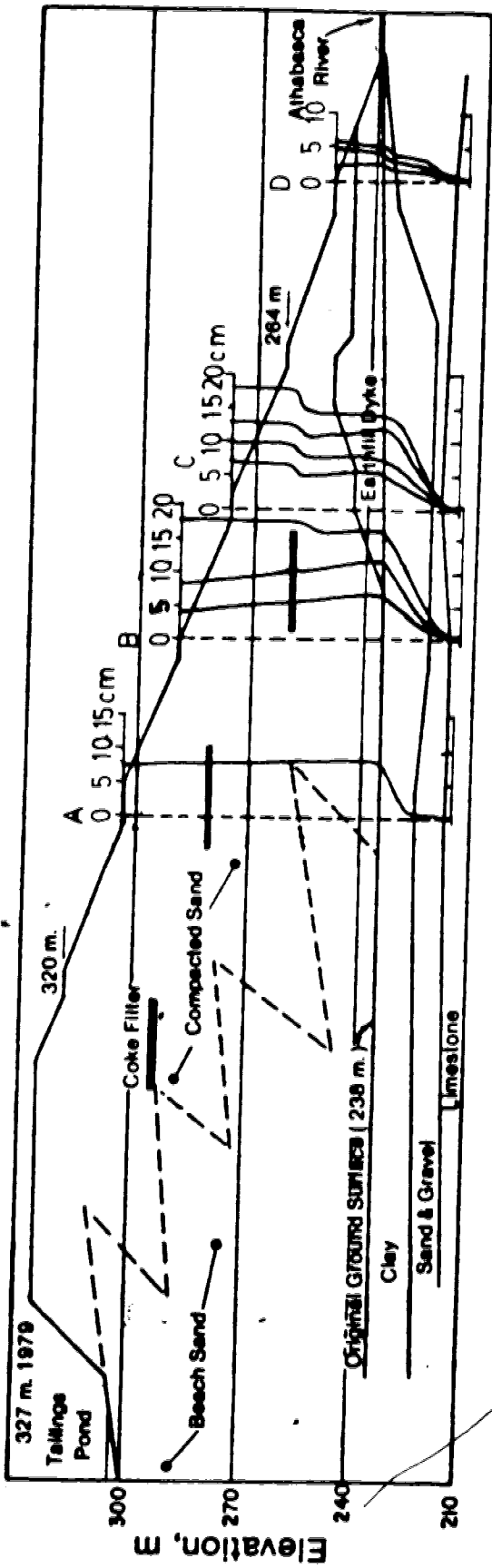
## 6. Analysis of Lateral Creep Movements in the Tar Island Dyke Clay Foundation

### 6.1 Introduction

The lateral movements of the clay foundation of Tar Island Dyke are examined in this chapter. As discussed in Chapter 2 it is considered that the time dependent movements displayed by the inclinometers are a consequence of creep rather than of lateral consolidation. The lateral creep movements of the clay foundation at Station 65+00 are shown in Figure 6.1.

A simple analysis of the lateral movements of one inclinometer is presented in this chapter. The analysis treats the boundary conditions in the immediate vicinity of the inclinometer as uniform and quasi-static. The form of the creep movements is similar for all inclinometers. A more rigorous creep analysis which would treat the inclinometer movements collectively requires the use of the finite element method because of the complex geometry and boundary conditions.

The creep problem must be considered as drained since pore pressures, where they are in excess of hydrostatic, have dissipated significantly over the duration of the creep movements analysed. It will be assumed as per Kavazanjian and Mitchell (1980) that the creep strain tensor can be decomposed into a volumetric and deviatoric component. There



Inclinometer No.	Position	Berm	Legend	Calibrated
S76-101 *	A	303 m		January 26, 1976
S76-103	B	291 m		November 2, 1976
S76-102 *	C	277 m		January 19, 1976
S76-104	D	251 m		September 16, 1976

\*Station 56+00

Inclinometer displacement profiles are shown for time intervals of one year after calibration

Figure 6.1 Lateral creep movements of the Tar Island Dyke clay foundation, Station 65+00

is some justification for this assumption in that the form of the shear strain versus depth profiles are similar for regions of the foundation that have different rates of excess pore pressure dissipation.

Lateral or horizontal strains with time have been negligible, in the order of 0.04 %, so volume change of the clay foundation must be accommodated primarily in the vertical direction. Vertical displacement readings for the clay foundation have not been recorded for Tar Island Dyke so the volumetric component of the creep strain tensor cannot be analysed. However, total volumetric strains from the the beginning of construction can be calculated from water content changes as determined from drilling. Using this method volumetric strains in excess of 20 % have occurred. Only the deviatoric component of the creep strain tensor will be analysed here.

It will be assumed for the purpose of this analysis that the creep deformations can be described by an equation of the Singh-Mitchell type. One justification for this assumption is that the laboratory creep of the clay described in Chapters 4 and 5 followed such a relationship.

The analysis then is concerned with defining the various parameters in the Singh-Mitchell equation. In order to do this it is first necessary to determine the stress state in the foundation and cast the Singh-Mitchell equation in a form applicable to this stress state.

## 6.2 State of Stress in Foundation Clay

### 6.2.1 Introduction

Tar Island Dyke has been constructed in stages from 1965 and by 1980 had reached an elevation of 327 m. It is intended to ultimately raise the dyke to 335 m. The dyke crest elevation and pond level elevation rise with time are shown in Figure 6.2. The effective stresses in the foundation clay with time are a function of the increase in dyke load with time and the dissipation of excess pore pressure with time. Since it is considered that effective stress governs the creep deformation of the soil it is necessary to determine these effective stresses for the period of the inclinometer readings. Two approaches, both of which use elastic constitutive relationships, to the solution of this problem will be described here. The use of the finite element method is necessary in both approaches because of the complex boundary conditions and incremental nature of construction.

One approach to this problem is to determine the effective stresses directly. Variations in this approach have been outlined by Eisenstein (1974), Law (1975), Nobari and Duncan (1972) and Lee and Idriss (1975). An advantage to this 'effective stress' approach is that material properties from drained or undrained laboratory shear tests with pore pressure measurements can be used directly in the finite element analysis. This procedure is necessary if

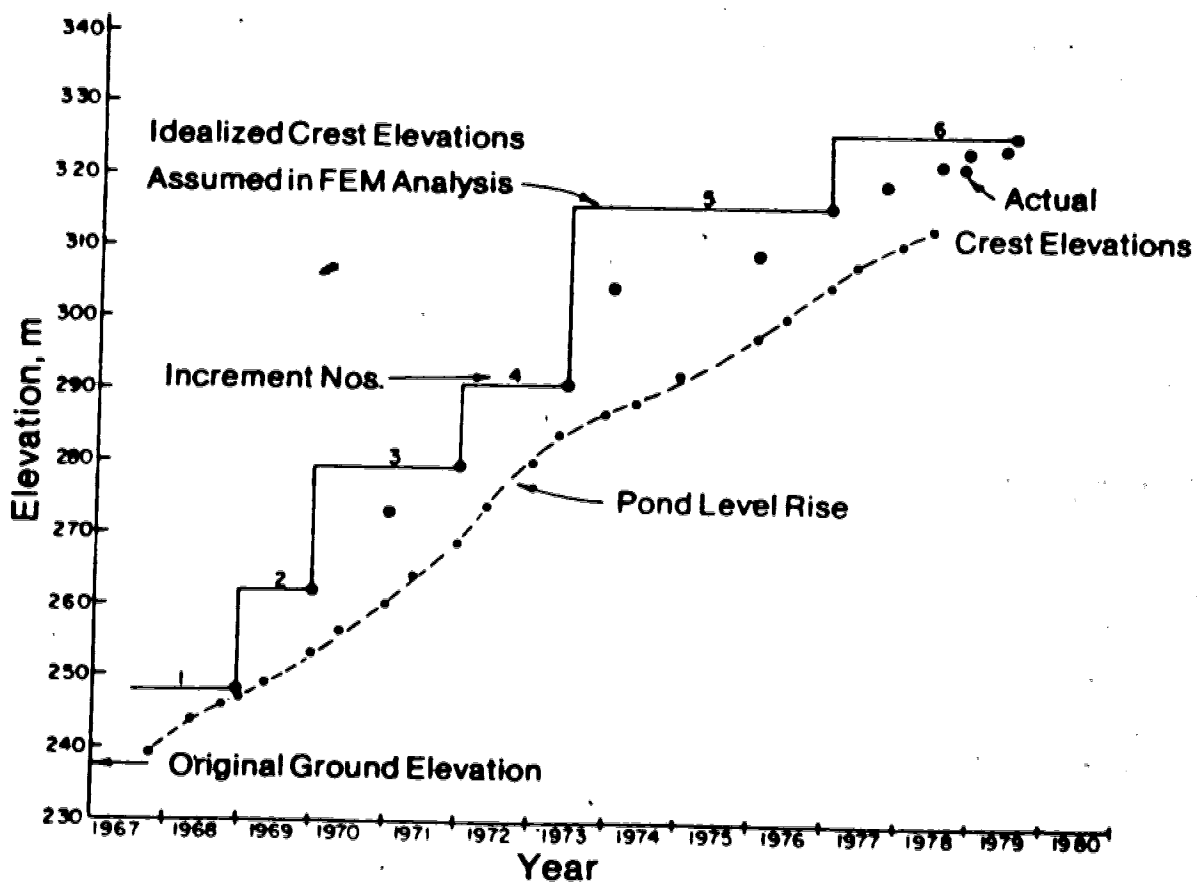


Figure 6.2 Dyke crest and pond level rise with time

displacements other than those arising from creep are to be predicted accurately. Since only stresses are required for this part of the analysis a simpler approach was adopted.

This approach employs the finite element method to determine the total stresses. The effective normal stresses are then calculated by subtracting known pore pressures measured in the field from the total stresses. This method is accurate for the determination of the effective vertical stress in the clay but is less accurate for the determination of the shear stress and the horizontal effective stress since both are highly dependent on the ratio of the material moduli and the value of Poisson's ratio. The next section describes the finite element stress analysis and the approximations used to overcome the difficulties of selecting the material parameters.

## 6.2.2 Total Stress Analysis

### 6.2.2.1 General

The finite element program, NLCP (nonlinear construction program), which was developed by Simmons (1981), was used to obtain the total stress configuration in the foundation clay. The program is reviewed in detail by Simmons (*op.cit.*) and only a brief summary of the features of the program used for this analysis will be discussed here.

The program employs quadrilateral elements. Both linear and nonlinear elastic constitutive relationships can be used. Materials can be modelled as either isotropic or cross-anisotropic. Computer graphics support programs were available for plotting displacements and mesh outlines.

#### 6.2.2.2 Boundary Conditions

The finite element mesh used for the program is shown on Figure 6.3. Plane strain was assumed for the analysis. The foundation stratigraphy is an idealized version of that at Station 65+00. The sand/limestone interface formed the lower boundary of the grid and was assigned a zero displacement boundary condition.

A total unit weight of  $1.97 \text{ Mg/m}^3$  was used for both the compacted zone and beach zone of the tailings dyke. Total unit weights for all materials are listed in Table 6.2. The construction boundary between these tailings zones is shown in Figure 6.3. The densities were taken to be equivalent on the basis of an extensive series of *in situ* density tests in Tar Island Dyke reported by Mittal and Hardy (1977), which revealed that for depths greater than 30 m the density of the beach zone was equal to that of the compacted zone.

The upstream boundary of the tailings dyke was modelled as a vertical surface with two degrees of freedom and a supporting thrust. The magnitude of the thrust was calculated on the basis of a heavy liquid with a unit weight equal to that of the beach zone. It must be emphasized that

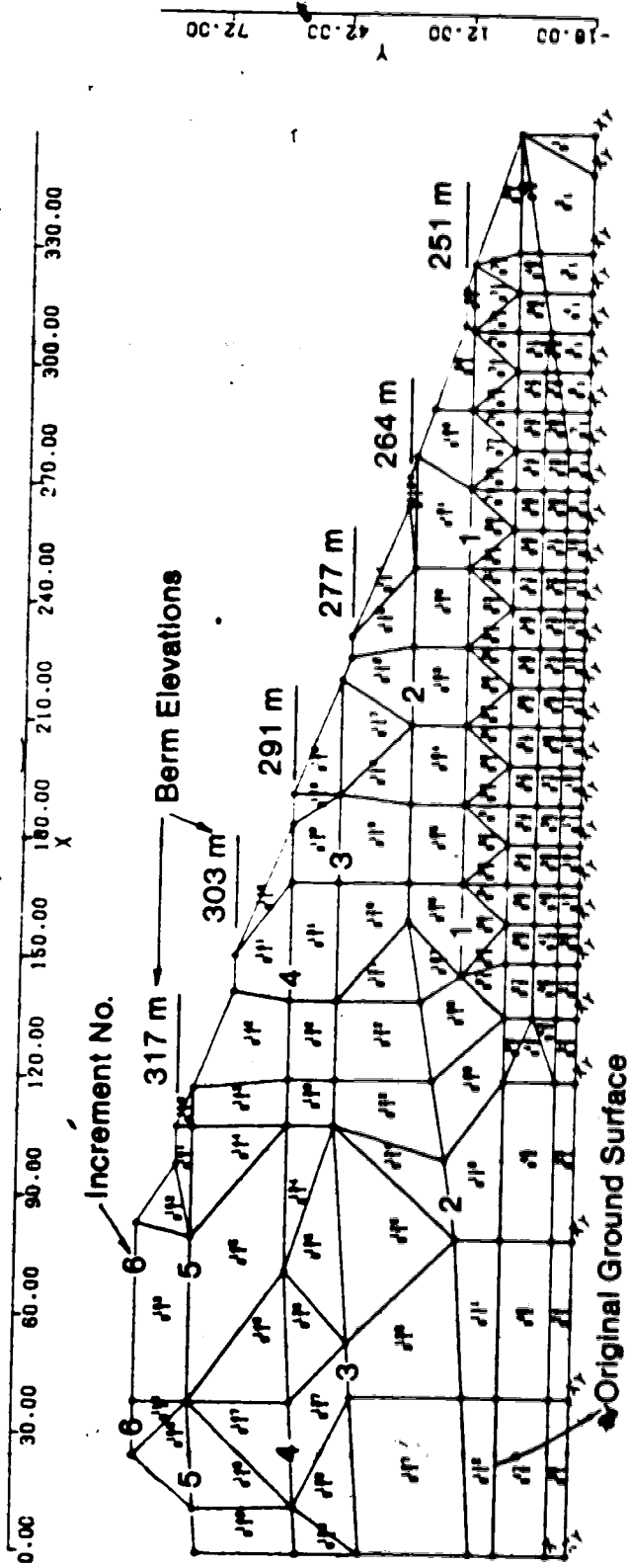


Figure 6.3 Tar Island Dyke stress analysis, finite element mesh



the thrust does not add to the shear stresses in the clay foundation but simply supports the assumed vertical/upstream boundary. The actual configuration of the upstream slope was not used because stresses and displacements in this portion of the dyke were not relevant to the analysis. As a check on this assumption a zero x-displacement upstream boundary condition was used in one analysis instead of the stress boundary condition. It was found that the stresses in the region of interest were not affected by the boundary condition change.

Dyke loads were incrementally applied to the foundation in the finite element analysis according to an idealized version of the actual dyke construction history as portrayed in G.C.O.S. (Great Canadian Oil Sands, now Suncor) Drawing No. TL-PL-009'E', entitled Construction History. Six increments were used and their timing and configuration are shown on Figures 6.2 and 6.3. The finite element program, NLCP, uses the nodal displacements and stresses calculated in the lower increments as input to the next increment. The total stresses in the foundation before dyke construction were calculated according to:

$$\sigma_v = \gamma_t \cdot D \quad 6.1$$

where  $\sigma_v$  = total vertical stress

$\gamma_t$  = total unit weight

D = depth

and:

$$\sigma_h = \sigma_v (1 - (\gamma'/\gamma_T) \sin \phi') \quad 6.2$$

where  $\sigma_h$  = total horizontal stress

$\gamma'$  = submerged unit weight

$\phi'$  = effective angle of shearing resistance

The incremental analysis provided an estimate of the stresses in the foundation at all stages of construction.

#### 6.2.2.3 Parametric Study

Two types of elastic analyses were performed to determine the foundation stresses. The first analysis was undertaken using a linear elastic constitutive relationship and the second analysis used a nonlinear elastic constitutive relationship. A constant Poisson's ratio of 0.49 was used in all analyses except for one linear elastic analysis where a value of 0.35 was used. Further parametric analysis should treat the value of Poisson's ratio in the sand as less than 0.49 .

A summary of the material parameters used is presented in Tables 6.1 and 6.2. One way of comparing the results of the different analysis is to plot the horizontal shear stress in the clay layer just beneath the tailings sand/clay interface along the downstream slope. Such a plot is shown in Figure 6.4. The shear stresses are those at the end of the sixth increment. It was found from the linear elastic analyses that the shear stresses depend on the ratio of the

Table 6.1 Summary of material constants used for linear elastic analyses

Analysis Number	Poisson's Ratio $\mu$	Modulus Ratio $E_s/E_c$
1	0.49	5
2	0.49	10
3	0.35	10

Table 6.2 Summary of material constants used for nonlinear elastic analyses

Material Type	Total Unit Weight (Kn/m <sup>3</sup> )	$K^{(1)}$	$n^{(1)}$	$\phi'$	$R_f^{(1)}$	$\mu$
Compacted Tailings sand	19.25	2000	.54	36°	0.91	0.49
Clay	19.32	350	0	24°	0.8	0.49

(1) Defined in Appendix D

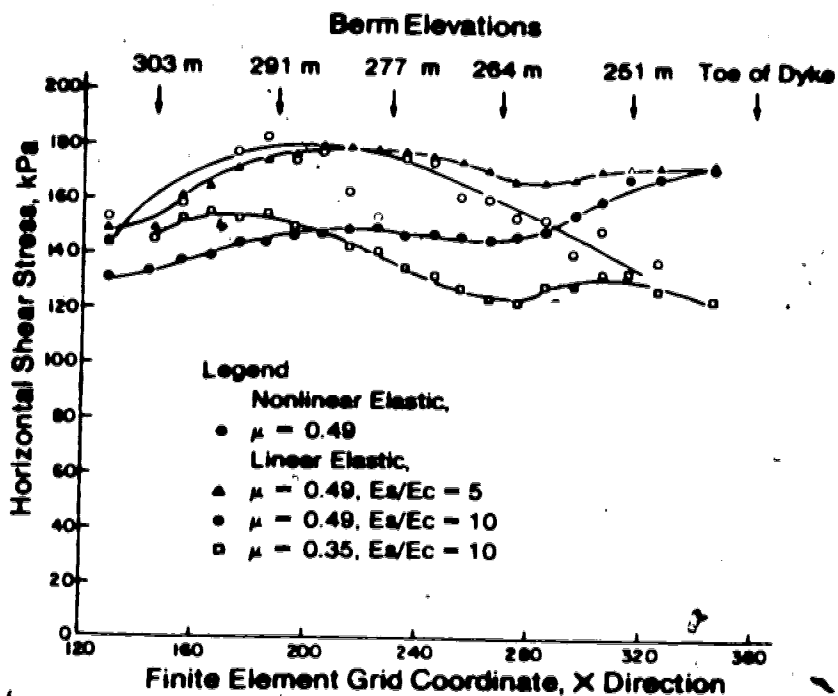


Figure 6.4 Horizontal shear stress in the upper half of the foundation clay along the downstream slope

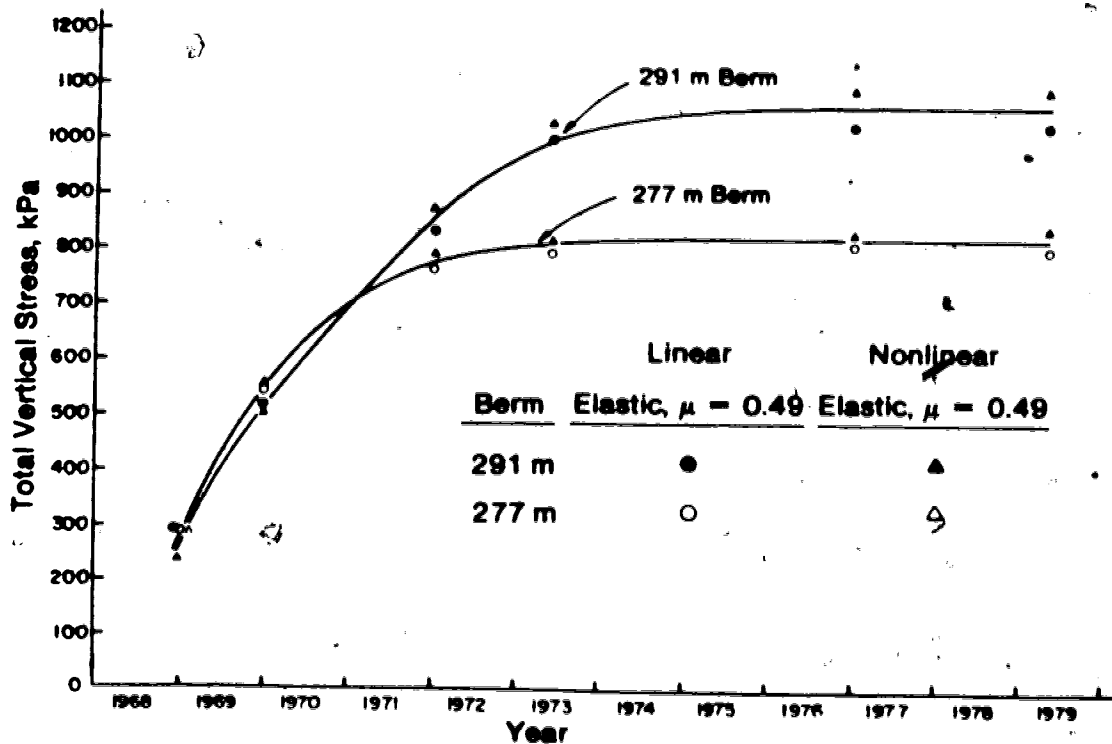


Figure 6.5 Total vertical stress with time in the upper half of the foundation clay for the 291 m and 277 m berms

Young's modulus of the sand to the clay,  $E_s/E_c$ , not on the magnitudes of the respective moduli. This is not true, of course, for the elastic displacements. Increasing the moduli ratio from 5 to 10 decreased the shear stresses in the clay by approximately 25 percent as illustrated in Figure 6.4.

For the linear elastic analysis the moduli ratio was not altered between increments. Allowing volume change in the clay by decreasing Poisson's ratio did not affect the horizontal shear stress substantially beneath the 291 m berm where the creep analysis will be performed. It did however decrease the shear stresses towards the toe of the embankment. It is considered that stresses downstream of the 264 m berm are not reliable for all of the analysis shown in Figure 6.4.

The nonlinear analysis was performed to investigate the effect of changing the moduli ratio between increments while keeping Poisson's ratio constant. The hyperbolic parameters listed in Table 6.2 for the clay are from the drained tests discussed in Chapter 5. The hyperbolic parameters for the tailings sand are based on the properties of a similar sand reported in the literature by Duncan and Chang (1970). It must be emphasized that the writer is not advocating the use of drained parameters in a total stress analysis. The drained parameters were used because it is considered that the tangent moduli ratio is applicable, not the absolute value of the moduli. The horizontal shear stress results are presented in Figure 6.4 and are within the range of the

linear elastic analyses.

Figure 6.5 illustrates the increase in vertical total stress with time for the foundation clay beneath the 291 m and 277 m berms. It is evident that the vertical stress is not sensitive to the selection of the material parameters.

### 6.2.3 Rationale for Simple Shear

Computed shear stresses with time in the foundation clay below the 291 m and 277 m berms are presented in Figures 6.6 and 6.7 respectively. The maximum shear stress as well as the horizontal shear stress are shown in these figures. It is apparent that a Poisson's ratio of 0.49 forces the principal stresses to rotate approximately  $45^\circ$ , that is, the horizontal and maximum shear stresses are approximately equal. The principal stresses for a Poisson's ratio of 0.35 do not rotate  $45^\circ$  but do rotate more than  $15^\circ$ .

A criterion for simple shear is that the principal stresses rotate during shear (see Edgers et.al., 1973 and Gale, 1981). Because the stress analyses indicate rotation of principal stresses and because the form of the creep strains from the inclinometers are similar to that determined from laboratory simple shear tests it is considered that the stress state applicable to the field situation is simple shear. Shear stresses are not dependent upon the magnitude of the pore water pressure so the shear stresses from the total stress analysis can be used in the creep analysis. This of course neglects the effect of

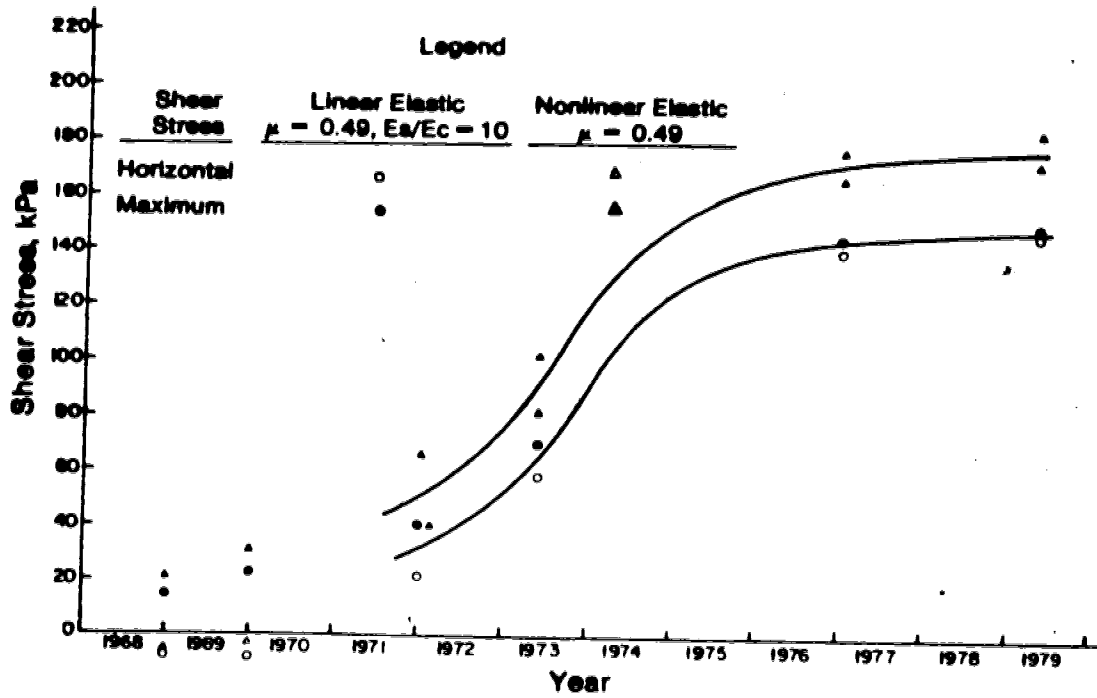


Figure 6.6 Shear stress with time in upper half of clay foundation below 291 m berm

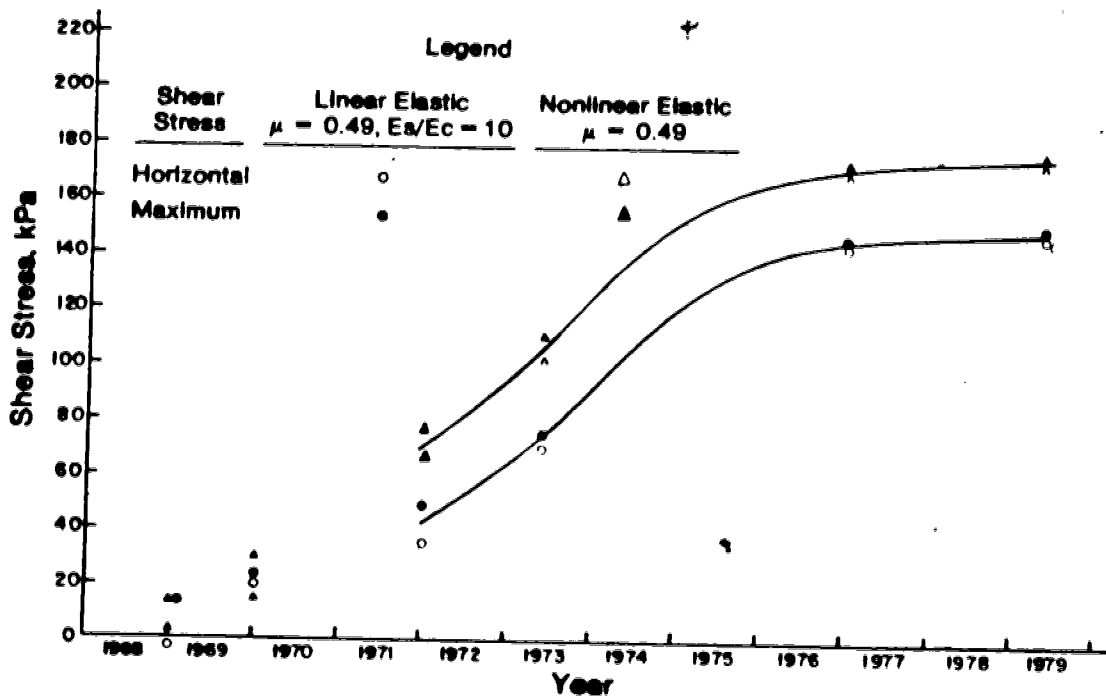


Figure 6.7 Shear stress with time in upper half of clay foundation below 277 m berm

changing material parameters during consolidation on shear stresses. The effective vertical stress is insensitive to material parameters.

### 6.3 Formulation of *In Situ* Creep Equation

#### 6.3.1 Introduction

A creep equation based on the Singh-Mitchell relationship is formulated in this section for the shear strain versus time curves from inclinometer S76-103. The methodology for obtaining shear strains from inclinometer readings is discussed in Chapter 2. The resultant shear strain versus depth plots for a number of inclinometers is included in Appendix A. These shear strain versus depth plots can also be displayed as shear strain versus time for each depth. Such a plot is shown for inclinometer S76-103 in Figures 6.8 and 6.9. The formulation derived here will be developed in terms of the curves shown in Figures 6.8 and 6.9.

Inclinometer S76-103 was chosen for the analysis because samples for the laboratory testing program were obtained nearby and, furthermore, because of the proximity of a reliable piezometer. The same analytical method to be presented here for S76-103 can also be applied individually to the other inclinometers.



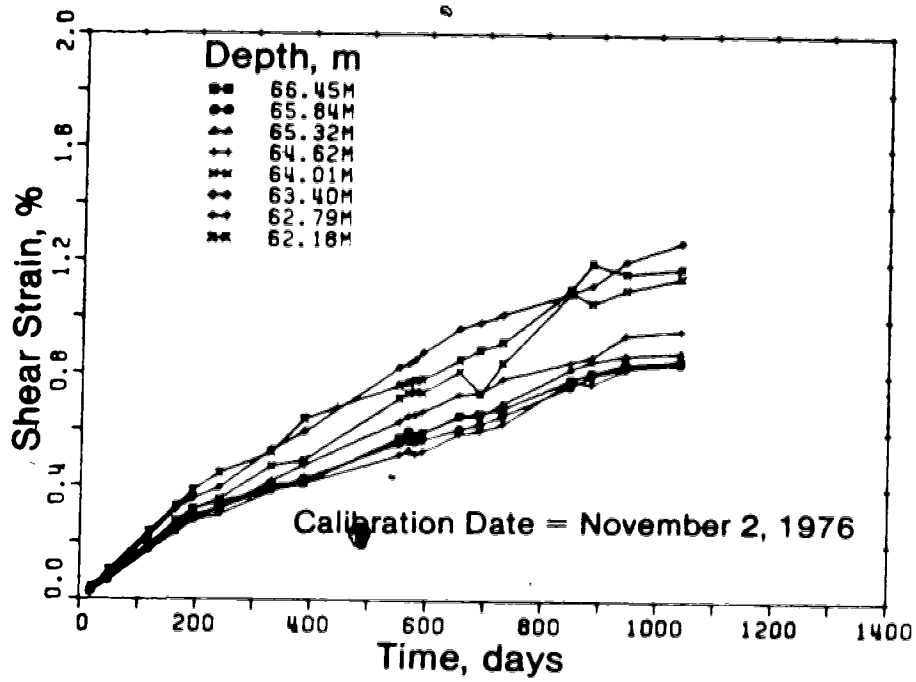
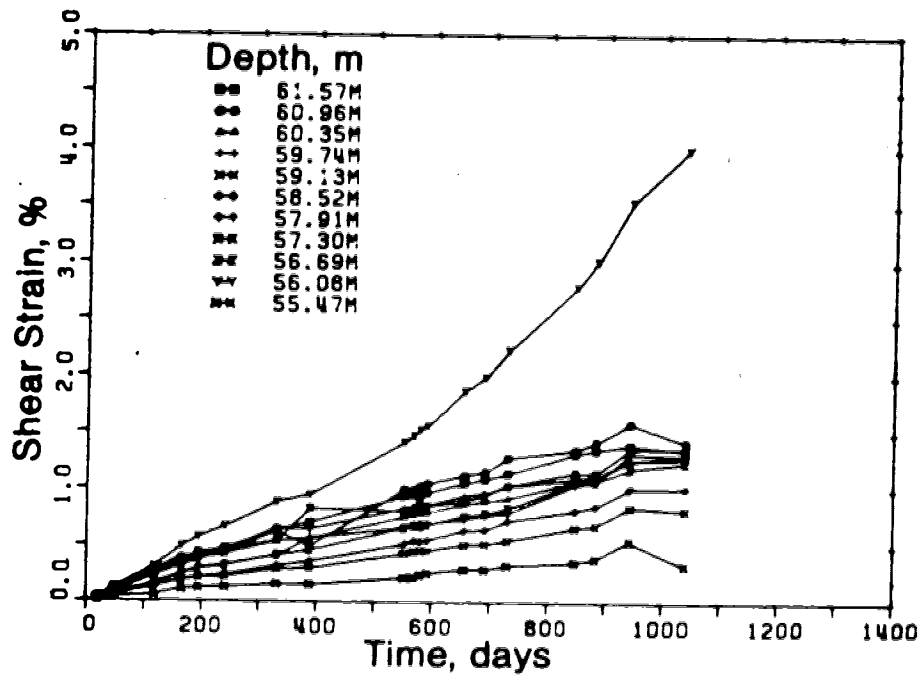


Figure 6.8 Shear strain versus time, inclinometer S76-103, above-upper half of clay, below-lower half of clay

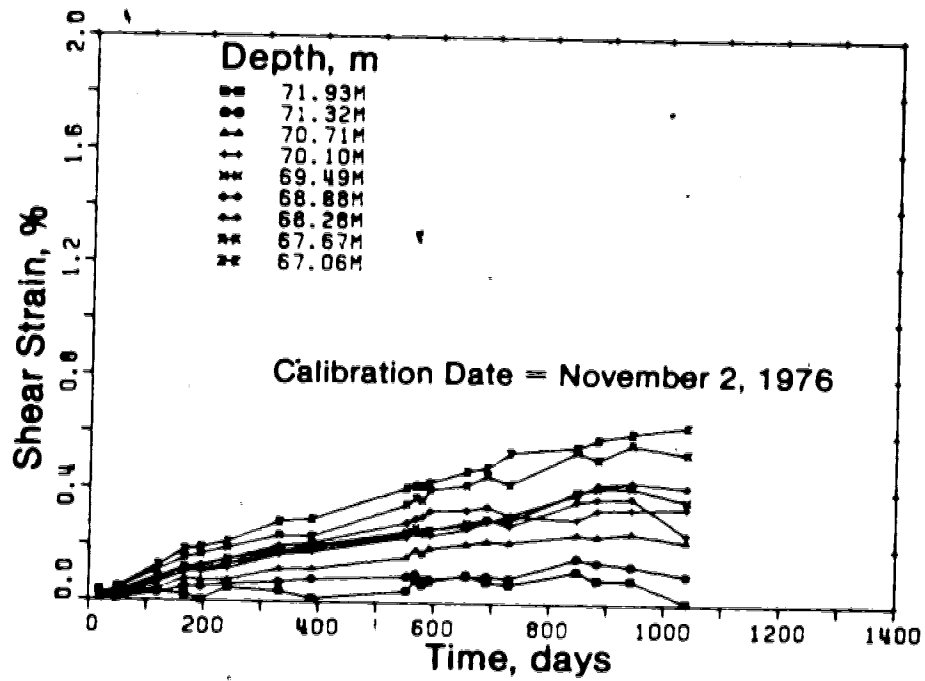


Figure 6.9 Shear strain versus time, inclinometer S76-103, basal sand

In Figure 6.8 it is apparent that the shear strains at a depth of 56.08 m do not have the same form as the other curves. The shear strains are much larger than at other depths and appear to have accelerated with time. The larger strains occur immediately below the tailings sand/clay contact and are evident in the other inclinometer plots at the same stratigraphic position. The Singh-Mitchell equation cannot be applied to these strains.

### 6.3.2 Multiaxial Form of Singh-Mitchell Equation

The Singh-Mitchell equation provides a relationship between axial strain rate, stress level and time for triaxial test results. In order to use this relationship for the field problem it is necessary to cast it in a multiaxial form and then extract the equation applicable to a simple shear stress state.

The generalization of a uniaxial creep relationship to a general multiaxial relationship has been outlined by Odqvist (1966). His approach is based on some similarities between creep and plastic deformation. Emery (1971) applied the work of Odqvist (*op.cit.*) to develop a multiaxial relationship for thawed soils as has Segó (1980) for frozen soils. The Singh-Mitchell equation is cast in a general multiaxial form according to the method of Odqvist (1966) in Appendix D. If simple shear boundary conditions are applied to the general equation the relationship between horizontal shear stress and shear strain rate becomes:

$$\dot{\gamma}_{xy} = \frac{3}{2} A e^{2\alpha \tau_h} (1/t)^m \quad 6.3$$

where  $\dot{\gamma}_{xy}$  = shear strain rate

$A, \alpha, m$  = triaxial stress state creep constants

$\tau_h$  = horizontal shear stress

It is apparent that Equation 6.3 is of the same form as the triaxial creep equation presented earlier as Equation 3.2. This theoretical observation has practical verification in the literature where creep equations describing the axial strain rate from triaxial creep tests have been shown to be of the same form as equations describing the shear strain rate from simple shear tests. Examples are given by Wu *et al* (1978), Edgers *et al* (1973) and Sego (1980).

To develop a field creep equation the constants in Equation 6.3 must now be determined from the shear strain versus time curves shown in Figures 6.8 and 6.9.

### 6.3.3 Derivation of Stress Level Term

Equation 6.3 predicts that the shear strain rate is an exponential function of the horizontal shear stress. The horizontal shear stress can be normalized to stress level in Equation 6.3 by making some assumptions about the state of stress in simple shear. This is done in Appendix D and the resulting normalized creep equation is:

$$\dot{\gamma}_{xy} = A_s e^{\bar{\alpha} \bar{D}} (1/t)^m \quad 6.4$$

Where  $A_s$  =  $3/2 A$

$\bar{\alpha}$  =  $2\alpha \delta' \tan \phi'$

$\bar{D}$  =  $\tau_h / \delta' \tan \phi'$

$\sigma_v'$  = effective vertical stress

$\phi'$  = effective angle of shearing resistance

It is apparent in Figures 6.8 and 6.9 that the creep strain rate, i.e. the slope of the shear strain versus time curves, decreases with increasing depth in the clay foundation. It is considered that the decrease in strain rate is a consequence of the decrease in stress level from the top to the bottom of the clay layer. The stress level decreases with depth because of the pore pressure decrease with depth in the clay horizon as shown in Figures 2.5 and 2.6. One method of determining the parameter,  $\bar{\alpha}$ , is to compare the strain rates at two depths where the stress levels are known.

Proceeding in this fashion the shear strain rates at two different depths are given by:

$$\dot{\gamma}_1 = A_1 e^{\bar{\alpha} \bar{\sigma}_1} (t_1/t)^m \quad 6.5$$

$$\dot{\gamma}_2 = A_1 e^{\bar{\alpha} \bar{\sigma}_2} (t_1/t)^m \quad 6.6$$

where  $A_1$  = strain rate at zero deviator stress at  $t=t_1$

The time,  $t_1$ , in Equations 6.5 and 6.6 is the time period from the effective initiation of the creep of the clay layer to the time at which the inclinometer was installed. A procedure for estimating  $t_1$  will be outlined in the next section.

If  $t$  is equal to  $t$ , then the term  $(t./t)^m$  reduces to one in Equations 6.5 and 6.6. The shear strain rates,  $\dot{\gamma}_1$ , and  $\dot{\gamma}_2$ , become the strain rates at  $t$ , or, in other words, the strain rates at the moment of installation of the inclinometer. If Equation 6.5 is divided by Equation 6.6 the result is:

$$\dot{\gamma}_1/\dot{\gamma}_2 = e^{\bar{\alpha}\bar{D}_1}/e^{\bar{\alpha}\bar{D}_2} \quad 6.7$$

The parameter  $A$ , cancels if it is assumed that the clay has identical creep properties at both depths. Solving for  $\bar{\alpha}$  yields:

$$\bar{\alpha} = (\ln \dot{\gamma}_1 - \ln \dot{\gamma}_2) / (\bar{D}_1 - \bar{D}_2) \quad 6.8$$

For an estimate of  $\bar{\alpha}$  from field data Equation 6.7 requires the strain rates at two depths for which the stress level is known.

A sample calculation of  $\bar{\alpha}$  for inclinometer S76-103 is given in Appendix D. The value of  $\bar{\alpha}$  calculated is 5.1. This compares favourably with the average value of  $\bar{\alpha}$  of 3 from the laboratory testing program.

#### 6.3.4 Derivation of $t$ , and $m$

It is customary when presenting the Singh-Mitchell equation as is done in Equation 6.4 to include unit time as the numerator in the time variable. The coefficient,  $A$ , is the corresponding strain rate at zero stress level at unit time. For this field case it is not known when the clay began to creep under its present stress level so  $A$  cannot be determined directly at unit time. It is therefore convenient

to replace the unit time numerator by the time corresponding to the period between initiation of creep at this stress level and the installation of the inclinometer. Equation 6.4 is then rewritten as:

$$\dot{\gamma}_{xy} = A_1 e^{\bar{\alpha}\bar{D}} (t_1/t)^m \quad 6.9$$

where  $t_1$  = duration of creep period to the time at which the inclinometer was installed

$A_1$  = shear strain rate at zero deviator stress at time  $t_1$ .

The parameter  $A_1$  is easily determined from the following since the shear strain rate and stress level are known at time  $t_1$ .

$$A_1 = \dot{\gamma}_1 / e^{\bar{\alpha}\bar{D}} \quad 6.10$$

where  $\dot{\gamma}_1$  = shear strain rate at  $t_1$ .

A procedure for determining  $\dot{\gamma}_1$  and stress level is presented in Appendix 4.

Implicit in Equation 6.8 is the assumption that the creep of the clay under the current stress level is independent of accumulated creep strains under previous stress levels. This concept has been discussed in Chapter 5 for incremental laboratory drained creep tests and is considered to be valid for this analogous field situation.

By making this assumption it is possible to derive a closed form solution for  $t_1$  that is independent of  $m$ . Two expressions are derived for  $t_1$  in Appendix D. One is valid

for  $m$  equal to one, the other is more general and valid for  $m$  of any magnitude. Values of  $t_1$  were determined by using strain rates calculated from the polynomial regression curves shown in Figure D.1. From the expression for  $m$  equal to one values of  $t_1$  were obtained ranging from 500,000 to 3,000,000 minutes. The general expression for  $t_1$  did not yield reasonable values for  $t_1$ . This occurred because the general expression, although mathematically correct, cannot account for the random component of the field strain rates.

To further delineate the value of  $t_1$ , a purely empirical approach was adopted. Strains were calculated for values of  $t_1$  ranging from 100,000 to 3,000,000 minutes for the initial strain rates and stress levels for depths of 67.06 m and 62.18 m in inclinometer S76-103. The magnitude of  $m$  was varied between 0.7 and 1.3 for each value of  $t_1$ . This range in  $m$  was used because it represents all reasonable values for soils according to Mitchell (1976). Shear strains were calculated from one of the following equations. For  $m$  not equal to one strains are given by:

$$\gamma = \gamma_1 + \frac{A_1 e^{\alpha \bar{\sigma}}}{1-m} (t_1)^m \left( (\Delta t + t_1)^{1-m} - (t_1)^{1-m} \right) \quad 6.11$$

where  $\gamma_1$  = accumulated strain at  $t_1$ ,  
 $\Delta t$  = net time past  $t_1$ ,

For  $m$  equal to one strains are given by:

$$\gamma = \gamma_1 + A_1 e^{\alpha \bar{\sigma}} (t_1)^m (\ln(\Delta t + t_1) - \ln t_1) \quad 6.12$$

Equations 6.10 and 6.11 are obtained by integrating Equation 6.8 with respect to time. It was assumed in the integration



of Equation 6.8 that the stress level is independent of time. This is certainly true at the base of the clay layer where the pore pressures are constant but not strictly true at depth 62.18 m where piezometer AP-75-18A has recorded substantial excess pore pressure dissipation with time. However the decrease in pore pressure only reduces the stress level by 6 percent so the stress level was assumed constant for the purpose of integration.

Time,  $t_1$ , was then selected on the basis that it must be the same for both depths and that it must result in strains that correctly match those recorded for both depths. The value of  $t_1$  determined in this way was approximately 1,800,000 minutes or about 3.5 years. The shear strain versus time curves produced using this value of  $t_1$  in Equations 6.11 and 6.12 are presented in Figure 6.10.

Inclinometer S76-103 was installed in late 1976. A value of  $t_1$  of 3.5 years predicts that the creep of the clay was initiated at this stress level in mid-1973. This appears reasonable since this time corresponds to the large increment in construction in 1973 as shown in Figure 6.2 and the resulting large increase in shear stress shown in Figure 6.6.

As shown in Figure 6.10 the value of  $m$  cannot be determined precisely from this approach. A value of 1.0 for  $m$  gives a reasonable fit to both curves. However it is possible to back calculate the magnitude of  $\gamma$  in Equation 6.11 given a  $t_1$  of 3.5 years. For values of  $m$  greater than

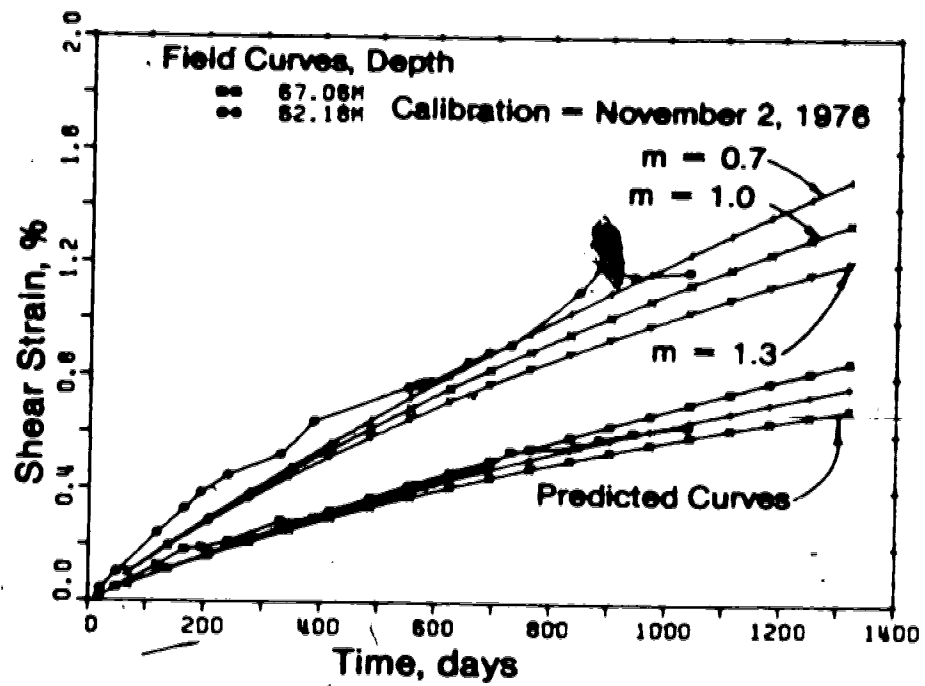


Figure 6.10 Actual and predicted field shear strain versus time curves

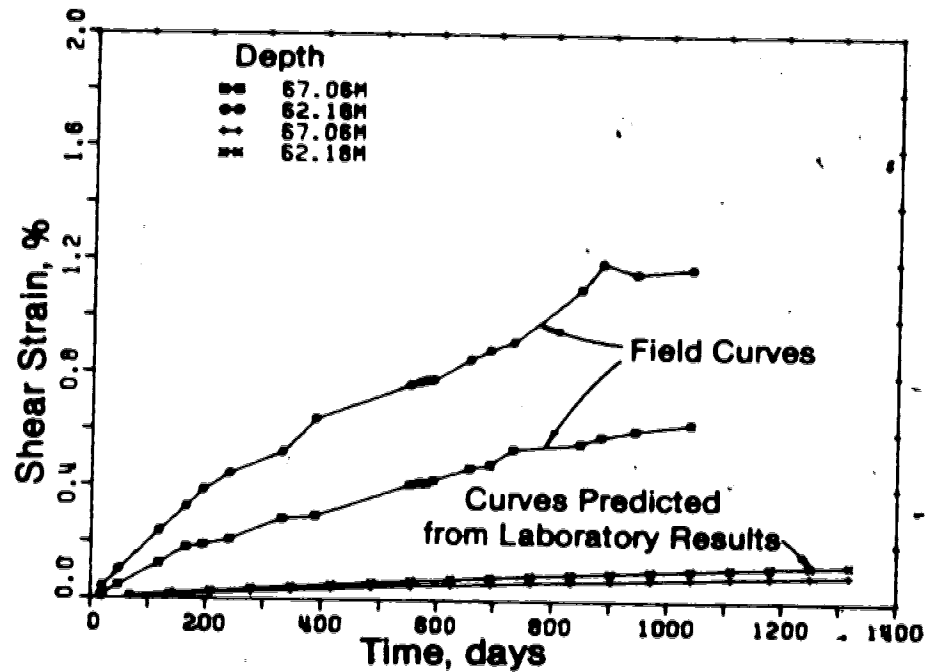


Figure 6.11 Field shear strain versus time curves and curves predicted from laboratory equation

1.0 high values of  $\gamma$ , are obtained, more reasonable values of  $\gamma$ , are obtained if  $m$  is taken to be in the range 0.7 to 1.0.

It is of interest to calculate the shear strain versus time curves predicted by the laboratory test results given a value of  $t$ , of 3.5 years. This is shown in Figure 6.11. It is apparent that Equation 5.2 underestimates the field shear strains. The discrepancy is considered to be primarily a result of the difference in the stress level parameter,  $\sigma$ , not in the value of  $t$ . Size effects between the laboratory and field are not considered to be the seat of the discrepancy.

#### 6.4 Concluding Remarks

It has been demonstrated that the shear strain versus time curves for two depths in inclinometer S76-103 follow similar patterns to those observed in laboratory creep tests. The key similarities are:

1. Shear strain rate decreases with time
2. Shear strain and shear strain rate are exponential functions of stress level.
3. A significant load increment ratio during stage construction of the dyke in 1973 caused creep strain rates to increase and then decay in a manner independent of the previously accumulated creep strains.

The shear strain versus time curves have been modelled with a Singh-Mitchell relationship by making various assumptions about the boundary conditions and the state of stress in the foundation clay. It has been shown that the time,  $t_c$ , can be approximated by assuming that the creep of the clay fits a Singh-Mitchell relationship. The best estimate of  $t_c$  is approximately 3.5 years. Simple procedures have been outlined for deriving the other creep parameters in the Singh-Mitchell relationship from the field data. The stress level term,  $\bar{\sigma}$ , is approximately 5. The damping term,  $m$ , is in the range 0.7 to 1.0. This approximation for  $m$  is tenuous since it is based on a back calculation which assumes a value of  $t_c$ .

## 7. Conclusions and Recommendations

### 7.1 Introduction

This thesis has examined the lateral creep deformation of the clay foundation of Tar Island Dyke. An analytical technique has been developed which enables creep parameters to be obtained from field inclinometer data. Extensive field data concerning foundation geology and soil properties, foundation pore pressures and dyke construction have been synthesized. A series of oedometer and drained triaxial creep tests have been performed on undisturbed clay foundation samples at different sample orientations, cell pressures and stress levels. A review of the creep literature on soils has been presented.

Conclusions and recommendations for further study arising from this research program are presented in the following sections.

### 7.2 Conclusions

#### 7.2.1 General

Tar Island clay is a normally consolidated Recent deposit which originated by infilling of an abandoned channel of the Athabasca River. The clay has deformed vertically and horizontally due to the continued construction of Tar Island Dyke which began in 1965. At

present, in situ piezometer records indicate that the clay has fully consolidated downstream of the 291 m berm and that significant excess pore pressures are dissipating upstream of this berm.

Inclinometers installed from the 303 m berm downstream show substantial time dependent lateral deformation. Horizontal shear strains (in some instances) are in excess of 5 % over a four year period while horizontal strains average 0.04 % over the same period. These small horizontal strains indicate only minor compression in the horizontal direction and are indicative of a creep mechanism rather than lateral consolidation for the shear strains. A further justification for postulated creep mechanism is that lateral movements resulting from horizontal shear straining occur where the clay is fully consolidated.

Vertical displacements of the clay layer have not been monitored directly but indirect estimates of vertical displacements can be obtained from water content changes and changes in the thickness of the deposit as recorded by drilling. Indirect estimates such as these reveal that the clay at some locations has compressed in excess of 3 m over the life of the project.

### 7.2.2 Laboratory Creep Tests

Both the oedometer and drained triaxial test results demonstrate that the axial creep strain rate decreases according to a power law with time. The average value of the

power law exponent,  $m$ , is 1.13 and is independent of the two stress states used. The drained triaxial test results demonstrate that  $m$  is independent of sample orientation, stress level and normal stress.

The triaxial test results show that the axial creep strain rate is an exponential function of stress level. This result together with the power law dependence of strain rate on time fulfill the requirements of a Singh-Mitchell model for creep strains. Transient consolidation effects at the beginning of the stress increments, disrupt the decay of creep strain rates with time and have been ignored in fitting the Singh-Mitchell model to the creep data.

Shear strength as determined from the drained triaxial creep test results are consistent with results from strain controlled tests. The effective angle of shearing resistance,  $\phi$ , is  $26.5^\circ$  for Tar Island Clay, and is independent of sample orientation.

### 7.2.3 *In Situ* Lateral Strains

The shear strain versus time curves from inclinometer S76-103 indicate that the shear strain rate decreases with time at all depths in the clay horizon except at the clay-tailings sand contact. At this location the shear strain rate has accelerated in the past and now appears to be steady. It is considered that the clay at this depth is in a state of local shear failure. Large strains are evident in the clay downstream of S76-103 at the same stratigraphic

position but the shear strain rates here are decreasing with time.

The shear strain rates for S76-103 are a function of stress level. Preliminary indications are that the shear strain rate is an exponential function of stress level. More investigation is needed to confirm this hypothesis.

Central to the understanding of the in situ creep behaviour of the clay is the estimation of the time period,  $t$ , that the clay has been creeping prior to the installation of the inclinometer. In order to make an estimate from this field data of  $t$ , it was first necessary to assume a creep model for the soil. It was assumed that the in situ creep behaviour could be described by the Singh-Mitchell relationship. Furthermore, it was assumed that the creep strain rates at the current stress level were independent of the accumulated creep strains at the previous stress levels. On this basis  $t$  is estimated to be approximately 3.5 years. This estimate of  $t$  appears to be reasonable since it correlates with a major episode of dyke construction during 1973.

### 7.3 Recommendations For Further Study



### 7.3.1 Drained Laboratory Creep Experiments

Further research is required to delineate the influence of stress state on the creep behaviour of undisturbed soils. A complete evaluation of the influence of stress state would involve oedometer, triaxial, plane strain and simple shear tests. It would be of benefit for practitioners to be able to estimate parameters for the Singh-Mitchell equation for field situations that involve complex stress states on the basis of oedometer tests.

Of particular importance to the estimation of the in situ creep behaviour of clay foundations beneath stage constructed embankments is the load increment ratio required to make the creep strain rates independent of the previously accumulated creep strains. It is considered that this load increment ratio is a function of stress level and the duration of the previous stress level. Its investigation at high stress levels is complicated by the small load increments required to cause undrained failure.

Creep tests on undisturbed soils of long duration similar to those of Lovenbury (1969) would be of benefit to the long term prediction of creep strains. Of particular interest are the strain instabilities at extended creep periods observed by Lovenbury (1969) and later by Tavenas *et al* (1978). Strain instabilities have not been displayed by the Tar Island Dyke inclinometers.

### 7.3.2 Lateral Creep Strains Beneath Tar Island Dyke

The analytical approach described in Chapter 6 can be applied individually to the other Tar Island Dyke inclinometers. The magnitude of  $t$ , should increase in the downstream direction. It would be of interest to install inclinometers at higher berms where the clay has been loaded recently by dyke construction and, of most interest, because an *a priori* assumption would not have to be made about the creep model which best fits the clay, to install an inclinometer in a position in the clay deposit where  $t$ , would be zero at some time in the future.

The next logical step in this analysis would be to treat the creep displacements of the clay collectively by solving the entire boundary value problem. This would involve the use of a finite element program that had coupled facilities for properly determining the effective stresses in the clay foundation.

## References

- Allen, J.R.L. 1965. Origin and characteristics of recent alluvial sediments. *Sedimentology*, Vol. 5, pp. 89-191.
- Arulanandan, K., Shen, C.K. and Young, R.B. 1971. Undrained creep behaviour of a marine organic silty clay. *Geotechnique*, Vol. 21, No. 4, pp. 359-375.
- Barden, L. 1965. Consolidation of clay with non-linear viscosity. *Geotechnique*, Vol. 25, No. 4, pp. 345-362.
- Barden, L. 1969. Time dependent deformation of normally consolidated clay. *Journal of the Soil Mechanics and Foundation Division, ASCE*, Vol. 95, No SM1, pp. 1-31.
- Barden, L. and Poskitt, T.J. 1969. Discussion. *Journal of the Soil Mechanics and Foundation Engineering Division, ASCE*, SM1, pp. 409-415.
- Berre, T. and Iversen, K. 1972. Oedometer tests with different specimen heights on a clay exhibiting large secondary compression. *Geotechnique*, Vol. 22, No. 1, pp. 53-70.
- Bishop, A.W. and Henkel, D.J. 1962. The measurement of soil properties in the triaxial test, Edward Arnold Publishers, 227 p.
- Bishop, A.W. and Lovenbury, H.T. 1969. Creep characteristics of two undisturbed clays. 7th International Conference on Soil Mechanics and Foundation Engineering, Mexico City, Vol. 1, pp. 29-37.
- Bjerrum, L. 1967. Engineering geology of normally consolidated clays as related to settlement of buildings. *Geotechnique*, Vol. 17, No. 2, pp. 81-118.
- Bjerrum, L. 1972. Shallow foundations: Discussion. *Proceedings of ASCE Specialty Conference on Performance of Earth and Earth Supported Structures*. Vol. 3, pp. 167-168.
- Bjerrum, L. 1973. Problems of soil mechanics and construction on soft clays. 8th International Conference on Soil Mechanics and Foundation Engineering, Vol. 3, pp. 111-159.

- Bjerrum, L. and Landva, A. 1966. Direct simple shear tests on a Norwegian quick clay. *Geotechnique*, Vol. 16, pp. 1-20.
- Buisman, A.S.K. 1936. Results of long duration settlement tests. 1st International Conference on Soil Mechanics and Foundation Engineering, Vol. 1, pp. 103-106.
- Campanella, R.G. 1965. Effect of temperature and stress on the time dependent behaviour in saturated clay. Ph.D. thesis, University of California, Berkeley, California.
- Campanella, R.G. and Vaid, Y.P. 1972. Creep rupture of a saturated natural clay. 6th International Congress on Rheology. Lyon, Fra
- Campanella, R.G. and Vaid, Y.P. 1974. Triaxial and plane strain creep rupture of an undisturbed clay. *Canadian Geotechnical Journal*, Vol. 11, No. 1, pp. 1-10.
- Chang, Y.C., Broms, B., and Peck, R.B. 1973. Relationship between the settlement of soft clays and excess pore pressures due to imposed loads. 8th International Conference on Soil Mechanics and Foundation Engineering, Moscow, Vol. 1.1, p. 93-96.
- Christensen, R.W. and Wu, T.H. 1964. Analysis of clay deformation as a rate process. *Journal of the Soil Mechanics and Foundation Engineering Division, ASCE*. Vol. 90, SM6, pp. 125-157.
- Christian, J.T. 1977. Two- and three- dimensional consolidation. In: *Numerical Methods in Geotechnical Engineering*. Edited by C.S. Desai and J.T. Christian. pp. 399-425.
- Christie, I.F. 1964. A re-appraisal of Merchant's contribution to the theory of consolidation. *Geotechnique*, Vol. 14, No. 4, pp. 309-320.
- Clough, R.W. and Woodward, R.J. 1966. Analysis of embankment stresses and deformations. *Stability and Performance of Slopes and Embankments*, ASCE. pp. 583-603.
- Cole, D.M. 1978. A technique for measuring radial deformation during repeated load triaxial testing. *Canadian Geotechnical Journal*, Vol. 15, No. 3, pp. 426-429.

- Collins, K. and McGown, A. 1974. The form and function of microfabric features in a variety of natural soils. *Geotechnique*, Vol. 24. No. 2, pp. 223-254.
- Crawford, C.B. 1964. Interpretation of the consolidation test. *Journal of the Soil Mechanics and Foundations Division, ASCE*, Vol. 90, No SM5, pp. 87-102.
- Crawford, C.B. and Sutherland, J.G. 1971. The Empress Hotel, Victoria, British Columbia, - sixty-five years of foundation settlements. *Canadian Geotechnical Journal*, Vol. 8, No. 1, pp. 77-98.
- da Fontoura, S.A.B. 1980. Time dependent response of rock masses during tunnelling. Ph.D. thesis, University of Alberta, 310 p.
- de Ambrosis, L.P. 1974. Settlement of foundations due to creep. Ph.D. thesis, Univeristy of Sydney, Australia.
- de Josselin de Jong, G. 1968. Consolidation models consisting of an assembly of viscous elements or a cavity channel network. *Geotechnique*, Vol. 18, No. 2, pp. 195-228.
- de Josselin de Jóng, G. and Verruijt, A. 1965. Primary and secondary consolidation of a spherical clay sample. 6th International Conference on Soil Mechanics and Foundation Engineering, Vol. 1.
- Design Review Panel. 1977. Report on Great Canadian Oil Sands Tar Island Tailings Dyke. 192 p.
- Duncan, J.M., Byrne, P., Wong, K.S. and Mabry, P. 1978. Strength, stress-strain and bulk modulus parameters for finite element analyses of stresses and movements in soil masses. Office of Research Services, University of California, Berkeley, California, Report No. UCB/GT/78-02 to National Science Foundation, 83 p.
- Duncan, J.M. and Chang, Y.Y. 1970. Nonlinear analysis of stress and strain in soils. *Journal of the Soil Mechanics and Foundations Division, ASCE*, Vol. 96, No. SM5, pp. 1629-1653.
- Dusseault, M.B. and Scafe, D. 1979. Mineralogical and engineering index properties of the basal McMurray clay shales. *Canadian Geotechnical Journal*, Vol. 16, No. 2, pp. 285-294.

- Eden, W.J. 1977. Evidence of creep in steep natural slopes of Champlain sea clay. Canadian Geotechnical Journal, Vol. 14, No. 4, pp. 620-627.
- Edgers, L., Ladd, C.C. and Christian, J.T. 1973. Undrained creep of Atchafalaya levee foundation clays. Research Report R73-16, M.I.T., Soils Publication 319, 600 pp.
- Eisenstein, Z. 1974. Application of finite element method to analysis of earth dams, State-of-the-Art Report, First Brazilian Seminar on Application of Finite Element Method in Soil Mechanics, Universidade Federal do Rio de Janeiro.
- El-Ruwayih, A.A. 1976. Design, manufacture and performance of a lateral strain device. Geotechnique, Vol. 26, No. 1, pp. 215-216.
- Emery, J.J. 1971. Finite element analysis of creep problems in soil mechanics. Ph.D thesis, U.B.C., 155 p.
- Emery, J.J. and Finn, W.D.L. 1972. Creep problems in soil mechanics. In: Applications of solid Mechanics. Edited by Charlwood, R.G., Wesner, D.S., Tabanok, B. Proc. Symp. Univ. Waterloo, June 26-27, 1972. pp. 417-437.
- Eyring, H. 1936. Viscosity, plasticity and diffusion as examples of absolute reaction rates. Journal of Chemical Physics, Vol. 4, pp. 283-291.
- Finn, W.D.L. and Shead, D.E. 1973. Creep and creep rupture of an undisturbed sensitive clay. 8th International Conference on Soil Mechanics and Foundation Engineering, Vol. 1.1, pp. 135-142.
- Fischer, K.P., Andersen, K.H. and Moum, J. 1978. Properties of an artificially cemented clay. Canadian Geotechnical Journal, Vol. 15, No. 3, pp. 322-331.
- Fung, Y.C. 1965. Foundations of solid mechanics. Eire Prentice Hall of Canada Ltd., 525 p.
- Gale, A.D. 1981. A high pressure simple shear apparatus. M.Sc. thesis, University of Alberta, 173 p.
- Geuze, E. and Tan, T.K. 1953. The mechanical behaviour of clays. Proceedings of 2nd International Congress of Rheology, Oxford. p. 247.

- Gibson, R.E. and Lo, K.Y. 1961. A theory of consolidation for soils exhibiting secondary compression. Norwegian Geotechnical Institute Publication No. 41.
- Glasstone, S., Laidler, K. and Eyring, H. 1941. The theory of rate processes. McGraw Hill Book Co., New York.
- Goldberg, D.T. 1964. Discussion. In: Design of Foundations For Control of Settlement, ASCE, pp. 463-467.
- Hansen, J.B. and Inan, S. 1969. Tests and formulas concerning secondary consolidation. 7th International Conference on Soil Mechanics and Foundation Engineering. Vol. 1, pp. 45-53.
- Hardy Associates (1978) Ltd. Numerous files and reports pertaining to the design of Tar Island Dyke.
- Holtz, R.D. 1980. SI units in geotechnical engineering. Geotechnical Testing Journal, Vol. 3, No. 2, pp. 73-79.
- Holzer, T.L., Hoeg, K. and Arulanandan, K. 1973. Excess pore pressures during undrained creep. Canadian Geotechnical Journal, Vol. 10, No. 1, pp. 12-24.
- Horn, H.M. and Lambe, T.W. 1964. Settlement of buildings on the M.I.T. campus. Journal of the Soil Mechanics and Foundations Division, ASCE, Vol. 90, No. SM5, pp. 181-196.
- Irwin, M.J. 1972. Discussion of use of servo-mechanisms for volume change measurement and Ko consolidation. Geotechnique, Vol. 22, No. 1, pp. 186-187.
- Kahn, M.H. and Hoag, D.L. 1979. A non-contacting transducer for measurement of lateral strains. Canadian Geotechnical Journal, Vol. 16, No. 2, pp. 409-411.
- Kavazanjian, E. and Mitchell, J.K. 1977. A general stress-strain-time formulation for soils. Proceedings, Specialty Session 9, 9th International Conference on Soil Mechanics and Foundation Engineering. pp. 113-120.
- Kavazanjian, E. and Mitchell, J.K. 1978. Discussion of Mesri, G. and Godlewski, P. M. 1977. Journal of the Geotechnical Engineering Division, Vol. 104, No. GT4, pp. 508-510.
- Kavazanjian, E. and Mitchell, J.K. 1980. Time dependent deformation behaviour of clays. Journal of the Geotechnical Engineering Division, ASCE, Vol. 106, No. GT6, pp. 611-630.

- Kenney, T.C., Moun, J. and Berre, T. 1967. An experimental study of bonds in a natural clay. Proceedings of the Geotechnical Conference Oslo, Vol. I, pp. 65-69.
- Klementev, I. 1974. Lever-type apparatus for electrically measuring volume change. Geotechnique, Vol. 24, No. 4, pp. 670-671.
- Komamura, F. and Huang, R.J. 1974. A new rheological model for soil behaviour. Journal of the Geotechnical Engineering Division, ASCE, Vol. 100, No. GT7, pp. 807-824.
- Krizek, R.J., Chawla, K.S. and Edil, T.B. 1977. Directional creep response of anisotropic clays. Geotechnique, Vol. 27, No. 1, pp. 35-51.
- Kwan, D. 1971. Observation of the failure of a vertical cut in clay at Welland, Ontario. Canadian Geotechnical Journal. Vol. 8, No. 2, pp. 283-298.
- Ladanyi, B. 1972. An engineering theory of creep in frozen soils. Canadian Geotechnical Journal, Vol. 9, pp. 63-80.
- Ladd, C.C., Aldrich, H.P. and Johnson, E.G. 1969. Embankment failure on organic clay. 7th International Conference of Soil Mechanics and Foundation Engineering, Vol. 2, pp. 627-634.
- Ladd, C.C. and Edgers, L. 1972. Consolidated undrained direct-simple shear tests on saturated clays. Department of Civil Engineering, MIT, Cambridge, Massachusetts, Research Report R72-82, 245 p.
- Ladd, C.C. and Preston, W.B. 1965. On the secondary compression of saturated clays. Research Report R65-59, Research in Earth Physics, Phase Report No. 6, Department of Civil Engineering, MIT, Cambridge, Massachusetts.
- Lambe, T.W. 1951. Soil testing for engineers, John Wiley and Sons, Inc, New York, 165 p.
- Lambe, T.W. 1953. The structure of inorganic soil. Proceedings of the ASCE, Vol. 79, Separate No. 315, October.
- Law, S.T.C. 1975. Deformations of earth dams during construction. Ph.D. thesis, University of Alberta, Edmonton, Alta., 364 p.



- Lee, K.L. and Idriss, I.M. 1975. Static stresses by linear and nonlinear methods. Journal of the Geotechnical Engineering Division, ASCE, Vol. 101, GT9, pp. 871-887.
- Lee, K.L. and Shen, C.K. 1969. Horizontal movements related to subsidence. Journal of the Soil Mechanics and Foundations Division, ASCE, Vol. 95, SM1, pp. 139-166.
- Leonards, G.A. and Altschaeffle, A.G. 1964. Compressibility of clays. Journal of the Soil Mechanics and Foundations Division, ASCE, Vol. 90, No. SM5, pp. 133-155.
- Leonards, G.A. and Girault, P. 1961. A study of the one dimensional consolidation test. 5th International Conference on Soil Mechanics and Foundation Engineering. Vol. 1, pp. 213-218.
- Leonards, G.A. and Ramiah, B.K. 1959. Time effects in the consolidation of clays. ASTM, STP 254, pp. 116-130.
- Lewin, P.I. 1971. Use of servo mechanisms for volume change measurement and Ko consolidation. Geotechnique, Vol. 21, No. 3, pp. 259-262.
- Lo, K.Y. 1961. Secondary compression of clays. Journal of the Soil Mechanics and Foundations Division, ASCE, Vol. 87, No. SM4, pp. 61-88.
- Lo, K.Y. and Stermac, A.G. 1965. Failure of an embankment founded on varved clay. Canadian Geotechnical Journal, Vol. 2, No. 1, pp. 234-253.
- Lohnes, R.A. and Demirel, T. 1978. SEM applications in soil mechanics. Scanning Electron Microscopy, Vol. 1, pp. 643-654.
- Lucks, A.S., Christian, J.T., Brandow, G.E. and Hoeg, K. 1972. Stress conditions in NGI simple shear tests. Journal of the Soil Mechanics and Foundations Division, ASCE, Vol. 98, No. SM1, pp. 155-160.
- McKeague, J.A. 1978. Manual on soil sampling and methods of analysis. Canadian Society of Soil Science.
- McRoberts, E.C. 1975. Some aspects of a simple secondary creep model for deformations in permafrost slopes. Canadian Geotechnical Journal, Vol. 12, No. 1, pp. 98-105.

- Medeiros, I. 1979. Deep excavations in stiff soils. Ph.D. thesis, University of Alberta.
- Menzies, B.K. 1975. A device for measuring volume change. *Geotechnique*, Vol. 25, No. 1, pp. 133-134.
- Menzies, B.K. 1976. Discussion. *Geotechnique*, Vol. 26, No. 3, pp. 542-544.
- Menzies, B.K. and Phillips, A.B. 1972. On the making of rubber membranes. *Geotechnique*, Vol. 22, No. 1, pp. 153-155.
- Mesri, G. 1973. Coefficient of secondary compression. *Journal of the Soil Mechanics and Foundations Division*. Vol. 99, No. SM1, pp. 123-137.
- Mesri, G. and Godlewski, P.M. 1977. Time and stress-compressibility interrelationship. *Journal of the Geotechnical Engineering Division, ASCE*, Vol. 103, No. GT5, pp. 417-430.
- Mesri, G. and Godlewski, P.M. 1979. Closure. *Journal of the Geotechnical Engineering Division*. Vol. 105, No. GT1, pp. 106-113.
- Mittal, H.K. and Morgenstern, N.R. 1977. Design and performance of tailings dams. *Geotechnical Practise for Disposal of Solid Waste Materials, ASCE*, pp. 475-492.
- Mitchell, J.K. 1964. Shearing resistance of soil as a rate process. *Journal of the Soil Mechanics and Foundations Division, ASCE*, Vol. 90, No. SM1, pp. 29-61.
- Mitchell, J.K. 1976. *Fundamentals of soil behaviour*. John Wiley and Sons, Inc, New York. 422 p.
- Mitchell, J.K. and Campanella, R.G. 1963. Creep studies on saturated clays. *ASTM STP 361*. pp. 90-103.
- Mitchell, J.K. Campanella, R.G. and Singh, A. 1968. Soil creep as a rate process. *Journal of the Soil Mechanics and Foundations Division, ASCE* Vol. 94, SM1, pp. 231-253.
- Mitchell, J.K., Seed, H.B. and Paduana, J. A. 1965. Creep deformation and strength characteristics of soils under the action of sustained stress. Report No. TE 65-8, *Soil Mechanics and Bituminous Materials Laboratory, University of California, Berkeley, California*.

- Mitchell, J.K., Singh, A. and Campanella, R.G. 1969. Bonding, effective stresses and strength of soils. *Journal of the Soil Mechanics and Foundations Division, ASCE*, Vol. 95, No. SM5, pp. 1219-1246.
- Mitchell, R.J. and Burn, K.N. 1971. Electronic measurement of changes in the volume of pore water during testing of soil samples. *Canadian Geotechnical Journal*, Vol. 8, No. 2, pp. 341-345.
- Mittal, H.K. and Hardy, R.M. 1977. Geotechnical aspects of a tar sand tailings dyke. *Geotechnical Practise For Disposal of Solid Waste Materials, ASCE*, pp. 327-347.
- Murayama, S. and Shibata, T. 1958. On the rheological characteristics of clay, part 1. *Bulletin No. 26, Disaster Prevention Research Institute, Kyoto University, Japan.*
- Muryama, S. and Shibata, T. 1961. Rheological properties of clays. *5th International Conference on Soil Mechanics and Foundation Engineering, Paris Vol.1, pp. 269-273.*
- Murayama, S. and Shibata, T. 1964. Flow and stress relaxation of clays. *Rheology and Soil Mechanics Symposium of the International Union of Theoretical and Applied Mechanics, Grenoble, France. pp. 99-129.*
- Nelson, J.D. and Thompson, E.G. 1977. A theory of creep failure on overconsolidated soil. *Journal of the Geotechnical Engineering Division, ASCE*, Vol. 103, No. GT11, pp. 1281-1294.
- Newland, P.L. and Allely, B.H. 1960. A study of the consolidation characteristics of a clay. *Geotechnique*, Vol. 10, No. 2, pp. 62-74.
- Nobari, E.S. and Duncan, J.M. 1972. Effect of reservoir filling on stresses and movements in earth and rockfill dams. *Report No. TE-72-1, University of California, Berkeley.*
- Odqvist, F.K.G. 1966. *Mathematical theory of creep and creep rupture. Oxford Mathematical Monograph, Clarendon press, Oxford, 268 p.*
- Odqvist, F.K.G. 1971. Theories of creep rupture under multiaxial state of stress. In: *Advances in Creep Design. Edited by Smith, A.L. and Nicholson, A.M. Applied Science Publishers Ltd., London, England, pp. 31-47.*

- Olson, R.E. and Mesri, G. 1970. Mechanisms controlling compressibility of clays. Journal of the Soil Mechanics and Foundations division, ASCE, Vol. 96, No. SM6, pp. 1863-1878.
- Poulos, H.G. 1972. Difficulties in prediction of horizontal deformations of foundations. Journal of the Soil Mechanics and Foundations Division, ASCE, Vol. 98, SM8, pp. 843-848.
- Poulos, H.G., de Ambrosis, L.P. and Davis, E.H. 1976. Methods of calculating long-term creep settlements. Journal of the Geotechnical Engineering Division, Vol. 102, No. GT7, pp. 787-804.
- Poulos, S.J. 1964. Control of leakage in the triaxial test. Harvard Soil Mechanics Series, No. 71, Cambridge, Mass., 230 p.
- Prevost, J.H. and Hoeg, K. 1976. Reanalysis of simple shear soil testing. Canadian Geotechnical Journal, Vol. 13, pp. 418-429.
- Prevost, J-H. and Hoeg, K. 1977. "Plasticity model for undrained stress-strain behaviour." 9th International Conference on Soil Mechanics and Foundation Engineering, Vol. 1, pp. 255-261.
- Pusch, R. and Feltham, P. 1980. A stochastic model of the creep of soils. Géotechnique, Vol. 30, No. 4, pp. 497-506.
- Pusch, R. and Feltham, P. 1981. Computer simulation of creep of clay. Journal of the Geotechnical Engineering Division, ASCE, Vol. 107, No. GT1, pp. 95-104.
- Roscoe, K.H. and Poorooshasb, H.B. 1963. A theoretical and experimental study of strains in triaxial compression tests on normally consolidated clays. Geotechnique, Vol. 13, No. 1, pp. 12-38.
- Rowlands, G.O. 1972. Apparatus for measuring volume change. Geotechnique, Vol. 22, No. 3, pp. 525-526.
- Rutledge, P.C. and Gould, J.P. 1973. Movements of articulated conduits under earth dams on compressible foundations. Embankment-Dam Engineering, Casagrande Volume, edited by Hirschfeld, R.C. and Poulos, S.J. pp. 209-237.

- Saito, M. 1965. Forecasting the time of occurrence of a slope failure. 6th International Conference on Soil Mechanics and Foundation Engineering, Vol. 2, pp. 537-541.
- Saito, M. 1969. Forecasting time of slope failure by tertiary creep. 7th International Conference on Soil Mechanics and Foundation Engineering, Vol. 2, pp. 677-683.
- Saito, M. and Vezawa, H. 1961. Failure of soil due to creep. 5th International Conference on Soil Mechanics and Foundation Engineering, Vol. 1, pp. 315-318.
- Savigny, K.W. 1980. In situ analysis of naturally occurring creep in ice rich permafrost soil. Ph.D. thesis, University of Alberta, 439 p.
- Schiffman, R.L. 1969. Secondary consolidation of clays - a viscoelastic analysis. Advances in Consolidation Theories for Clays, Proceedings of Specialty Session No. 12, 7th International Conference on Soil Mechanics and Foundation Engineering.
- Schiffman, R.L., Ladd, C.C. and Chen, A.T.F. 1964. The secondary consolidation of clay. Symp. of Rheology and Soil Mech., International Union of Theoretical and Applied Mechanics, Grenoble.
- SEGO, D.C. 1980. DEFORMATION OF ICE UNDER LOW STRESSES. PH.D. THESIS, UNIVERSITY OF ALBERTA, EDMONTON, ALTA., 429 P.
- Sharpe, P. 1978. A device for automatic measurement of volume change. Geotechnique, Vol. 28, No. 3, pp. 348-350.
- Shen, C.K., Arulanandan, K. and Smith, W.S. 1973. Secondary consolidation and strength of a clay. Journal of the Soil Mechanics and Foundations Division, Vol. 99, SM1, pp. 95-111.
- Shibata, T. and Karube, D. 1969. Creep rate and creep strength of clays. 7th International Conference on Soil Mechanics and Foundation Engineering, Vol. 1, pp. 361-367.
- Simmons, J. 1981. Ph.D. thesis (in preparation), University of Alberta, Edmonton, Alta.

- Singh, A. and Mitchell, J.K. 1968. General stress-strain-time function for soils. Soil Mechanics and Foundation Division, ASCE, Vol. 94, SM1, pp. 21-46.
- Singh, A. and Mitchell, J.K. 1969. Closure. Journal of the Soil Mechanics and Foundation Engineering Division, Vol. 95, SM6, pp. 1526-1527.
- Singh, A. and Mitchell, J.K. 1969. Creep potential and creep rupture of soils. 7th International Conference on Soil Mechanics and Foundation Engineering, Mexico City, Mexico, Vol. 1, pp. 379-383.
- Skempton, A.W. 1977. Slope stability of cuttings in brown London clay. 9th International Conference on Soil Mechanics and Foundation Engineering. Vol. 3, pp. 261-270.
- Stermac, A.G., Lo, K.Y. and Barsvary, A.K. 1967. The performance of an embankment on a deep deposit of varved clay. Canadian Geotechnical Journal, Vol. 4, No. 1, pp. 45-61.
- Suklje, L. 1961. A landslide due to long term creep. 5th International Conference on Soil Mechanics and Foundation Engineering, Vol. 2, pp. 727-735.
- Tavenas, F., Des Rosiers, J.P., Leroueil, S., La Rochelle, P. and Roy, M. 1979. The use of strain energy as a yield and creep criterion for lightly overconsolidated clays. Geotechnique, Vol. 29, No. 3, pp. 285-303.
- Tavenas, F. and Leroueil, S. 1977. Effects of stresses and time on yielding of clays. 9th International Conference on Soil Mechanics and Foundation Engineering, Vol. 1, pp. 319-326.
- Tavenas, F., Leroueil, S., La Rochelle, P. and Roy, M. 1978. Creep behaviour of an undisturbed lightly overconsolidated clay. Canadian Geotechnical Journal, Vol. 15, No. 3, pp. 402-423.
- Tavenas, F., Mieussens, C. and Bourges, F. 1979. Lateral displacements in clay foundations under embankments. Canadian Geotechnical Journal, Vol. 16, No. 3, pp. 532-550.
- Taylor, D.W. 1942. Research on consolidation of clays. Massachusetts Institute of Technology, Department of Civil Engineering, Serial 82.

- Taylor, D.W. and Merchant, W. 1940. A theory of clay consolidation accounting for secondary compression. *Journal Math. Phys.*, Vol. 19, No. 2, pp. 167-185.
- Ter-Stepanian, G. 1975. Creep of a clay during shear and its rheological model. *Geotechnique*, Vol. 25, No. 2, pp. 299-320.
- Terzaghi, K. 1941. Undisturbed clay samples and undisturbed clays. *Journal of the Boston Society of Civil Engineers*, Vol. 28, No. 3, pp. 211-231.
- Vaid, Y.P. and Campanella, R.G. 1977. Time-dependent behaviour of undisturbed clay. *Journal of the Geotechnical Engineering Division, ASCE*, Vol. 103, No. GT7, pp. 693-709.
- Vaid, Y.P., Robertson, P.K. and Campanella, R.G. 1979. Strain rate behaviour of Saint Jean Vianney clay. *Canadian Geotechnical Journal*, Vol. 16, No. 1, pp. 34-42.
- Wahls, H.E. 1962. Analysis of primary and secondary consolidation. *Journal of the Soil Mechanics and Foundations Division, ASCE*, Vol. 88, No. SM6, pp. 207-231.
- Walker, L.K. 1969a. Secondary compression in the shear of clays. *Journal of the Soil Mechanics and Foundations Division, ASCE*, Vol. 95, No. SM1, pp. 167-188.
- Walker, L.K. 1969b. Undrained creep in a sensitive clay. *Geotechnique*, Vol. 19, No. 4, pp. 515-529.
- Walker, L.K. 1969c. Discussion. *Journal of the Soil Mechanics and Foundation Engineering Division, ASCE*, SM1, pp. 409-415.
- Watts, K.S. 1980. A device for automatic logging of volume change in large scale triaxial tests. *Geotechnical Testing Journal*, Vol. 3, No. 1, pp. 41-44.
- Wilson, N.E. and Lo, M.B. 1965. Discussion. *Journal of the Soil Mechanics and Foundations Division*, Vol. 91, No. SM1, pp. 231-233.
- Wu, T.H., El Refai, A.N.A.A. and Hsu, J.R. 1978. Creep deformation of clays. *Journal of the Geotechnical Engineering Division, ASCE*, Vol. 104, No. GT1, pp. 61-76.

Wu, T.H., Resiendiz, D. and Neukirchner, R.J. 1966. Analysis of consolidation by rate process theory. Journal of the Soil Mechanics and Foundation Engineering Division, ASCE, Vol. 92, SM6, pp. 229-248.

Yen, B.C. 1969. Stability of slopes undergoing creep deformations. Journal of the Soil Mechanics and Foundations Division, ASCE, Vol. 95, No. 4, pp. 1075-1096.

Yudhbir and Mathur, S.K. 1977. Path dependent drained creep of clays. 9th International Conference on Soil Mechanics and Foundation Engineering. Vol. 1, pp. 353-356.



**Appendix A**  
**Field Instrumentation Data**

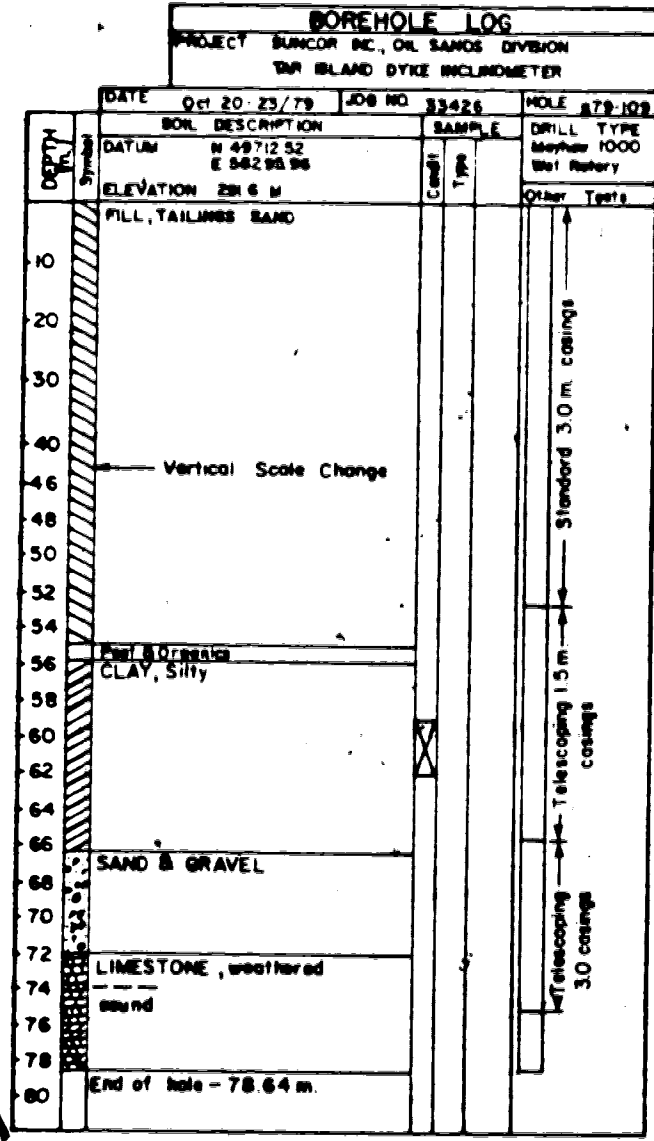


Figure A.1 Test hole log S79-109 at which samples for laboratory testing were obtained

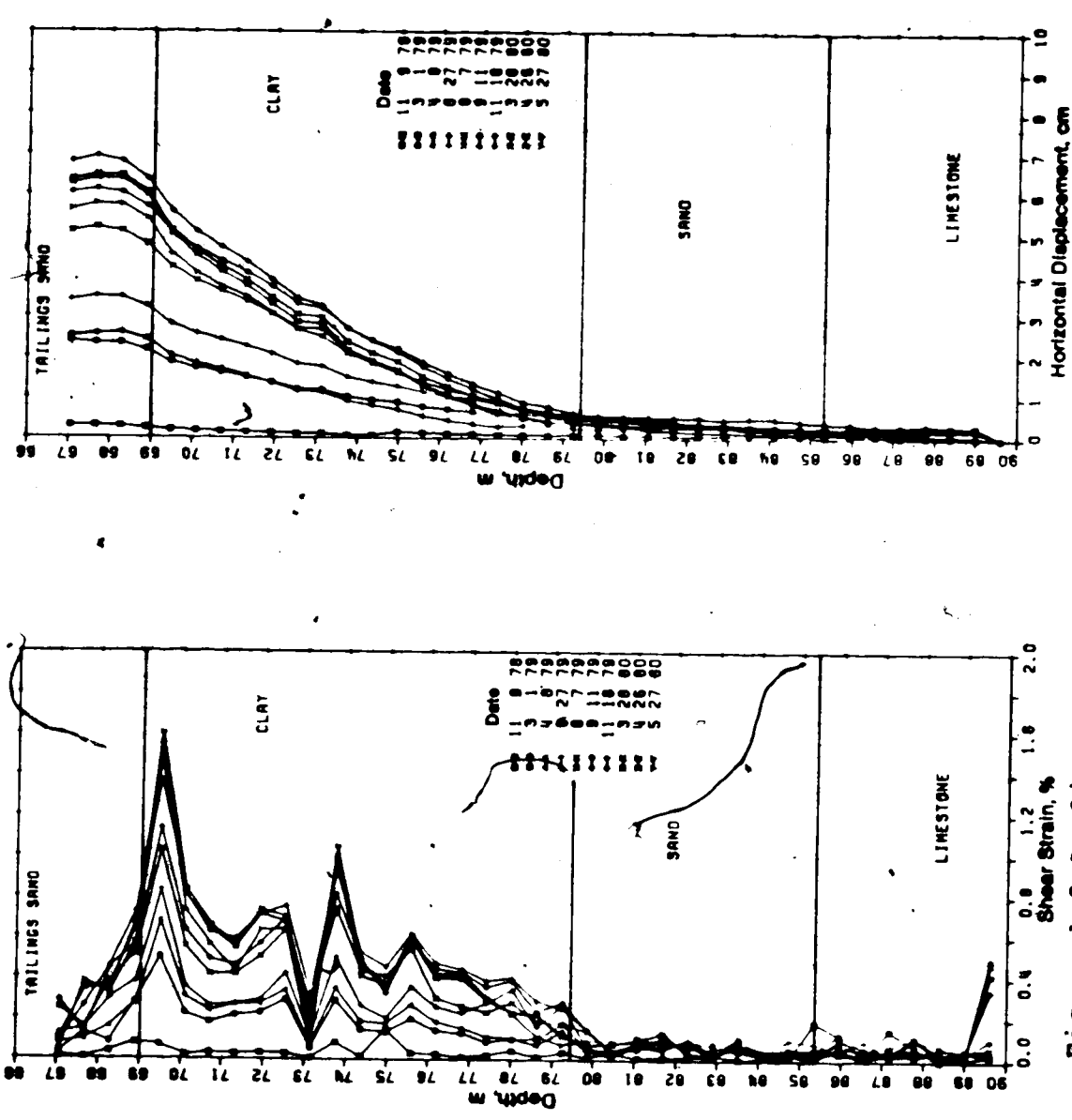


Figure A.2 Inclinometer S78-101S, calibrated November 26, 1978

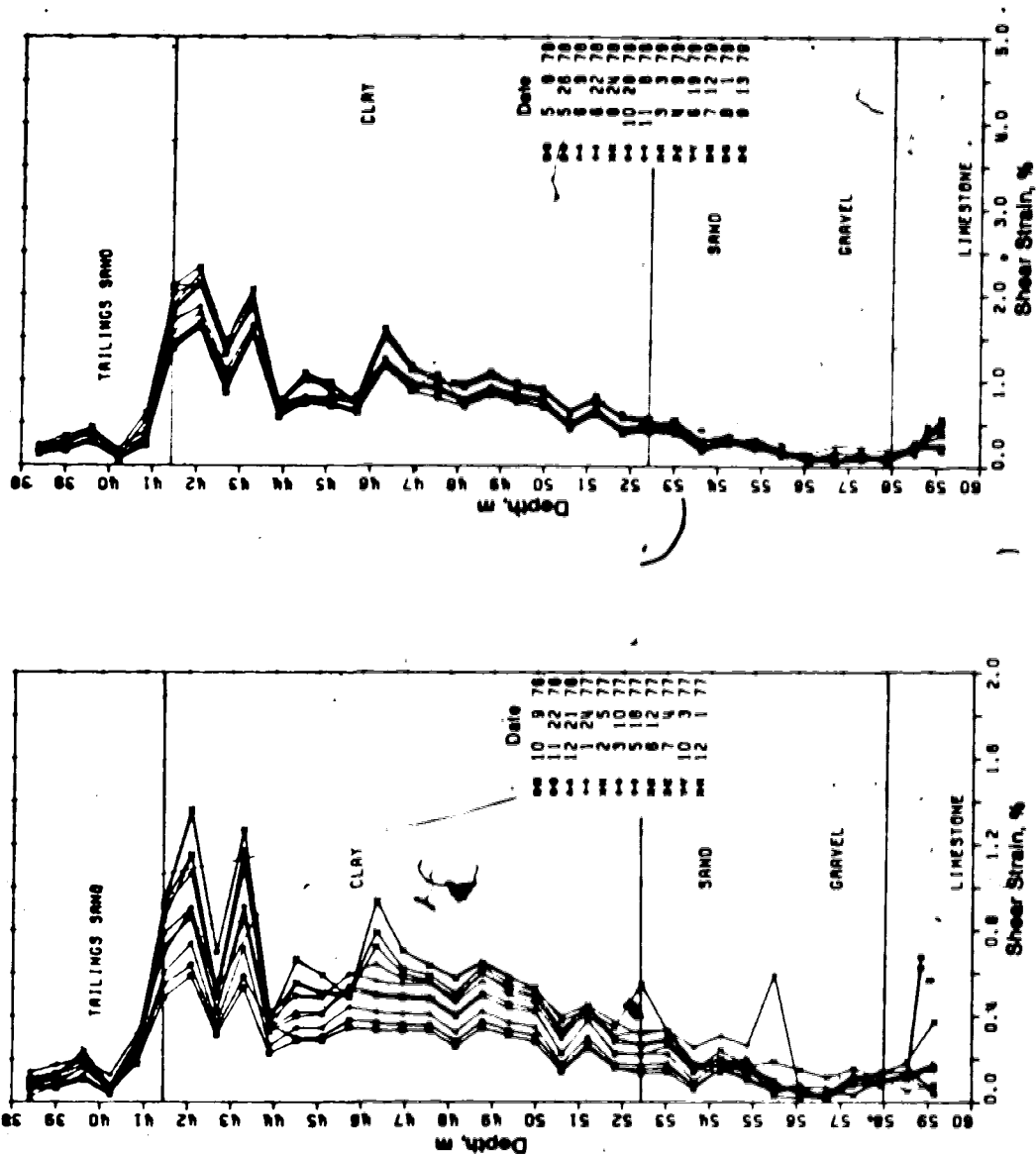


Figure A.3 Inclinometer S75-102, calibrated January 19, 1976, shear strain



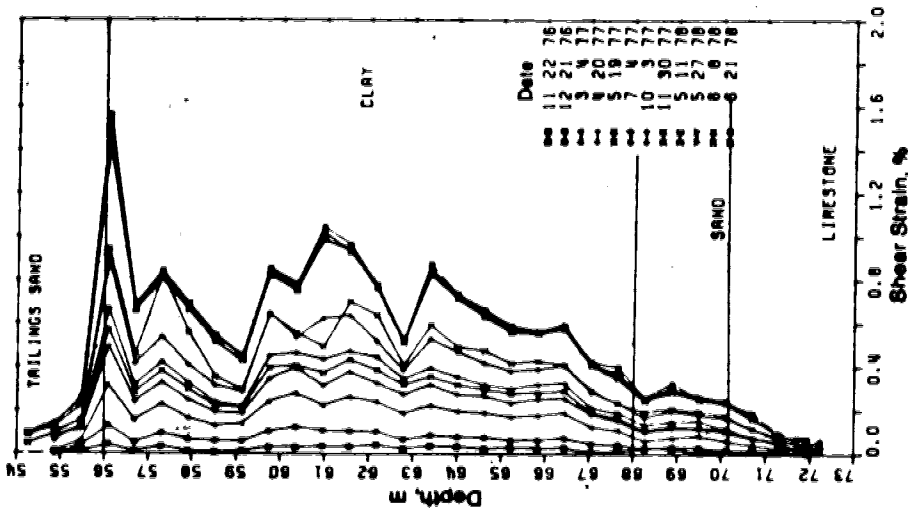
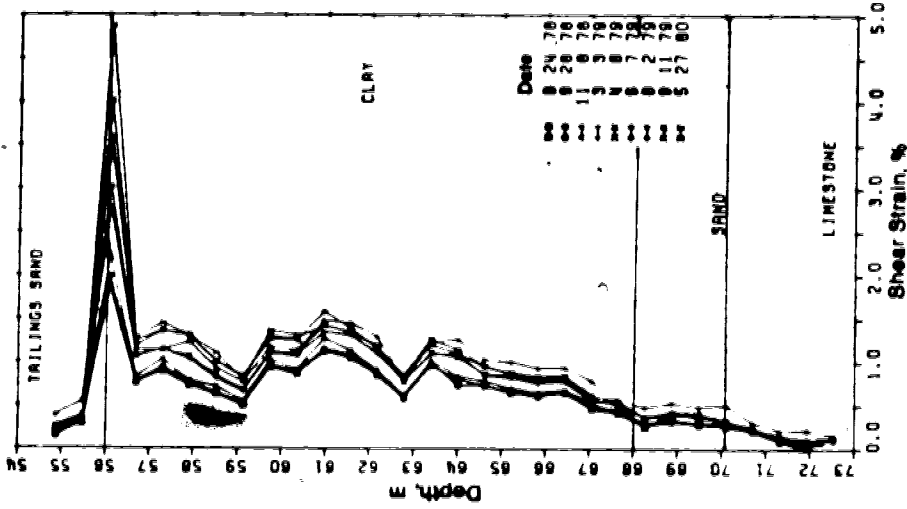


Figure A.5 Incliner S76-103, calibrated November 2, 1976, shear strain

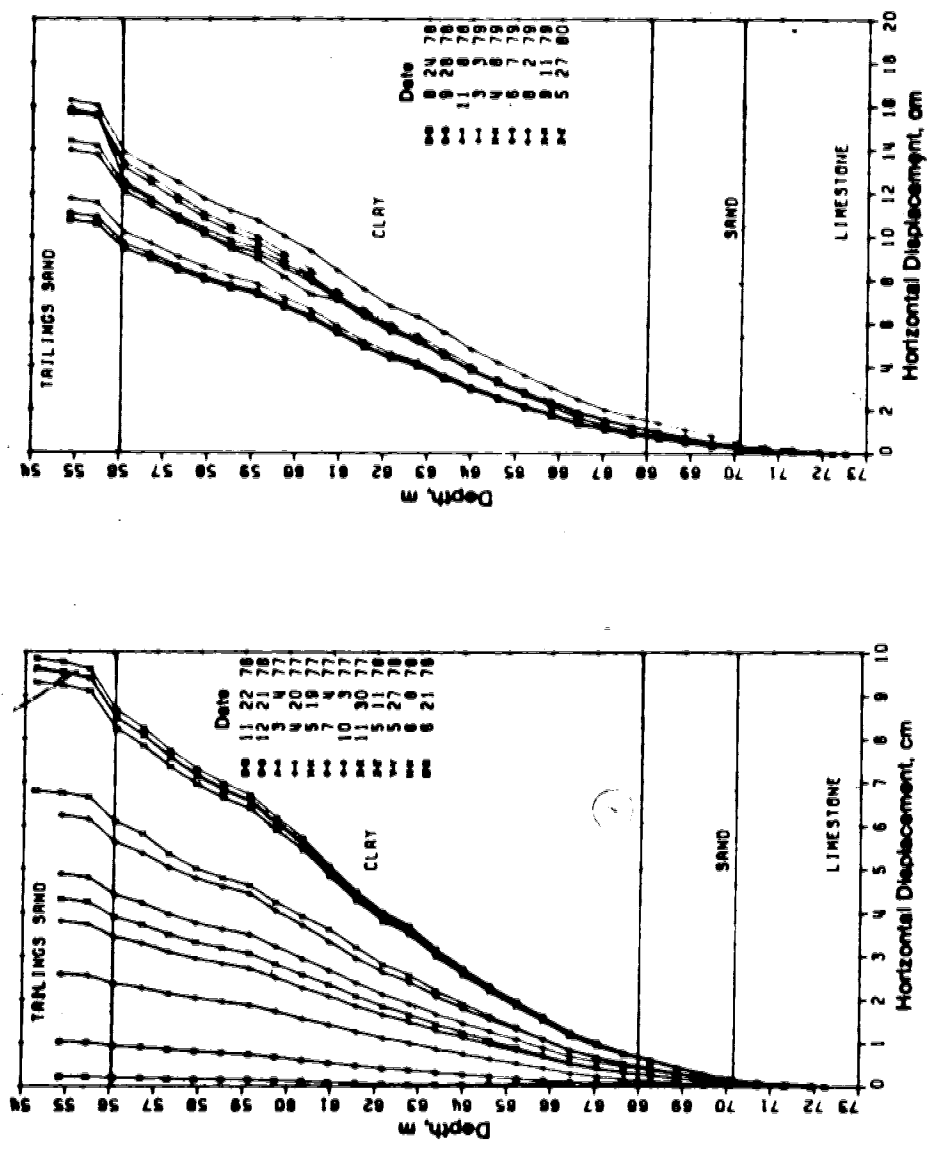


Figure A.6 Inclinometer S76-103, calibrated November 2, 1976, horizontal displacement

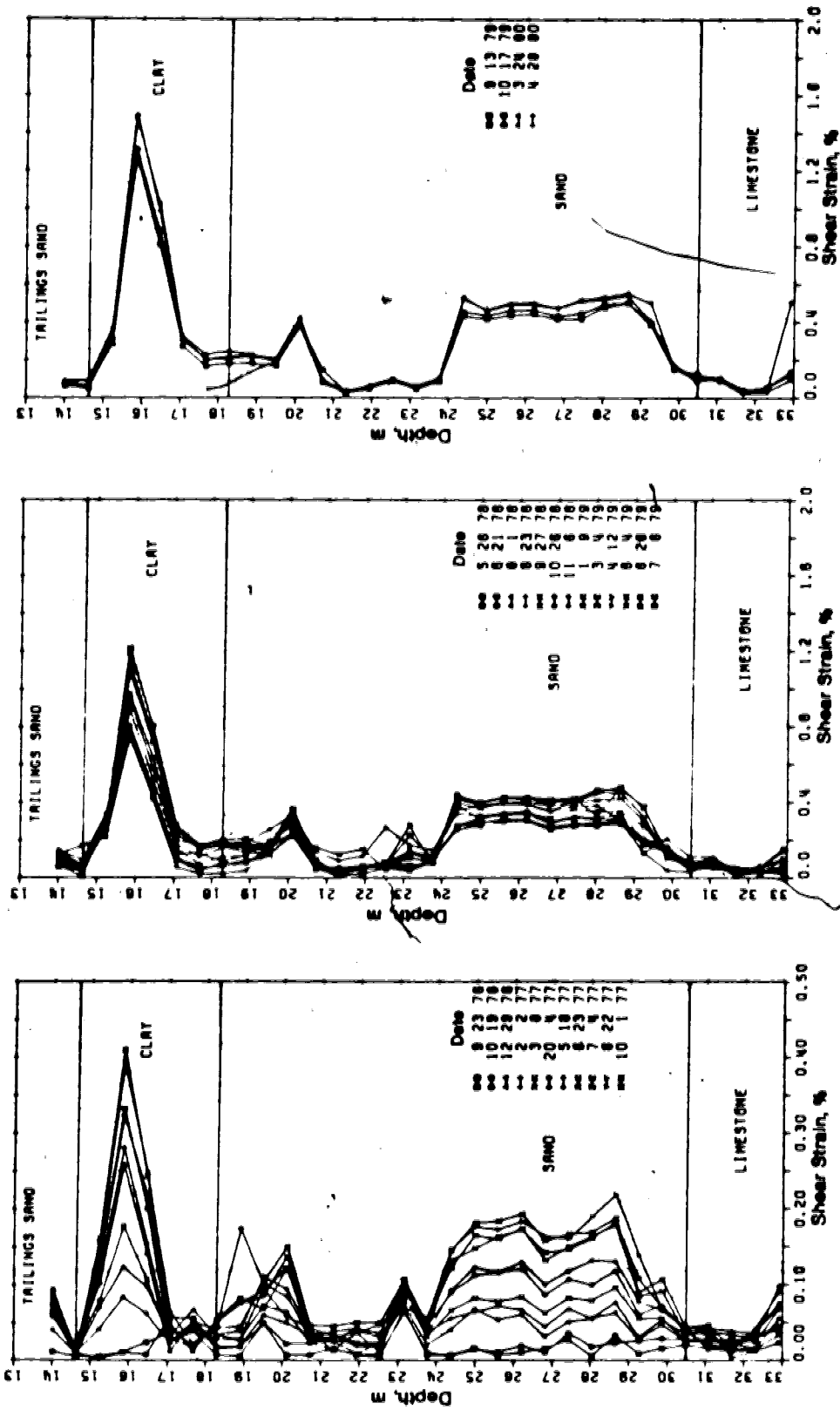


Figure A.7 Inclinerometer S75-104,calibrated September 16,1976,shear strain



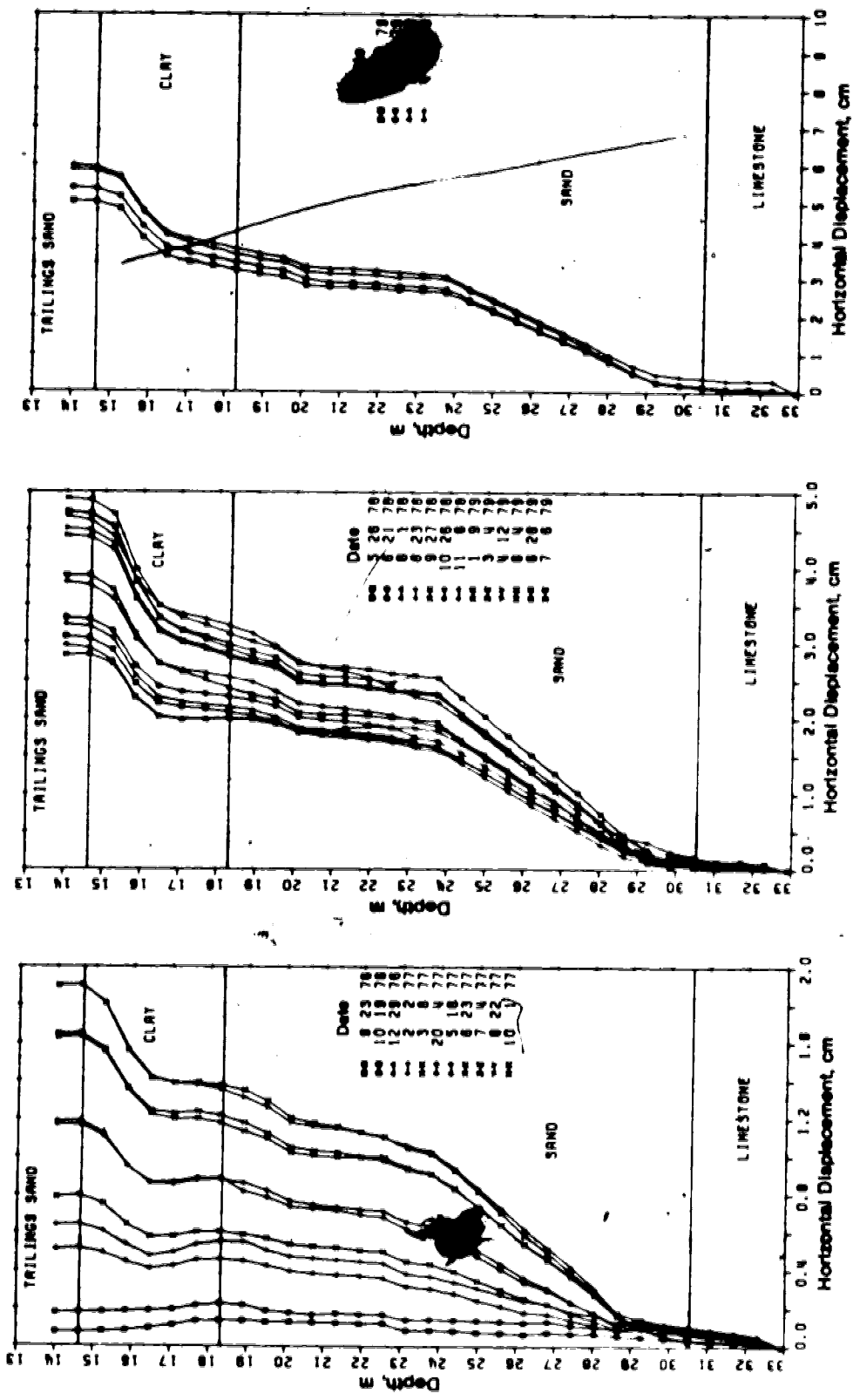


Figure A.8 Inclinometer S75-104, calibrated September 16, 1976, horizontal displacement

**Appendix B**  
**Grain Size Curves, Scanning Electron Micrographs and**  
**Oedometer Test Results**

**B.1 Derivation of Equation 4.3**

For a given change in vertical total stress the effective stresses immediately after loading are:

$$\sigma'_{3f} = \sigma'_{3i} - A\Delta\sigma_1 \quad \text{B.1}$$

$$\sigma'_{1f} = \sigma'_{1i} + \Delta\sigma_1(1-A) \quad \text{B.2}$$

where  $\sigma'_{3i}$  = effective radial stress at the beginning of the increment

$\sigma'_{3f}$  = effective radial stress at the end of the increment

$\sigma'_{1i}$  = effective axial stress at the beginning of the increment

$\sigma'_{1f}$  = effective axial stress at the end of the increment

It follows that:

$$\sin\phi' = \frac{\sigma'_{1i} + \Delta\sigma_1 - \Delta\sigma_1 A - \sigma'_{3i} + \Delta\sigma_1 A}{\sigma'_{1i} + \Delta\sigma_1 - \Delta\sigma_1 A + \sigma'_{3i} - \Delta\sigma_1 A} \quad \text{B.3}$$

Solving for  $\Delta\sigma_1$ :

$$\Delta\sigma_1 = \sigma'_i(1 - \sin\phi') - \sigma'_i(1 + \sin\phi') / (1 - 2A)\sin\phi' - 1) \quad \text{B.4}$$

Table B.1 Oedometer test results, sample C2

Incr. No.	Stress (kPa)	Elapsed Time (min)	Void Ratio Change $\Delta e$	$C_v^{(1)}$ (cm <sup>2</sup> /sec)	$C_a$	$m^{(2)}$	Unit Strain Rate <sup>(3)</sup> (%/min)
1	31.3	1700	0 <sup>(4)</sup>	-	-	-	-
2	62.5	2620	.0055	-	.0030	1.19	.059
3	125.5	5331	.0157	-	.0010	1.23	.21
4	250.0	4483	.0236	-	.0016	1.16	.19
5	500.0	2362	.0315	-	.0021	1.09	.16
6	1000.0	2937	.0463	.00065	.0030	1.11	.30
7	1996.0	4011	.0719	.00045	.0052	1.12	.69
8	4000	11502	.0928	.00025	.0060	1.15	.77

(<sup>1</sup>) Calculated only at stresses above the preconsolidation stress where possible

(<sup>2</sup>) Slope of the logarithm of volumetric strain versus logarithm of time curves

(<sup>3</sup>) Intercept of logarithm of volumetric strain versus logarithm of time at  $t=1$  min, ignoring consolidation effects

(<sup>4</sup>) Sample swelled slightly

Table B.2 Oedometer test results, sample C3

Incr. No.	Stress (kPa)	Elapsed Time (min)	Void Ratio Change $\Delta e$	$C_v^{(1)}$ (cm <sup>2</sup> /sec)	$C_a$	$m^{(2)}$	Unit Strain Rate <sup>(3)</sup> (%/min)
1	39.30	2691	.0157	-	.0003	-	-
2	78.0	4555	.0202	-	.0015	-	-
3	158.9	2482	.0296	-	.0020	1.29	0.71
4	314.0	2676	.0375	-	.0025	1.19	0.41
5	624.0	4093	.0493	-	.0033	1.18	0.56
6	1251	4687	.0743	.00015	.0052	1.15	0.72
7	2502	4180	.0963	.00010	.0071	1.17	1.15
8	5027	2865	.0686	.00011	-	1.16	-

(<sup>1</sup>) Calculated where possible at stresses above the preconsolidation stress

(<sup>2</sup>) Slope of the logarithm of volumetric strain versus logarithm of time curves

(<sup>3</sup>) Intercept of logarithm of volumetric strain versus logarithm of time at  $t=1$  min, ignoring transient consolidation effects

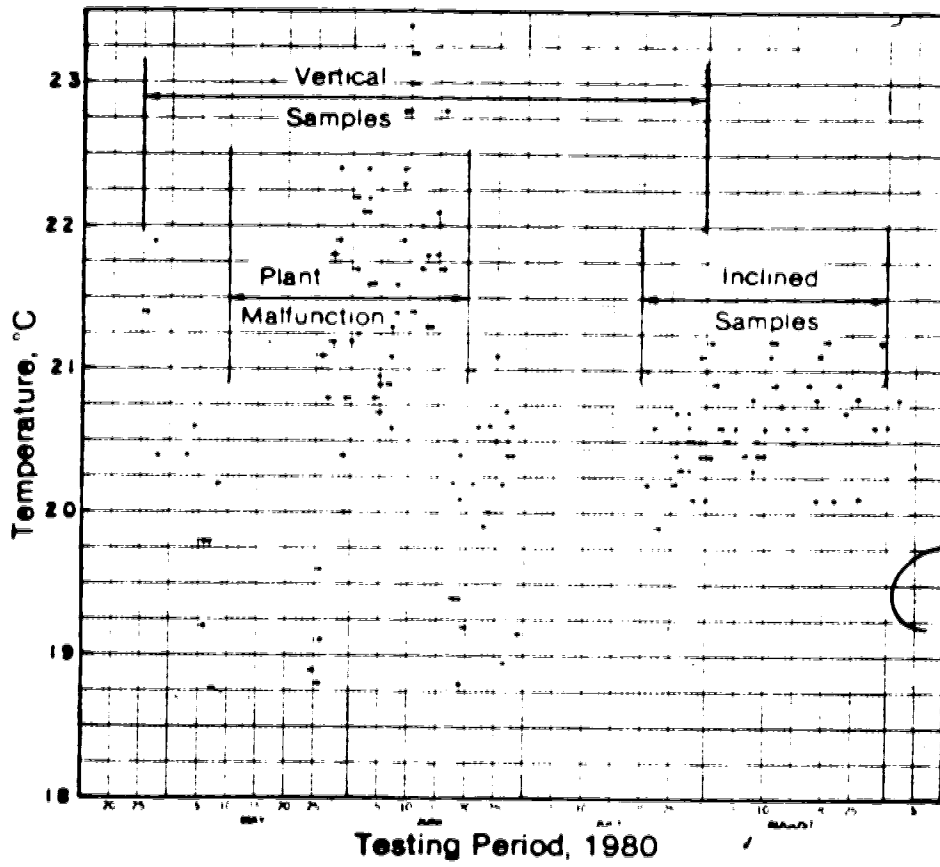


Figure B.1 Room temperature versus time

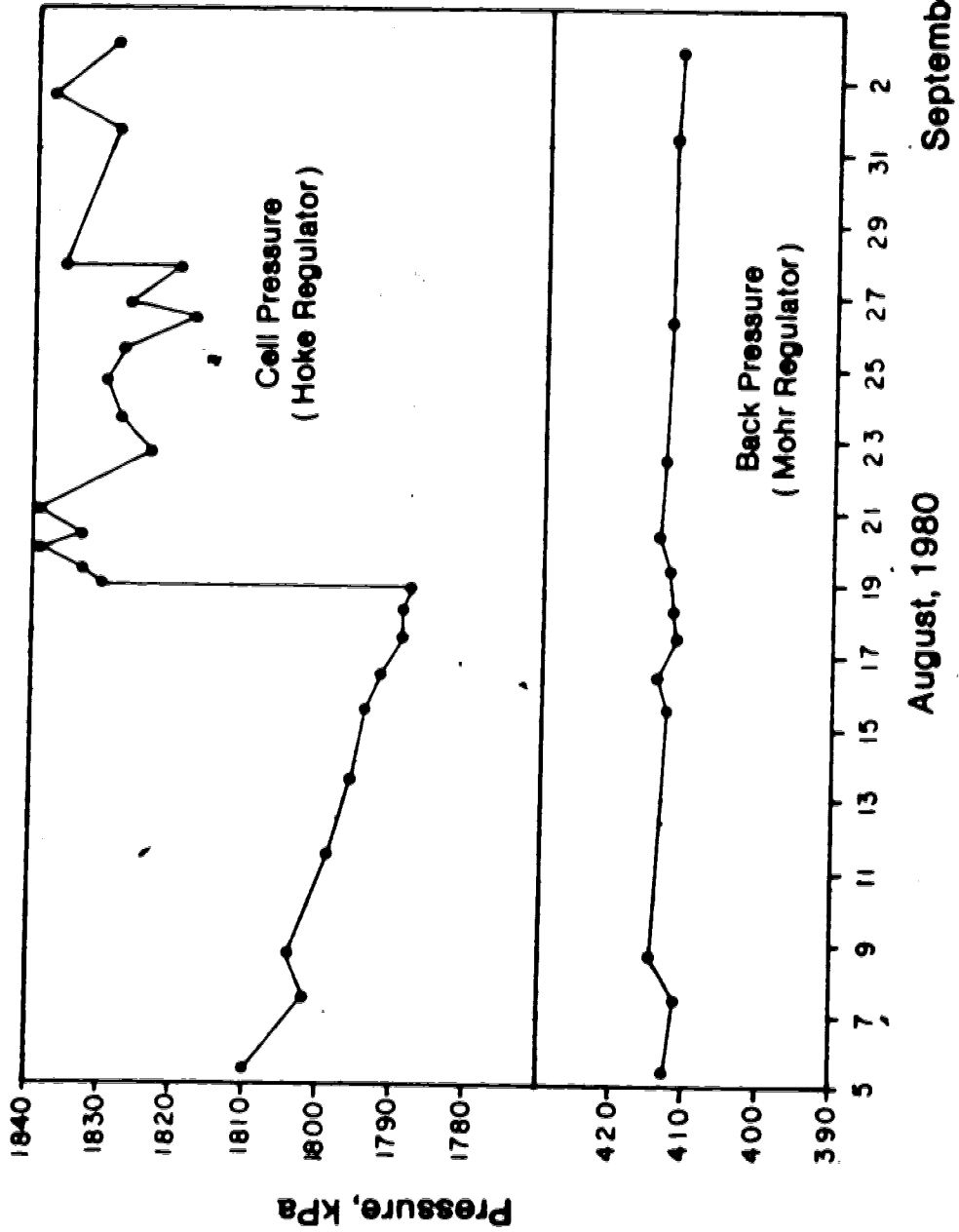


Figure B.2 Cell pressure and back pressure versus time, sample 12

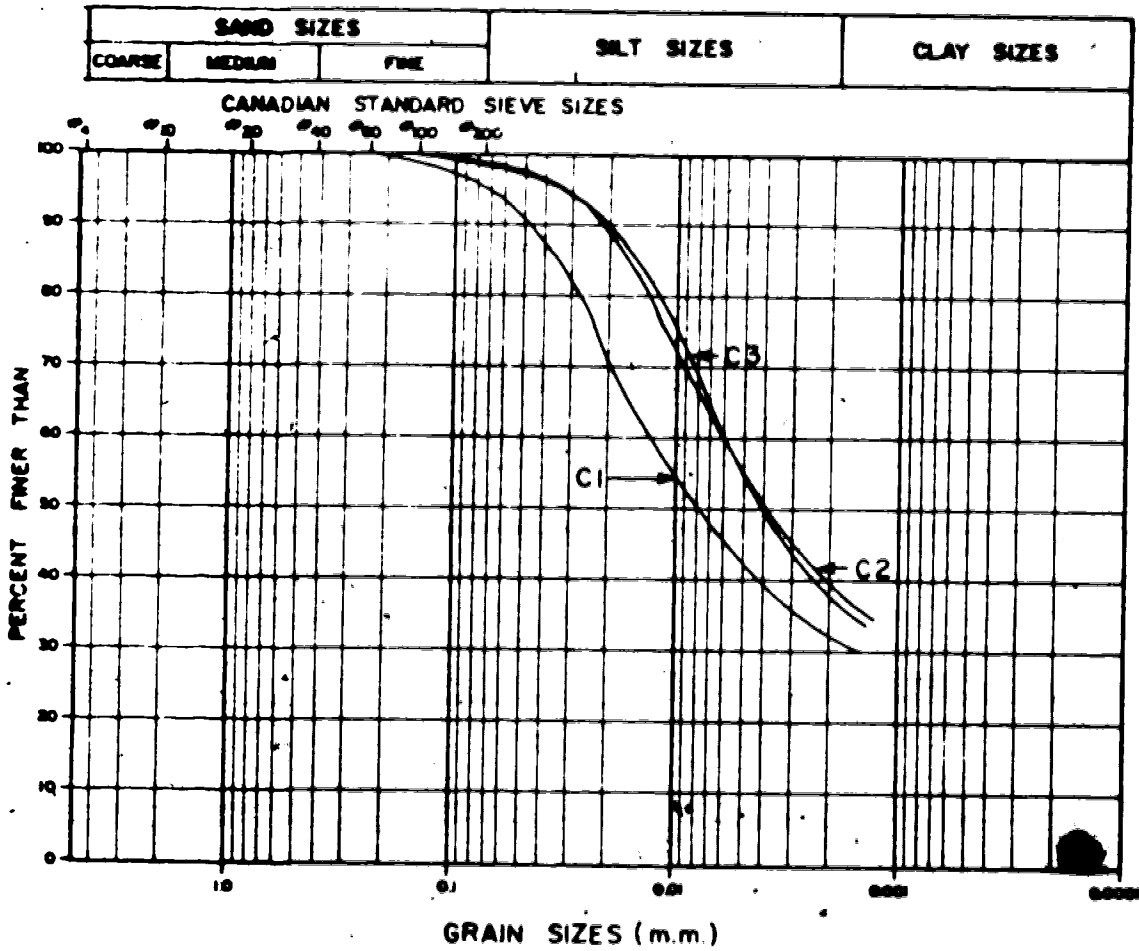


Figure B.3 Grain size analysis, samples C1, C2 and C3

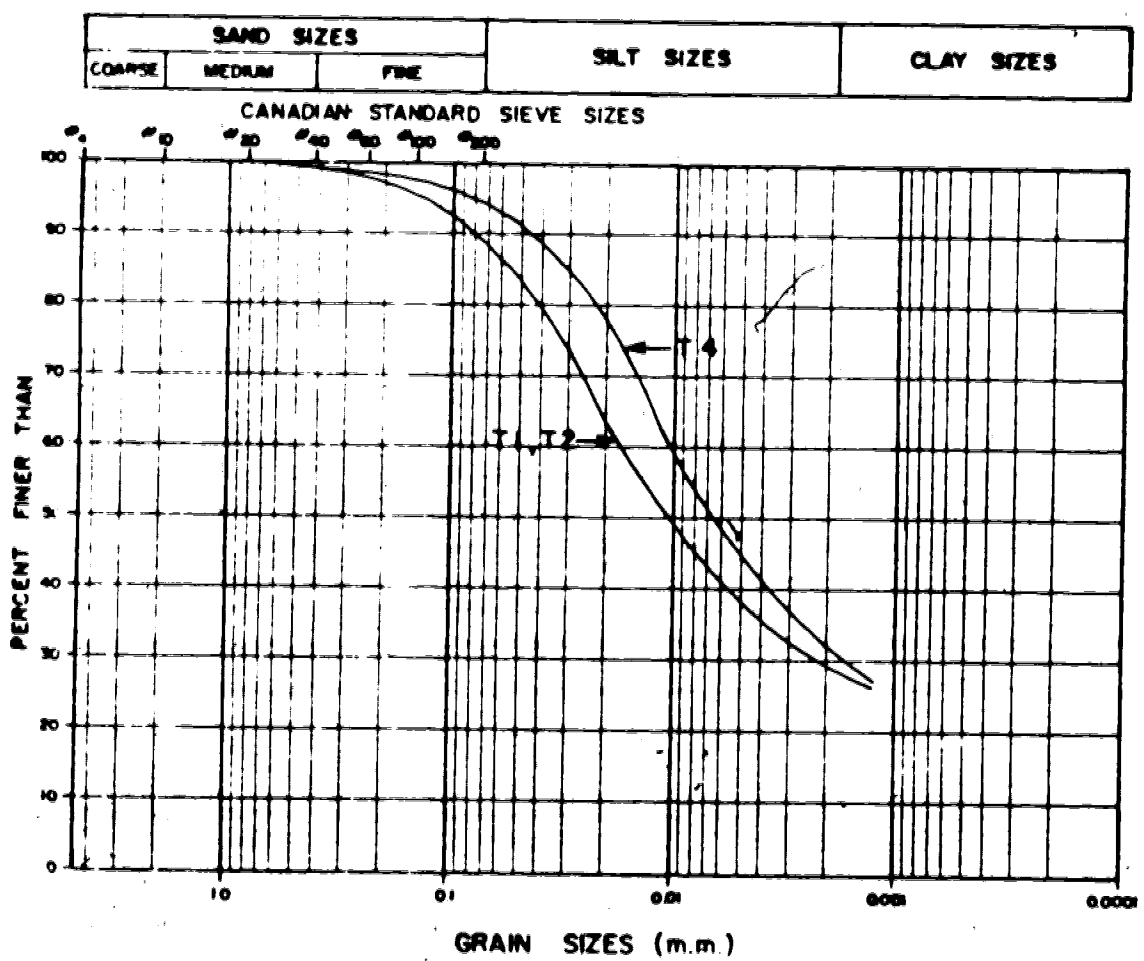


Figure B.4 Grain size analysis, samples T1, T2 and T4





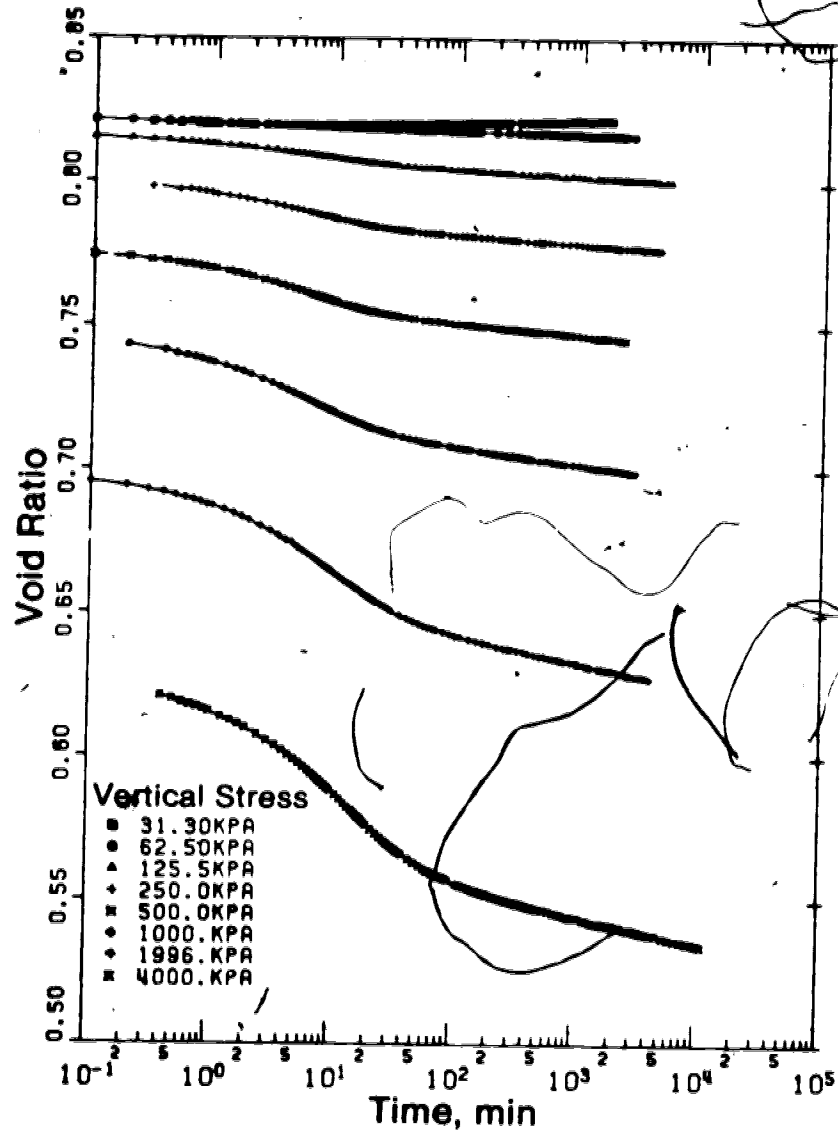


Figure B.6 Void ratio versus time, sample C2

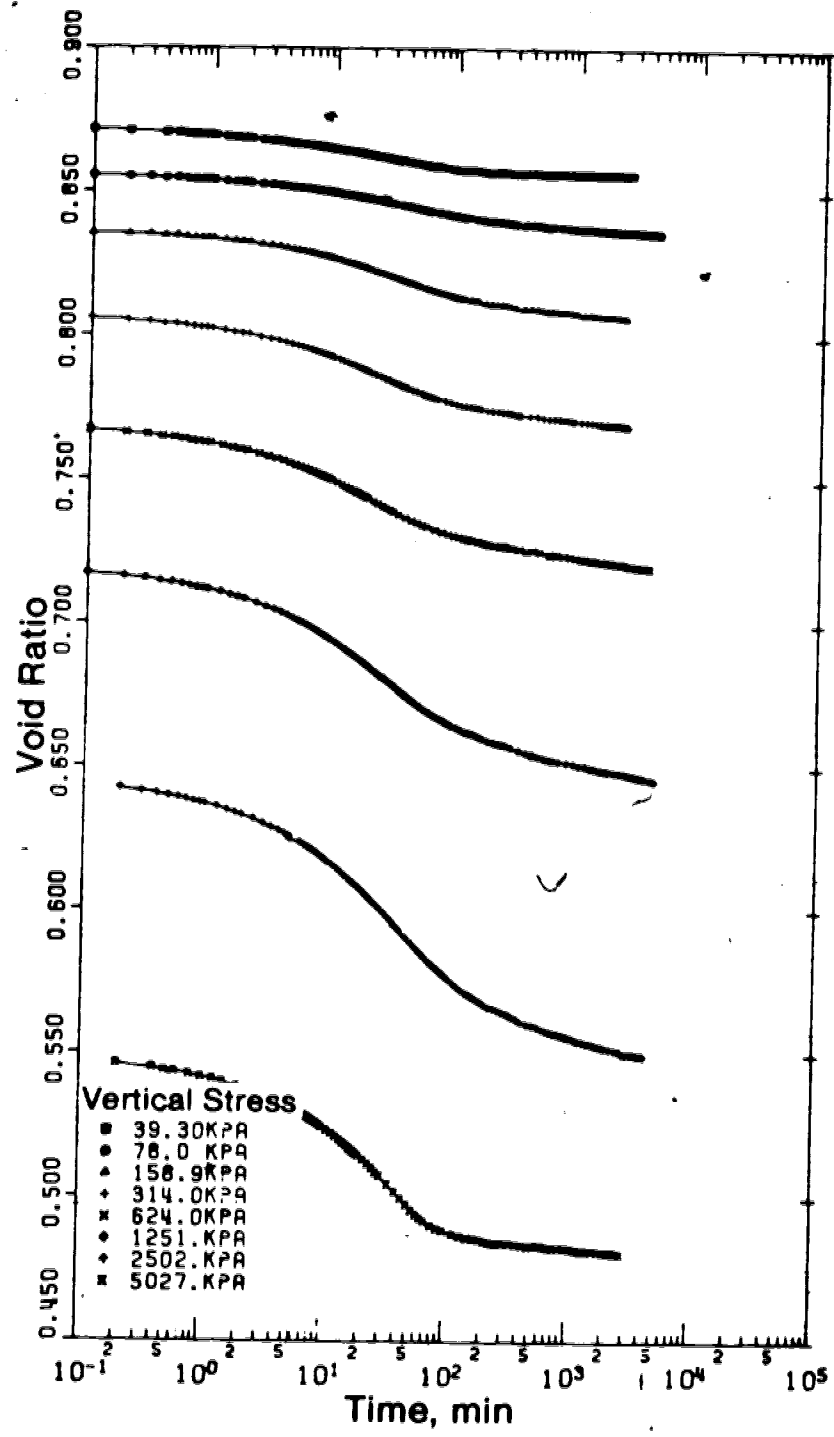


Figure B.7 Void ratio versus time, sample C3

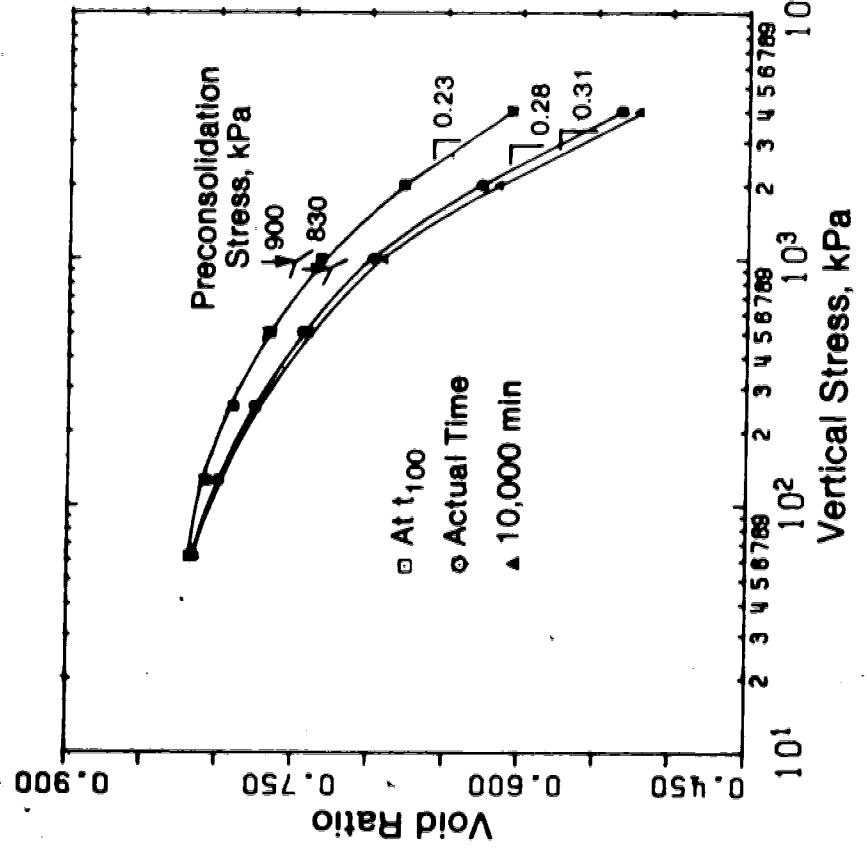
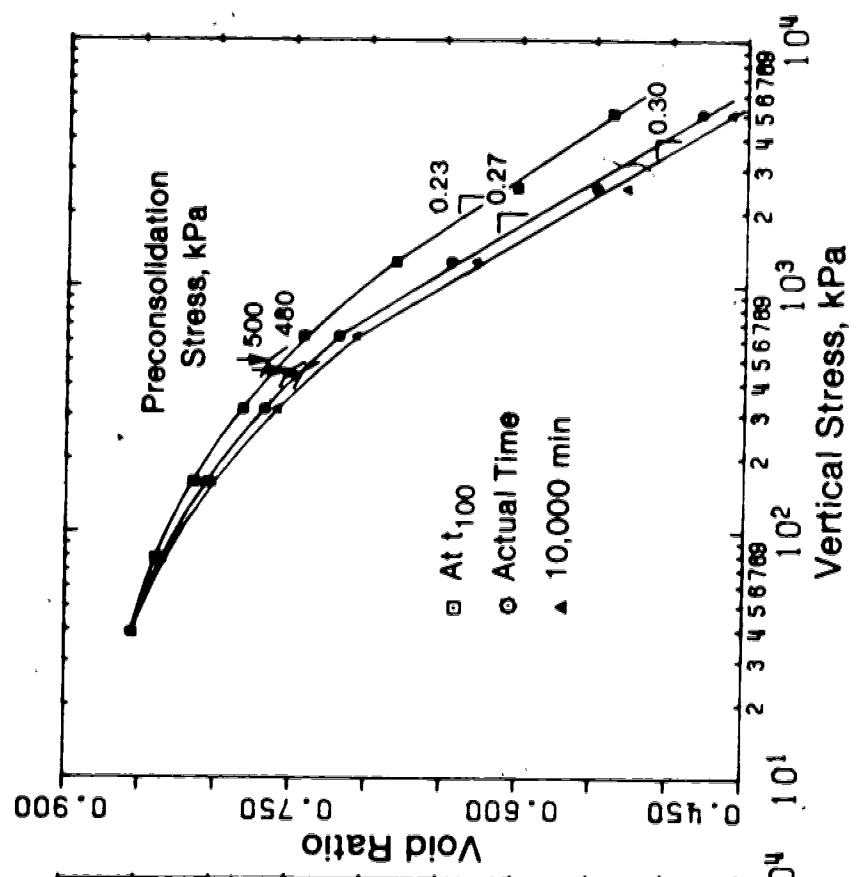


Figure B.8 Void ratio versus effective stress, sample C2-left, sample C3-right

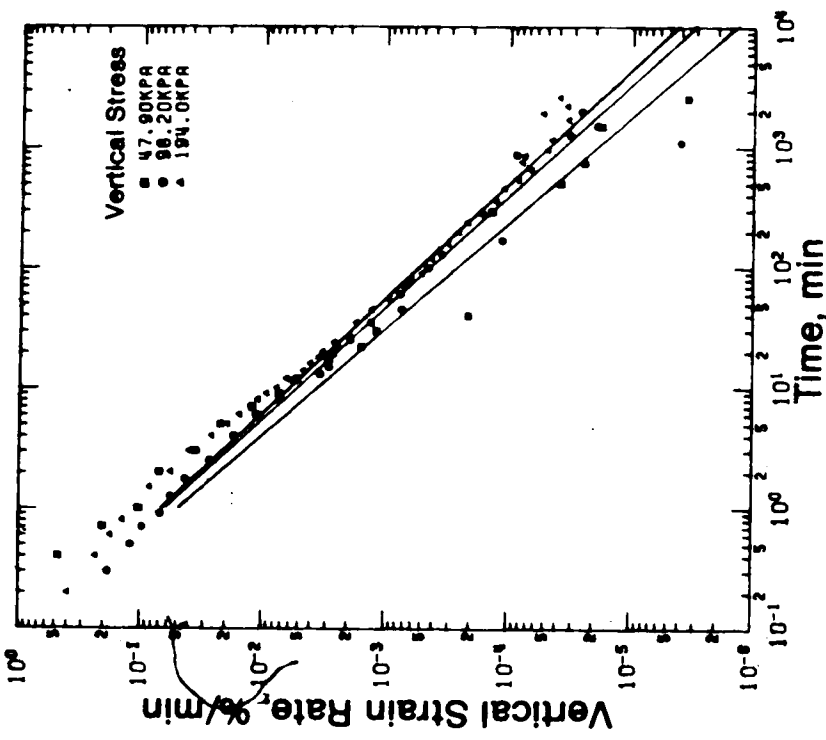
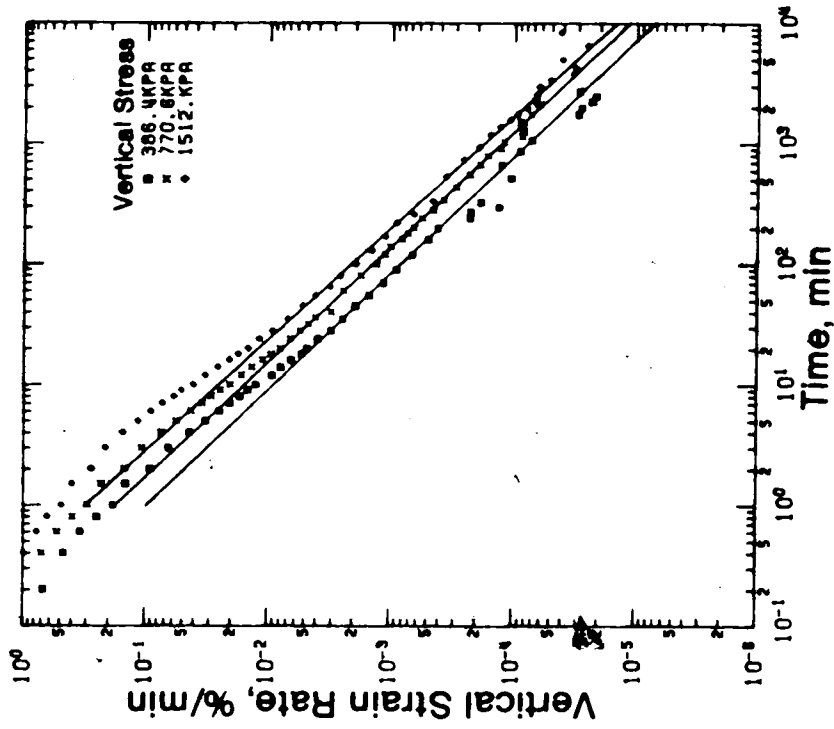
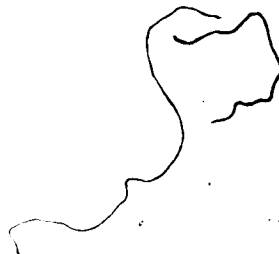


Figure B.9 Vertical strain rate versus time, sample C1



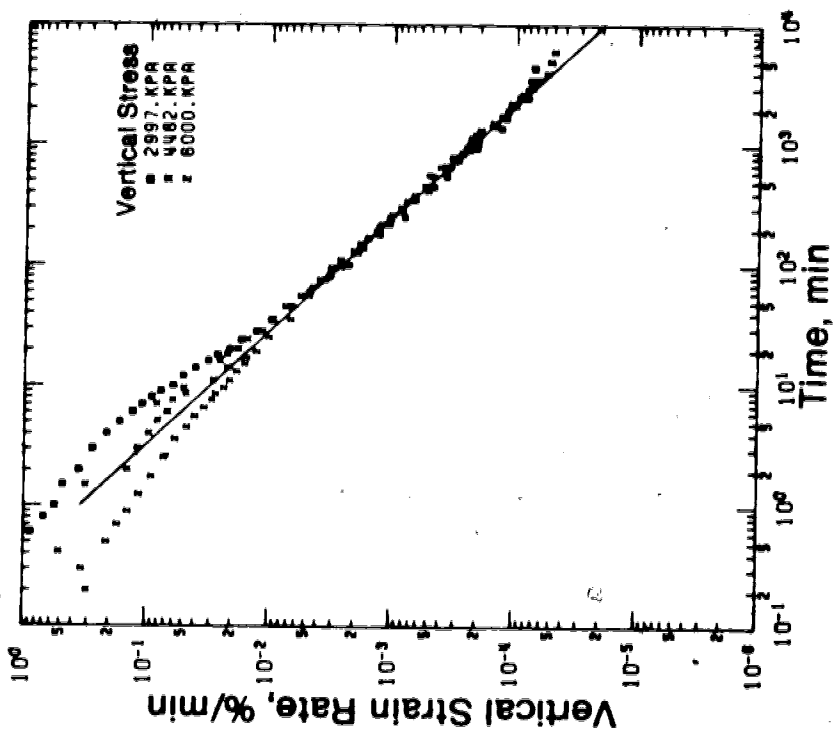


Figure B.10 Vertical strain rate versus time, sample C1

U

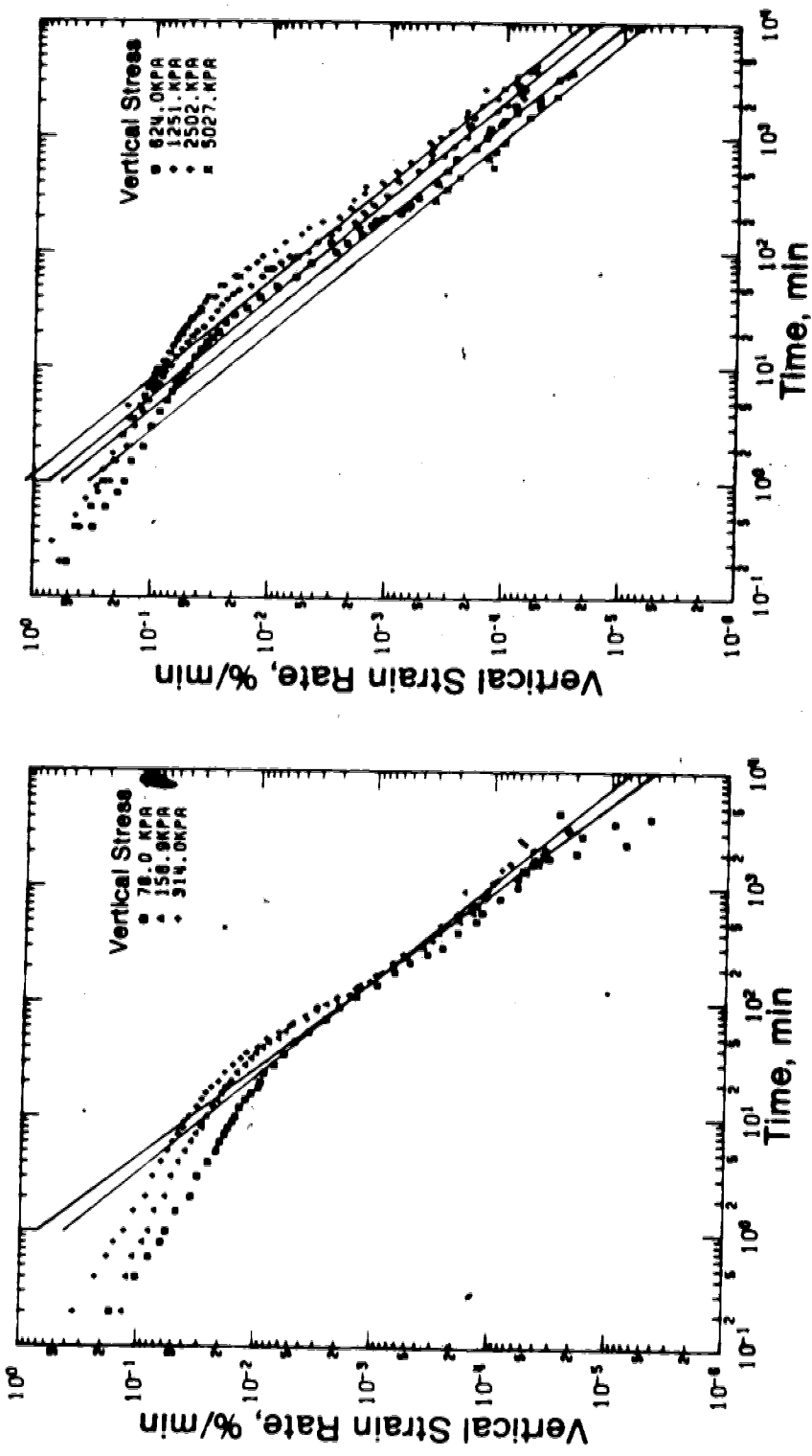


Figure B.11 Vertical strain rate versus time, sample C3

**Appendix C**

**Triaxial Creep Test Results**



Table C.1 Summary of incremental creep test results, sample T1

Incr. No.	Deviator Initial (kPa)	Stress Final (kPa)	Stress Level (%)	Time (min)	Axial Strain (%)	Cumulative Axial Strain (%) <sup>(2)</sup>
1	181	181	8.3	20	0.10	0.10
2	326	326	15.0	1875	0.27	0.37
3	515	514	23.6	16742	0.58	0.95
4	681	681	31.2	5636	0.33	1.28
5	892	891	40.9	1339	0.35	1.63
6	1087	1077	49.9	15754	1.51	3.14
7	1263	1259	58.0	5885	0.56	3.70
8	1467	1467	67.4	27255	1.57	5.27
9	1530	1530	70.3	1334	0.06	5.33
10	1595	1592	73.2	5692	0.33	5.66
11	1649	1645	75.7	3019	0.27	5.93
12	1695	1688	77.8	4573	0.60	6.53
13	1720	1718	78.9	1104	0.15	6.68
14	1781	1764	81.8	5918	1.29	7.97
15	1804	1804	82.8	4224	0.39	8.36
16	1881	1881	86.4	1517	0.39	8.75
17	1959	1959	90.0	5572	3.41	12.16
18	1998	1998	91.8	4149	0.37	12.53
19	2030	2030	93.2	280	0.07	12.60

(cont'd)

Table C.1 (cont'd)

Incr. No.	Deviator Initial (kPa)	Stress Final (kPa)	Stress Level (%)	Time (min)	Axial Strain (%)	Cumulative Axial Strain (%) <sup>(2)</sup>
20	2049	2047	94.1	350	0.08	12.68
21	2089	2085	95.9	808	0.26	12.94
22	2126	2104	97.6	1475	1.70	14.64
23	2143	2085	98.4	3130	3.42	18.06
24	2116	21145	97.2	270	0.09	18.15
25	2152	2141	98.8	1020	0.61	18.76
26 <sup>(1)</sup>	2178	2155	100.0	1430	2.87	21.63

Total duration of test=120371 mins,  $\sigma_3=1103$  kPa

<sup>(1)</sup> Failure

<sup>(2)</sup> Strain at the end of the increment

Table C.2 Summary of incremental creep test results, sample T2

Incr. No.	Deviator Initial (kPa)	Stress Final (kPa)	Stress Level (%)	Time (min)	Axial Strain (%)	Cumulative Axial Strain (%) <sup>(1)</sup>
1	186	186	13.5	1645	0.14	0.14
2	366	365	26.7	17171	0.48	0.62
3	490	490	35.7	2736	0.14	0.76
4	615	614	44.8	2686	0.44	1.20
5	738	740	53.8	17418	0.86	2.06
6	864	863	63.0	2574	0.37	2.42
7	986	970	71.9	1181	1.18	3.60
8	1055	1082	76.9	20418	1.89	5.49
9	1122	1121	81.7	1187	0.06	5.55
10	1161	1157	84.6	4603	0.45	6.00
11	1187	1186	86.6	1395	0.21	6.21
12	1216	1206	88.6	5911	1.05	7.26
13	1243	1238	90.6	4159	0.55	7.81
14	1312	1299	95.6	1457	1.25	9.06
15 <sup>(1)</sup>	1372	1307	100.0	380	5.30	14.36

Total duration of test=84921 mins,  $\sigma_1$ =758 kPa

<sup>(1)</sup> Failure did not occur, sample strained vertically 5.3%

<sup>(2)</sup> Strain at the end of the increment

Table C.3 Summary of incremental creep test results, sample I1

Incr. No.	Deviator Stress (kPa)	Stress Final (kPa)	Stress Level (%)	Time (min)	Axial Strain (%)	Cumulative Axial Strain (%) <sup>(2)</sup>
1	233	233	20.5	505	0.48	0.48
2	413	412	36.3	6800	0.85	1.33
3	594	593	52.2	1280	0.55	1.88
4	775	767	68.1	1431	1.68	3.56
5	949	948	83.4	13189	3.44	6.99
6	1064	1064	93.9	2850	0.47	7.47
7 <sup>(1)</sup>	1138	1131	100.0	212	0.63	8.10

Total Duration of Test=26267 mins,  $\sigma_3=743$  kPa

<sup>(1)</sup> Failure

<sup>(2)</sup> Strain at the end of the increment

Table C.4 Summary of incremental creep test results, sample I2

Incr. No.	Deviator Initial (kPa)	Stress Final (kPa)	Stress Level (%)	Time (min)	Axial Strain (%)	Cumulative Axial Strain (%) <sup>(2)</sup>
1	356	356	17.5	1331	0.47	0.47
2	696	691	34.2	7103	1.74	2.21
3	894	892	43.9	1648	0.42	2.63
4	1079	1073	53.0	1190	0.96	3.59
5	1290	1288	63.3	10180	2.53	6.12
6	1531	1525	75.2	1350	0.67	6.79
7	1648	1640	80.9	310	0.62	7.41
8	1729	1693	84.9	1380	2.72	10.13
9	1744	1740	85.6	1070	0.28	10.41
10	1793	1785	88.0	8845	0.82	11.23
11	1821	1820	89.4	1461	0.06	11.29
12	1895	1892	93.0	1264	0.13	11.42
13	1966	1963	96.5	340	0.13	11.55
14 <sup>(1)</sup>	2037	2024	100.0	330	0.72	12.27

Total Duration of Test=37802 mins,  $\sigma_1$ =1386 kPa

(1) Failure

(2) Strain at the end of the increment

Table C.5 Summary of incremental creep test results, sample I3

Incr. No.	Deviator Initial (kPa)	Stress Final (kPa)	Stress Level (%)	Time (min)	Axial Strain (%)	Cumulative Axial Strain (%) <sup>(1,2)</sup>
1	291	291	17.5	1281	0.45	0.45
2	539	539	32.4	7123	0.07	0.52
3	695	693	41.7	1667	0.44	0.96
4	834	832	50.1	1240	0.42	1.38
5	1022	1021	61.4	10110	1.69	3.07
6	1205	1201	72.4	1318	0.47	3.54
7	1290	1287	77.5	310	0.34	3.88
8	1350	1339	81.0	1400	1.10	4.98
9	1402	1397	84.2	9915	1.41	6.39
10	1466	1464	88.0	1461	0.14	6.53
11	1525	1522	91.6	1264	0.25	6.78
12	1588	1583	95.3	330	0.34	7.12
13	1621	1599	97.4	1095	1.58	8.70
14	1636	1626	98.3	410	0.78	9.48
15 <sup>(1)</sup>	1665	1648	100.0	230	1.18	10.66

Total Duration of Test=39154 mins,  $\sigma'_v=1090$  kPa

<sup>(1)</sup> Failure

<sup>(2)</sup> Strain at the end of the increment

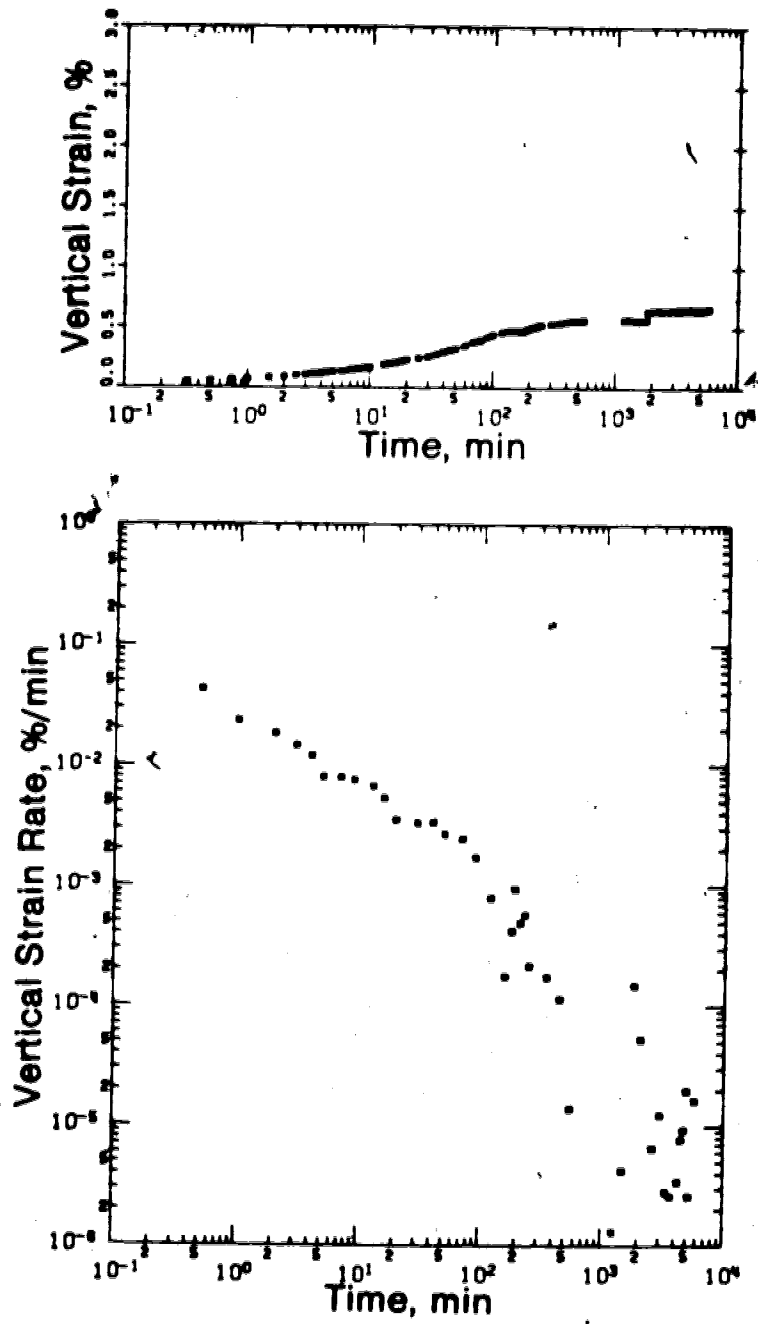


Figure C.1 Vertical strain and strain rate versus time, sample 11, consolidation pressure=365 kPa

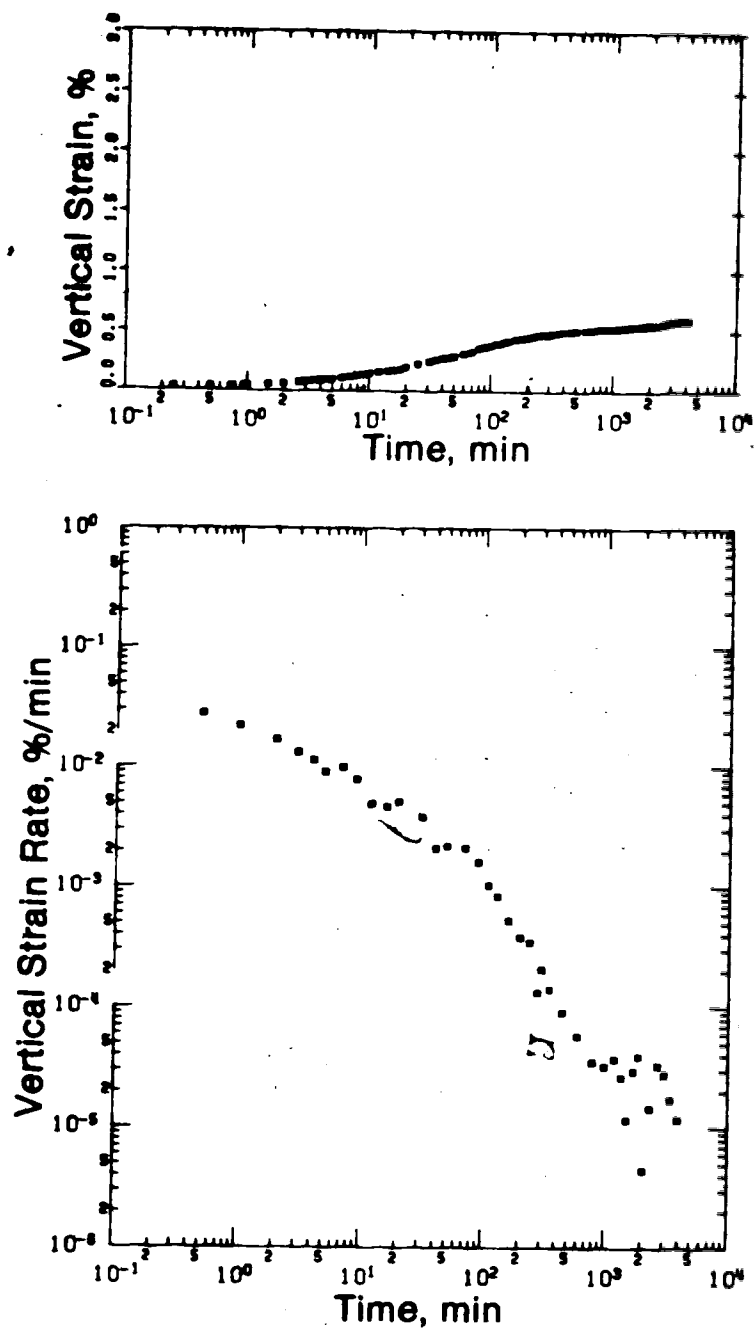


Figure C.2 Vertical strain and strain rate versus time, sample I1, consolidation pressure=743 kPa



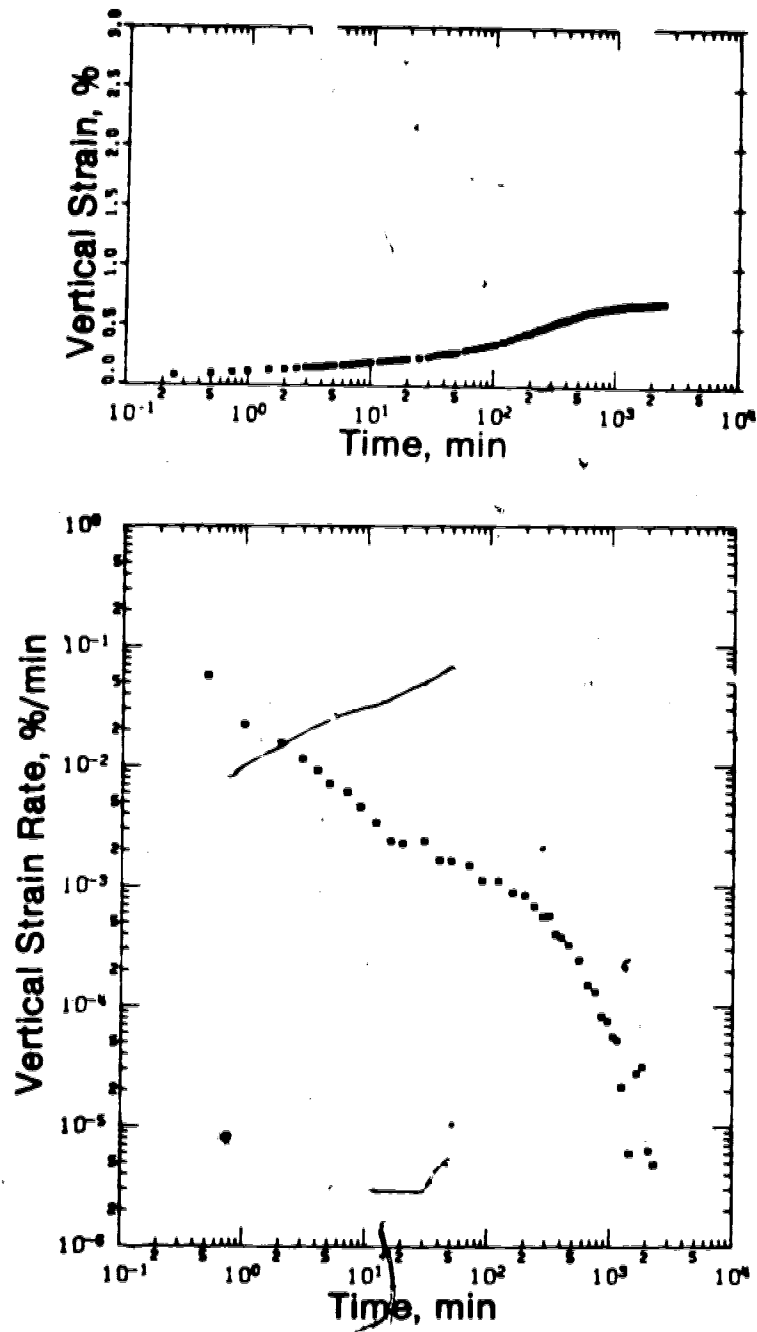


Figure C.3 Vertical strain and strain rate versus time, sample 12, consolidation pressure=334 kPa

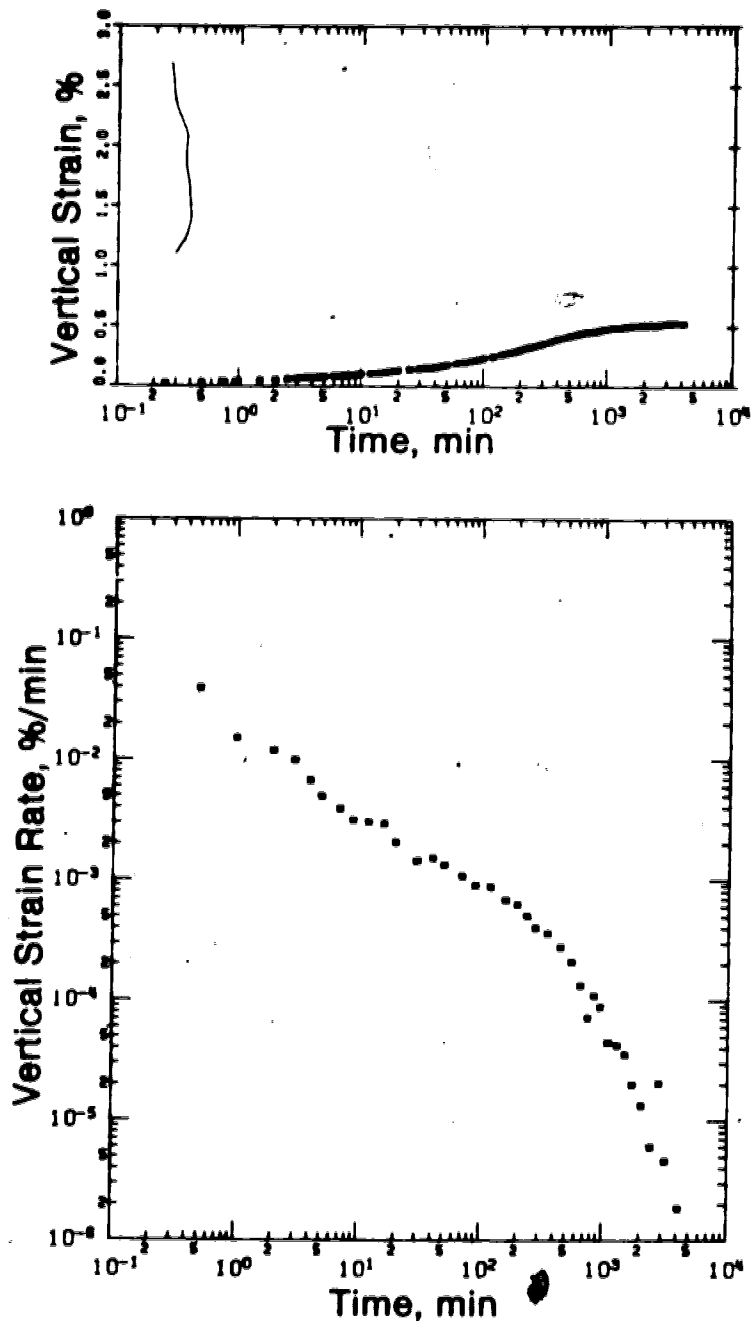


Figure C.4 Vertical strain and strain rate versus time, sample 12, consolidation pressure=672 kPa

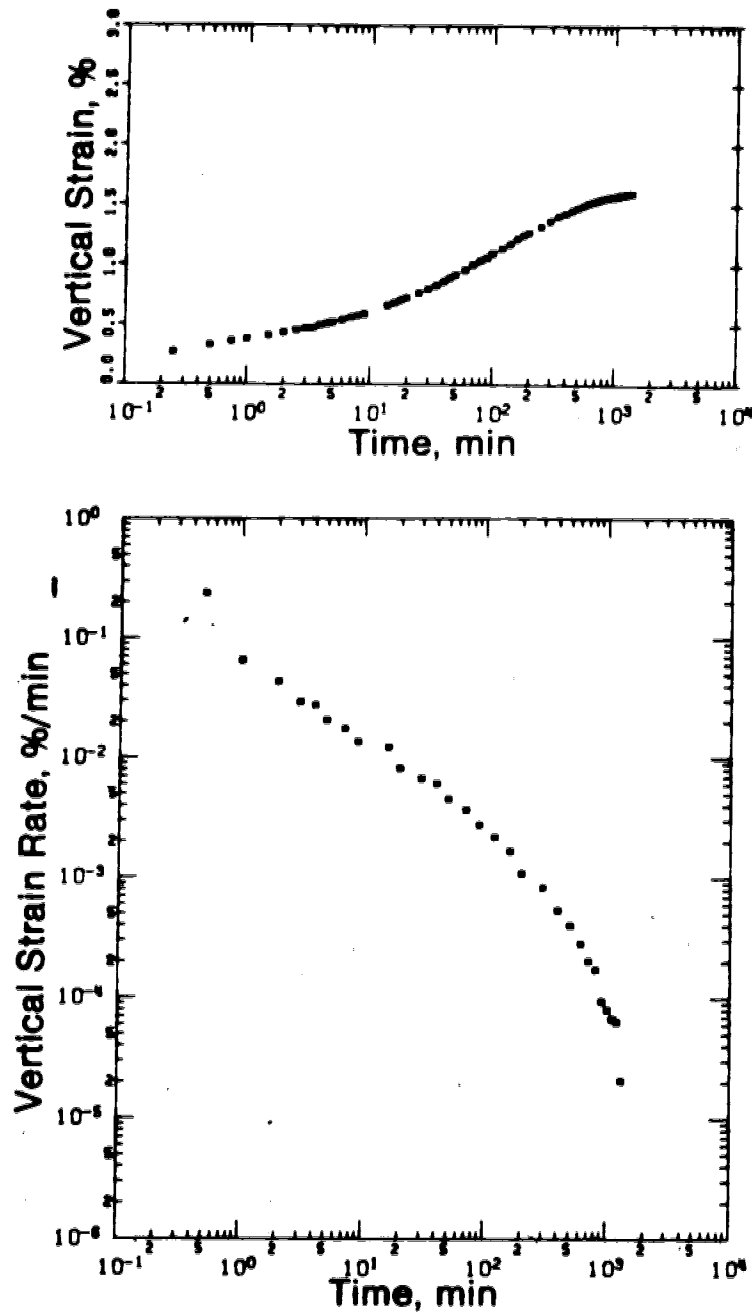


Figure C.5 Vertical strain and strain rate versus time, sample 13, consolidation pressure=271 kPa

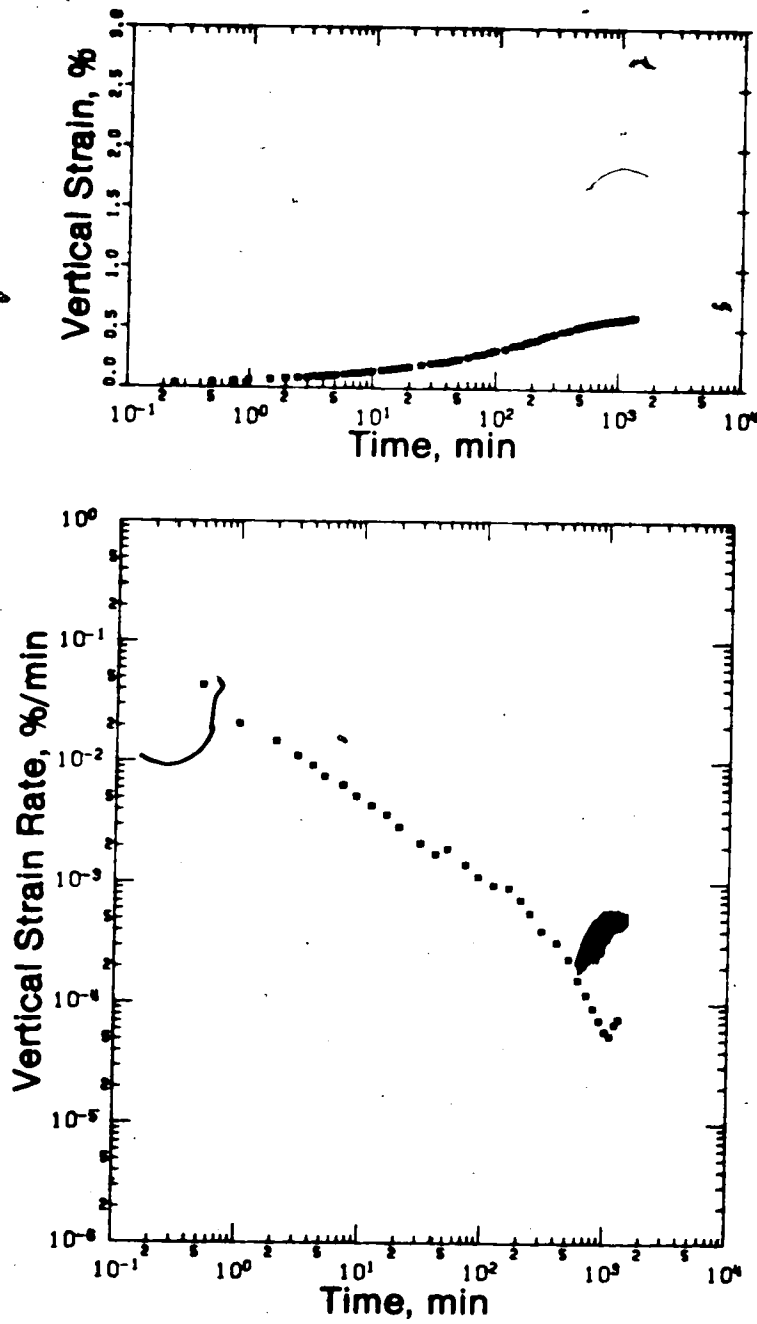


Figure C.6 Vertical strain and strain rate versus time, sample 13, consolidation pressure=548 kPa

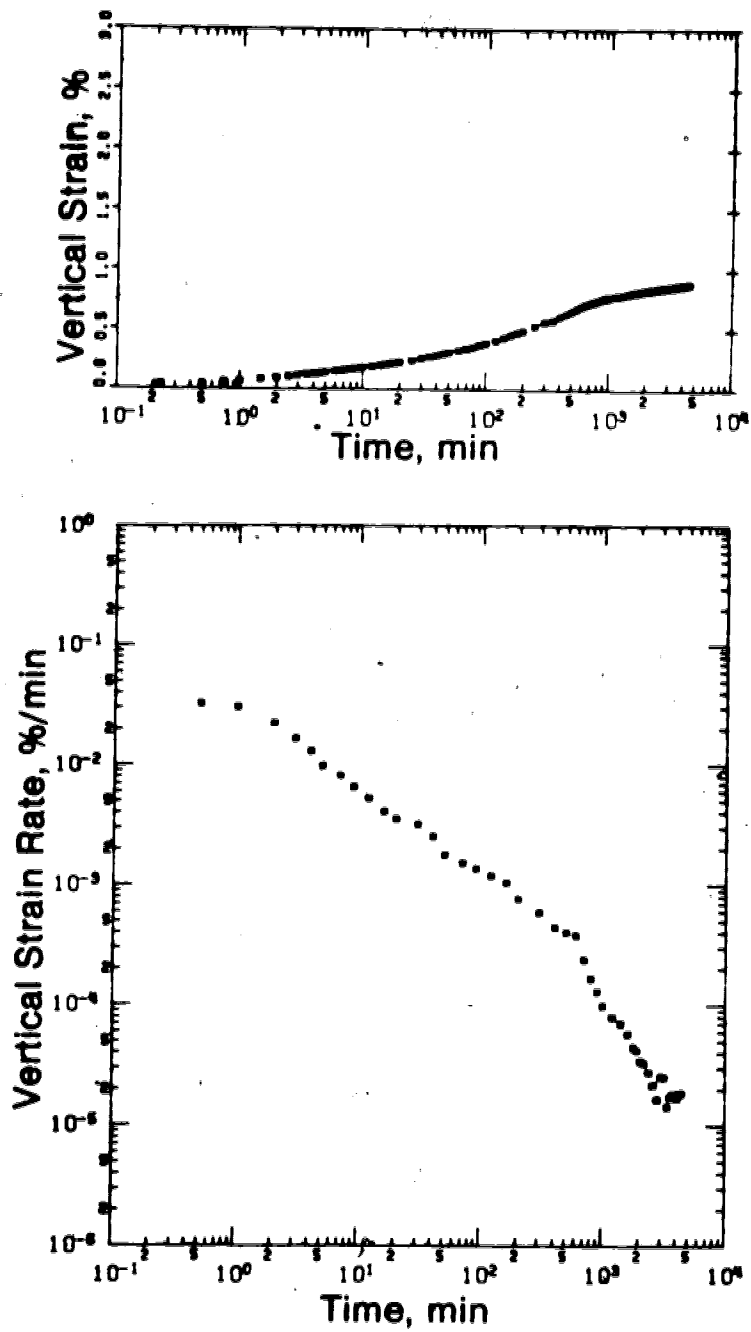


Figure C.7 Vertical strain and strain rate versus time, sample I3, consolidation pressure=1090 kPa

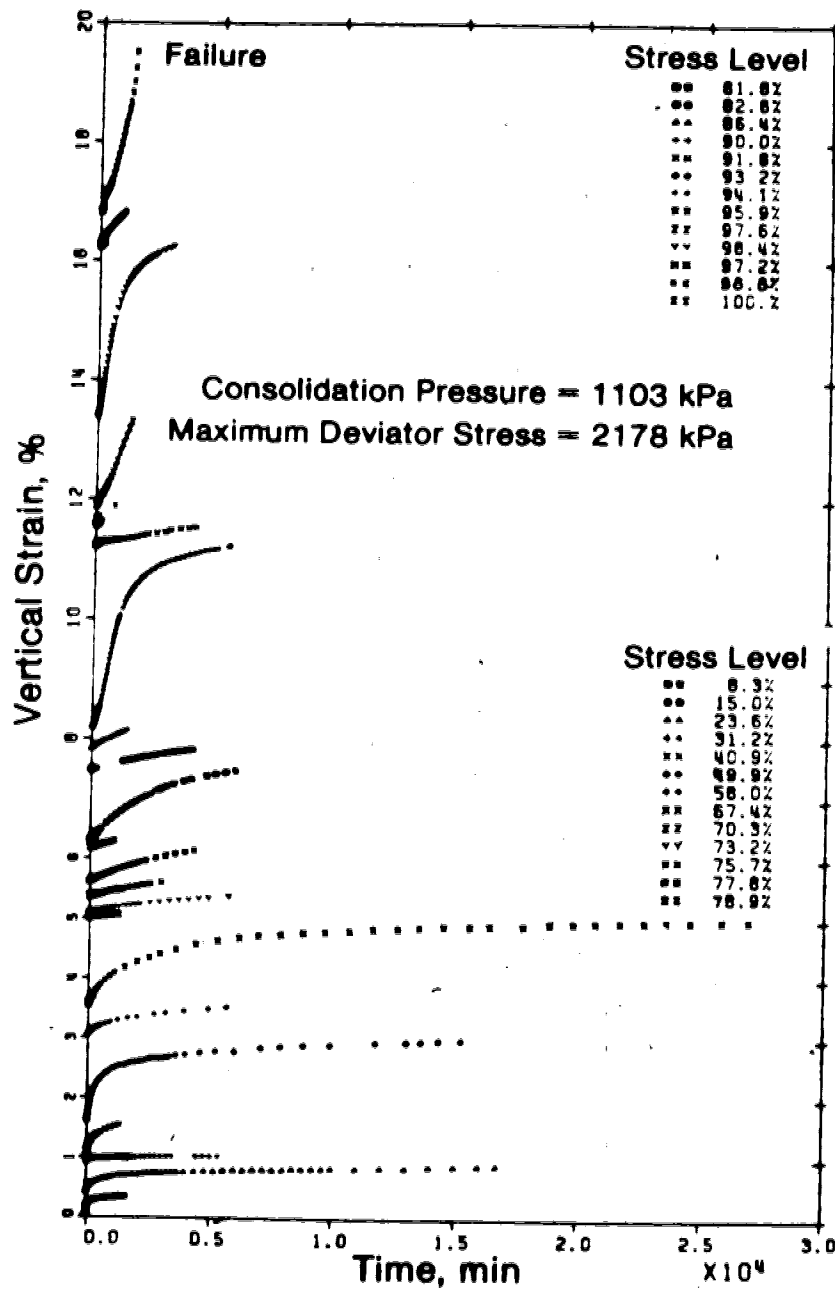


Figure C.8 Vertical strain versus time, sample T1

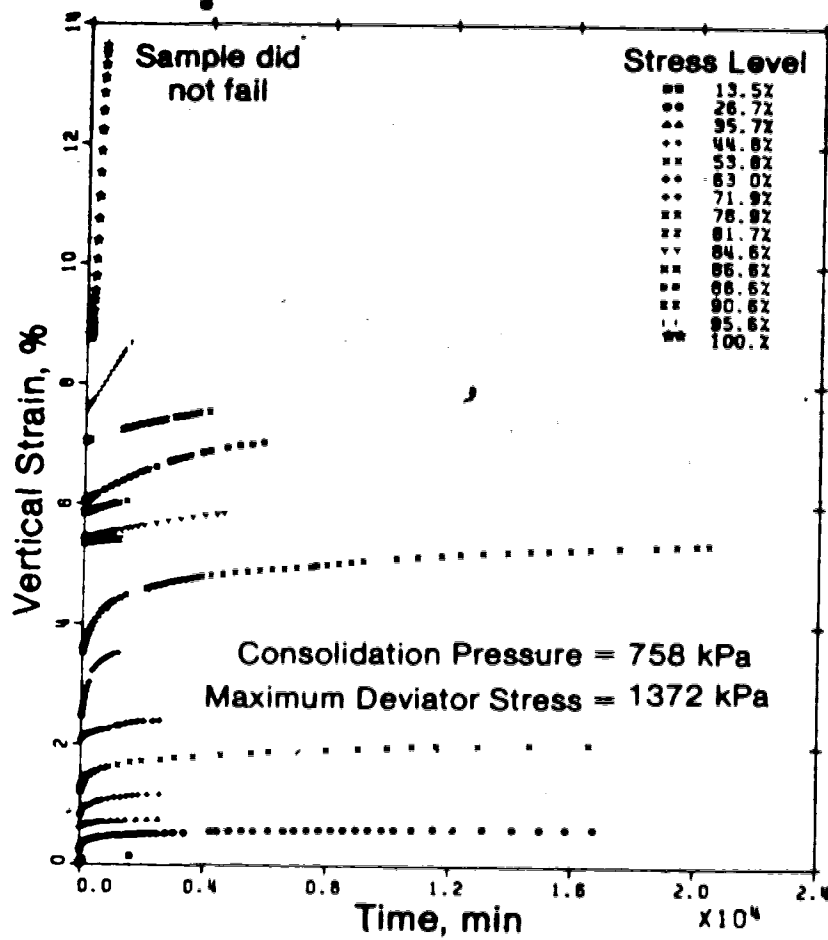


Figure C.9 Vertical strain versus time, sample T2

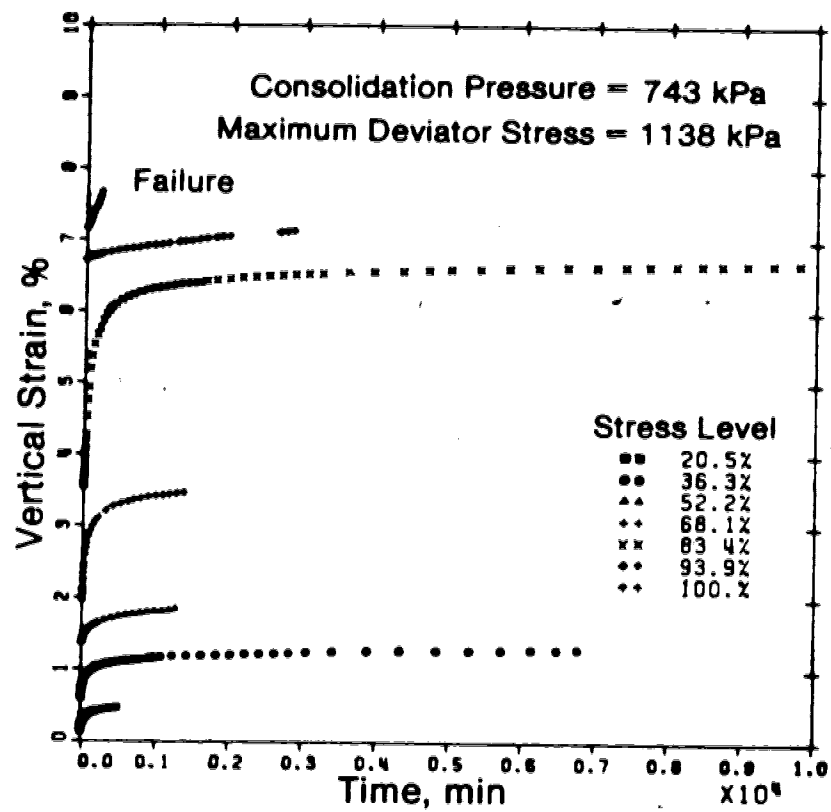


Figure C.10 Vertical strain versus time, sample I1



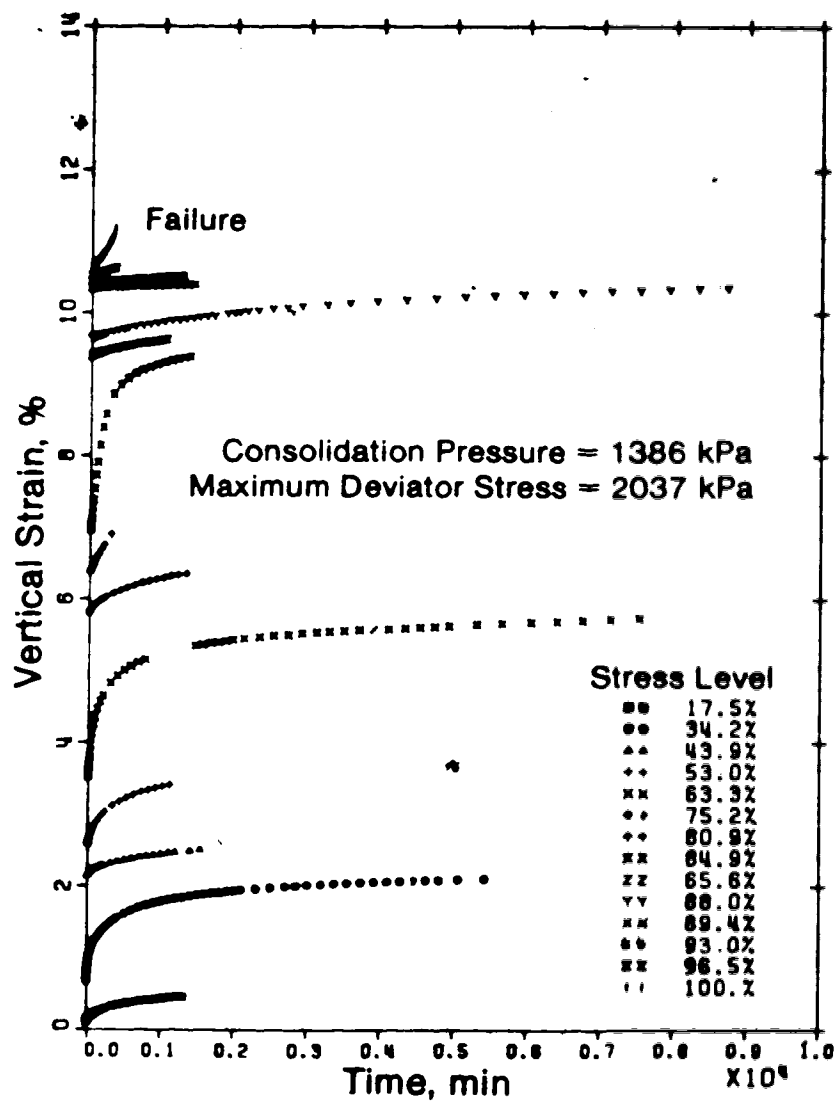


Figure C.11 Vertical strain versus time, sample 12

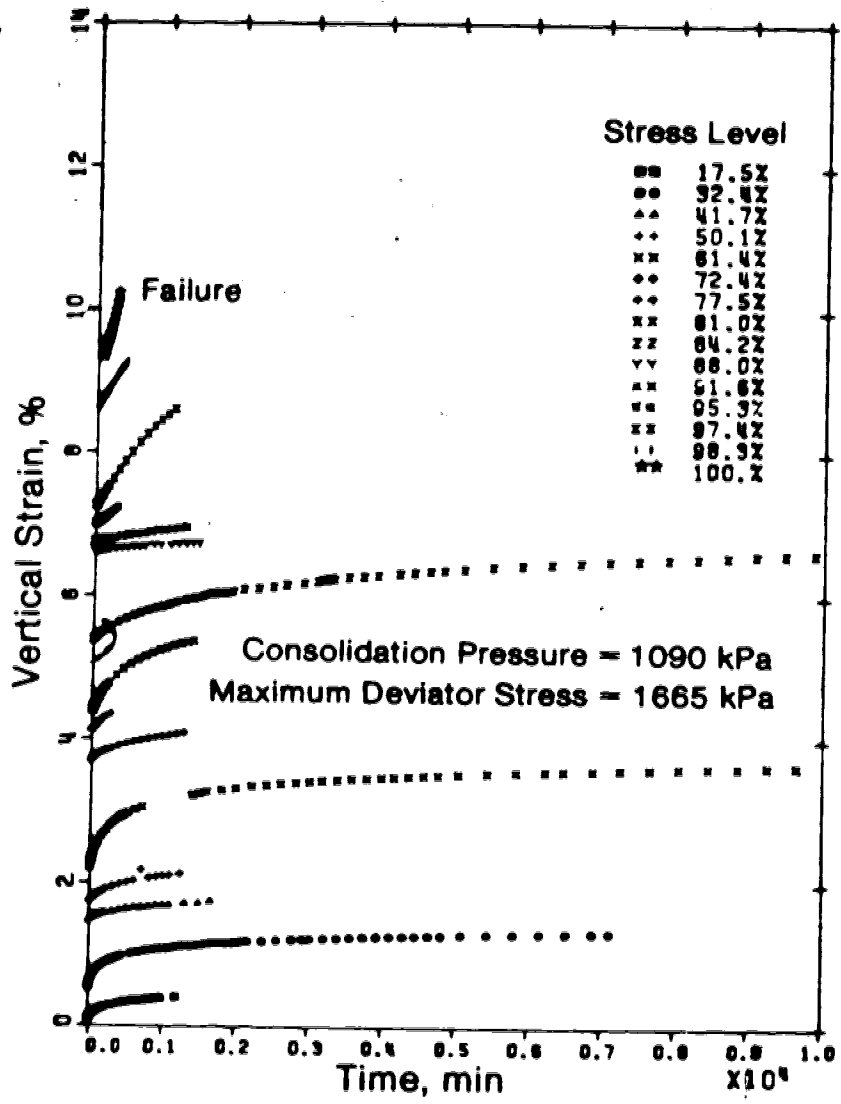


Figure C.12 Vertical strain versus time, sample 13

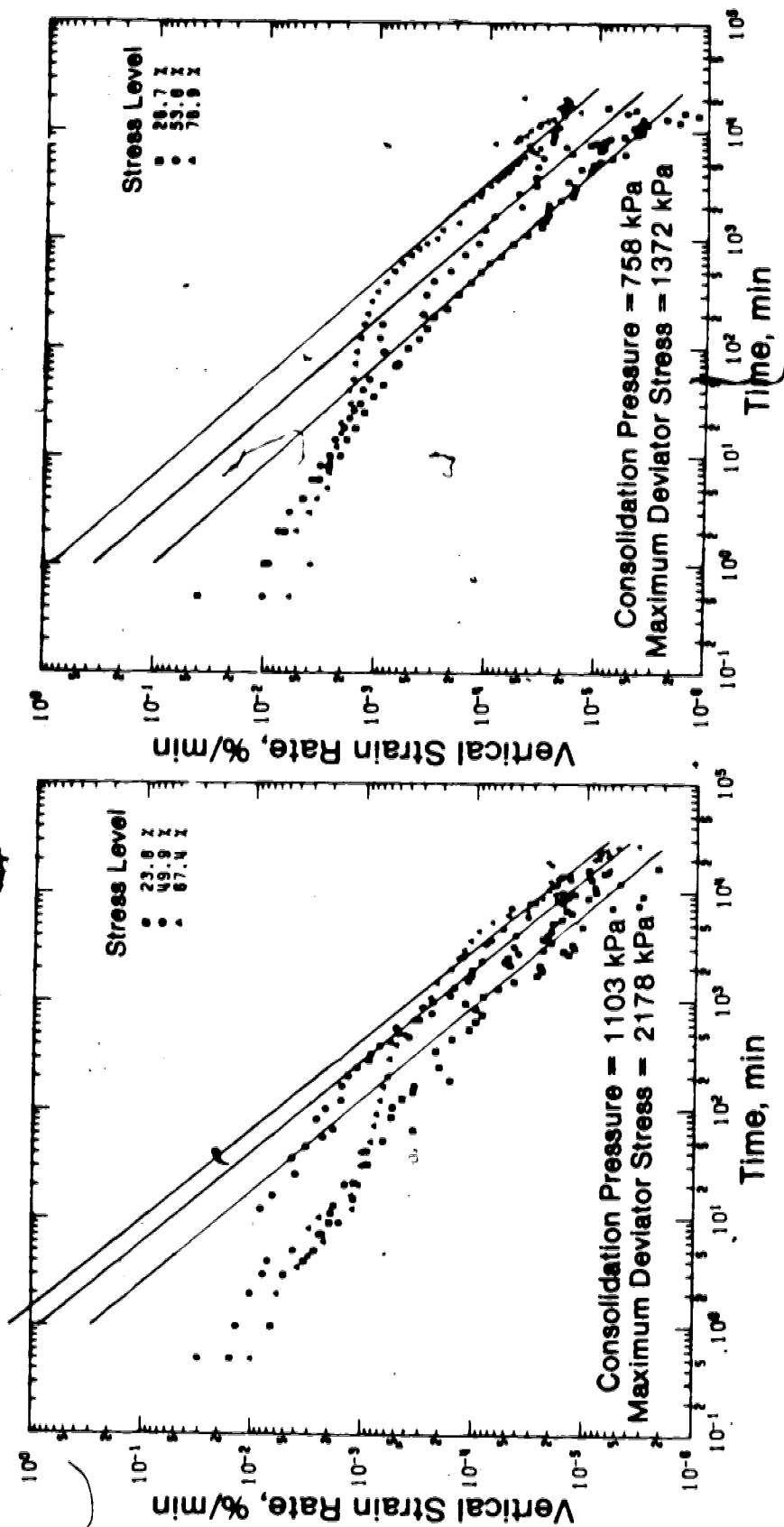


Figure C.13 Vertical strain rate versus time, left-sample T1, right-sample T2

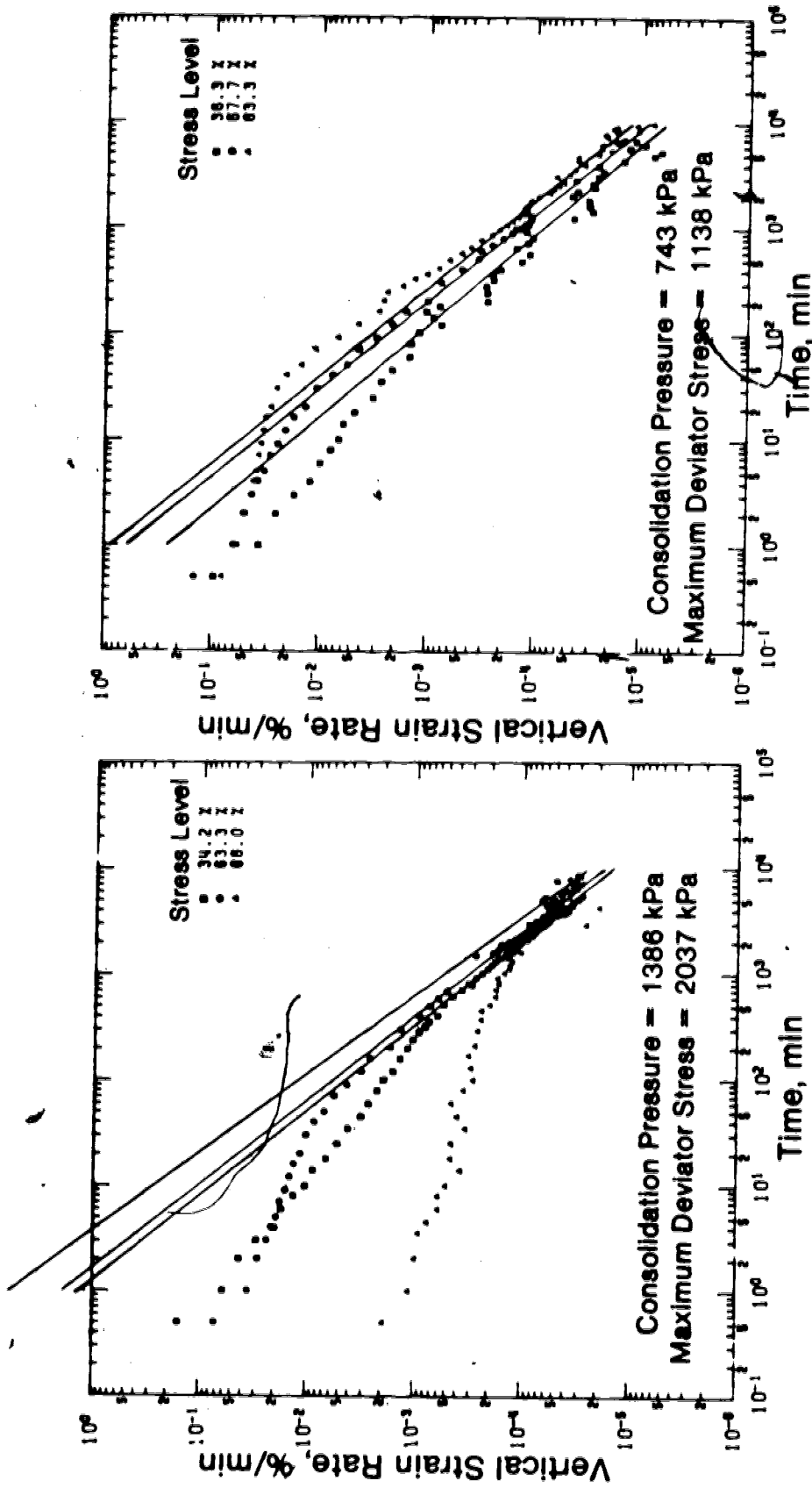


Figure C.14 Vertical strain rate versus time, left-sample I2, right-sample I1

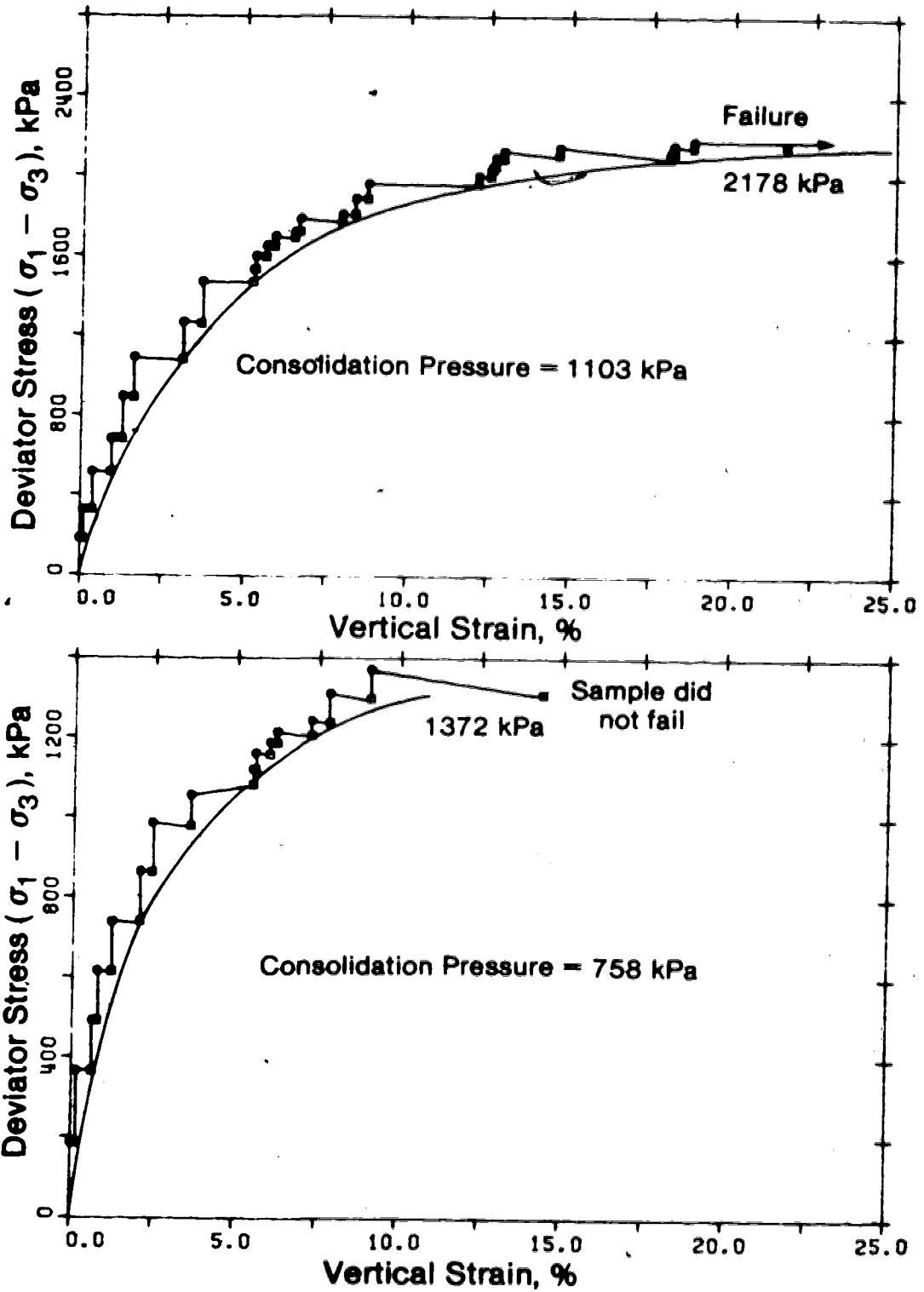


Figure C.15 Stress strain curves, sample T1-upper, sample T2-lower

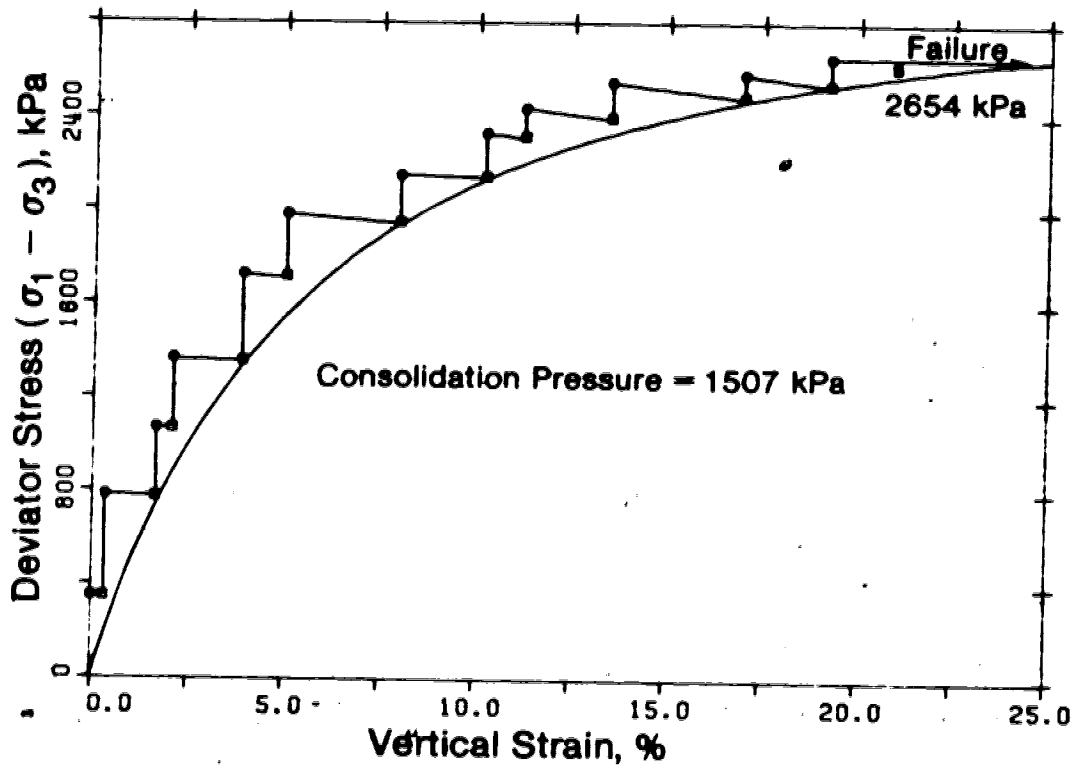


Figure C.16 Stress strain curve, sample t4

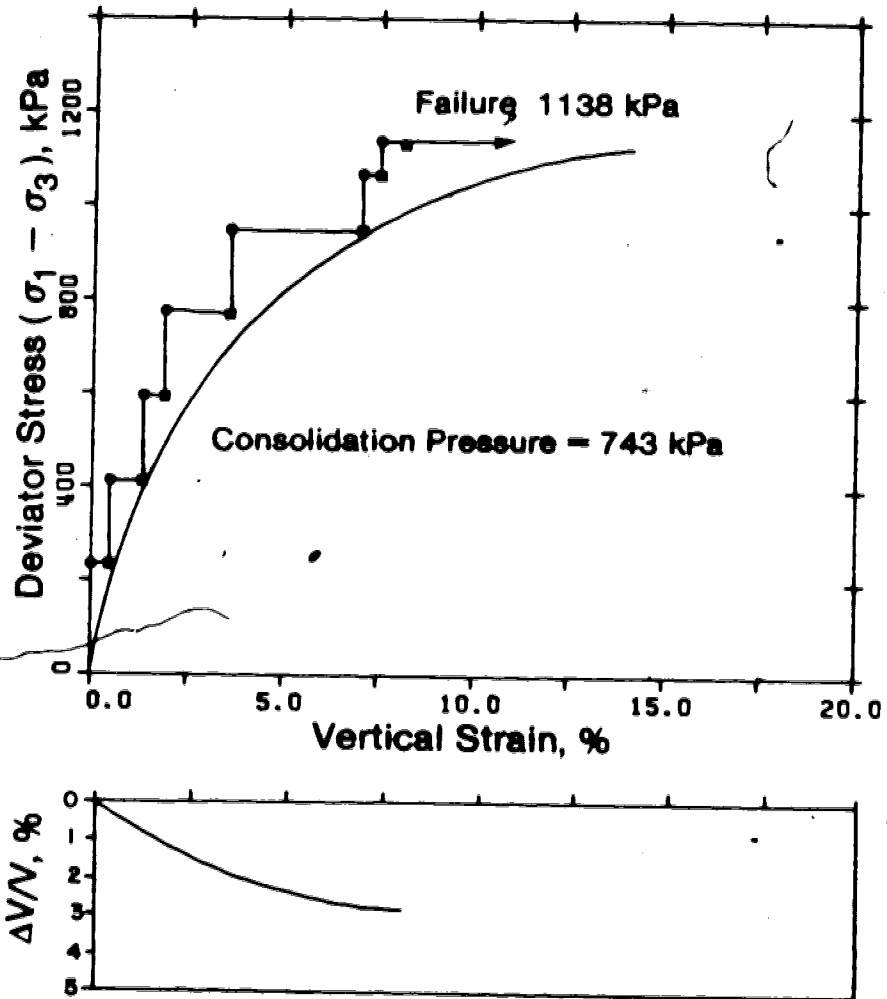


Figure C.17 Stress strain curve, sample I1

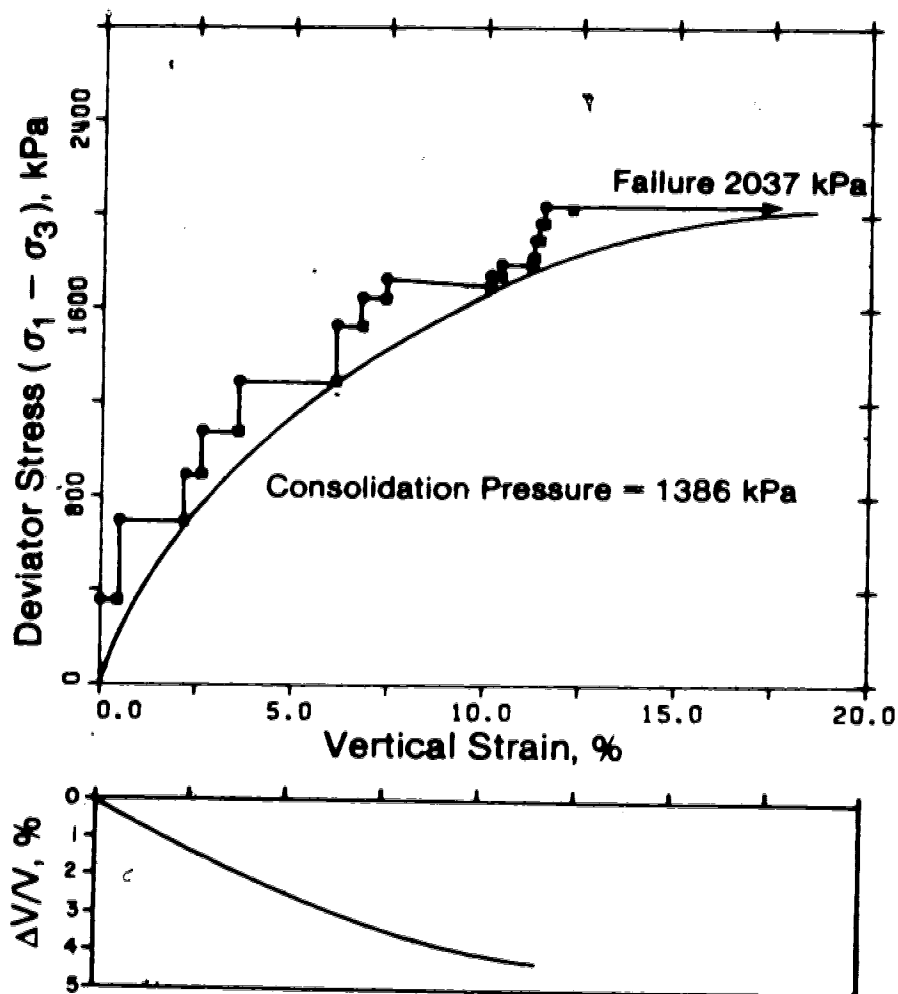


Figure C.18 Stress strain curve, sample I2



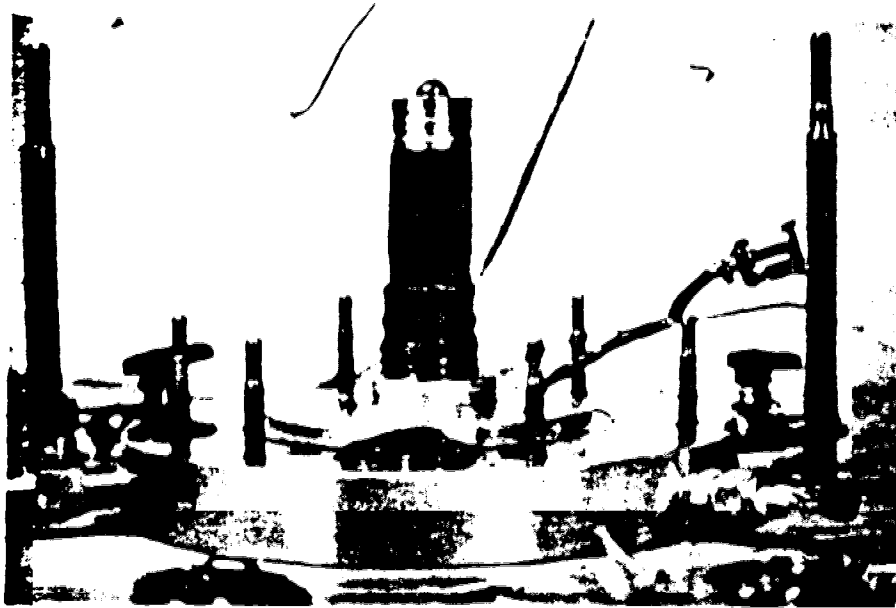


Plate C.1 Sample T1-upper, sample T2-lower, after failure

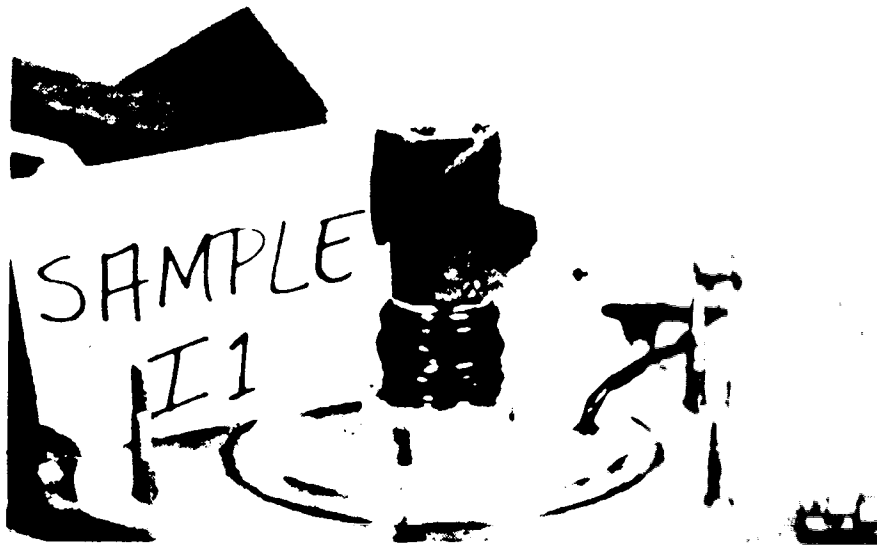
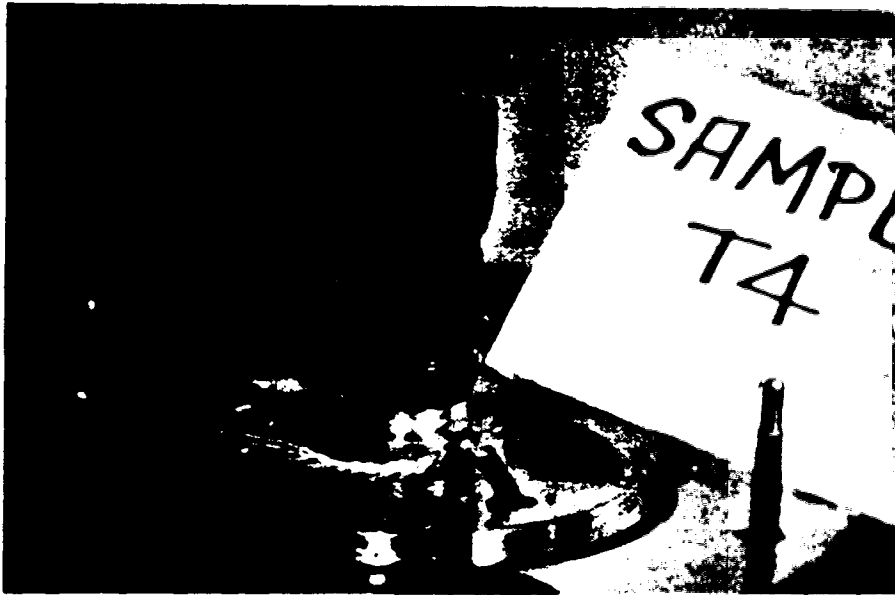


Plate C.2 Sample T4-upper, sample I1-lower, after failure



Plate C.3 Sample 12-upper, sample 13-lower, after failure

## Appendix D

### Derivation of Formulas for Analysis

#### D.1 Definition of Nonlinear Elastic Material Parameters

Nonlinear elastic constitutive relationships in soil mechanics can be derived from the observation that stress strain curves can be described by the equation for a hyperbola. This was first reported by Kondner (1963) and later popularized by Duncan and Chang (1970). Reference should be made to this latter publication for a more detailed explanation than is given here.

A stress strain curve can be represented by an equation for a hyperbola of the form:

$$(\sigma_1 - \sigma_3) = \frac{\epsilon}{1/E_t + \epsilon/(\sigma_1 - \sigma_3)_{ult}} \quad \text{D.1}$$

where

$(\sigma_1 - \sigma_3)$  = deviator stress

$\epsilon$  = strain

$E$  = initial tangent modulus

$(\sigma_1 - \sigma_3)_{ult}$  = asymptotic value of deviator stress as represented by hyperbolic equation

The compressive strength of the soil is related to  $(\sigma_1 - \sigma_3)_{ult}$  by:

$$R_f = (\sigma_1 - \sigma_3)_f / (\sigma_1 - \sigma_3)_{ult} \quad \text{D.2}$$

where  $R_f$  = failure ratio

The initial tangent modulus varies with confining stress according to:

$$E_i = K p_a \left( \frac{\sigma_3}{p_a} \right)^n \quad \text{D.3}$$

where  $K$  = modulus number

$n$  = modulus exponent

$p_a$  = atmospheric pressure in chosen units

The Mohr Coulomb failure criterion is given by:

$$(\sigma_1 - \sigma_3)_f = \frac{2c \cos \phi' + 2\sigma_3 \sin \phi'}{1 - \sin \phi'} \quad \text{D.4}$$

By differentiating Equation D.1 with respect to strain and substituting Equations D.2, D.3 and D.4 the tangent modulus is given by:

$$E_t = \left[ 1 - \frac{R_f (1 - \sin \phi') (\sigma_1 - \sigma_3)}{2c \cos \phi' + 2\sigma_3 \sin \phi'} \right]^2 K p_a \left( \frac{\sigma_3}{p_a} \right)^n \quad \text{D.5}$$

Poisson's ratio can be described by an equation which accounts for its dependence on normal stress and shear stress (for contractant materials only) as per Duncan *et al* (1978). Poisson's ratio was taken as a constant since this analysis was assumed undrained.

## D.2 Transformation of Singh-Mitchell Equation To a Multiaxial State of Stress

The following formulation follows that of Odqvist (1966). Odqvist begins his formulation by drawing from the theory of plasticity. He defines the rate of dissipation of

energy in a creep test by:

$$\dot{W}_{ij} = \delta s_{ij} v_{ij} \quad \text{D.6}$$

where  $\dot{W}_{ij}$  = change in rate of dissipation of energy

$\delta s_{ij}$  = increment of stress deviator tensor

$v_{ij}$  = strain rate tensor

Equation D.6 provides a relationship between the stress deviator tensor and strain rate tensor. He continues by stating that  $W$  is a flow potential and dependent on some scalar function. He calls the scalar function the 'effective' stress and defines it in terms of the second stress invariant as:

$$\begin{aligned} \sigma_e^2 &= 3/2 s_{ij} s_{ij} & \text{D.7} \\ &= \sigma_{11}^2 + \sigma_{22}^2 + \sigma_{33}^2 - \sigma_{11}\sigma_{22} - \sigma_{22}\sigma_{33} - \sigma_{33}\sigma_{11} \\ &\quad + 3(\sigma_{12}^2 + \sigma_{23}^2 + \sigma_{31}^2) \end{aligned}$$

Equation D.6 can now be manipulated as follows:

$$v_{ij} = \frac{dW}{d\sigma_e} \times \frac{\partial \sigma_e}{\partial s_{ij}} = \frac{W}{d\sigma_e} \times \frac{1}{2\sigma_e} \times \frac{\partial \sigma_e^2}{\partial s_{ij}} = 3/2 \times \frac{dW}{d\sigma_e} \times \frac{s_{ij}}{\sigma_e} \quad \text{D.8}$$

The preceding assumes coaxiality of the tensors of strain rate and stress. It also assumes no volume change and isotropy.

For the case of uniaxial stress:

$$s_{11} = 2\sigma_{11}/3$$

$$\sigma_e = \sigma_{11}$$

$$s_{22} = s_{33} = -\sigma_{11}/3$$

Now Equation D.8 will be manipulated so that it reduces to the Singh-Mitchell equation for a uniaxial stress state.

$$v_{11} = 3/2 \frac{\partial W}{\partial \sigma_e} \frac{2}{3} \frac{\sigma_{11}}{\sigma_{11}} = A e^{\alpha \sigma_{11}} (1/t)^m \quad \text{D.9}$$

This reduces to:

$$\frac{\partial W}{\partial \sigma_e} = A e^{\alpha \sigma_e} \left(\frac{1}{t}\right)^m \quad \text{D.10}$$

Substituting D.10 into D.8 we have:

$$\dot{\epsilon}_{ij} = \frac{3}{2} A e^{\alpha \sigma_e} \left(\frac{1}{t}\right)^m \frac{\sigma_{ij}}{\sigma_e} \quad \text{D.11}$$

Equation D.11 is a general multiaxial equation relating each term in the strain rate tensor to each term in the stress deviator tensor. The relationship desired for the analysis is one between horizontal shear strain and horizontal shear stress for a simple shear stress state. It will be assumed that a pure shear stress state is representative of a simple shear stress state at zero normal stress. The assumptions of pure shear result in the following:

$$\begin{aligned} \sigma_1 = \tau_h, \sigma_2 = 0, \sigma_3 = -\tau_h \\ s_{11} = -s_{33} = \tau_h, s_{22} = 0 \end{aligned} \quad \text{D.12}$$

The effective stress as given by Equation D.2 reduces to the following:

$$\sigma_e = 2 \tau_h \quad \text{D.13}$$

If this is now substituted into Equation D.7 the following results:

$$\dot{\gamma}_{xy} = 2 \times \frac{3}{2} A e^{\alpha 2 \tau_h} \left(\frac{1}{t}\right)^m \frac{\tau_h}{2 \tau_h} \quad \text{D.14}$$

Reducing:

$$\dot{\gamma}_{xy} = \frac{3}{2} A e^{2\alpha \tau_h} \left(\frac{1}{t}\right)^m \quad \text{D.15}$$

### D.3 Definition of Stress Level For Simple Shear Stress Conditions

In order to define the stress level in simple shear it is necessary to make some assumptions about the state of stress (see Ladd and Edgers, 1972) and Gale, 1981). One assumption is that the horizontal plane is the failure

plane, another is that the horizontal plane is the plane of maximum shear stress. These two assumptions converge as the effective angle of shearing resistance decreases. For an angle of shearing resistance of  $24^\circ$  of the foundation clay, the maximum difference between these assumptions in defining the shear stress level is less than 10 percent. It will be assumed that the horizontal plane is the failure plane.

The tangent of the angle of shearing resistance for a simple shear test is then defined as:

$$\tan\phi' = \tau_{max} / \sigma'_v \quad D.16$$

where  $\tau_{max}$  = shear stress on horizontal plane at failure

$\sigma'_v$  = effective normal stress on horizontal plane at failure

The shear stress level is defined by:

$$\bar{D} = \tau_h / \tau_{max} \quad D.17$$

where  $\bar{D}$  = shear stress level

$\tau_h$  = shear stress on the horizontal plane

The stress level term  $\bar{D}$  in Equation 6.3 then becomes:

$$\bar{D} = \tau_h / \sigma'_v \tan\phi' \quad D.18$$

It is of interest to compare the stress level terms from a triaxial and a simple shear test. In a triaxial test:

$$\bar{\alpha}_T = \alpha / 2 (\sigma_1 - \sigma_3) / f \quad D.19$$

In a simple shear test:

$$\bar{\alpha}_S = \alpha \sigma'_v \tan\phi'$$



If the approximation is made that  $\sigma_v \tan \phi' = 1/2(\sigma_1 - \sigma_3)$  then:

$$\bar{\alpha}_s = \bar{\alpha}_T \quad \text{D.21}$$

#### D.4 Sample Calculation of $\bar{\alpha}$

The shear strain versus time curves for inclinometer S76-103 will be used to determine a value of  $\bar{\alpha}$  from Equation 6.7. Two depths in the clay layer are required for the calculation of  $\bar{\alpha}$  at which the pore pressures, hence the stress levels, are known. The obvious choices for inclinometer S76-103 are the base of the clay layer which is at a depth of 67.07 m and the depth corresponding to the piezometer AP-75-18A of 62.18 m.

The stress level at the base of the clay is given by:

$$\begin{aligned} \bar{D}_1 &= \tau_h / \sigma_v' \tan \phi' \\ &= 224 \text{ kPa} / (1353 \text{ kPa} - 110 \text{ kPa}) \tan 24^\circ \\ &= 0.40 \end{aligned}$$

The stress level at 62.18 m is:

$$\begin{aligned} \bar{D}_2 &= 175 \text{ kPa} / (1120 \text{ kPa} - 350 \text{ kPa}) \tan 24^\circ \\ &= 0.51 \end{aligned}$$

In order to use Equation 6.7 the strain rates at  $t_i$  are required. This was done by passing the best fit second order polynomial through the shear strain versus time curves and then calculating the shear strains at  $t_i$ . Inserting these values into Equation 6.7 results in:

$$\bar{\alpha} = \frac{\ln(5.9 \times 10^{-7} \%/\text{min}) - \ln(1.04 \times 10^{-6} \%/\text{min})}{.40 - .51} \quad \text{D.22}$$

$$= 5.1$$

#### D.5 Procedure For Determining $t_1$ .

The procedure detailed here for the determination of  $t_1$  is based on the assumption that  $m$  is constant, i.e. the slope of the natural logarithm of strain rate versus the natural logarithm of time is a straight line. The equation of such a line is given by:

$$\ln \dot{\gamma}_2 = \ln \dot{\gamma}_1 - m \ln \left( \frac{\Delta t_2 + t_1}{t_1} \right) \quad \text{D.23}$$

where  $\dot{\gamma}_1$  = shear strain rate at time  $t_1$ ,

$\dot{\gamma}_2$  = shear strain rate at time  $\Delta t_2 + t_1$ .

If  $m$  is equal to 1 then  $t_1$  can be found from:

$$t_1 = \Delta t_2 / (\dot{\gamma}_1 / \dot{\gamma}_2) - 1 \quad \text{D.24}$$

If  $m$  is not equal to one then two equations are needed to solve for  $T_1$ . Another expression similar to D.23 can be written for the same line as:

$$\ln \dot{\gamma}_3 = \ln \dot{\gamma}_1 - m \ln \left( \frac{\Delta t_3 + t_1}{t_1} \right) \quad \text{D.25}$$

Solving for  $m$  in Equation D.25 and substituting this expression into Equation D.23 yields:

$$\frac{\ln \dot{\gamma}_3 - \ln \dot{\gamma}_1}{\ln \dot{\gamma}_2 - \ln \dot{\gamma}_1} = \frac{\ln((\Delta t_3 + t_1)/t_1)}{\ln((\Delta t_2 + t_1)/t_1)} \quad \text{D.26}$$

The left hand side of Equation D.26 is a constant and will be called  $P$ . Rearranging D.26 yields:

$$\left( \frac{\Delta t_2 + t_1}{t_1} \right)^P = \frac{\Delta t_3 + t_1}{t_1} \quad \text{D.27}$$

A solution for  $t_1$  is a root of Equation D.27. The roots of Equation D.27 can be obtained by using a numerical technique such as Newton-Raphson. To proceed in this way Equation D.27

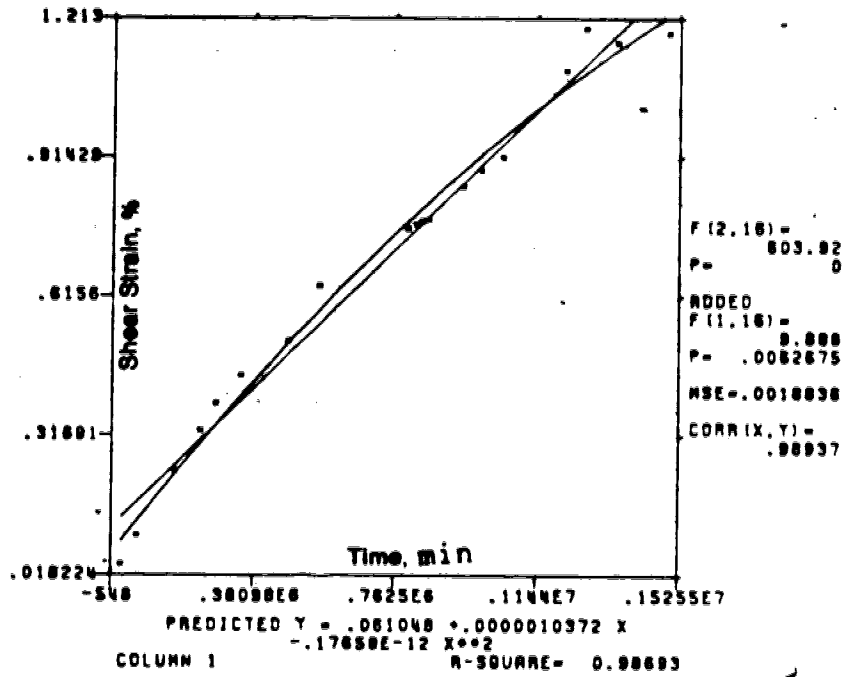
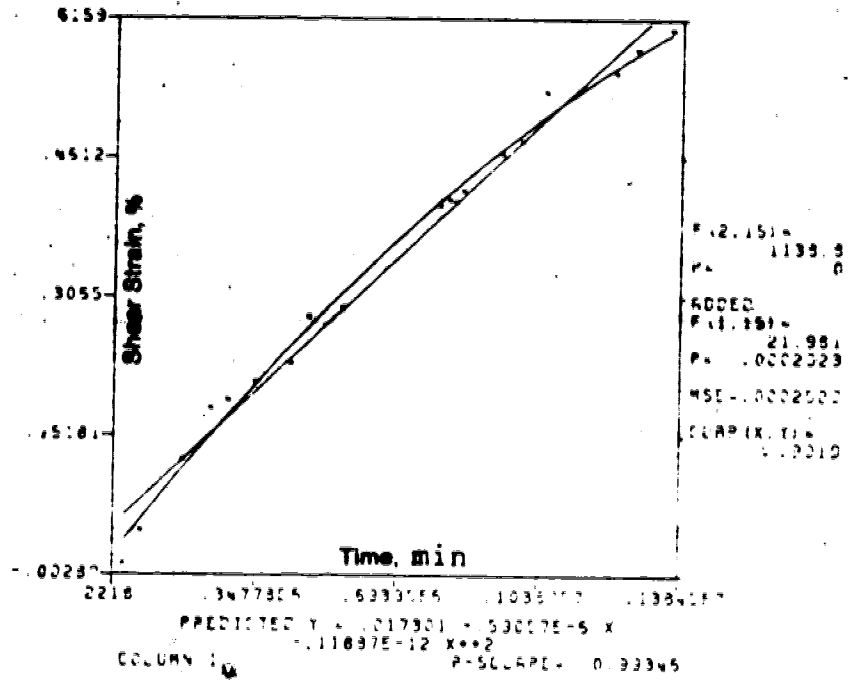


Figure D.1 Regression analysis of shear strain versus time at depths 67.06 m (upper) and 62.18 m (lower) for inclinometer S76-103

must be rearranged as follows:

$$(X+1)^P - KX - 1 = 0$$

where  $X = \Delta t_2 / t_1$

$K = \Delta t_2 / \Delta t_1$

D.28